

**Novel Roles of Matrix Metalloproteinase-2 in Mitochondrial and
Endoplasmic/Sarcoplasmic Reticulum Dysregulation**

by

Wesam Mohamed Elsayed Bassiouni Farag

A thesis submitted in partial fulfillment of the requirements for the degree of

Doctor of Philosophy

Department of Pharmacology

University of Alberta

©Wesam Mohamed Elsayed Bassiouni Farag, 2024

ABSTRACT

Matrix metalloproteinase-2 (MMP-2) is a ubiquitous multifunctional protease that cleaves both extracellular and intracellular proteins. MMP-2 is synthesized as an inactive zymogen. It is rapidly activated inside the cell in response to oxidative stress during different cardiac pathologies such as myocardial ischemia-reperfusion (IR) injury as well as doxorubicin (DXR)-induced cardiotoxicity. This occurs by the action of peroxynitrite-induced S-glutathiolation which exposes its catalytic site. Upon activation in the heart, MMP-2 induces the cleavage of several cardiac sarcomeric proteins resulting in cardiac contractile dysfunction. An important isoform of MMP-2, known as N-terminal truncated MMP-2 (MMP-2_{NTT76}), is constitutively active and gets expressed in cardiomyocytes in response to oxidative stress. MMP-2 is localized to several intracellular compartments including the cytosol, sarcomere, cytoskeleton, nuclei, mitochondria and mitochondrial-endoplasmic reticulum (ER)-associated membrane (MAM), while MMP-2_{NTT76} is localized to the intermembranous space of mitochondria. However, how MMP-2 affects mitochondrial and ER functions is not well investigated.

Mitochondria and ER play significant roles in the regulation of several biological processes. A specialized form of the ER, known as the sarcoplasmic reticulum (SR), found only in striated muscle, interacts with the T-tubules to regulate intracellular calcium level. As MMP-2 is localized at the MAM, I hypothesize that MMP-2, activated in response to oxidative stress, disrupts mitochondrial function, ER homeostasis and the T-tubule-SR interaction, by proteolyzing specific mitochondrial and/or ER/SR proteins localized at or near the MAM, leading to the development of cardiac pathologies.

A fundamental role of mitochondria during cellular injury is the proteolytic processing of apoptosis-inducing factor (AIF), a mitochondrial flavoprotein that mediates staurosporine (STS)-

induced cell death. I investigated whether MMP-2 activity is affected in response to STS and if it mediates AIF cleavage in human fibrosarcoma HT1080 cells. I found a significant increase in MMP-2 activity in response to STS treatment, prior to the induction of cell necrosis. However, mitochondrial AIF cleavage is independent of the proteolytic activity of MMP-2.

Interestingly, enhanced oxidative stress which occurs during myocardial IR injury also impairs mitochondrial function which is regulated by different proteins including mitofusin-2 (Mfn-2). Oxidative stress and mitochondrial dysfunction also trigger the NLRP3 inflammasome response. In isolated hearts from mice subjected to IR injury, I found that increased MMP-2 activity and MMP-2_{NTT76} mRNA expression are associated with a reduction in post-ischemic recovery of cardiac contractile function, the loss in mitochondrial Mfn-2 level, enhanced inflammasome response and increased infarct size, compared to aerobically perfused hearts. All these changes were attenuated by MMP-2 inhibition. An association between MMP-2 and Mfn-2 was observed in aerobic and IR hearts. IR also impaired the rate of mitochondrial oxygen consumption in muscle fibers freshly isolated from mouse hearts, whereas MMP-2 inhibitors attenuated this reduction.

Upon investigating how MMP-2 activation affects ER homeostasis using the same model of IR injury, I found that MMP-2 is not involved in the induction of the ER stress response itself. However, it affects the unfolded protein response (UPR) by targeting and cleaving the UPR sensor, inositol-requiring enzyme 1 α (IRE1 α). MMP-2 inhibitors are able to preserve IRE1 α levels and protect against the progression of ER stress-mediated myocardial cell death. An association between MMP-2 and IRE1 α was also observed in aerobic and IR hearts. Finally, the Schulz lab previously showed that junctophilin-2 (JPH-2), a membrane protein that tethers T-tubules to the SR, is proteolyzed by MMP-2 during IR injury. I investigated the involvement of MMP-2-

mediated JPH-2 proteolysis in DXR-induced cardiotoxicity. I found that myocytes in hearts from DXR-treated mice had abnormally swollen T-tubules and mitochondria, accompanied by JPH-2 cleavage. These changes were also attenuated by MMP inhibitors. Loss in JPH-2 and impaired calcium transients were also observed in response to DXR in neonatal rat ventricular cardiomyocytes, while MMP-2 inhibition attenuated these changes.

In conclusion, MMP-2, activated in response to oxidative stress, plays a fundamental role in MAM dysregulation by affecting different downstream pathways that are essential for cardiac function including mitochondrial and ER homeostasis and T-tubule-SR interaction. Potential MMP-2 proteolytic targets whose loss could mediate these pathophysiological changes include Mfn-2, IRE1 α and JPH-2. Therefore, MMP-2 inhibition could be a promising adjunct therapy that can be used to protect against cardiac dysfunction in patients with ischemic heart disease or receiving anthracycline treatment for cancer.

PREFACE

This thesis is an original work done by Wesam Mohamed Elsayed Bassiouni Farag. All experimental animal procedures included in this thesis were approved by the University of Alberta Health Sciences Welfare Committee (University of Alberta Animal Welfare, ACUC, study ID #AUP329 for Dr Richard Schulz, and AUP330 for Dr John Seubert) and conducted according to guidelines provided by the Guide to the Care and Use of Experimental Animals.

A part of **Chapter 1** (Introduction) has been published as a review article as **Wesam Bassiouni**, Mohammad A.M. Ali, Richard Schulz (2021). Multifunctional intracellular matrix metalloproteinases: implications in disease. *FEBS J.* 288:7162-82. I was responsible for reviewing, collecting and summarizing data from the literature and writing the manuscript. I also designed and edited the figures. Richard Schulz and Mohammad A.M. Ali were the supervisory authors who were involved with concept formation, reviewing and editing the manuscript.

A version of **Chapter 3** has been published as **Wesam Bassiouni**, John M. Seubert, Richard Schulz (2022). Staurosporine-induced cleavage of apoptosis-inducing factor in human fibrosarcoma cells is independent of matrix metalloproteinase-2. *Can J Physiol Pharmacol.* 100:184-91. I was responsible for designing and performing the experiments, analyzing the data and writing the manuscript. Richard Schulz and John M. Seubert were the supervisory authors who were involved with concept formation, reviewing and editing the manuscript.

A version of **Chapter 4** has been published as **Wesam Bassiouni**, Robert Valencia, Zabed Mahmud, John M. Seubert, Richard Schulz (2023). Matrix metalloproteinase-2 proteolyzes mitofusin-2 and impairs mitochondrial function during myocardial ischemia-reperfusion injury. *Basic Res Cardiol.* 118:29. I was responsible for designing and performing the experiments, analyzing the data and writing the manuscript. Robert Valencia helped with the qPCR experiment.

Zabed Mahmud did the 3D protein structure analysis. Richard Schulz and John M. Seubert were the supervisory authors who were involved with concept formation, reviewing and editing the manuscript.

A part of **Chapter 5** has been submitted to *J Mol Cell Cardiol* as **Wesam Bassiouni**, Zabed Mahmud, Thomas Simmen, John M. Seubert, Richard Schulz. MMP-2 inhibition attenuates ER stress-mediated cell death during myocardial ischemia-reperfusion injury by preserving IRE1 α . I was responsible for designing and performing the experiments, analyzing the data and writing the manuscript. Zabed Mahmud did the 3D protein structure analysis. Thomas Simmen collaborated in designing some experiments and was involved with concept formation. Richard Schulz and John M. Seubert were the supervisory authors who were involved with concept formation, reviewing and editing the manuscript.

A version of **Chapter 6** is under revision with *J Physiol* as **Wesam Bassiouni**, Brandon Y.H. Chan, Andrej Roczkowsky, Zabed Mahmud, Woo Jung Cho, Richard Schulz. Junctophilin-2 proteolysis and T-tubule remodeling are consequences of matrix metalloproteinase-2 activation during doxorubicin-induced cardiotoxicity. I was responsible for designing and performing the immunoblotting, N-deglycosylation and neonatal rat ventricular cardiomyocytes experiments. I analyzed the data and wrote the manuscript. Brandon Y.H. Chan contributed equally to the manuscript. He performed the *in vivo* mouse doxorubicin treatment, analyzed the echocardiography results and helped with the immunoblotting experiment. Andrej Roczkowsky helped with the *in silico* protein structure analysis. Zabed Mahmud did the 3D protein structure analysis. Woo Jung Cho did the transmission electron microscopy imaging. Richard Schulz was the primary investigator and the supervisory author who was involved with concept formation, reviewing and editing the manuscript.

This dissertation is dedicated with love, appreciation and gratitude to my

parents, wife, daughter, brother and sister

Thank you for your unconditional love and support

ACKNOWLEDGEMENTS

First of all, I am grateful to Allah for providing me with the strength, patience and capability to proceed with this work successfully and for always being by my side.

I would like to express my sincerest gratitude to my supervisors, Dr Richard Schulz and Dr John Seubert. I am greatly thankful to Dr Schulz for his continuous motivation, guidance and thoughtful advice throughout my PhD. His expertise, knowledge and understanding have greatly added to my experience and made everything easier during this long journey. He gave me a great opportunity to be a member of his lab and allowed me the space to work independently and be a part of the scientific society. I am also thankful to Dr Seubert for his continuous assistance, patience, motivation and constant support. He has enlightened my scientific path and nourished my interests. His continuous help and insightful comments have greatly contributed to the accomplishment of this research. They both have saved no effort to guide me and improve my work and I am deeply grateful for all the opportunities they generously provided me with.

I am also grateful to my supervisory committee member, Dr Frances Plane, for the continuous support and valuable time she gave me throughout my program. Her kindness and generosity have always been inspiring, and her advice and feedback have been of great help to me.

I would also like to thank Dr Thomas Simmen for his advice and collaboration that helped me accomplish a significant part of my research. I am also thankful to Dr Mohammad Ali for his advice and support before starting and throughout my PhD. I also need to acknowledge the great work done by Woo Jung Cho who helped us with the electron microscopy imaging and analysis.

I would like to extend my thanks and appreciation to my past and present lab colleagues, Robert Valencia, Deanna Sosnowski, Ala' Yousef, Joshua Kranrod, Liye Fang and Mobina

Darmani for being such great colleagues and for their continuous assistance, scientific input, support and encouragement. Special thanks go to Dr Ahmed Darwesh and Dr Brandon Chan who have taught me most of the techniques I learnt since starting my PhD, and Dr Zabed Mahmud for being a great lab colleague and for all the protein structure analyses he has done for me. I would also like to thank our lab technicians Andy Huang and Kamala Lamsal for their generous help and dedication to keep our work going.

I am thankful to Alberta Innovates for financially supporting me through the Alberta Innovates Graduate Student Scholarship (2020-2023). I would also like to thank the generous support provided to me by the University of Alberta and the Department of Pharmacology in the form of several other scholarships and awards including Ivy A Thomson and William A Thomson Graduate Scholarship, Alberta Graduate Excellence Scholarship, Andrew Stewart Memorial Graduate Prize, Faculty of Medicine and Dentistry Dean's Doctoral Award, Dr Edwin E. Daniel Pharmacology Graduate Award, among others. Finally, I need to thank the Canadian Institutes of Health Research (CIHR) for funding our research work.

My sincerest indebtedness goes to my beloved parents, brother and sister for their endless love, prayers and encouragement. They were very supportive and provided me with all the amenities to be who I am today. No words could be fair to express the virtue of their presence as a part of my life. Finally, I would have never been able to reach this milestone without the continuous support of my special lovely wife, Sarah. She has always been my source of strength, wisdom and inspiration and helped me get through difficult times. Thank you for being there for me and for your unconditional love and encouragement. No words can describe how great partner you are. Last but not least, a special thanks goes to my lovely newborn daughter, Sama, who fills my life with hope and happiness and makes me always think how to be a better person for her.

TABLE OF CONTENTS

CHAPTER I. GENERAL INTRODUCTION	1
1.1. Matrix metalloproteinase-2	2
1.1.1. The history of matrix metalloproteinases	2
1.1.2. Classification of MMPs	3
1.1.3. MMP-2 structural domains	4
1.1.4. Mechanisms of intracellular localization of MMP-2	6
1.1.4.1. Inefficient secretion	6
1.1.4.2. Post-secretion re-entry	6
1.1.4.3. Organelle localization signals	7
1.1.5. Mechanisms of MMP-2 activation and its regulation	9
1.1.6. Intracellular locales and substrates of MMP-2	12
1.1.6.1. Cytosol	12
1.1.6.2. Muscle sarcomere and cytoskeleton	12
1.1.6.3. Caveolae	13
1.1.6.4. Mitochondria, mitochondrial associated membranes and endoplasmic reticulum	13
1.1.6.5. Nucleus/Nucleolus	14
1.1.7. MMP-2 inhibitors	18
1.1.7.1. Endogenous MMP-2 inhibitors	18
1.1.7.2. Synthetic MMP-2 inhibitors	19
1.1.8. Role of MMP-2 in pathologies	20
1.1.8.1. Kidney injury	20
1.1.8.2. Inflammatory diseases	20
1.1.8.3. Malignancy	21
1.1.8.4. Cardiovascular diseases	21

1.2. Myocardial ischemia-reperfusion injury	24
1.2.1. Pathophysiology of myocardial IR injury	24
1.2.2. Cardioprotective interventions to protect against reperfusion injury	27
1.2.3. Myocardial stunning vs necrosis	27
1.2.4. Role of MMP-2 in IR injury and its proteolytic targets	28
1.2.5. Role of MMP-2 in myocardial cell death	30
1.3. Doxorubicin-induced cardiotoxicity	31
1.3.1. Pathophysiology of DXR-induced cardiotoxicity	31
1.3.2. Therapeutic approaches to protect against DXR-cardiotoxicity	32
1.3.3. Role of MMP-2 in DXR cardiotoxicity and its proteolytic targets	33
1.4. Mitochondrial-ER-associated membrane	34
1.4.1. Regulatory functions of the MAM in cardiac cells	34
1.4.2. MMP-2 localization to the MAM	36
1.4.3. Mitochondria and their regulation	37
1.4.3.1. Structure of mitochondria	37
1.4.3.2. Functions of mitochondria in cardiac cells	38
1.4.3.3. Mitochondria and IR injury	38
1.4.3.4. Mitochondrial quality control mechanisms	39
1.4.3.4.1. Mitochondrial biogenesis	40
1.4.3.4.2. Mitochondrial dynamics	40
1.4.3.4.3. Mitochondrial autophagy/mitophagy	42
1.4.3.5. Functions of mitofusin-2 in cardiomyocytes	44
1.4.3.6. Mitochondrial respiratory chain and oxidative phosphorylation	45
1.4.3.7. Role of mitochondria in apoptotic cell death	49
1.4.3.7.1. Apoptosis-inducing factor	49
1.4.3.7.2. Bcl-2/Bax/Bak signalling pathway	50

1.4.4. Inflammasomes and IR injury	51
1.4.4.1. Inflammasome structure and activation	51
1.4.4.2. Crosstalk between inflammasomes and mitochondria	52
1.4.4.3. Role of inflammasome response in myocardial IR injury	53
1.4.5. Endoplasmic reticulum and its regulation	53
1.4.5.1. Role of ER in protein synthesis/folding and calcium regulation	53
1.4.5.2. ER stress and misfolded proteins	55
1.4.5.3. The unfolded protein response	56
1.4.5.4. ER stress-mediated cell death	58
1.4.5.5. ER stress and the UPR in IR injury	60
1.5. Sarcoplasmic reticulum/T-tubule junction	63
1.5.1. Role of the SR-T-tubule junction in cardiac excitation-contraction coupling	63
1.5.2. SR-T-tubule junctional alterations in heart disease	64
1.5.3. Junctophilin-2 and its role in cardiac contractility	65
1.5.3.1. JPH-2 structure, localization and function	65
1.5.3.2. Effect of JPH-2 loss on cardiac contractile function	68
1.5.4. Impairment of excitation-contraction coupling and T-tubule distortion during DXR cardiotoxicity	69
1.5.5. MMP-2 association with T-tubule-SR junction and calcium transient	70
1.6. Thesis overview	71
1.6.1. Rationale	71
1.6.2. Overall hypothesis	72
1.6.3. Thesis objectives	72
1.6.3.1. Staurosporine-induced cleavage of apoptosis-inducing factor in human fibrosarcoma cells is independent of matrix metalloproteinase-2 (Chapter 3)	72

1.6.3.2. Matrix metalloproteinase-2 proteolyzes mitofusin-2 and impairs mitochondrial function during myocardial ischemia-reperfusion injury (Chapter 4)	73
1.6.3.3. Matrix metalloproteinase-2 inhibition attenuates ER stress-mediated cell death during myocardial ischemia-reperfusion injury by preserving IRE1 α (Chapter 5)	73
1.6.3.4. Junctophilin-2 proteolysis and T-tubule remodeling are consequences of matrix metalloproteinase-2 activation during doxorubicin-induced cardiotoxicity (Chapter 6)	74
CHAPTER II. GENERAL METHODS	75
2.1. Animals	76
2.2. Isolated heart perfusion	76
2.3. Preparation of cellular or tissue extracts and subcellular fractionation	79
2.4. Measuring protein concentration	80
2.5. Gelatin zymography	80
2.6. Immunoblotting	82
2.7. Co-immunoprecipitation	83
2.8. RNA isolation and qPCR	84
CHAPTER III. Staurosporine-Induced Cleavage of Apoptosis-Inducing Factor in Human Fibrosarcoma Cells Is Independent of Matrix Metalloproteinase-2	85
3.1. Introduction	87
3.2. Methods	88
3.2.1. Cell experiments	88
3.2.2. MMP-2 knockdown using siRNA	89
3.2.3. Subcellular fractionation	89
3.2.4. Cytotoxicity determination	90
3.2.5. Gelatin zymography	90
3.2.6. Immunoblotting	90

3.2.7. Determination of the ability of MMP inhibitors to penetrate cells at an effective concentration	91
3.2.8. <i>In silico</i> predicted cleavage sites of AIF by different proteases	91
3.2.9. Statistics	92
3.3. Results	92
3.3.1. STS induces activation of MMP-2 in HT1080 cells before induction of necrosis	92
3.3.2. STS induces the release of 60 and 45 kDa AIF fragments into the cytosol	92
3.3.3. STS-induced cleavage of AIF is independent of MMP-2 or calpain activities	93
3.3.4. <i>In silico</i> prediction of possible proteases that mediate AIF cleavage	94
3.4. Discussion	107
CHAPTER IV. Matrix Metalloproteinase-2 Proteolyzes Mitofusin-2 and Impairs Mitochondrial Function During Myocardial Ischemia-Reperfusion Injury	111
4.1. Introduction	114
4.2. Methods	117
4.2.1. Isolated heart perfusion	117
4.2.2. Preparation of ventricular extracts	117
4.2.3. Measurement of MMP-2 activity	118
4.2.4. Immunoblotting	118
4.2.5. Co-immunoprecipitation	118
4.2.6. qPCR	119
4.2.7. Mitochondrial respiration	120
4.2.8. Infarct size measurement	121
4.2.9. LDH release measurement	122
4.2.10. <i>In vitro</i> proteolysis of Mfn-2 by MMP-2	122
4.2.11. <i>In silico</i> analysis of Mfn-2 cleavage by MMP-2	123
4.2.12. 3D crystal structure analysis	123

4.2.13. Statistics	124
4.3. Results	124
4.3.1. MMP-2 preferring inhibitors improve the recovery of contractile function after IR injury	124
4.3.2. MMP-2 preferring inhibitors prevent impaired mitochondrial respiration in IR injury	124
4.3.3. MMP-2 is activated during myocardial IR injury	125
4.3.4. Inflammasome response is attenuated by MMP-2 preferring inhibitors	126
4.3.5. Mitochondrial Mfn-2 level is diminished after IR injury and preserved by MMP-2 preferring inhibitors	126
4.3.6. Mfn-2 is proteolyzed by MMP-2	127
4.3.7. MMP-2 preferring inhibitors attenuate IR-induced myocardial infarction	128
4.4. Discussion	144
CHAPTER V. MMP-2 Inhibition Attenuates ER Stress-Mediated Cell Death During Myocardial Ischemia-Reperfusion Injury by Preserving IRE1α	151
5.1. Introduction	154
5.2. Methods	156
5.2.1. Isolated heart perfusion	156
5.2.2. Preparation of ventricular extracts	157
5.2.3. Immunoblotting	157
5.2.4. Co-immunoprecipitation	157
5.2.5. qPCR	158
5.2.6. <i>In vitro</i> proteolysis of IRE1 α by MMP-2	158
5.2.7. <i>In silico</i> analysis of IRE1 α cleavage by MMP-2	159
5.2.8. 3D crystal structure analysis	159
5.2.9. Measurement of caspase activity	159
5.2.10. Thioflavin T binding assay	160

5.2.11. Statistics	161
5.3. Results	161
5.3.1. MMP-2 preferring inhibitors protect against IR-induced cardiac contractile dysfunction	161
5.3.2. MMP-2 is not involved in the induction of ER stress response during IR injury	162
5.3.3. MMP-2 preferring inhibitors preserve IRE1 α protein level after IR injury	162
5.3.4. MMP-2 preferring inhibitors attenuate ER stress-mediated apoptosis during IR injury	164
5.3.5. IRE1 α is proteolyzed by MMP-2	164
5.3.6. MMP-2 preferring inhibitors preserve IRE1 α during ischemia prior to progression into myocardial cell death	165
5.4. Discussion	181
CHAPTER VI. Junctophilin-2 Proteolysis and T-Tubule Remodeling Are Consequences of Matrix Metalloproteinase-2 Activation During Doxorubicin-Induced Cardiotoxicity	188
6.1. Introduction	191
6.2. Methods	193
6.2.1. Induction of DXR cardiotoxicity	193
6.2.2. Echocardiography	194
6.2.3. Preparation of ventricular extracts and N-deglycosylation of glycoproteins	194
6.2.4. Isolation and cultivation of neonatal rat ventricular cardiomyocytes	195
6.2.5. Cytotoxicity determination	196
6.2.6. Measurement of cytosolic calcium using fluorescent microscopy	196
6.2.7. Immunoblotting	197
6.2.8. Transmission electron microscopy	197

6.2.9. <i>In silico</i> analysis of JPH-2 cleavage by MMP-2	198
6.2.10. 3D crystal structure analysis	198
6.2.11. Statistics	199
6.3. Results	199
6.3.1. MMP inhibitors attenuate DXR-induced systolic and diastolic dysfunction	199
6.3.2. MMP inhibitors prevent the cleavage of JPH-2 during DXR-induced cardiotoxicity	201
6.3.3. MMP-2 favors the cleavage of JPH-2 at the joining region between its MORN repeats	201
6.3.4. JPH-2 is N-glycosylated	202
6.3.5. MMP inhibitors preserve T-tubule shape and size and mitochondria size in hearts from DXR-treated mice	203
6.3.6. MMP inhibition attenuates DXR-induced reduction in JPH-2 and calcium transients in neonatal rat ventricular cardiomyocytes	203
6.4. Discussion	212
CHAPTER VII. CONCLUSIONS	219
7.1. Conclusions	220
7.2. Limitations	225
7.2.1. Limitations of Chapter 3	225
7.2.2. Limitations of Chapter 4	226
7.2.3. Limitations of Chapter 5	228
7.2.4. Limitations of Chapter 6	229
7.3. Future directions	231
REFERENCES	234
APPENDIX	281
A.1. Introduction	282

A.2. Methods	283
A.2.1. Isolated heart perfusion	283
A.2.2. Preparation of ventricular extracts	283
A.2.3. Immunoblotting	284
A.2.4. Statistics	284
A.3. Results	284
A.3.1. Hearts subjected to shorter ischemia showed improved recovery of cardiac contractile function	284
A.3.2. IR-mediated reduction in mitochondrial Mfn-2 level occurs during early reperfusion and with shorter ischemia	285
A.3.3. Changes in mitochondrial Drp-1 showed a different pattern than Mfn-2	285
A.3.4. MMP-2 inhibition preserves mitochondrial and cytosolic Drp-1 levels during IR injury	286
A.3.5. IR induces a reduction in mitochondrial parkin, but not PINK-1	286
A.4. Discussion	291

LIST OF TABLES

Table 1.1.	Summary of known MMP-2 intracellular locales and identified substrates in different cell types	16
Table 2.1.	Gelatin zymography 8% separating gel	81
Table 2.2.	Gelatin zymography stacking gel	81
Table 3.1.	<i>In silico</i> predicted cleavage sites of human apoptosis-inducing factor (AIF) by different intracellular proteases listed in alphabetical order, according to Procleave	102
Table 4.1.	Primer sequences used for qPCR in Chapter 4	119
Table 5.1.	Primer sequences used for qPCR in Chapter 5	158
Table 6.1.	Cardiac function and morphology in control and doxorubicin (DXR)-treated mice with or without doxycycline (Doxy) or ONO-4817 (ONO) following 28 days of treatment	200

LIST OF FIGURES

Figure 1.1.	Structural domains of MMP-2 isoforms	5
Figure 1.2.	Mechanisms of intracellular localization of MMP-2	8
Figure 1.3.	Diverse mechanisms of intracellular and extracellular MMP-2 activation	11
Figure 1.4.	Intracellular locales and a partial overview of identified substrates of MMP-2	17
Figure 1.5.	Role of intracellular MMP-2 in selected pathological conditions	23
Figure 1.6.	Pathophysiological changes during myocardial ischemia-reperfusion injury	26
Figure 1.7.	Mechanisms of mitochondrial quality control	43
Figure 1.8.	The mechanism of oxidative phosphorylation	48
Figure 1.9.	Adaptive and maladaptive signalling pathways in the unfolded protein response (UPR)	62
Figure 1.10.	Mechanism of cardiac excitation-contraction coupling	67
Figure 2.1.	Schematic diagram of the experimental protocol of ischemia-reperfusion (IR) injury and the groups of isolated perfused mouse hearts	78
Figure 3.1.	Staurosporine (STS) induces activation of MMP-2 in HT1080 cells	95
Figure 3.2.	Effect of MMP-2 or calpain inhibitors on staurosporine (STS)-induced cytotoxicity in HT1080 cells	96
Figure 3.3.	Staurosporine (STS) induces the cytosolic release and cleavage of apoptosis-inducing factor (AIF)	97
Figure 3.4.	Changes in MMP-2 activity in HT1080 cell lysates by MMP-2 preferring inhibitors	98

Figure 3.5.	Effect of MMP-2 preferring inhibitors on staurosporine (STS)-induced apoptosis-inducing factor (AIF) cleavage	99
Figure 3.6.	Effect of MMP-2 knockdown on staurosporine (STS)-induced apoptosis-inducing factor (AIF) cleavage	100
Figure 3.7.	Effect of calpain inhibitors on staurosporine (STS)-induced apoptosis-inducing factor (AIF) cleavage	101
Figure 4.1.	Hearts perfused with MMP-2 preferring inhibitors showed improved post-ischemic contractile function	129
Figure 4.2.	MMP-2 preferring inhibitors have no effect on post-ischemic heart rate during IR injury	130
Figure 4.3.	MMP-2 preferring inhibitors have no effect on cardiac contractile function under aerobic conditions	131
Figure 4.4.	MMP-2 preferring inhibitors improve mitochondrial respiration in cardiac muscle fibers isolated from IR mouse hearts	132
Figure 4.5.	MMP-2 preferring inhibitors have no effect on mitochondrial respiration in cardiac muscle fibers isolated from aerobically perfused mouse hearts	133
Figure 4.6.	MMP-2 is activated in response to myocardial IR injury	134
Figure 4.7.	Mitochondrial or cytosolic MMP-2 protein levels are not affected by IR injury	135
Figure 4.8.	MMP-2 isoform expression in mouse hearts subjected to IR injury	136
Figure 4.9.	MMP-2 preferring inhibitors attenuate IR injury-induced increase in NLRP3 and active interleukin-1 β (IL-1 β) levels in the cytosolic fraction	137
Figure 4.10.	MMP-2 preferring inhibitors have no effect on inflammasome response in aerobically perfused hearts	138

Figure 4.11.	MMP-2 preferring inhibitors attenuate IR injury-induced reduction in Mfn-2 level in the mitochondria-enriched fraction	139
Figure 4.12.	MMP-2 preferring inhibitors have no effect on Mfn-2 levels in the mitochondria-enriched fractions prepared from aerobically perfused hearts	140
Figure 4.13.	Mfn-2 is proteolyzed by MMP-2	141
Figure 4.14.	Long exposure of immunoblot in Figure 4.13A	142
Figure 4.15.	MMP-2 preferring inhibitors attenuate IR-induced myocardial infarction	143
Figure 4.16.	Schematic diagram showing the potential role of MMP-2 in mitochondrial dysfunction and inflammasome activation during myocardial ischemia-reperfusion (IR) injury	150
Figure 5.1.	MMP-2 preferring inhibitors improve post-ischemic contractile function in isolated mouse hearts subjected to IR injury	167
Figure 5.2.	Myocardial IR injury is associated with ER stress response	168
Figure 5.3.	MMP-2 preferring inhibitors prevent IRE1 α loss during IR injury	169
Figure 5.4.	MMP-2 preferring inhibitors have no effect on ER stress or UPR markers in aerobically perfused hearts	170
Figure 5.5.	Changes in XBP1s in hearts subjected to IR injury.	171
Figure 5.6.	IRE1 α and PERK protein levels correlate with cardiac mechanical function	172
Figure 5.7.	MMP-2 preferring inhibitors attenuate ER stress-mediated apoptosis during IR injury	173
Figure 5.8.	MMP-2 preferring inhibitors attenuate the IR-induced increase in caspases-3 and -9 cleavage	174

Figure 5.9.	MMP-2 preferring inhibitors have no effect on CHOP or Bax in aerobically perfused hearts	175
Figure 5.10.	IRE1 α is proteolyzed by MMP-2	176
Figure 5.11.	GRP78 is upregulated during myocardial ischemia	177
Figure 5.12.	MMP-2 preferring inhibitors prevent IRE1 α loss during myocardial ischemia	178
Figure 5.13.	ER stress-mediated apoptosis is not developed during myocardial ischemia	179
Figure 5.14.	Changes in caspases-3 and -9 protein levels during myocardial ischemia	180
Figure 5.15.	Schematic diagram showing the potential role of MMP-2 in ER stress-mediated cell death during myocardial IR injury	187
Figure 6.1.	MMP inhibitors attenuate JPH-2 cleavage in hearts from DXR-treated mice	205
Figure 6.2.	The levels of JPH-2 63 and 25 kDa fragments in hearts from DXR-treated mice are negatively correlated to cardiac functional parameters	206
Figure 6.3.	<i>In silico</i> analysis of the predicted cleavage sites within JPH-2 by MMP-2	207
Figure 6.4.	JPH-2 is N-glycosylated in mouse hearts	208
Figure 6.5.	MMP inhibitors prevent T-tubule and mitochondria derangements in cardiac myocytes in hearts from DXR-treated mice	209
Figure 6.6.	MMP-2 inhibition attenuates JPH-2 cleavage in DXR-treated neonatal rat ventricular cardiomyocytes	210
Figure 6.7.	MMP-2 inhibition improves cytosolic calcium transients in DXR-treated neonatal rat ventricular cardiomyocytes	211

Figure 6.8.	Schematic representation of the role of MMP-2 in JPH-2 cleavage during DXR-induced cardiotoxicity	218
Figure A.1.	Cardiac contractile function in hearts subjected to IR injury with different durations of ischemia	287
Figure A.2.	Changes in mitochondrial Mfn-2 and Drp-1 levels in hearts subjected to different durations of ischemia and/or reperfusion	288
Figure A.3.	MMP-2 preferring inhibitors attenuate IR injury-induced reduction in Drp-1 level	289
Figure A.4.	MMP-2 preferring inhibitors attenuate IR injury-induced reduction in mitochondrial parkin	290

LIST OF ABBREVIATIONS

ADP	Adenosine diphosphate
AFC	7-Amino-4-(trifluoromethyl)coumarin
AIF	Apoptosis-inducing factor
Akt	Protein kinase B
AMC	7-Amino-4-methylcoumarin
AMPK α	AMP-activated protein kinase- α
ANOVA	Analysis of variance
ASC	Apoptosis-associated speck-like protein containing caspase-recruitment domain
ASK1	Apoptosis signal-regulating kinase 1
ATF	Activating transcription factor
ATP	Adenosine triphosphate
B2M	Beta-2-microglobulin
Bak	Bcl-2 homologous antagonist/killer
Bax	Bcl-2-associated X protein
BCA	Bicinchoninic acid
Bcl-2	B-cell lymphoma-2
Bcl-XL	B-cell lymphoma-extra large
BiP	Binding immunoglobulin protein
BSA	Bovine serum albumin
cDNA	Complementary DNA
CHOP	C/EBP homologous protein

CIB1	Calcium and integrin binding protein 1
C _t	Cycle threshold
DAMPs	Danger-associated molecular pattern
DMEM	Dulbecco's Modified Eagle Medium
DMSO	Dimethyl sulfoxide
DNA	Deoxyribonucleic acid
Drp-1	Dynamin-related protein-1
DXR	Doxorubicin
eIF2 α	Eukaryotic translation initiator factor 2 α
ER	Endoplasmic reticulum
ERK	Extracellular signal regulated kinase
FAD	Flavin adenine dinucleotide
FADH ₂	Reduced flavin adenine dinucleotide
FBS	Fetal bovine serum
FCCP	Carbonyl cyanide p-trifluoro-methoxyphenyl hydrazone
GAPDH	Glyceraldehyde 3-phosphate dehydrogenase
GRP75	75 kDa glucose-related protein
GRP78	78 kDa glucose-related protein
HR	Heart rate
IL	Interleukin
IP3R	Inositol 1,4,5-triphosphate receptor
IR	Ischemia-reperfusion
IRE1 α	Inositol-requiring enzyme 1 α

JNK	c-Jun N-terminal kinase
JPH-2	Junctophilin-2
LDH	Lactate dehydrogenase
LVDP	Left ventricular developed pressure
MAM	Mitochondrial-ER-associated membrane
MAPK	Mitogen-activated protein kinase
Mfn	Mitofusin
Miro	Mitochondrial Rho GTPase proteins
MMP	Matrix metalloproteinase
MORN	Membrane occupation and recognition nexus
mPTP	Mitochondrial permeability transition pore
mRNA	Messenger ribonucleic acid
mtDNA	Mitochondrial DNA
NAD	Nicotinamide adenine dinucleotide
NADH	Reduced nicotinamide adenine dinucleotide
NADPH	Nicotinamide adenine dinucleotide phosphate
NF κ B	Nuclear factor kappa B
NLR	Nucleotide-binding oligomerization domain (NOD)-like receptor
NLRP3	NLR family pyrin domain-containing protein 3
NTT	N-terminal truncated
OCR	Oxygen consumption rate
OPA-1	Optical atrophy-1
PAMPs	Pathogen-associated molecular pattern

PARP-1	Poly ADP ribose polymerase-1
PBS	Phosphate buffered saline
PDB	Protein data bank
PDI	Protein disulfide isomerase
PERK	Protein kinase R-like ER kinase
PGC1 α	PPAR γ coactivator 1 α
PINK1	PTEN-induced kinase-1
PPAR γ	Peroxisome proliferator-activated receptor γ
PRR	Pattern-recognition receptor
PVDF	Polyvinylidene difluoride
qPCR	Quantitative real-time polymerase chain reaction
RCR	Respiratory control ratio
RFU	Relative fluorescence unit
RIPA	Radioimmunoprecipitation assay
RONS	Reactive oxygen-nitrogen species
rRNA	Ribosomal ribonucleic acid
SAVES	Structural analysis and verification server
SDS	Sodium dodecyl sulfate
SEM	Standard error of the mean
SERCA2a	Sarcoplasmic/endoplasmic reticulum Ca ²⁺ ATPase 2a
siRNA	Small interfering RNA
SR	Sarcoplasmic reticulum
STS	Staurosporine

TBS-T	Tris-buffered saline with Tween
ThT	Thioflavin T
TIMPs	Tissue inhibitors of metalloproteinases
TnI	Troponin I
UPR	Unfolded protein response
VDAC	Voltage-dependent anion channel
XBP1	X box-binding protein 1
XBP1s	Spliced XBP1

Chapter I

General Introduction

A part of this chapter has been published as a review article:

Wesam Bassiouni, Mohammad A.M Ali, Richard Schulz (2021). Multifunctional intracellular matrix metalloproteinases: implications in disease. *FEBS J.* 288:7162-82.

1.1. Matrix metalloproteinase-2

1.1.1. The history of matrix metalloproteinases

Matrix metalloproteinases (MMPs) are a family of multifunctional zinc-dependent endopeptidases that were first discovered in 1962 by Gross and Lapiere who identified the presence of collagen-degrading activity in amphibian tissue that was found later to be the collagenase activity of MMP-1 [1]. For decades, MMPs were known as secreted proteases that target and cleave a variety of extracellular matrix proteins during different physiological conditions such as angiogenesis, cell differentiation and wound healing as well as pathological conditions such as inflammation, cancer metastasis, tumor growth, atherosclerosis and myocardial infarction [2-7].

Almost 20 years ago, the Schulz group identified the first intracellular substrate of a ubiquitous MMP isoform “MMP-2”, also known as gelatinase-A or 72-kDa Type IV collagenase, in the heart. They found that, during myocardial ischemia-reperfusion (IR) injury, MMP-2 induces the cleavage of the cardiac sarcomeric protein, troponin I (TnI), resulting in cardiac contractile dysfunction. [8, 9]. At this time, it was unknown how MMP-2 remains intracellular given its signal sequence that targets it to be secreted outside the cell. Currently there are 28 MMP isoforms identified in vertebrates of which 24 are found in humans [10, 11]. Beside MMP-2, several other MMPs were found to also function intracellularly in diverse cell types including MMP-1, -3, -7, -8, -9, -10, -11, -12, -14, -23 and -26 [12-17].

MMP biology is now greatly expanding as new functions of MMPs are discovered inside cells. Understanding the biological functions of MMPs inside the cell is crucial not only towards understanding their physiological roles but also for discovering new therapeutic targets for the treatment of different pathologies.

1.1.2. Classification of MMPs

MMPs can be classified under different schemes. One method of their classification is based on the difference in their structural domains according to which they are classified into: classical structured MMPs, MMP-1, -3, -8, -10, -12, -13, and -19; furin-activated MMPs, MMP-11, -21 and -28 [18]; Cys/IgG-like MMP, MMP-23; transmembrane MMPs, MMP-14, -16 and -24; glycosylphosphatidylinositol-anchored MMPs, MMP-17 and -25 and the gelatin-binding MMPs, MMP-2 and -9 [19].

Another classification scheme is based on their substrates and subcellular localization. Collagenases are MMPs which degrade collagen. These include MMP-1, -8, -13, -18 as well as MMP-14 which cleaves fibrillar collagen [20]. Specific forms of MMP-2 and -9 are also thought to have some collagenolytic activity [19, 21]. Gelatinases are MMPs which degrade gelatin (denatured collagen) and type IV collagen including MMP-2 and -9 [22]. Stromelysins include MMP-3, -10 and -11 and are capable of degrading extracellular matrix proteins other than fibrillar collagen [23]. Membrane type MMPs, as stated earlier, are membrane-anchored and have a furin recognition site. They include MMP-14, -15, -16, -17, -23, -24 and -25 [20].

Some other MMPs have different substrates and, in this regard, are classified into different types, particularly, the matrilysins (MMP-7 and -26) [24], enamelysin (MMP-20) [25] and metalloelastase (MMP-12) [26]. However, some MMPs cannot be included into any of these classes and include MMP-19, -21, -27 and -28.

In the next sections, I will focus on MMP-2, the most important and ubiquitous intracellular MMP isoform, and discuss its structure, localization, mechanisms of intracellular activation and pathophysiological role in diseases.

1.1.3. MMP-2 structural domains

Like most of the other MMPs, the structure of MMP-2 contains three domains; a pro-peptide, catalytic and hemopexin-like C-terminal domain which is linked to the catalytic domain by a flexible hinge region [18] (**Figure 1.1**). The catalytic domain contains a zinc ion that confers its proteolytic activity as it binds through coordinate bonds to three histidine residues forming the active site that binds to MMP-2 substrates. The pro-peptide domain contains a cysteine residue (part of the cysteine switch, see below) that interacts with the catalytic zinc, preventing the enzyme from binding to the substrate, and subsequently keeping the MMP inactive [19]. The hemopexin-like C-terminal domain contains the site of interaction with the tissue inhibitors of metalloproteinases (TIMPs) and is also essential for MMP subcellular localization and protein specificity [27]. MMP-2 has three fibronectin type II repeats incorporated before the zinc-binding sequence, which allow its binding to gelatin and type IV collagen [19].

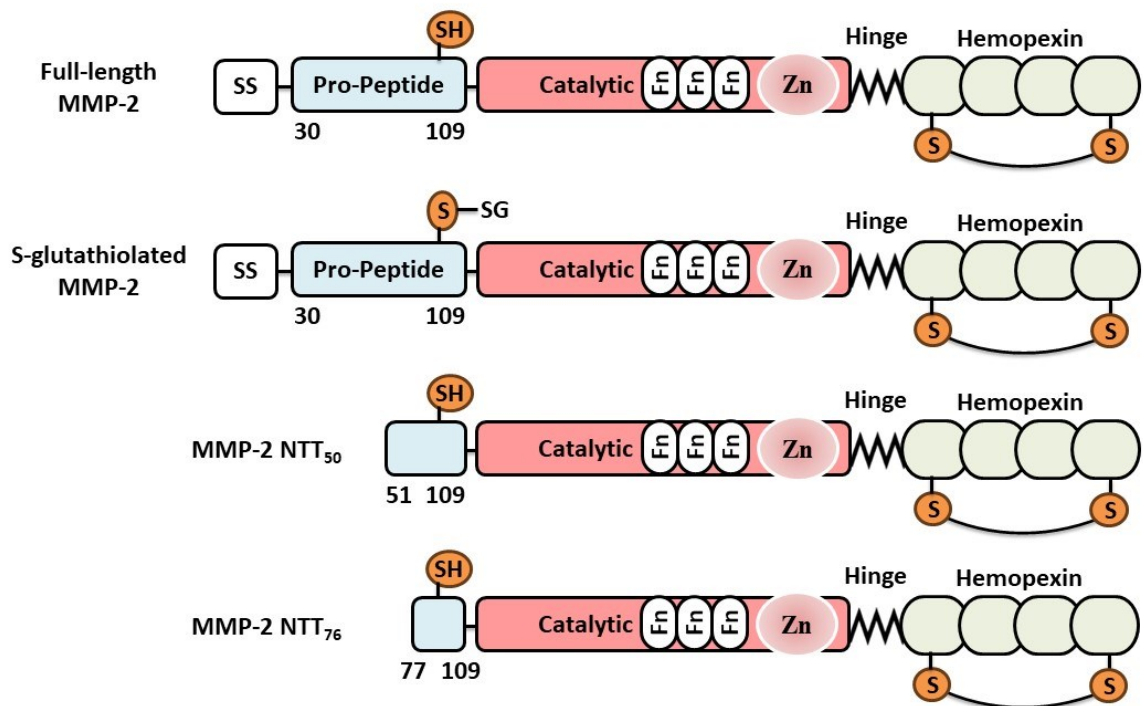


Figure 1.1. Structural domains of MMP-2 isoforms. Full length MMP-2 is composed of three domains; a pro-peptide, catalytic and hemopexin-like C-terminal domain which is linked to the catalytic domain by a flexible hinge region. The catalytic domain contains a zinc ion that confers its proteolytic activity. The pro-peptide domain contains a cysteine residue that interacts through its sulfhydryl (-SH) residue with the catalytic zinc, preventing the enzyme from binding to the substrate and keeping it inactive. It also has fibronectin type II repeats incorporated before the zinc-binding sequence and an N-terminal signal sequence that targets it to the secretory pathway. S-glutathiolated MMP-2 has the cysteine residue in the pro-peptide domain bound to glutathione which prevents it from binding to the catalytic zinc resulting in its activation. MMP-2_{NTT50} and MMP-2_{NTT76} lack the first 50 or 76 amino acids respectively, including the signal sequence and are constitutively active. Fn, fibronectin; G, glutathione; MMP-2, matrix metalloproteinase-2; NTT, N-terminal truncated; SH, sulfhydryl; SS, signal sequence; Zn, zinc.

1.1.4. Mechanisms of intracellular localization of MMP-2

Despite not being fully understood, different mechanisms by which MMP-2 is localized intracellularly, and to specific sub-organelles, are summarized below and depicted in **Figure 1.2**.

1.1.4.1. Inefficient secretion

For newly synthesized MMP to be secreted, its N-terminal signal sequence targets it to the endoplasmic reticulum (ER) for subsequent secretion outside the cell. The signal sequence is ~20-29 amino acids found on most MMPs which are secreted extracellularly [17, 28, 29]. The Schulz group described at least two mechanisms by which MMP-2 can reside inside the cell. MMP-2 has an inefficient secretory signal sequence which results in about 50% of nascent protein escaping the secretory pathway and remaining in the cytosol (**Figure 1.2 A**) [29]. In addition, there is a splice variant which lacks the first 50 amino acid residues including the signal sequence (N-terminal truncated MMP-2 “MMP-2_{NTT50}”), which is expressed in neonatal and adult human cardiomyocytes. MMP-2_{NTT50} is elevated in response to oxidative stress and enhances the degradation of intracellular MMP-2 substrates [29]. In addition, another intracellular variant lacking the first 76 amino acids (MMP-2_{NTT76}) is transcriptionally induced by oxidative stress as part of the innate immune response (**Figures 1.1 and 1.2 A**) [30].

1.1.4.2. Post-secretion re-entry

MMP-2, after being secreted, can undergo endocytosis by binding to the low-density lipoprotein related protein-1 receptor allowing it to re-enter the cell [31]. Caveolin-1 and -3 scaffolding domains are suggested to bind MMP-2 so that endocytic caveolae can bring MMP-2 to the endosomes (**Figure 1.2 B**) [32, 33].

1.1.4.3. Organelle localization signals

MMP-2 can be localized to specific compartments inside the cell. MMP-2 possesses a nuclear localization sequence at its C-terminus that allows it to be localized and targeted to the nucleus (**Figure 1.2 C**) [34, 35]. MMP-2 may also undergo post-translational modifications that could explain its nuclear localization via the Golgi-ER-nucleus route [36]. However, in a study that used an agent disrupting Golgi endosomal structure, nuclear localization of MMP-2 was not affected, suggesting that its localization to the nucleus is stable and independent from this pathway [37]. The mechanism of MMP-2 and MMP-2_{NTT76} localization to the mitochondria and the mitochondrial-ER associated membrane (MAM) is still unclear.

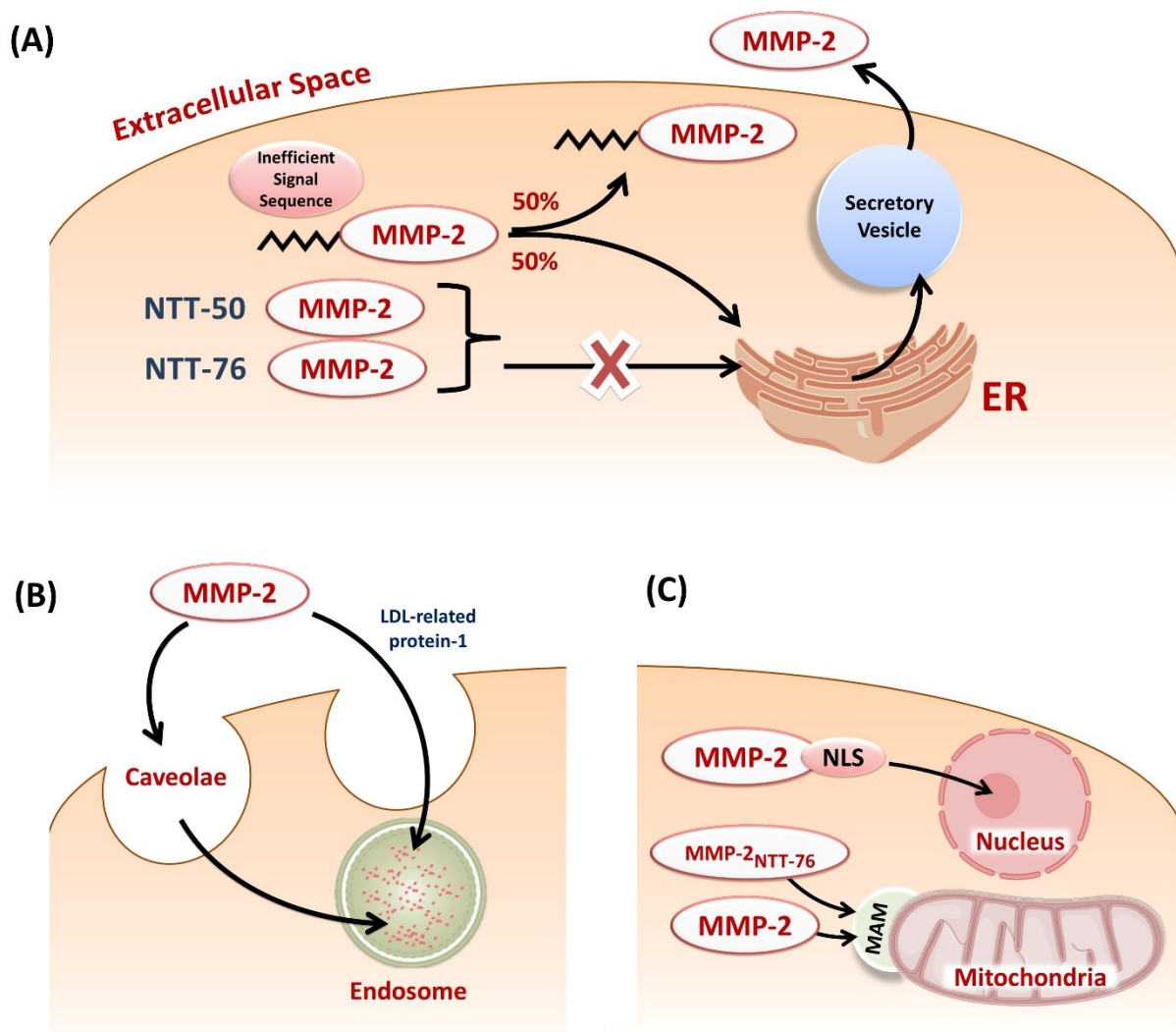


Figure 1.2. Mechanisms of intracellular localization of MMP-2. (A) Inefficient secretion: MMP-2 has an inefficient signal sequence that allows approximately half of it to remain inside the cell. MMP-2_{NTT50} and _{NTT76} lack the signal sequence and therefore remain inside the cell. (B) Post-secretion re-entry: MMP-2 re-enters the cell after being secreted through endocytosis by binding to LDL-related protein-1 or caveolin-1 and -3. (C) Organelle localization signals: MMP-2 possesses a nuclear localization sequence that targets it to the nucleus. MMP-2 and MMP-2_{NTT76} are localized to mitochondria and the mitochondrial associated membrane by an unknown mechanism. ER, endoplasmic reticulum; LDL, low density lipoprotein; MAM, mitochondrial-ER-associated membrane; MMP, matrix metalloproteinase; NLS, nuclear localization sequence; NTT, N-terminal truncated (*Figure was created using BioRender*).

1.1.5. Mechanisms of MMP-2 activation and its regulation

Generally, under basal conditions, the sulfhydryl group of the cysteine residue at the C-terminus of the MMP pro-peptide domain binds to the catalytic zinc in the active site, acting as an inactivating ligand to keep the enzyme inactive. In order for MMPs to be active proteases, this interaction between the cysteine residue and the catalytic zinc must be disrupted where the sulfhydryl group is replaced by water to allow substrate access to the catalytic site. This is known as “the cysteine switch” [19, 38, 39]. Extracellular activation of MMP-2 occurs via proteolytic removal of the pro-peptide domain by the action of MMP-14 and its interaction with TIMP-2 at the cell surface [40]. However, intracellular activation of MMP-2 occurs by a different mechanism that does not involve proteolytic cleavage. This occurs by post-translational modifications of the cysteine switch, including peroxynitrite-induced S-glutathiolation in response to oxidative or nitrosative stress, that results in exposing the active site without the removal of the pro-peptide domain. Generation of reactive oxygen-nitrogen species (RONS) induces oxidation of the sulfhydryl moiety within the cysteine switch preventing its interaction with the catalytic zinc (**Figure 1.3**) [41-43].

Peroxyntirite is the reaction product of nitric oxide and superoxide and itself is reported to induce MMP-2 activation in perfused rat hearts [44]. It peaks in cardiac cells during IR injury in the first 30 seconds of reperfusion [45], which in turn induces MMP-2 activation within 2-5 minutes of reperfusion [8]. Pro-inflammatory cytokines also activate MMP-2 intracellularly in myocardium by enhancing peroxynitrite biosynthesis in the myocardium [46, 47]. Inhibition of MMP activity reduces oxidative stress-induced contractile dysfunction of the heart and prevents cleavage of several sarcomeric proteins [48]. In vascular smooth muscle, S-glutathiolation of MMP-2 occurs in response to endotoxemia [42].

Post-translational modification by phosphorylation also affects MMP-2 activity, as its dephosphorylation by alkaline phosphatase increases its activity, while phosphorylation of MMP-2 by protein kinase C attenuates its activity. Phosphorylation of MMP-2 occurs at threonine 250, tyrosine 271 and serines 32, 160 and 365 [49].

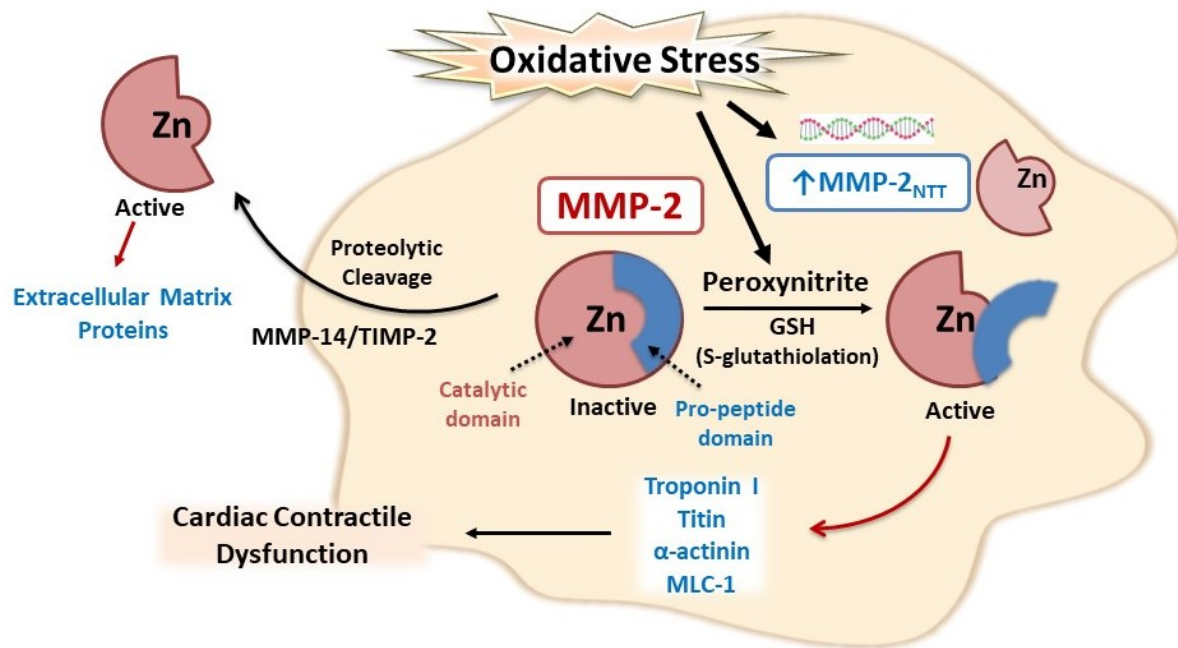


Figure 1.3. Diverse mechanisms of intracellular and extracellular MMP-2 activation. Extracellular: MMP-2 is activated extracellularly via proteolytic removal of the pro-peptide domain by the action of MMP-14 and its interaction with TIMP-2 at the cell surface. Intracellular: in response to oxidative stress, reactive oxygen-nitrogen species activate MMP-2 by S-glutathiolation of the cysteine switch resulting in the exposure of its catalytic site without proteolytic removal of the pro-peptide domain. Oxidative stress also transcriptionally induces MMP-2_{NTT} which is constitutively active. Upon activation, MMP-2 targets and cleaves different cardiac sarcomeric proteins resulting in cardiac contractile dysfunction. GSH, glutathione; MMP-2, matrix metalloproteinase-2; MLC-1, myosin light chain-1; NTT, N-terminal truncated; TIMP, tissue inhibitor of metalloproteinase; Zn, zinc (*Figure was created using BioRender*).

1.1.6. Intracellular locales and substrates of MMP-2

1.1.6.1. Cytosol

MMP-2 is one of the most abundant proteases in cardiomyocytes that can be directly activated in the cytosol as a result of oxidative stress. Its cytosolic activity can be regulated by S-glutathiolation, phosphorylation as well as by the action of intracellular TIMPs, as TIMP-4 is also found to be located in the sarcomere of cardiomyocytes [43, 49-51]. One of the identified cytosolic substrates of MMP-2 is glycogen synthase kinase-3 β which regulates several metabolic pathways in the cell. MMP-2 cleaves its N-terminal auto-inhibitory domain resulting in enhanced glycogen synthase kinase-3 β activity which may also contribute to cardiac injury in response to oxidative damage [52]. Likewise, MMP-2 is found in the cytoplasm of human platelets and contributes to the process of platelet activation and regulation of hemostasis [53-56]. Intracellular MMP-2, for example, targets and proteolyzes the cytoskeletal protein, talin, which in turn activates the fibrinogen receptor, glycoprotein IIb/IIIa, the final step required for platelet activation [57].

1.1.6.2. Muscle sarcomere and cytoskeleton

The sarcomere is the functional contractile unit of cardiac and skeletal muscles which effects muscle contraction. When the Schulz lab first discovered that MMP-2 has intracellular proteolytic effects, they were focused on cardiac muscle and found that many initially characterized targets of MMP-2 are associated with the sarcomere and cytoskeleton of cardiomyocytes (see [10, 58] for reviews). Analysis by confocal immunohistochemistry [59] and immunogold electron microscopy [60] showed that MMP-2 colocalizes with titin primarily at the Z-disk region of the sarcomere of cardiomyocytes. Upon IR injury, MMP-2 induced titin cleavage in rat and human hearts [59]. Furthermore, MMP-2 is reported to target several other sarcomeric

and cytoskeletal proteins such as TnI, α -actinin and myosin light chain-1 in similar conditions characterized by oxidative stress damage to the heart [9, 50, 59, 61]. Upon activation, MMP-2-mediated degradation of these sarcomeric/cytoskeletal proteins resulted in cardiac contractile dysfunction and, importantly, inhibition of MMP-2 preserved the contractile function of the heart [9].

1.1.6.3. Caveolae

Caveolae are plasma membrane invaginations that regulate several cellular functions such as endocytosis and various cell signalling pathways [62]. Caveolin-1 and -3 scaffolding domains bind MMP-2 and may bring it to the endosomes. MMP-2 is associated with caveolins in cardiomyocytes, fibroblasts and endothelial cells. In cardiac cells, caveolin-1 negatively regulates MMP-2 activity, however, the significance of this regulation is not yet defined [32, 33].

1.1.6.4. Mitochondria, mitochondrial associated membranes and endoplasmic reticulum

MMP-2 is suggested to be one of the negative regulators of myocardial mitochondrial function. In transgenic mice with cardiac-specific expression of full length MMP-2, impaired mitochondrial structure and function, along with decreased mitochondrial respiration and lipid peroxidation, are observed [63]. MMP-2 and MMP-2_{NTT76} are reported to be localized to the intermembranous space of the mitochondria and the MAM and may induce cleavage of different mitochondria-associated proteins [64-66].

Possible mitochondrial targets of MMP-2, that were identified using proteomic analysis in rat cardiomyocytes, may include adenosine triphosphate (ATP) synthase β 1-subunit, cytochrome

c oxidase subunit 5A, electron transfer flavoprotein subunit β , reduced nicotinamide adenine dinucleotide (NADH) dehydrogenase-1 α subcomplex subunit 5 among others [67]. Another substrate for MMP-2_{NTT76} in mitochondria is the inhibitor of kappa B-alpha. When cleaved by MMP-2 in response to oxidative stress, inhibitor of kappa B-alpha releases the pro-inflammatory nuclear factor kappa B (NF κ B) which is translocated to the nucleus, resulting in mitochondrial-nuclear stress observed in innate immune responses [66]. In retinal endothelial cells, both mitochondrial MMP-2 levels and activity are increased in response to hyperglycemia, and this is associated with subsequent decrease in the mitochondrial level of heat shock protein 60 as well as the mitochondrial membrane gap junction protein connexin 43 [68].

Regarding the ER, MMP-2 was recently found in sarcoplasmic reticulum (SR)-enriched microsomes from cardiomyocytes where it induces degradation of sarcoplasmic/endoplasmic reticulum calcium-ATPase 2a (SERCA2a), an essential factor for the coordination of cardiac excitation-contraction coupling [69]. Moreover, calreticulin, an ER-calcium binding chaperone protein, can be proteolyzed by MMP-2, which is predicted to affect mitochondrial-ER communication and cardiac function [65].

Another protein targeted by MMP-2 in cardiomyocytes is junctophilin-2 (JPH-2), a membrane-binding protein that tethers the transverse (T)-tubule to the SR which is required for myocardial excitation-contraction coupling. Cleavage of JPH-2 by MMP-2 during myocardial IR injury results in cardiac contractile dysfunction [70].

1.1.6.5. Nucleus/Nucleolus

The Schulz group was the first to report MMP-2 activity in nuclear extracts from both human heart and rat liver. Immunogold electron microscopy confirmed the nuclear localization of

MMP-2 in rat cardiomyocytes [35]. Nuclear localization of MMP-2 was also reported in pulmonary artery endothelial cells [71]. During cerebral ischemia, MMP-2 targets deoxyribonucleic acid (DNA) repair proteins poly adenosine diphosphate (ADP) ribose polymerase-1 (PARP-1), X-ray repair cross complementing protein-1 and 8-oxoguanine DNA glycosylase-1 and decreases their activity in rat cortical neurons during IR injury [72]. The Schulz group recently detected MMP-2 inside the nucleolus of osteosarcoma cell lines where it promotes ribosomal ribonucleic acid (rRNA) transcription and cell proliferation via, at least in part, cleavage of the N-terminal tail of histone H3 [73].

A summary of the intracellular localizations of MMP-2 and some of its known or putative targets is shown in **Table 1.1** and **Figure 1.4**.

Table 1.1. Summary of known MMP-2 intracellular locales and identified substrates in different cell types

Subcellular location/organelle	Intracellular substrate	Cell	Reference
Cytosol	GSK-3 β	Cardiomyoblast	[52]
	Calponin-1	Smooth muscle	[42]
	Talin	Platelet	[57, 74]
	?	Megakaryocyte	[75]
	?	Fibroblast	[76]
	?	Fibrosarcoma	[49]
	?	HEK 293, Cardiomyocyte	[29]
T-tubule -sarcoplasmic reticulum interface	JPH-2	Cardiomyocyte	[70]
Sarcomere	TnI	Cardiomyocyte	[9]
	Titin		[59]
	MLC-1		[61]
	α -actinin		[50]
Mitochondria	Hsp60	Retinal endothelial	[68]
	CX43		
	I κ B	Cardiomyocyte	[66]
Mitochondrial-associated membrane	Calreticulin	Cardiomyocyte	[65]
Sarcoplasmic reticulum	SERCA2a	Cardiomyocyte	[69]
Caveolae	Caveolin-1	Cardiomyocyte, Fibroblast, Endothelial	[32, 33]
Nucleus	Histone H3	Osteosarcoma	[73]
	8-oxodG	Cerebral neuron	[72]
	PARP-1		
	XRCC-1		
	?	Megakaryocyte	[75]

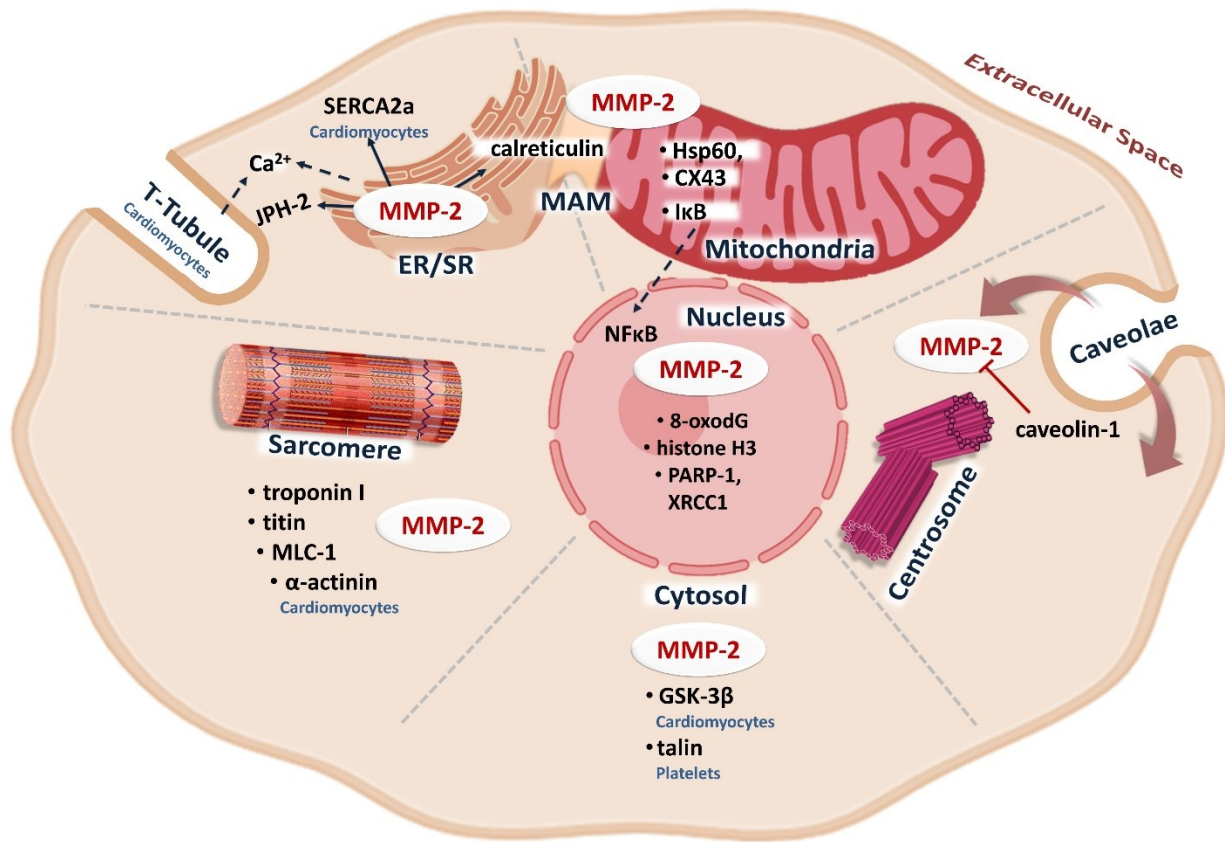


Figure 1.4. Intracellular locales and a partial overview of identified substrates of MMP-2. Schematic representation of the intracellular localization of MMP-2 as well as some of its identified intracellular targets. MMP-2 intracellular targets are depicted in black and the cell or tissue type is in blue. 8-oxodG, 8-oxoguanine DNA glycosylase-1; CX, connexin; ER, endoplasmic reticulum; GSK, glycogen synthase kinase; Hsp, heat shock protein; IκB, inhibitor of kappa B-alpha; JPH, junctophilin; MLC-1, myosin light chain-1; MMP-2, matrix metalloproteinase-2; NFκB, nuclear factor kappa B; PARP, Poly ADP ribose polymerase; SERCA, sarcoplasmic/endoplasmic reticulum calcium ATPase; XRCC, X-ray repair cross complementing protein (Figure was created using BioRender).

1.1.7. MMP-2 inhibitors

1.1.7.1. Endogenous MMP-2 inhibitors

Several endogenous inhibitors of MMPs are known to regulate the function of MMPs both inside and outside the cell. TIMPs are endogenous regulatory proteins that inhibit MMPs activity with four identified members (TIMP-1, -2, -3 and -4). They possess an N-terminal inhibitory domain which interacts with zinc in the catalytic site of MMPs preventing their binding to the target substrates, while the C-terminal domain binds to the MMP hemopexin-like domain to increase the stability of the formed complex [77]. The four TIMPs have little selectivity for a specific MMP, except for TIMP-1 which lacks the ability to inhibit membrane-type MMPs [78]. However, TIMP-2 can play an additional role as it interacts with MMP-14 at the cell surface to activate MMP-2 outside the cell [79, 80]. α 2-Macroglobulin is another MMP inhibitor [81]. When proteolytically cleaved at a specific sequence called the bait region, it undergoes conformational changes that expose its thiol ester group which in turn covalently binds to the MMP and inhibits its activity [82]. α 2-Macroglobulin usually functions when TIMPs are deficient [83]. It eliminates the MMP by targeting the formed complex to endocytosis via a specific cell surface receptor, low density lipoprotein receptor-related protein [84]. β -Amyloid precursor protein is an integral membrane protein that acts as a precursor of β -amyloid peptide [85]. It is also reported to act as an MMP-2 inhibitor, as its secreted portion has a proteinase inhibitory domain in its C-terminus that selectively interacts with the catalytic domain of MMP-2 to inhibit extracellular matrix degradation [86, 87].

1.1.7.2. Synthetic MMP-2 inhibitors

Several synthetic inhibitors of MMPs are also available and were first developed as anticancer drugs [88]. *o*-Phenanthroline, batimastat, marimastat, ilomastat (GM-6001), and PD-166793 were shown to inhibit a wide range of MMPs [89]. Some antimicrobials, particularly tetracyclines, were also shown to exert an MMP inhibitory action. Among the tetracyclines, doxycycline and minocycline are the two most potent MMP inhibitors and their MMP inhibitory effect is independent of their antibacterial effect. Doxycycline inhibits MMP activity at sub-antimicrobial plasma concentration [90, 91]. It was shown to exhibit beneficial effects on the heart in patients with acute myocardial infarction and left ventricular dysfunction [92]. A series of chemically-modified tetracyclines were synthesized and some were found to be devoid of antimicrobial properties but still able to inhibit MMP activity [93]. These inhibitors act as zinc chelators. They bind to zinc in the catalytic site which in turn prevents MMP binding to its substrate [4]. Other more MMP-2 selective synthetic inhibitors include hydroxamates (ONO-4817), carboxylates (BAY12-9566) and sulfonamide-based compounds (ARP-100, ARP-101). The selectivity profile for ONO-4817 in guinea pig joint cartilage is as follows; MMP-12 > -2 > -8 = -13 > -9 > -3 > -7 [94], while for ARP-100, its selectivity profile in human fibrosarcoma cells is as follows; MMP-2 > -9 > -3 > -1 and -7 [95]. Therefore, ARP-100 and ONO-4817 are considered to be MMP-2 preferring inhibitors. To date, doxycycline is the only MMP inhibitor approved for clinical use by the US Food and Drug Administration and by Health Canada. It is used as a sub-antimicrobial dose formulation (20 mg, two times per day) which was shown to have a beneficial effect in patients with chronic periodontal inflammation [96]. It is also used in a sub-antimicrobial dose for treatment of rosacea, a chronic inflammatory skin condition [97].

1.1.8. Role of MMP-2 in pathologies

1.1.8.1. Kidney injury

In acute kidney injury caused by subjecting mice to unilateral renal IR, MMP-2_{NTT76} is found to be highly expressed along with MMP-2 in lesser amount in epithelial cells of proximal renal tubules. This intracellular MMP-2 activity induces mitochondrial permeability transition, loss of defined cristae structure and swelling and rupture of the mitochondria. MMP-2_{NTT76} also triggers an innate immune response and upregulation of pro-inflammatory cytokines which induce inflammatory and necrotic responses in tubular epithelial cells [98].

1.1.8.2. Inflammatory diseases

MMP-2 also plays a significant role in inflammation. Through cleavage of different metabolic regulators such as lipoproteins and lipoprotein receptors, MMP-2 is suggested to modulate intracellular inflammatory pathways and lipid metabolism. MMP-2 deficiency in humans and transgenic mice is reported to induce inflammation and affect cardiac metabolism [99]. This effect is suggested to be mediated by the action of a pro-inflammatory cytokine known as monocyte chemoattractant protein-3 which is normally proteolytically cleaved and inactivated by MMP-2 [100]. A similar effect is shown in the liver where MMP-2 deficiency is reported to induce hepatic dysfunction as a result of the enhanced inflammatory response [101]. On the other hand, cardiac-specific overexpression of MMP-2_{NTT76} induces an innate immune response and enhanced level of pro-inflammatory cytokines, associated with apoptosis and inflammatory cell infiltration of the heart [66].

1.1.8.3. Malignancy

In osteosarcoma cells, nucleolar MMP-2 promotes rRNA transcription and cancer cell proliferation via cleaving the N-terminal tail of histone H3 [73]. Moreover, in ovarian cancer cells, zoledronic acid is reported to suppress tumor growth and angiogenesis via inactivation of an intracellular MMP-2/p38 pathway [102, 103].

1.1.8.4. Cardiovascular diseases

The first decades of investigating the role of MMPs in cardiovascular pathology uncovered several important actions on extracellular matrix remodeling in myocardial infarction, atherosclerosis, hypertension, hypertrophy and heart failure [5, 104]. However, in the past 20 years since discovering intracellular MMPs activity, research has shown that intracellular MMPs are also importantly involved in the pathogenesis of many cardiovascular diseases. For example, myocardial-specific overexpression of constitutively active full length MMP-2 in mice, even in the absence of external injury, results in several cardiac pathological changes that lead to TnI proteolysis, cardiac mitochondrial dysfunction, left ventricular remodeling and systolic heart failure [105, 106]. Upon activation in response to IR injury, MMP-2 induces degradation of several cardiac sarcomeric proteins including TnI, myosin light chain-1 and titin resulting in cardiac contractile dysfunction [9, 29, 59]. Moreover, in vascular smooth muscle, MMP-2 mediates angiotensin-II induced vascular injury by triggering inflammation and the immune response [107]. Intracellular MMP-2 activity is also associated with vascular hyporeactivity to vasoconstrictors during endotoxemia [108] via degradation of calponin-1 [42]. Recently, MMP-2 activity is also detected as an early event during cardiotoxicity caused by anthracyclines used in cancer

chemotherapy and induces proteolysis of cardiac titin resulting in myofilament lysis, adverse ventricular remodeling and impaired cardiac contraction [60].

In diabetic cardiomyopathy, both MMP-2 and MMP-2_{NTT76} are expressed in cardiac tissue where MMP-2 is mainly localized to the sarcomere, whereas MMP-2_{NTT76} isoform is localized to the mitochondria, sarcomeric Z-line, intercalated discs and nuclei. Induction of mitochondrial permeability transition is correlated with MMP-2_{NTT76} expression in the diabetic heart [109]. These findings suggest that intracellular MMP-2 may contribute to the development of diabetic cardiomyopathy [109] and open new avenues in the management of diabetes complications. Indeed, the MMP inhibitor doxycycline reduced the negative alterations in cardiac contractile function, action potential duration and calcium handling in streptozotocin-induced diabetic rats [110].

A summary of the role of intracellular MMP-2 in pathologies is shown in **Figure 1.5**. Here I will be focusing on two particular cardiac pathological conditions: myocardial IR injury and anthracycline-induced cardiotoxicity, and the pathophysiological role played by MMP-2 in these conditions.

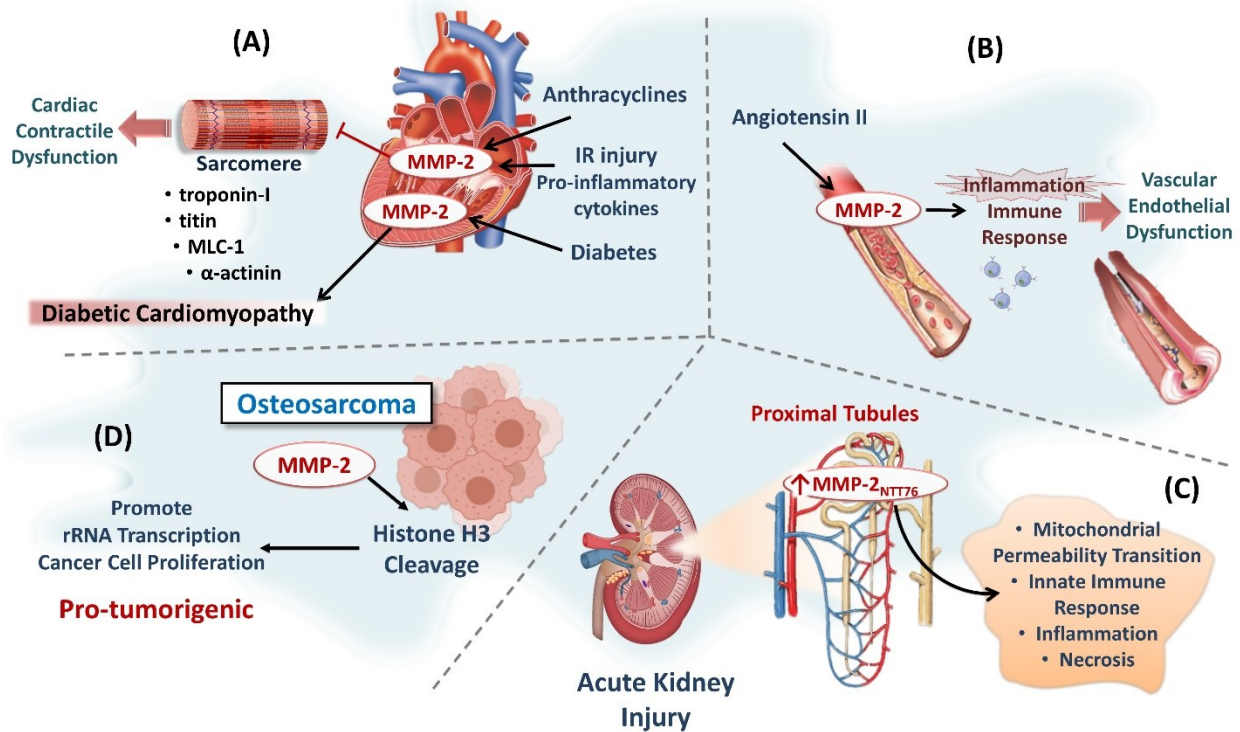


Figure 1.5. Role of intracellular MMP-2 in selected pathological conditions. (A) MMP-2 is activated in the heart in response to anthracycline-cardiotoxicity, ischemia/reperfusion injury, pro-inflammatory cytokines or diabetes resulting in degradation of cardiac sarcomeric proteins and cardiac contractile dysfunction. (B) In response to angiotensin II-induced vascular injury, MMP-2 is activated in vascular smooth muscle and triggers inflammation and endothelial dysfunction. (C) In acute kidney injury, MMP-2_{NTT76} is expressed in the proximal tubules and induces structural changes, innate immune response and inflammation. (D) In osteosarcoma, MMP-2 promotes rRNA transcription and cancer cell proliferation via cleavage of N-terminal tail of histone H3. IR, ischemia/reperfusion; MLC-1, myosin light chain-1; MMP-2, matrix metalloproteinase-2; MMP_{NTT}, N-terminal truncated MMP (Figure was created using BioRender).

1.2. Myocardial ischemia-reperfusion injury

1.2.1. Pathophysiology of myocardial IR injury

Ischemic heart disease or myocardial ischemia occurs when there is a reduction in blood flow to the heart, preventing the heart muscle from receiving enough oxygen. It is caused by a partial or complete occlusion of the coronary arteries as a result of coronary artery diseases such as atherosclerosis, coronary spasm or blood clot, and eventually leads to heart attack, heart failure or sudden death [111]. Irreversible injury resulting from severe, prolonged myocardial ischemia induces myocardial infarction as a result of rupture or erosion of coronary artery plaque and initiation of thrombosis. It can also occur in presence of coronary atherosclerosis when blood flow redistributes away from the myocardial region supplied by a coronary artery with stenosis [112]. Globally, ischemic heart disease is considered the leading cause of death worldwide and according to the American Heart Association and Heart and Stroke Foundation of Canada reports, it is considered the second leading cause of death in Canada. According to the Canadian Chronic Disease Surveillance System in 2018, about 1 in 12 or 2.6 million Canadian adults aged above 20 live with diagnosed heart disease [113-115].

When the heart undergoes ischemia, it is important to restore the blood flow to affected heart muscle, known as reperfusion, to rescue the heart from developing infarction, either by mechanical approaches such as percutaneous coronary intervention, coronary artery bypass grafting, cardiac transplantation or pharmacological approaches using thrombolytic/fibrinolytic agents [116-118]. However, reperfusion paradoxically leads to further cardiac injury due to cellular changes in response to the enhanced oxidative stress it causes, leading ultimately to myocardial cell death. This is known as IR injury [119]. As shown in **Figure 1.6**, during ischemia, there is a reduction in blood flow/fuel delivery to the heart, buildup of cellular metabolites which

are not washed-out, and lack of oxygen supply to the heart. Upon reperfusion, re-introduction of blood flow through coronary circulation induces endothelial dysfunction and a burst of RONS including peroxynitrite [45, 120]. This necessitates the use of adjunct cardioprotection during reperfusion. The pathophysiology of IR injury is not fully understood, and this resulted in the failure of translating preclinical studies into clinical practice [121]. We therefore need to understand the precise molecular mechanisms of IR injury to discover new therapeutic options for its treatment.

Myocardial infarction is synonymous with death of cardiac muscle by several cell death pathways. It involves mitochondrial and sarcolemma rupture as a result of the loss of cellular homeostasis and swelling due to water and electrolyte accumulation, as well as failure of ion pumps due to the reduction in ATP production by ATP hydrolysis, and acidosis due to the accumulation of lactic acid [122, 123]. Acidosis induces intracellular sodium overload due to increased Na^+/H^+ exchange which in turn results in an induction of reverse $\text{Na}^+/\text{Ca}^{2+}$ exchange that leads to calcium overload [124]. This increase in cytosolic calcium induces mitochondrial dysfunction and mitochondrial permeability transition pore (mPTP) opening which in turn increase the formation of mitochondrial RONS and induce DNA, protein and lipid damage [125]. Reperfusion, on the other hand, induces excessive formation of RONS, leukocyte infiltration and uncoordinated contraction in response to calcium overload. It also intensifies the morphological changes associated with necrosis such as mitochondrial rupture and mPTP opening (**Figure 1.6**) [126].

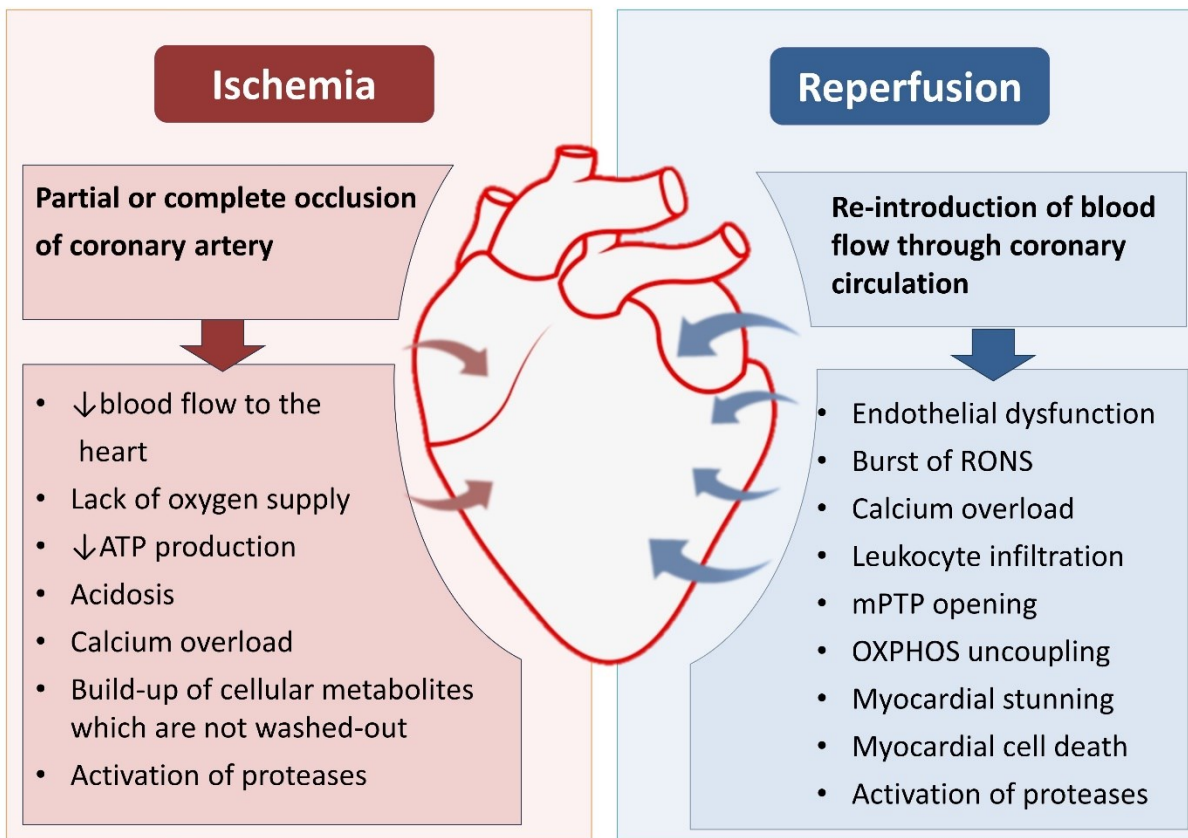


Figure 1.6. Pathophysiological changes during myocardial ischemia-reperfusion injury. Ischemia occurs when there is a reduction in blood flow to the heart as a result of partial or complete occlusion of the coronary arteries. This results in reduction in oxygen supply to the heart, reduced ATP production, acidosis due to the accumulation of lactic acid, calcium overload, activation of intracellular proteases and build up of cellular metabolites which are not washed out. Reperfusion, on the other hand, occurs upon the reintroduction of blood flow through the coronary circulation. Although it is essential to restore the normal blood flow to the heart, this paradoxically leads to further cardiac injury due to the cellular changes in response to enhanced oxidative stress. This includes endothelial dysfunction, increased RONS formation, calcium overload, leukocyte infiltration, mPTP opening, oxidative phosphorylation uncoupling and intracellular proteases activation, which collectively lead to myocardial stunning and/or cell death. ATP, adenosine triphosphate; mPTP, mitochondrial permeability transition pore; OXPHOS, oxidative phosphorylation; RONS, reactive oxygen-nitrogen species.

1.2.2. Cardioprotective interventions to protect against reperfusion injury

Some cardioprotective interventions to reduce reperfusion injury include therapeutic hypothermia, vagal stimulation and beta-blockers such as metoprolol [127-129]. Ischemic preconditioning is another approach to reduce infarct size by introducing several cycles of short, brief ischemia and reperfusion that protect the heart from more prolonged episodes of ischemia and prevent endothelial cell dysfunction [130]. For example, in isolated perfused mouse hearts, subjecting the heart to repeated cycles of 5 min ischemia followed by 5 min reperfusion or shorter prior to the global no-flow ischemia, induces ischemic preconditioning [131]. This works by stimulating adenosine A₁ receptors to activate protein kinase C signalling and open the mitochondrial ATP-sensitive potassium channels which in turn results in shortening of action potential duration and reducing calcium entry to cytosol. This eventually inhibits cardiac contractility, reduces energy consumption and increases the tolerance to ischemia [132].

1.2.3. Myocardial stunning vs necrosis

The duration of ischemia affects the degree of cardiac injury and how the heart recovers upon reperfusion. It ranges from mild, reversible injury caused by shorter ischemic duration, known as stunning, to more severe, irreversible injury caused by longer ischemia that leads to necrosis (infarction) [133]. Myocardial stunning is a post-ischemic ventricular dysfunction that occurs following a brief period of ischemia. It resolves within days to weeks depending on the restoration of normal blood flow and the absence of irreversible damage, and although it induces contractile abnormalities, it does not lead to myocardial cell death [134]. Cardiac mechanical dysfunction during stunning injury appears to be a result of the cellular changes that occur during reperfusion, as mentioned earlier, rather than the short deprivation of cardiac muscle from blood supply. However, there is no stunning without ischemia [135].

Necrosis, on the other hand, is death of myocardial tissue that results from prolonged ischemia leading to myocardial infarction [136]. Myocardial necrosis is associated with inflammation and tissue invasion by monocyte-macrophages and neutrophils. It is also accompanied by the release of biomarkers including TnI, lactate dehydrogenase (LDH), myoglobin and creatine kinase in circulating blood [137]. The resulting cardiac dysfunction and cell death during necrosis are net results of the damage accompanying both ischemic injury and reperfusion [138]. For example, in isolated perfused mouse hearts, subjecting the heart to 30-35 min of global no-flow ischemia is reported to be optimal as it results in ~50% infarction and allows testing the recovery of contractile function. A shorter duration of ~20-25 min ischemia can induce stunning injury, while a longer duration of >35 min ischemia results in necrosis [139].

MMP-2 activation is reported to be directly involved in the development of myocardial stunning during IR injury, as evidenced by the marked release of MMP-2 during early reperfusion and its negative correlation to the post-ischemic recovery of cardiac function in hearts subjected to 20 min ischemia [8]. However, there is evidence that MMP-2 activity is also increased during myocardial infarction when the heart is subjected to 90 min ischemia [140], indicating the critical role played by MMP-2 in the pathophysiology of both conditions.

1.2.4. Role of MMP-2 in IR injury and its proteolytic targets

MMP-2 is rapidly activated during oxidative stress by peroxynitrite-induced S-glutathiolation [43]. It contributes to IR-mediated contractile dysfunction by inducing the proteolysis of different proteins of the sarcomere including titin, TnI and myosin light chain-1 [8, 9, 50, 59, 61]. It was also reported to be activated in human hearts in response to IR injury. Plasma samples and left atrial biopsies, obtained from patients undergoing coronary artery bypass graft

surgery following stable angina, showed an increase in MMP-2 activity and reduction in TIMP-1 level [141].

MMP-2 is localized at the Z-line of cardiac sarcomere and co-localizes with TnI, the thin myofilament protein that regulates actin-myosin interaction. MMP-2 mediates TnI proteolysis during IR resulting in impairment of cardiac mechanical function. MMP inhibitors prevented the loss of TnI and caused the improvement of cardiac contractile function post-IR [9]. Another sarcomeric protein associated with MMP-2 is myosin light chain-1 (MYL3), particularly at the thick myofilament, and its degradation by MMP-2 also contributes to the impaired recovery of mechanical function in rat hearts subjected to IR injury [61]. Titin, the largest mammalian and myofilament protein, is co-localized with MMP-2 at the Z-disc region of cardiac sarcomere and is proteolyzed by MMP-2 in rat hearts subjected to IR injury. The loss of titin was prevented by either pharmacological or genetic inhibition of MMP-2 [59]. JPH-2, which tethers the T-tubules to SR and mediates excitation-contraction coupling, was identified as another MMP-2 proteolytic target during IR injury. It is localized close to the Z-disc of the sarcomere where MMP-2 is localized [70]. Using the same model of IR injury in rat hearts, MMP-2 was found to target and cleave SERCA2a, which controls calcium re-entry to SR during diastole, resulting in calcium overload and myocardial cell death [69].

Mice with cardiac-specific transgenic expression of active, full length MMP-2 showed a greater impairment in contractile function and larger infarct size when subjected to IR injury compared to wild-type mice. In addition, abnormalities in mitochondrial structure, respiration and lipid peroxidation were more pronounced in hearts from transgenic mice [63]. Similarly, cardiac-specific expression of MMP-2_{NTT76} in mice delayed the recovery of ventricular function and caused more severe myocardial infarction in response to IR injury [30]. Inhibition of MMP-2 activity was

also suggested to mediate the cardioprotective effect of carvedilol during myocardial IR injury [142]. The mechanism by which carvedilol inhibits MMP-2 activity is unknown.

1.2.5. Role of MMP-2 in myocardial cell death

Enhanced oxidative stress in cardiomyocytes triggers myocardial cell death pathways [143]. Models of myocardial IR injury leading to infarction show evidence of apoptotic cell death in heart tissue [144, 145]. MMP-2 is reported to play a fundamental role in this process. In adult rat cardiomyocytes, MMP-2 was shown to mediate β -adrenergic receptor-stimulated apoptosis by disruption of β 1-integrin survival signalling and activation of the c-Jun N-terminal kinase (JNK)-mediated mitochondrial cell death pathway. Inhibition of MMP-2 activity by SB-3CT, a selective gelatinase inhibitor, attenuated the increased cytochrome C release and the reduced mitochondrial membrane potential, resulting in inhibition of apoptosis [146]. MMP-2 has been also shown to target and cleave glycogen synthase kinase-3 β in H9c2 cardiomyoblasts subjected to hydrogen peroxide to induce oxidative stress, resulting in an increase in its kinase activity and promoting apoptosis, considering its important role in cellular functions regulating apoptotic pathways [52, 147]. Inhibiting MMP-2 activity in cultured neonatal rat ventricular cardiomyocytes also reduced tumor necrosis factor α -mediated apoptosis, pro-apoptotic B-cell lymphoma-2 (Bcl-2)-associated X protein (Bax) expression and caspase-3 activity and increased the anti-apoptotic Bcl-2 expression [148].

In hearts from rats subjected to *in vivo* IR injury leading to infarction, MMP-2 activity was shown to be higher in the infarct zone and area at risk [140]. Ilomastat, a nonselective MMP inhibitor, reduced infarct size in rat hearts subjected to *in vivo* IR injury [149]. Cardiac-specific expression of MMP-2_{NTT76} in mouse hearts activated nuclear factor of activated T-cell and NF- κ B signalling and innate immune response, by elevating interleukin (IL)-6, monocyte chemoattractant

protein-1, interferon regulatory factor-7 and pro-apoptotic transcripts, resulting in induction of cardiac cell death [30].

1.3. Doxorubicin-induced cardiotoxicity

1.3.1. Pathophysiology of DXR-induced cardiotoxicity

Anthracyclines are a class of chemotherapeutic agents that have been used since the 1960s for treatment of a wide range of solid tumors such as sarcoma, breast and lung cancers as well as blood malignancies including leukemia, lymphoma and multiple myeloma [150, 151]. Doxorubicin (DXR), a member of the anthracyclines, is considered one of the most effective chemotherapeutic agents. However, its use is limited by the dose-dependent development of severe, irreversible cardiotoxicity including heart failure and left ventricular dysfunction [152]. In a study by Von Hoff and colleagues, among over 4000 patients receiving DXR as a treatment, 2.2% developed signs of congestive heart failure [153]. Subsequent studies showed a dose-dependent reduction in left ventricular ejection fraction in patients under anthracycline chemotherapy with a cumulative DXR dose $> 350 \text{ mg/m}^2$ of body surface area [154, 155]. The dose-related risk of developing DXR-induced congestive heart failure rises from 0.2 to 8.7% at cumulative doses of 150 and 600 mg/m^2 respectively [156, 157]. In addition to left ventricular dysfunction, some studies reported development of arrhythmia and pericarditis with acute anthracycline cardiotoxicity [158, 159]. Anthracycline-cardiotoxicity is considered irreversible as it is characterized by not only cardiac dysfunction but also induction of myocardial cell death [156].

The mechanisms underlying DXR-induced cardiotoxicity include RONS formation subsequent to DXR metabolism, in addition to altered iron metabolism, degradation of sarcomeric proteins, dysregulation of calcium signalling and induction of apoptosis [160]. DXR is reduced by

mitochondrial respiratory chain complex I NADH dehydrogenase to form a semiquinone radical which in turn reacts with molecular oxygen and forms superoxide radical with subsequent formation of hydrogen peroxide [161, 162]. DXR also forms a complex with non-heme iron that catalyzes the conversion of hydrogen peroxide to hydroxyl radical which in turn increases the generation of RONS [163]. The formation of RONS induces apoptotic cell death via opening of mPTP, cytochrome C release and activation of caspase cascade [164, 165]. DXR also directly interacts with the mitochondrial phospholipid, cardiolipin, resulting in disrupting its association with the inner mitochondrial membrane proteins and induction of mitochondrial dysfunction and apoptosis [166]. Another mechanism contributing to DXR-cardiotoxicity is calcium dysregulation which results from the changes in calcium regulatory proteins such as SERCA2a, the $\text{Na}^+/\text{Ca}^{2+}$ exchanger and phospholamban, reducing mitochondrial calcium retention capacity and increasing calcium release from SR resulting in depleting SR intracellular stores. Eventually this leads to the development of mitochondrial and cardiac contractile dysfunction [167-169].

1.3.2. Therapeutic approaches to protect against DXR-cardiotoxicity

Several approaches have been proposed to protect against DXR-induced cardiotoxicity, particularly by reducing the generation of RONS and attenuating myocardial oxidative stress. This includes the use of antioxidants, angiotensin converting enzyme inhibitors, angiotensin II receptor antagonists, beta blockers and alpha-1 receptor agonists [170]. Carvedilol, a beta blocker that possesses antioxidant properties, was shown to be effective in relieving DXR-cardiotoxicity [171]. The alpha-1A adrenergic receptor agonist, dabuzalgron, has been also shown to exert a cardioprotective effect by activation of extracellular signal regulated kinase (ERK)-1 and -2 pathways and inhibition of apoptosis [172]. The use of PEGylated liposomes for DXR delivery is another approach for its selective uptake by tumor cells to limit its cardiotoxic effect [173].

1.3.3. Role of MMP-2 in DXR cardiotoxicity and its proteolytic targets

MMP-2 is the main MMP whose level and activity are reported to be affected during anthracycline-induced cardiotoxicity [174]. DXR was reported to induce a time-dependent activation of MMPs, specifically MMP-2, in mouse heart and aorta [175]. Being one of the main mechanisms underlying DXR-induced heart failure, oxidative stress developing during this type of cardiotoxicity enhances intracellular MMP-2 activity. Chan et al. showed that, in neonatal rat ventricular cardiomyocytes, DXR induces activation of intracellular MMP-2 in response to enhanced oxidative stress. This response occurs either by direct activation of full-length MMP-2 and/or de novo expression of MMP-2_{NTT} [174]. The level of the sarcomeric protein, TnI, was reduced by DXR. However, this effect was independent on the proteolytic activity of MMP-2 [174]. Another study of a mouse model of DXR-induced cardiotoxicity showed that titin could be a proteolytic target of MMP-2, resulting in myofilament lysis, as it showed that the use of the MMP inhibitors, doxycycline or ONO-4817, prevented titin proteolysis, attenuated extracellular matrix remodeling and protected against DXR-induced cardiac systolic and diastolic dysfunction [60]. Similarly, myocardial MMP-2 activation was reported to mediate DXR-induced left ventricular dysfunction in rats [176].

MMP-2 activation in cardiomyocytes in response to DXR is regulated via ERK/JNK/p38 mitogen-activated protein kinase (MAPK) pathway. Attenuation of MMP-2 activation appears as a result of inhibition of nicotinamide adenine dinucleotide phosphate (NADPH) oxidase whose transcription is modulated by ERK/JNK pathway [177]. In rats treated with DXR, MMP-2 activity was increased in plasma after the end of treatment and MMP-2 activity was increased in the left ventricle in association with enhanced expression of RONS, activation of caspase-3 and stimulation of the protein kinase B (Akt) pathway [178]. On day 2 of DXR treatment in mice,

MMP-2 and MMP-9 gene transcription was increased in heart ventricles, whereby MMP-2 gene expression occurred earlier on day 1 and was doubled on day 2, suggesting that both isoenzymes contribute to the development of DXR-cardiotoxicity [179]. However, in hearts from DXR-treated mice, only MMP-2 activation was observed with no evidence of MMP-9 activity [60].

A study investigating the cardioprotective effect of erythropoietin against DXR-cardiotoxicity in rats reported increased MMP-2 protein level in the heart together with induction of cardiac fibrosis and TIMP-2 downregulation in response to DXR treatment, while erythropoietin was able to reverse all these changes, including the increased MMP-2 protein expression [180].

1.4. Mitochondrial-ER-associated membrane

The MAM or mitochondria-ER contact site is the interface between the ER and mitochondria. It was first identified in 1969 by Ruby et al. as a possible interplay between both organelles and was later introduced in 1990 as a biochemical entity that plays a fundamental role in intracellular homeostasis by Jean Vance at the University of Alberta [181, 182].

1.4.1. Regulatory functions of the MAM in cardiac cells

The MAM serves as the connection between ER and mitochondria that regulates several intracellular processes required for determining cell fate such as calcium homeostasis, apoptosis, lipid metabolism and exchange of molecules between the ER and mitochondria [183]. It is also involved in the inflammasome response, ER stress, autophagy and mitochondrial morphology and function regulation [184].

MAM is required for the tethering of the ER to mitochondria which in turn is essential for calcium transit between the two organelles. Calcium transport from ER to mitochondria occurs through the inositol 1,4,5-triphosphate receptor (IP3R)- 75kDa glucose-related protein (GRP75)-

voltage-dependent anion channel-1 (VDAC1) complex which is a part of the MAM tethering proteins [185]. IP3R allows the release of calcium from the ER, while VDAC1 serves as the calcium uptake channel as a part of the outer mitochondrial membrane, and both channels are connected through their cytosolic domains via GRP75 [184]. Disruption of this interaction was associated with the development of cardiac and mitochondrial dysfunction [186]. Mitochondrial calcium homeostasis is also critical for the regulation of ATP production and mitochondrial quality control in the heart [187]. Reduced calcium transfer to mitochondria impairs the function of electron transport chain and ATP production and activates autophagy [188], while excessive calcium transfer to mitochondria results in mitochondrial calcium overload, mPTP opening and induction of apoptosis [189].

MAM tethering proteins are also involved in phospholipid biosynthesis and transport which in turn is essential for the formation of cellular membranes and signal transduction [190]. MAM-associated caveolin-1 can bind to cholesterol and mediates its transport from the ER to the plasma membrane which in turn regulates atherogenesis [191, 192]. The MAM also modulates ER stress signalling, and many of the proteins involved in ER regulation and the unfolded protein response (UPR) are localized to the MAM. Disruption of ER-mitochondria communication could trigger an ER stress response [193]. Oxidative stress is another cellular stress response that is regulated in part by the MAM, as excessive calcium transfer to mitochondria can enhance mitochondrial RONS production by disrupting oxidative phosphorylation which in turn triggers myocardial cell death during different cardiac conditions including IR injury [194].

In addition to the role of MAM in mitochondrial calcium transit, it also regulates mitochondrial function, morphology and quality control mechanisms including fusion, fission and mitophagy [193]. Mitofusin-2 (Mfn-2), which regulates mitochondrial fusion, is localized to the

MAM [195]. Dynamin-related protein-1 (Drp-1), which regulates mitochondrial fission, upon activation is recruited in close proximity to the MAM where the fission process takes place [196]. MAM also plays a role in mitochondrial motility via the mitochondrial Rho GTPase proteins (Miro)-1 and -2 which mediate mitochondria trafficking, positioning and transportation along the microtubules [197]. Loss of Miro-2 and impaired inter-mitochondrial communication are reported in hearts from mice subjected to transverse aortic constriction [198]. The mitophagy regulatory protein, PTEN-induced kinase-1 (PINK1), is shown to be localized to the MAM and recruits parkin to the MAM upon induction of mitophagy [199]. The PINK1/parkin interaction induces Mfn-2 ubiquitination and dissociates mitochondria from the ER which in turn triggers mitophagy [200].

Mitochondrial damage is one of the cellular stimuli that trigger the activation of the inflammasome. The MAM serves as the site where the nucleotide-binding oligomerization domain (NOD)-like receptors (NLRs) family pyrin domain-containing protein 3 (NLRP3) inflammasome complex assembles [201]. Several mitochondrial factors at the MAM are involved in the interaction between NLRP3 and mitochondria such as Mfn-2, cardiolipin and mitochondrial antiviral-signalling protein [202]. NLRP3 localization to the MAM is suggested to contribute to the recognition and sensing of mitochondrial damage and the associated release of mitochondrial DNA (mtDNA) [203].

1.4.2. MMP-2 localization to the MAM

MMP-2 was found to be localized to several intracellular organelles, among them is the MAM [65]. Using immunogold electron microscopy and immunofluorescence, it was found that the majority of mitochondrial MMP-2 is actually associated with the MAM, which was confirmed by detection of MMP-2 in the purified MAM fraction subcellularly isolated from mouse heart [65]. The same finding was reported in hearts from DXR-treated mice using immunogold electron

microscopy [60], suggesting that MMP-2 may be involved in the pathophysiological changes accompanying this peculiar structure during cellular injury. However, the exact role of MMP-2 and its potential proteolytic targets at the MAM are not well known.

1.4.3. Mitochondria and their regulation

Mitochondria are the powerhouse of the cell. They comprise one third of the cellular volume and provide approximately 90% of the ATP required for cellular functions, making them vital for the high energy-demanding organs such as the heart [204, 205]. Therefore mitochondrial dysfunction and failure to produce the ATP required for cardiac muscle contraction is considered a primary mechanism of cardiac dysfunction [206].

1.4.3.1. Structure of mitochondria

The mitochondrion is composed of a matrix surrounded by two phospholipid membranes, termed the inner and outer mitochondrial membranes. The space between them is called the intermembrane space [207]. The two mitochondrial membranes have different characteristics regarding their lipid composition and the functions of the transmembrane proteins embedded within them. The outer membrane has a lipid composition more similar to that of the plasma membrane, while the inner membrane has a higher protein to lipid ratio and forms invaginations into the matrix, called cristae, that provide more space for chemical reactions [208]. The outer membrane has also different permeability than the inner as it allows the transport of ions and small molecules through VDACs, while the inner membrane only permits the free passage of water, oxygen and carbon dioxide. This selective permeability of the inner membrane forms an electrochemical gradient which is required for the function of electron transport chain and ATP

production [209, 210], see **section 1.4.3.6**. The cristae membrane contains the respiratory chain complexes that regulate the electron transport required for ATP synthesis [208].

1.4.3.2. Functions of mitochondria in cardiac cells

Mitochondria play significant roles in the regulation of cardiac function through ATP production and regulation of cellular metabolism and apoptosis [211]. Mitochondria are the source of NADH and ATP via the tricarboxylic acid cycle and oxidative phosphorylation, particularly the electron transport chain which generates the proton gradient that drives the phosphorylation of ADP to ATP [212]. They provide the intermediates for lipid and pyrimidine nucleotide through fatty acid β -oxidation [213], as well as iron and sulfur homeostasis which are important for electron transport chain and DNA repair proteins [214]. In addition, mitochondria contribute to apoptotic pathways through the release of apoptosis-inducing factor (AIF) as well as the Bax-mediated release of cytochrome C and induction of the caspase cascade [215]. Calcium uptake by mitochondria via the mitochondrial calcium uniporter is also essential for regulation of the level of intracellular calcium which in turn affects cardiac metabolism, contractility and cellular stress responses [216]. Therefore, impaired mitochondrial homeostasis contributes to the pathophysiology of cardiac diseases.

1.4.3.3. Mitochondria and IR injury

The lack of oxygen during ischemia inhibits electron flow within the electron transport chain which in turn results in reduced ATP production that does not meet myocardial demand [217]. Subsequently, the reduction in ATP and the increased production of lactate, that induces a drop in intracellular pH, inhibit the activity of Na^+/K^+ ATPase and activates the Na^+/H^+ exchanger to restore normal intracellular pH. This increases the intracellular Na^+ concentration which in turn

activates the $\text{Na}^+/\text{Ca}^{2+}$ exchanger resulting in calcium overload. This eventually leads to myocardial damage by activating proteolytic enzymes and mediating myocardial cell death [218]. However, the acidic environment during ischemia caused by lactic acid accumulation inhibits mPTP opening [219].

Upon reperfusion, RONS biosynthesis and calcium overload induce more cellular injury. With the washout of lactic acid and restoration of physiological pH, oxidative stress and calcium overload trigger mPTP opening and reduce the calcium retention capacity of mitochondria which makes the cardiomyocyte more sensitive to calcium overload [220, 221]. The mPTP is a high conductance channel located at the interface between the inner and outer mitochondrial membranes and allows for nonselective mitochondrial permeabilization and the communication between mitochondrial matrix and cytoplasm [222]. It is normally closed, and opens when stimulated by adenine nucleotides, mitochondrial calcium accumulation or oxidative stress [218]. mPTP opening leads to the uncoupling between electron transport and phosphorylation reactions in oxidative phosphorylation, disruption of ATP synthesis, loss of mitochondrial membrane potential, osmotic swelling, enhanced production of mitochondrial RONS and the release of cytochrome C which collectively lead to myocardial cell death [223]. Mitochondrial respiratory chain complex-mediated oxygen consumption is also reported to be impaired following IR injury [224].

1.4.3.4. Mitochondrial quality control mechanisms

Given the fundamental role played by mitochondria in cellular homeostasis, mitochondrial quality must be regulated to protect against cellular dysfunction. Mitochondrial quality control mechanisms help protect the mitochondria in response to cellular stress [225]. They include: mitobiogenesis, mitochondrial dynamics (fusion and fission) and mitophagy [226]. Impairment of

mitochondrial quality control and homeostasis is reported to be associated with cardiac dysfunction [227]. This drove the attention of researchers to target these mechanisms in the attempt to preserve cardiac function. A summary of the mitochondrial quality control mechanisms and their regulatory proteins is shown in **Figure 1.7**.

1.4.3.4.1. Mitochondrial biogenesis

Mitobiogenesis means the synthesis of new mitochondria from pre-existing ones, and it is regulated by different proteins, among them is AMP-activated protein kinase- α (AMPK α) and peroxisome proliferator-activated receptor γ (PPAR γ) coactivator 1 α (PGC1 α) [228]. AMPK α regulates cellular energy homeostasis by activating glucose and fatty acid uptake and regulates mitobiogenesis by phosphorylation of metabolic enzymes, nutrient transporters and epigenetic factors such as DNA methyltransferase 1, retinoblastoma binding protein 7 and histone acetyltransferase 1, promoting transactivation of nuclear genes involved in mitochondrial biogenesis and function. It also induces phosphorylation and activation of PGC1 α [229]. PGC1 α regulates mitochondrial biogenesis through activation of PPAR and mitochondrial transcription factor A, enhancing the expression of mitochondrial respiratory chain enzymes and increasing mtDNA content [230]. PGC1 α regulates the replication of mtDNA and the transcription of mitobiogenesis genes [231].

1.4.3.4.2. Mitochondrial dynamics

Mitochondria are dynamic organelles as they continuously undergo fusion and fission. These two processes are essential for cell survival, growth and division [232]. Mitochondrial fusion includes the merging of the salvageable portions of two distinct, partially damaged mitochondria to maintain mitochondrial quality and morphology and prevent permanent loss of essential components including the mitochondrial proteins required for oxidative phosphorylation

and ATP synthesis. This process is regulated by several proteins including Mfn-1 and -2 and optic atrophy-1 (OPA-1). These three proteins are dynamin-like GTPases, meaning that they possess GTPase activity [233, 234]. Mfn-2 mediates outer mitochondrial membrane fusion by interacting with Mfn-1 and contributes to the maintenance and operation of the mitochondrial network. This is driven by GTP hydrolysis that induces conformational changes of the outer mitochondrial membrane and dimerization of Mfn from adjacent mitochondria, allowing their merger [235, 236]. OPA-1, on the other hand, regulates inner mitochondrial membrane fusion and senses the changes in mitochondrial membrane potential which is critical for maintaining the electrochemical gradient required for ATP production [237]. OPA-1 is also involved in the process of oxidative phosphorylation and ATP production [238].

Mitochondrial fission, on the other hand, divides mitochondria into two separate organelles. When mitochondria are damaged, the fission process separates the injured mitochondrial segments which in turn are delivered to and degraded by lysosomes, and is regulated by Drp-1 [234]. Drp-1 is a cytosolic protein which is recruited to the outer mitochondrial membrane to induce fission by interaction with mitochondrial-bound proteins including fission 1, mitochondria fission factor and 49 kDa and 51 kDa mitochondrial dynamics proteins [238, 239]. This involves ER recruitment around mitochondria to mark the sites for mitochondrial fission as well as the induction of outer mitochondrial membrane constriction at the MAM with subsequent GTP hydrolysis and Drp-1 oligomerization [196]. This process also involves Drp-1 phosphorylation to increase its GTPase activity [240]. Although mitochondrial fission is required to get rid of the damaged mitochondria, excessive or unbalanced fission can affect healthy mitochondria and induce mitochondrial fragmentation which leads to enhanced RONS production and progression of cell death [241].

1.4.3.4.3. Mitochondrial autophagy/mitophagy

Mitochondrial autophagy or mitophagy is the removal of damaged mitochondria by autophagosome-lysosomal degradation and is regulated by PINK1 and parkin [242]. PINK1 regulates mitophagy by identifying damaged mitochondria and targeting them for degradation. Damaged mitochondria have low membrane potential which results in PINK1 accumulation on the outer membrane which in turn recruits parkin to target the damaged mitochondria for autophagy [243]. Parkin is a cytosolic E3 ubiquitin ligase that allows ubiquitination of damaged proteins which directs them to degradation by proteasomes or lysosomes [244]. It translocates to the depolarized mitochondria upon PINK1-mediated phosphorylation which also activates its ubiquitin ligase activity [245]. Once recruited to mitochondria, parkin induces the ubiquitination of several mitochondrial proteins followed by induction of proteasomal degradation. Following that, the autophagic protein, p62, is recruited to damaged mitochondria to mediate autophagosome formation around them which ultimately fuse with lysosomes to lyse the damaged mitochondria [225].

Failure of mitochondrial quality control will result in mitochondrial dysfunction and accumulation of damaged mitochondria which in turn predispose cellular dysfunction [246]. The release of mitochondrial RONS such as superoxide anion radical can be a result of mitochondrial dysfunction and is generated from complexes I and III leading to nuclear DNA and lipid damage [125]. mPTP opening, resulting from calcium overload and high RONS production, causes mitochondrial swelling, bursting and the release of mitochondrial components [218]. Collectively, this will result in the impairment of ATP production and cardiac contractility, dysregulation of metabolic and calcium signalling, disruption of iron and sulfur homeostasis and the induction of apoptotic cell death.

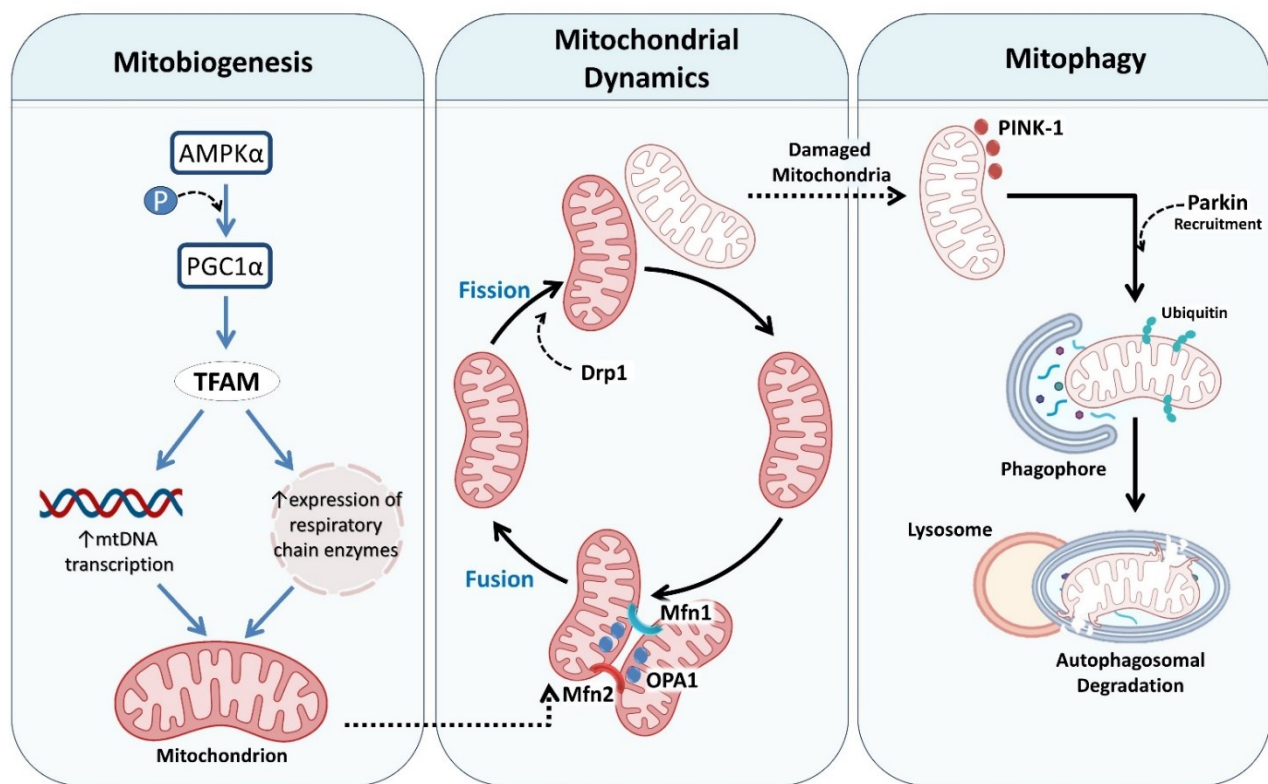


Figure 1.7. Mechanisms of mitochondrial quality control. Mitobiogenesis is regulated by different proteins including AMPK α and PGC1 α . AMPK α induces the phosphorylation and activation of different downstream regulators including PGC1 α , which in turn activates TFAM that induces mtDNA and mitobiogenesis gene transcription and increases the expression of respiratory chain enzymes. Mitochondrial dynamics involves fusion and fission: Mfn-1 and -2 regulate outer mitochondrial membrane fusion, while OPA-1 regulates inner mitochondrial membrane fusion, where two distinctive mitochondria merge together. Drp-1, on the other hand, mediates mitochondrial fission to separate injured mitochondrial segments which are delivered to degradation by lysosomes through mitophagy. During mitophagy, PINK1 identifies damaged mitochondria and accumulates on the outer membrane to recruit parkin, an E3 ubiquitin ligase that induces ubiquitination of damaged mitochondria and directs them to proteasomes or lysosomes for autophagosomal degradation. AMPK, AMP-activated protein kinase; Drp, dynamin-related protein; Mfn, mitofusin; mtDNA, mitochondrial DNA; OPA, optic atrophy; PGC1, peroxisome proliferator-activated receptor γ coactivator 1; PINK, PTEN-induced kinase; TFAM, mitochondrial transcription factor A (*Figure was created using BioRender*).

1.4.3.5. Functions of mitofusin-2 in cardiomyocytes

Mfn-2 is a mitochondrial fusion protein that was first discovered in *Drosophila melanogaster* and was found to have a conserved structure among different species [247, 248]. It consists of a cytosolic N-terminal GTPase domain, followed by a first coiled-coil heptad repeat domain, two transmembrane domains which cross the outer mitochondrial membrane and, finally, a second C-terminal heptad-repeat domain [236]. It is reported to be localized at the MAM, which in turn supports its role in mediating mitochondrial fusion [195]. Mfn-1 and -2 also have functions distinct from their role in mitochondrial fusion, but the loss of both would induce deleterious effects on mitochondrial morphology and regulation [249], as cardiac-specific double knockout of Mfn-1/Mfn-2 in mice resulted in disrupted mitochondrial structure and cardiac contractile function [250]. However, deletion of Mfn-2, but not Mfn-1, in the mouse heart resulted in impaired mitochondrial calcium uptake and respiration. Mfn-1 knockout, on the other hand, did not affect mitochondrial structure or function [251]. Cardiac-specific knockout of Mfn-2 in mice also showed impaired cardiac contractile function, while mice lacking Mfn-1 had normal heart function [252].

Mfn-2 plays several other crucial roles in the cell as it is essential for the tethering between mitochondria and ER and subsequently calcium transit between both organelles [195]. Previous studies reported that deletion of Mfn-2 disrupts mitochondria-ER tethering and ER morphology, induces mitochondrial fragmentation and impairs mitochondrial respiration and ATP production [195, 253, 254]. It also reduces mitochondrial calcium uptake in cardiomyocytes [255]. As discussed earlier, mitochondria-ER tethering and calcium uptake by mitochondria are essential for the function of the electron transport chain. This explains why a loss in Mfn-2 would also result in impaired mitochondrial respiratory function.

Mfn-2 also plays a role in mitophagy. Mfn-2 is phosphorylated by PINK1 to induce parkin translocation from cytosol to mitochondria which in turn induces Mfn-2 ubiquitination. This interaction induces mitophagy which rids the cell of damaged mitochondria by recruiting p62 to the ubiquitinated mitochondrial proteins as discussed earlier [256]. This was supported by Chen and Dorn who showed that cardiac-specific knockout of Mfn-2 in the mouse heart resulted in defective ubiquitination and mitophagy by preventing parkin migration to mitochondria, which in turn resulted in mitochondrial respiratory dysfunction due to accumulation of damaged mitochondria [252]. Additionally, Mfn-2 is suggested to play a role in mitochondria transport and their attachment to microtubules by interaction with Miro and Milton motor proteins. This role was first discovered in neuronal cells and is yet to be investigated in cardiomyocytes [257].

1.4.3.6. Mitochondrial respiratory chain and oxidative phosphorylation

The most important function of mitochondria is the generation of ATP, the energy source of the cell. Mitochondria consume oxygen in order to generate ATP, which can be referred to as mitochondrial respiration [205, 258]. ATP generation by mitochondria is regulated via two main processes, the electron transport chain defined as the flow of electrons from the electron carriers, NADH and reduced flavin adenine dinucleotide (FADH₂), across a series of respiratory chain complexes to create a proton gradient across the inner mitochondrial membrane [259], and chemiosmosis which involves the generation of ATP by ATP synthase driven by the force of proton gradient. The two processes collectively are known as oxidative phosphorylation as they involve oxygen consumption and phosphorylation of ADP into ATP (see **Figure 1.8**) [260, 261].

There are a series of four complexes (I-IV) across the inner mitochondrial membrane that mediate electron transport chain reactions [262]. Complexes I, III and IV, but not II, have transmembrane proton channels that allow the passage of the positively charged protons from the

mitochondrial matrix to the intermembrane space upon acquiring enough energy which is mainly obtained by electron transport [263, 264]. The tricarboxylic acid cycle, which takes place in the mitochondrial matrix, is the main source of NADH and FADH₂ which undergo a series of redox reactions in the matrix to generate protons and electrons. The protons remain in the mitochondrial matrix, while electrons are transferred to the respiratory complexes [265]. NADH is converted into NAD⁺ and H⁺ and passes two electrons to complex I, resulting in its activation that triggers proton pumping across the inner membrane [266]. Then complex I transfers electrons to another molecule called co-enzyme Q10 (ubiquinone) which subsequently transfers them to complex III. FADH₂, on the other hand, is converted into FAD and two H⁺ and generates two electrons that are passed to complex II which on its own does not allow proton pumping across the membrane but transfers its electrons to co-enzyme Q10 and subsequently to complex III [267, 268]. Upon being charged, complex III pumps protons across the inner membrane and passes its electrons to cytochrome C which transfers them to complex IV to repeat the same process [260]. Finally, complex IV transfers electrons to their final acceptor, oxygen, which undergoes a redox reaction to form water [269].

The passage of protons from the mitochondrial matrix to the intermembrane space generates a proton gradient across the membrane which is considered the driving force for ATP synthesis [270]. Protons accumulating in the intermembrane space start to flow back to the matrix through the ATP synthase complex which serves as a proton channel within the inner membrane [271, 272]. The flow of protons across this channel induces activation of the ATP synthase subunit that triggers the phosphorylation of ADP into ATP to produce a massive amount of ATP. This also restores protons to the matrix to allow their passage again across the respiratory complexes and continue the same cycle [273, 274]. These series of oxidative phosphorylation reactions are,

therefore, crucial for ATP production and disruption of any of these steps will impair mitochondrial respiratory function.

Another important regulator of mitochondrial oxidative phosphorylation is the level of calcium. In quiescent cardiac cells, mitochondrial calcium concentration is maintained at ~100 nM, which is close to the cytosolic calcium level. The mitochondria calcium buffering capacity is also critical for maintaining intracellular calcium at its optimal level [275, 276]. Whether the changes in mitochondrial calcium concentration follows the beat-to-beat changes in its cytosolic concentration is questionable [277]. Regulation of mitochondrial calcium is also essential for the function of mitochondria themselves, as mitochondrial calcium induces the activation of NADPH-generating dehydrogenases resulting in increased NADH production which in turn provides the electrons to complex I during the electron transport chain and stimulates ATP production [194]. However, increased mitochondrial calcium can also activate mitochondrial proteases like calpain, impair the function of complexes I and III and increase mitochondrial RONS production [189, 278, 279]. Therefore, maintaining an adequate mitochondrial calcium level is critical for mitochondrial respiration.

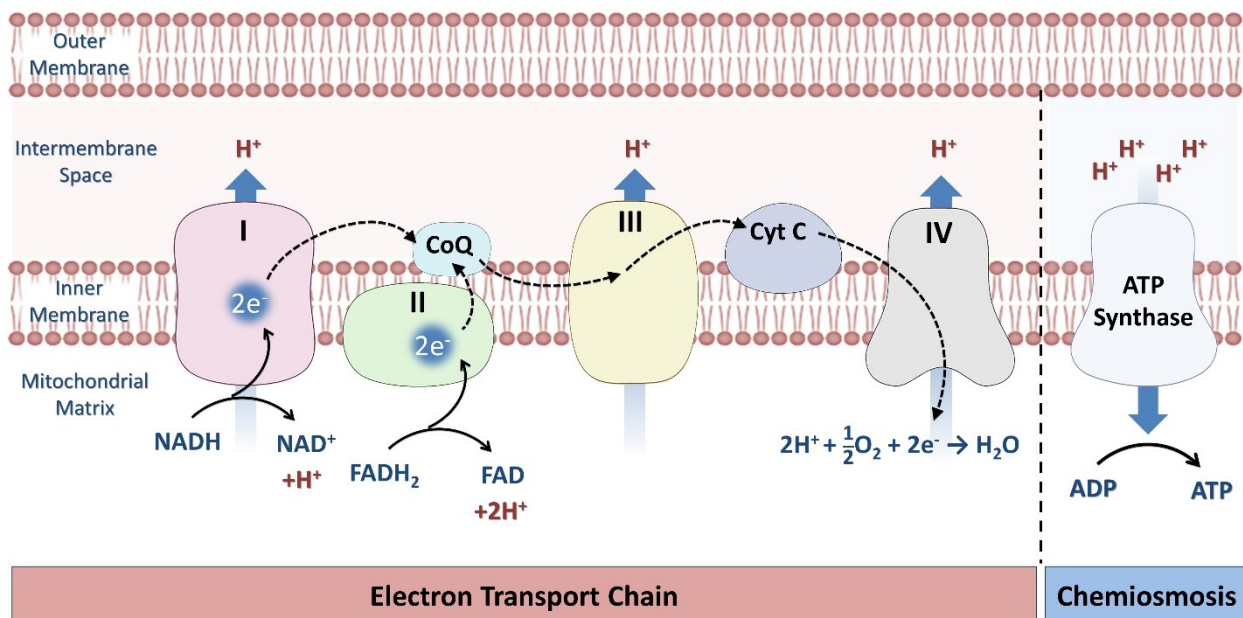


Figure 1.8. The mechanism of oxidative phosphorylation. ATP generation by mitochondria is regulated by two processes: the electron transport chain and chemiosmosis, collectively known as oxidative phosphorylation. The electron transport chain is the process of electron flow from the electron carriers, NADH and FADH₂, across a series of respiratory chain complexes (I-IV), which creates a proton gradient across the inner mitochondrial membrane, till electrons reach their final acceptor, oxygen, which undergoes a redox reaction to form water. This proton gradient across the membrane is the driving force for ATP synthesis through the chemiosmosis (phosphorylation) process. The flow of protons across the ATP synthase complex induces the activation of ATP synthase subunit to trigger the phosphorylation of ADP into ATP, and thus producing energy. ADP, adenosine diphosphate; ATP, adenosine triphosphate; CoQ, co-enzyme Q10; Cyt C, cytochrome C; FADH₂, reduced flavin adenine dinucleotide; NADH, reduced nicotinamide adenine dinucleotide (Figure was created using BioRender).

1.4.3.7. Role of mitochondria in apoptotic cell death

1.4.3.7.1. Apoptosis-inducing factor

Mitochondria play a pivotal role in cell death signalling in mammalian cells, particularly in apoptosis [280]. One of the major pathways involved in mitochondria-mediated apoptotic cell death is the release of AIF from mitochondria. AIF is a flavoprotein anchored to the mitochondrial inner membrane [281], and binds to FAD which allows it to exhibit a NADH oxidase activity that is suggested to be important for the function of mitochondrial respiratory chain complexes and energy homeostasis [282-284]. Independent from its redox activity, AIF induces apoptosis in a caspase-independent manner as inhibition of caspase activity does not affect the pro-apoptotic action of AIF [282, 285].

AIF is synthesized as a 67 kDa protein that contains a mitochondrial-localization sequence within its N-terminal domain that targets it to mitochondria. Subsequently, it gets cleaved by the mitochondria processing peptidase into a mature 62 kDa protein [281, 284, 286]. In addition to the mitochondrial-localization sequence, AIF has two nuclear localization sequences and NAD and FAD-binding motifs [282]. In mitochondria, 62 kDa AIF is further cleaved into a 57 kDa form which is translocated to the cytosol in response to cellular stressors which induce intracellular calcium overload, such as calcium influx, or ER stress that results in induction of calcium release from the ER. These stressors eventually induce mPTP opening and AIF release [287, 288]. Cleaved AIF is then translocated to the nucleus via its nuclear localization sequence identified by nuclear transport receptors to induce apoptosis via mediating DNA fragmentation and chromatin condensation [289]. This occurs by displacing chromatin-associated proteins and stimulating the formation of degradosomes, DNA-degrading complexes, via the recruitment of proteases and nucleases to the nucleus [290].

Some studies reported that the cleavage and release of AIF into the cytosol is calpain-1-dependent, being a calcium-dependent protease. This is encountered during staurosporine (STS)-induced cell death in tumor cell lines [287]. However, the role of calpain in AIF cleavage is questionable as, in neuroblastoma cells, it was reported that calpain is not involved in AIF processing [291]. AIF cleavage is also reported to occur via calcium-independent proteases such as cathepsin, specifically cathepsins-B, -L and -S [292]. However, this has been also contradicted by the results of another study showing that cathepsin knockdown does not affect AIF processing [293]. The exact protease responsible for mitochondrial AIF cleavage and release requires further investigation.

1.4.3.7.2. Bcl-2/Bax/Bak signalling pathway

Another mechanism by which mitochondria regulate apoptosis is the Bcl-2/Bax/Bak pathway. The Bcl-2 family of proteins are important regulators of this process. They are composed of pro-apoptotic proteins such as Bax and Bcl-2 homologous antagonist/killer (Bak), which initiate apoptotic signalling pathways as well as anti-apoptotic members such as Bcl-2 and B-cell lymphoma-extra large (Bcl-XL), which inhibit the pro-apoptotic proteins [294]. Bax is normally localized in the cytosol and translocates to the mitochondria in response to apoptotic stimuli [295]. Subsequently, it induces permeabilization of the outer mitochondrial membrane and cytochrome C release from mitochondria, which in turn activates apoptotic peptidase activating factor 1 that contains a caspase recruitment domain and can induce caspase activation and apoptosis [296]. Interestingly, Bax levels were shown to be upregulated in rat hearts subjected to IR injury [297] and Bax-deficient mice showed protection against myocardial IR injury [298]. The Bcl-2/Bax/Bak pathway is also involved in ER stress-mediated apoptosis as discussed in **section 1.4.5.4**.

1.4.4. Inflammasomes and IR injury

1.4.4.1. Inflammasome structure and activation

Inflammasomes are multiprotein complexes that regulate the innate immune response, the first line of defense against infections in our body [299, 300]. The innate immune response is activated as an immediate, non-specific response against harmful stimuli including foreign antigens, pathogens, irritants or nucleic acids, resulting in induction of cytokine and chemokine pathways that induce the inflammatory response [301]. While insufficient inflammation leads to persistent infections, excessive inflammatory response can result in the progression of chronic inflammatory disease and cell damage [302]. The innate immune response is initiated by the recognition of pathogen-associated molecular patterns (PAMPs) which are derived from pathogens such as pore forming toxins, bacteria, virus, viral RNA, lipopolysaccharide, β -glucans and hyphae or danger-associated molecular pattern (DAMPs) which originate from endogenous stress such as ATP, amyloid- β , alum, asbestos, glucose, hyaluronan and RONS [303, 304]. PAMPs and DAMPs are recognized by what is known as pattern-recognition receptors (PRRs) which, upon stimulation, activate downstream signalling inflammatory cascades by the production of pro-inflammatory cytokines and type I interferon [305, 306].

PRRs are components of the inflammasome complex and consist of several families including the NLRs, toll-like receptors, C-type lectin receptors and AIM2-like receptors among others. The NLR family contains a central nucleotide-binding and oligomerization domain surrounded by leucine-rich repeats, caspase activation and recruitment domain and pyrin domain [307]. An NLR subfamily member, known as NLRP3, has been reported to be associated with several chronic inflammatory diseases including metabolic disorders such as atherosclerosis, type-2 diabetes and obesity, neurodegenerative diseases such as Alzheimer's and Parkinson's diseases

and multiple sclerosis as well as hypertension, inflammatory bowel disease, respiratory disease and cancer [308].

The NLRP3 is normally localized at the ER and the cytosol and, upon stimulation, relocates to the MAM and assembles with the apoptosis-associated speck-like protein containing caspase-recruitment domain (ASC) that binds to pro-caspase-1 to form a complex called the NLRP3 inflammasome which induces the release of pro-inflammatory cytokines by cleaving caspase-1 and the activation of IL1 β and IL18 followed by induction of pyroptosis, an inflammatory form of cell death [201]. Two signals are involved in this process: signal I is the priming signal whereby NLRP3 expression is upregulated along with inducing NF κ B-dependent expression of pro-IL1 β and IL18. Signal II is the assembly phase where the inflammasome complex is formed with subsequent activation of caspase-1 and pro-inflammatory cytokines [309, 310]. Active caspase-1 not only converts pro-IL1 β and pro-IL18 into their mature forms, but also induces maturation of gasdermin D which mediates pyroptosis [311].

1.4.4.2. Crosstalk between inflammasomes and mitochondria

The NLRP3 is activated in response to variable stimuli including the generation of mitochondrial RONS, potassium efflux out of the cell, the release of mtDNA into the cytoplasm or outside the cell, lysosomal rupture or upon interaction of NLRP3 with cardiolipin, uric acid, cathepsins or ATP. There is a crosstalk between mitochondrial damage and NLRP3 activation [299]. The mitochondrial respiratory chain damage induces elevation of mitochondrial RONS production which in turn results in the activation of NLRP3 [312]. Meanwhile, the active caspase-1 resulting from NLRP3 inflammasome assembly is reported to be attracted to the mitochondrial outer membrane and inhibits mitophagy via cleavage of parkin, resulting in accumulation of damaged mitochondria [313].

1.4.4.3. Role of inflammasome response in myocardial IR injury

Several studies have reported the association between the inflammasome response and pyroptosis with myocardial IR injury [314-316]. Activation of the inflammasome response can lead to cardiomyocyte damage, inflammation and cell death [317]. Myocardial IR injury induces a sterile inflammatory response that eventually contributes to the infarct size [318]. NLRP3 activation is reported during IR injury [318, 319]. Pharmacological inhibition of the NLRP3 inflammasome using INP4E, a synthetic NLRP3 inhibitor, has been shown to attenuate myocardial IR injury [320]. NLRP3 was shown to be upregulated in cardiac fibroblasts following myocardial infarction and its genetic knockout can also improve cardiac function in mice subjected to IR injury [318]. In diabetic rats, NLRP3-mediated pyroptosis in response to hyperglycemia aggravates myocardial IR injury [316]. Taken together, this shows the strong association between NLRP3 activation and the pathophysiological consequences of IR injury which can be linked to the development of mitochondrial dysfunction.

1.4.5. Endoplasmic reticulum and its regulation

The second compartment of the MAM is the ER, a large dynamic network of membrane that was discovered in the 1950s by George Palade and was later introduced as the main site for membrane-associated and secreted protein synthesis [321, 322]. ER stress, the disruption of ER homeostasis, is involved in the pathophysiology of several cardiac disorders including heart failure, cardiac hypertrophy and ischemic heart disease [323].

1.4.5.1. Role of ER in protein synthesis/folding and calcium regulation

The ER is the major site for protein synthesis, transport and release as well as lipid and steroid biosynthesis, carbohydrate metabolism and calcium storage and homeostasis [324]. It

serves as the site for synthesis of both membrane integrated proteins as well as secreted proteins which are transported outside the cell [325]. Protein translation is initiated in the cytosol and then ribosomes containing messenger ribonucleic acids (mRNAs) are transferred to the ER where the translation process is continued [326]. Following protein synthesis, secreted proteins must undergo folding process by ER chaperones and folding enzymes to acquire their three-dimensional conformation and post-translational modifications including oligomerization, N-glycosylation or disulfide bond formation. Following that, proteins either reside in the ER or translocate to Golgi to be transferred to their final destination in the cell [324]. Proper folding of proteins is essential for them to acquire their native structure which is required for their proper function and activity [327].

The ER is also a major site of intracellular calcium storage. Several calcium channels are located in the ER such as ryanodine receptors and the IP3R which mediate calcium release from the ER to the cytosol when its cytosolic level is diminished in order to maintain calcium balance within the cell [328]. This occurs via G protein-coupled receptor-dependent stimulation of phospholipase C which cleaves phosphatidylinositol 4,5-bisphosphate into diacyl glycerol and inositol 1,4,5-triphosphate, which in turn stimulates IP3R to release calcium [329]. Ryanodine receptors, on the other hand, are activated when there is an increase in cytosolic calcium level as calcium binds to them and induces more calcium release from the ER, a process known as calcium-induced calcium release [330]. If the calcium level in cytosol is elevated, calcium can be transported back to the ER via the action of SERCA2a [331].

A specialized network of membranes with similar structure to ER, known as the SR, was identified in striated muscle cells such as cardiomyocytes. Its main function is calcium storage [332]. The SR lacks ribosomes, so it is not involved in protein synthesis. However, it can serve as

a site for lipid synthesis [333]. The SR surrounds the myofilament and interacts with the T-tubules, deep sarcolemmal invaginations, to regulate calcium release from the SR to the cytosol which in turn is required for cardiac muscle contraction. As I will discuss later, this process is known as excitation-contraction coupling [334].

1.4.5.2. ER stress and misfolded proteins

Maintenance of the ER homeostasis and function is critical for proper protein folding, and any physiological or pathological stimuli that disrupt this homeostasis will result in accumulation of misfolded proteins, a process known as ER stress [323]. Accumulation of misfolded proteins is the primary cause of different pathological conditions such as Parkinson's disease, Alzheimer's disease, Huntington's disease, cystic fibrosis, and other degenerative disorders [327]. The harmful effect of misfolded protein accumulation, also known as proteotoxicity, is either due to the loss of function like what happens in cystic fibrosis or α 1-antitrypsin deficiency, or unfavorable gain of function as seen in numerous neurodegenerative diseases where misfolded proteins induce the formation of amyloid plaques [335]. Although the direct relationship between intracellular misfolded protein aggregation and cardiac diseases is unclear, association between both has been reported in some cardiomyopathies such as desmin-related cardiomyopathy which results from a mutation in the desmin gene or its chaperone, resulting in accumulation of insoluble proteins and the progression into muscle weakness [336, 337]. Several driving factors can disrupt the ER homeostatic function and induce ER stress such as ischemia, hypoxia, genetic mutation, oxidative stress, and increased protein synthesis [338].

1.4.5.3. The unfolded protein response

ER stress triggers the activation of complex adaptive mechanisms known as the UPR to correct for protein misfolding and restore the normal function of the ER [339]. The UPR is a signalling pathway that maintains the balance of protein folding and is activated in response to accumulation of unfolded or misfolded proteins in the ER which increases the load on the molecules responsible for protein folding [340]. It works through pro-survival mechanisms including lowering the number of proteins that need to be folded by transcriptional downregulation of secretory proteins, increasing the folding ability of the ER or increasing the removal of misfolded or slowly folding proteins via stimulating another process known as ER-associated degradation [339, 341].

As shown in **Figure 1.9**, the UPR in mammalian cells is mediated via three ER transmembrane proteins: inositol-requiring enzyme 1 α (IRE1 α), protein kinase R-like ER kinase (PERK) and activating transcription factor 6 (ATF6) [342, 343]. IRE1 α is the most conserved UPR protein among different species. It is a kinase and endonuclease that, in response to the release and dissociation of the ER chaperone, 78kDa glucose-related protein (GRP78) also known as binding immunoglobulin protein (BiP), dimerizes and undergoes autophosphorylation and becomes activated to stimulate the UPR [344]. Active IRE1 α induces the splicing of transcription factor X box-binding protein 1 (XBP1) encoding mRNA by excising a 26-nucleotide-long intron, resulting in the expression of the active transcription factor, spliced XBP1 (XBP1s), which translocates to the nucleus to induce the transcriptional upregulation of UPR target genes, folding enzymes and ER chaperones that correct for protein misfolding [345]. Subsequently PERK is activated to inhibit protein synthesis and reduce the number of proteins that need to be folded through the phosphorylation of eukaryotic translation initiator factor 2 α (eIF2 α), which in turn induces the

translation of another transcription factor, ATF4, which controls the transcription of genes involved in redox balance, autophagy and apoptosis [346, 347]. ATF6 is also activated during the UPR by being transported to the Golgi where it undergoes proteolytic cleavage by S1 and S2 proteases and subsequent translocation to the nucleus to activate transcription of target genes that promote the UPR [348].

The UPR components are not only involved in the ER stress response, but also regulate several cellular functions such as energy homeostasis, lipid metabolism, inflammation and cell differentiation [349]. IRE1 α also plays an indirect role in calcium homeostasis through regulating its release from ER via the IP3R [350]. Calcium release through the IP3R is inhibited by calcium and integrin binding protein 1 (CIB1) [351]. However, CIB1-IP3R interaction is inhibited by another adaptor molecule, apoptosis signal-regulating kinase 1 (ASK1), that dissociates CIB1 from the IP3R, resulting in induction of calcium release from the ER [352]. IRE1 α , on the other hand, acts as a negative regulator for ASK1 as it reduces its interaction with CIB1, resulting in enhancing CIB1-mediated inhibition of calcium release and preventing calcium overload [353].

Overactivation or failure of the UPR to reduce ER stress and restore homeostasis will result in induction of cellular dysfunction and apoptosis. Therefore, ER stress plays a critical role in the development of different disease conditions, particularly cardiovascular diseases [354]. It is considered one of the pathophysiological characteristics involved in the development of cardiac hypertrophy and heart failure [355]. Maladaptive, prolonged ER stress triggers apoptosis through activation of C/EBP homologous protein (CHOP) as well as JNK and the caspase cascade to eliminate unhealthy cells and their accumulated misfolded proteins, which signifies the transition from an adaptive to a maladaptive response or from cell survival to cell death [356-359].

1.4.5.4. ER stress-mediated cell death

A persistent ER stress response means that the UPR signal is not enough to correct for protein misfolding [360]. This in turn induces a maladaptive response, which involves induction of different apoptotic pathways that are triggered by the UPR components following either loss of the UPR proteins or overactivation of them in an attempt to resolve the persistent ER stress response (see **Figure 1.9**) [356, 357]. Therefore, both overexpression and reduction in the UPR proteins can lead to induction of ER stress-mediated cell death. Maintaining their balance is critical for pro-survival mechanisms. One of these cell death pathways is the IRE1 α /XBP1s-mediated activation of the JNK/p38 MAPK pathway [361]. IRE1 α , upon prolonged ER stress, can recruit an adaptor molecule called TNF-receptor-associated factor 2 and ASK1 to form a complex that induces the activation of JNK/p38 MAPK [362]. Subsequently, JNK and p38 MAPK suppress the anti-apoptotic activity of Bcl-2 and activate other pro-apoptotic proteins such as Bax and Bak [363].

Another important pathway involves enhanced CHOP expression. CHOP signalling is dependent on PERK activation and the induction of ATF4 translation [364]. CHOP transcriptional upregulation can be triggered by IRE1 α -mediated XBP1s splicing [365], while p38 MAPK increases its activity by post-translational phosphorylation to mediate apoptosis [366]. CHOP can induce apoptosis via several pathways. For instance, as a transcription factor, CHOP can act as either a transcriptional activator or repressor. It inhibits the transcription of the anti-apoptotic Bcl-2 and Bcl-XL and upregulates pro-apoptotic Bax and Bak, allowing their translocation from the cytosol to mitochondria to induce cytochrome C release that eventually activates the caspase cascade, particularly caspases-3, -9 and -12, to induce apoptosis [367, 368]. CHOP can also trigger

apoptosis by upregulating tribbles homolog 3 that inhibits the anti-apoptotic activity of Akt, resulting in greater activation of caspase-3 [369, 370].

Studies demonstrated that impaired UPR signalling can also trigger ER stress-mediated cell death. In mice with alcohol-induced pancreatic damage, XBP1 deficiency resulted in CHOP upregulation and induction of apoptosis. Counter-adaptive activation of PERK, in response to XBP1 deficiency, was suggested to be the cause of CHOP upregulation [371]. Another study showed that inactivation of IRE1 α induces CHOP upregulation and disrupts calcium homeostasis leading to cell death [353]. In a mouse model of type-1 diabetes, loss of ATF6 was shown to induce beta cell death [372].

ER stress-mediated apoptosis also plays a role in cardiac diseases. Myocardial CHOP mRNA expression was found to be higher in patients with heart failure and in mice undergoing transaortic constriction. CHOP knockout improved cardiac function and attenuated the extent of cardiac hypertrophy and fibrosis [373]. Similarly, mice with dilated cardiomyopathy exhibited increased CHOP expression and aggregation of misfolded proteins that resulted in apoptosis [374]. ASK1 knockout mice also showed protection against cardiac dysfunction and apoptosis following transaortic constriction [375]. Therefore, preserving balance in the UPR and preventing the progression into maladaptive cell death during the ER stress response is critical for maintaining proper cardiac function and protecting against cardiac disease. That is why pharmacological agents modulating the UPR showed promising effects in the treatment of cardiovascular disease. An eIF2 α phosphatase inhibitor showed protection against ER stress-mediated cardiac apoptosis in a rat model of myocardial infarction [376]. Administration of 4-phenylbutyric acid, a chemical chaperone that inhibits ER stress, showed efficacy in protecting against apoptosis and pressure overload-induced cardiac hypertrophy in mice [377]. Ginkgolide K, a biologically active lactone,

protected against cardiomyocyte death in response to ER stress stimuli both *in vivo* and *in vitro* by selectively activating the IRE1 α /XBP1 pathway and inhibiting JNK activation [378].

1.4.5.5. ER stress and the UPR in IR injury

ER stress and the UPR have been implicated in ischemic heart disease. Ischemia, particularly the lack of oxygen, impairs protein folding in the ER which in turn activates the UPR [379, 380]. Moreover, as protein folding depends on redox homeostasis, oxidative stress and RONS production can alter the redox status in the ER and trigger protein misfolding that induces ER stress [381, 382].

Cultured cardiomyocytes subjected to oxygen and glucose deprivation exhibited an early induction in GRP78, XBP1 splicing and eIF2 α activation indicating the induction of the UPR. However, prolonged stress resulted in upregulation of CHOP and propagation of apoptotic signalling [383]. GRP78 expression was also increased in cardiomyocytes from the hearts of mice subjected to permanent myocardial infarction induced by left anterior descending coronary artery ligation [380]. In mouse hearts subjected to *in vivo* IR, XBP1 splicing, eIF2 α activation and increased expression of CHOP were observed early during reperfusion [384]. These studies suggest that although activation of the UPR is essential to protect against ER stress-mediated cellular damage during ischemia/hypoxia, prolonged ischemia with a persistent ER stress response can trigger myocardial apoptotic cell death (see [385] for review). Therefore, keeping the balance of the UPR components is critical for cell survival during ischemia and IR injury. ER stress can also activate other cellular components such as inflammasomes, which in turn aggravate cardiac damage in response to myocardial IR injury [386].

The protective role of IRE1 α /XBP1 was reported in studies with myocardial IR injury. Cardiac-specific knockout of XBP1 in mouse hearts subjected to *in vitro* IR injury showed profound impairment of cardiac contractile function and an increase in infarct size, while its induced expression caused the opposite [387]. Similarly, cardiac-specific expression of active ATF6 also showed better functional recovery and reduced apoptosis following *in vitro* IR injury [388]. Meanwhile, CHOP-deficient mice showed protection against myocardial damage following *in vivo* IR injury [384]. Chemical inhibition of the ER stress response during *in vitro* IR with 4-phenylbutyric acid improved cardiac post-ischemic contractile recovery, attenuated myocardial apoptosis and reduced the expression of ER stress and pro-apoptotic proteins [389]. This suggests that modulating UPR proteins and their downstream signalling pathways could be a potential therapeutic target to protect against myocardial IR injury.

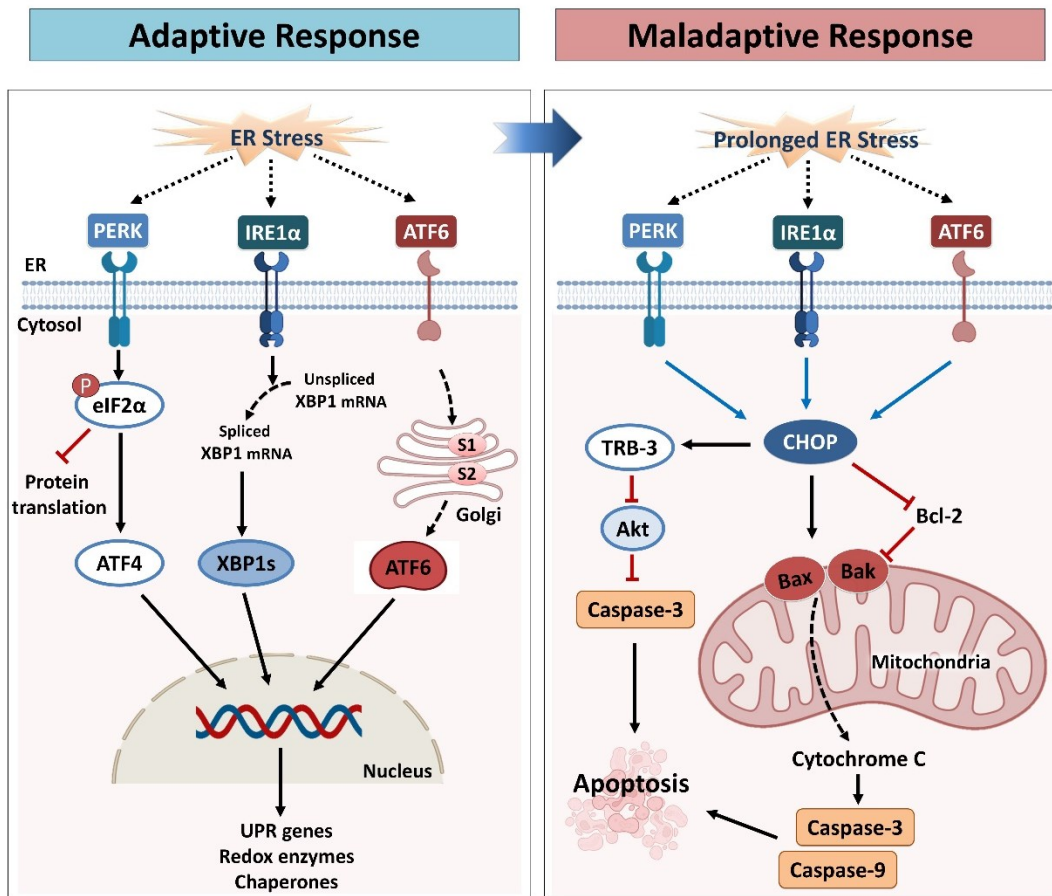


Figure 1.9. Adaptive and maladaptive signalling pathways in the unfolded protein response (UPR). ER stress triggers the UPR to correct for protein misfolding. The UPR is mediated via three ER transmembrane proteins: IRE1 α , PERK and ATF6. IRE1 α dimerizes, undergoes autophosphorylation and induces the splicing of XBP1 encoding mRNA, resulting in the expression of XBP1s that induces transcriptional upregulation of UPR target genes. PERK induces phosphorylation of eIF2 α which inhibits protein synthesis and stimulates expression of ATF4, that controls the transcription of genes involved in redox balance. Finally, ATF6 translocates to the Golgi, undergoes proteolytic cleavage by S1 and S2 proteases and translocates to the nucleus to promote transcription of UPR genes. Prolonged, unresolved ER stress results in the transition from an adaptive to a maladaptive response via CHOP-mediated TRB3 upregulation that inhibits Akt activity and induces more activation of caspase-3. CHOP also transcriptionally inhibits Bcl-2 and upregulates Bax and Bak to be translocated to mitochondria and in turn induce cytochrome C release, and activate caspases-3 and -9 to induce apoptosis. Akt, protein kinase B; ATF, activating transcription factor; Bak, Bcl-2 homologous antagonist/killer; Bax, Bcl-2-associated X protein; Bcl, B-cell lymphoma; CHOP, C/EBP homologous protein; eIF2 α , eukaryotic translation initiator factor 2 α ; ER, endoplasmic reticulum; IRE1 α , inositol-requiring enzyme 1 α ; PERK, protein kinase R-like ER kinase; TRB3, tribbles homolog 3; UPR, unfolded protein response; XBP, X box-binding protein (Figure was created using BioRender).

1.5. Sarcoplasmic reticulum/T-tubule junction

In cardiac muscle, transverse or T-tubules are invaginations in the cell membrane occurring at the Z-line of sarcomere and make contact with the SR at junctions called “dyads” [390]. The cardiac dyad is a specialized signalling nexus whose main function is the initiation of cardiac contraction [391]. This structural organization allows the connection between the voltage-gated L-type calcium channels in the T-tubule membrane and type 2 ryanodine receptors in the SR, which is required for excitation-contraction coupling [392].

1.5.1. Role of the SR-T-tubule junction in cardiac excitation-contraction coupling

Cardiac excitation-contraction coupling refers to the process of transforming the electrical stimulation of myocytes into muscle contraction [334]. T-tubules and SR play a significant role in this process through the dyads [393]. Type 2 ryanodine receptors are the predominant ryanodine receptor isoform in cardiac muscle. They are homo-tetrameric ion channels, possessing a cytoplasmic domain that contains binding sites for different cytoplasmic regulators including calcium and ATP. Cytoplasmic calcium is considered the most important activator of type 2 ryanodine receptors in cardiac cells [393, 394].

As shown in **Figure 1.10**, upon depolarization, the action potential passes across the T-tubules and stimulates the opening of voltage-gated L-type calcium channels to induce calcium influx into the cell. This increased intracellular calcium triggers type 2 ryanodine receptors to release a larger amount of calcium from the SR into the cytosol, known as the calcium spark. This process is referred to as calcium-induced calcium release [391, 395]. Calcium in turn binds to cardiac troponin resulting in sliding of the thin and thick myofilaments and cell shortening to induce cardiac contraction [396]. For relaxation, after calcium is released, it is recycled to the SR

by the action of SERCA2a to replenish its stores or is transported outside the cell by the action of $\text{Na}^+/\text{Ca}^{2+}$ exchanger and plasma membrane Ca^{2+} ATPase, resulting in a reduction in cytosolic calcium which in turn triggers cardiac relaxation [397, 398].

1.5.2. SR-T-tubule junctional alterations in heart disease

Impairment of T-tubule and junctional SR organization is reported in cardiac diseases and the distortion of their interaction, referred to as dyadic degradation, is widely described and contributes to impaired cardiac contractility [399, 400]. It is well-established that, in cardiac hypertrophy and heart failure, the defective calcium transient is directly linked to the reduction in excitation-contraction coupling and disorganized dyad architecture [401]. In patients with dilated or ischemic cardiomyopathy, the T-tubule-SR junctional interaction was reduced as evidenced by the loss in volume density and surface area of both T-tubules and junctional SR [402]. T-tubule remodeling is one of the manifestations accompanying the progression from cardiac hypertrophy into heart failure [403]. Tachycardia pacing-induced heart failure *in vivo* also showed a reduction in T-tubule and L-type calcium channel densities in the ventricular myocytes isolated from these failed hearts [404]. Ventricular myocytes from spontaneously hypertensive rats exhibited an increased T-tubule distortion from the Z-line with a reduction in their ability to induce calcium release from the SR leaving behind what is termed as “orphaned” ryanodine receptors that lead to a loss in calcium spark synchronization and impaired cardiac contractility [405]. Besides, in failing hearts, T-tubule folding was deranged along with reduced numbers and electrophysiological activities of the L-type calcium channels [406]. Therefore T-tubular dysfunction is considered a major contributing factor to cardiac contractile dysfunction and heart failure [407].

Impaired ryanodine receptor activity and disorganized SR structure is another characteristic of cardiac abnormalities. In cardiomyocytes isolated from rats with myocardial

infarction, disorganized type 2 ryanodine receptor clusters and slower calcium release were observed, along with a reduced number of ryanodine receptors per cluster [408]. In cardiomyocytes from failing human hearts, impaired calcium handling, characterized by a diminished calcium transient and slower decay, as well as reduced calcium uptake into SR stores, were reported [409]. In hearts from mice with ventricular arrhythmias, impaired calcium handling was associated with structural remodeling of the junctional SR, reduced T-tubule-SR contact sites and decreased type 2 ryanodine receptor protein expression [410]. Therefore, preserving dyad architecture and the T-tubule-SR interaction is critical for proper cardiac function. Any stimulus that disrupts this interaction would result in impaired calcium handling and cardiac contractile dysfunction.

1.5.3. Junctophilin-2 and its role in cardiac contractility

1.5.3.1. JPH-2 structure, localization and function

Junctophilins are a family of junctional membrane proteins which anchor the T-tubules to the terminal cisternae of the SR [411, 412]. JPH-2 was identified by Takeshima et al. as the predominant isoform expressed in cardiomyocytes [411]. It is localized in close proximity to the Z-disc region of the sarcomere where MMP-2 is also localized [59], as well as type 2 ryanodine receptors [413]. Being required for T-tubule-SR interaction, JPH-2 is essential for excitation-contraction coupling, calcium transients from/to SR and cardiac contractility [414].

JPH-2 has a peculiar structure that allows its interaction with the T-tubules and the junctional SR across the dyad [411]. It possesses eight highly conserved, lipophilic membrane occupation and recognition nexus (MORN) domains at its N-terminus that are associated with the T-tubule membrane, with a joining region separating the first six from the last two domains. The MORN repeats are followed by an α -helix that composes most of the dyadic junctional space and maintain the ideal space between the L-type calcium channels in the T-tubule sarcolemma and

type 2 ryanodine receptors in the SR. Adjacent to the α -helix, there is a divergent region which has a specific structure for JPH-2 isoform and is highly conserved among the different species. Finally, its C-terminus ends with a transmembrane domain that is embedded in the SR [411, 415, 416].

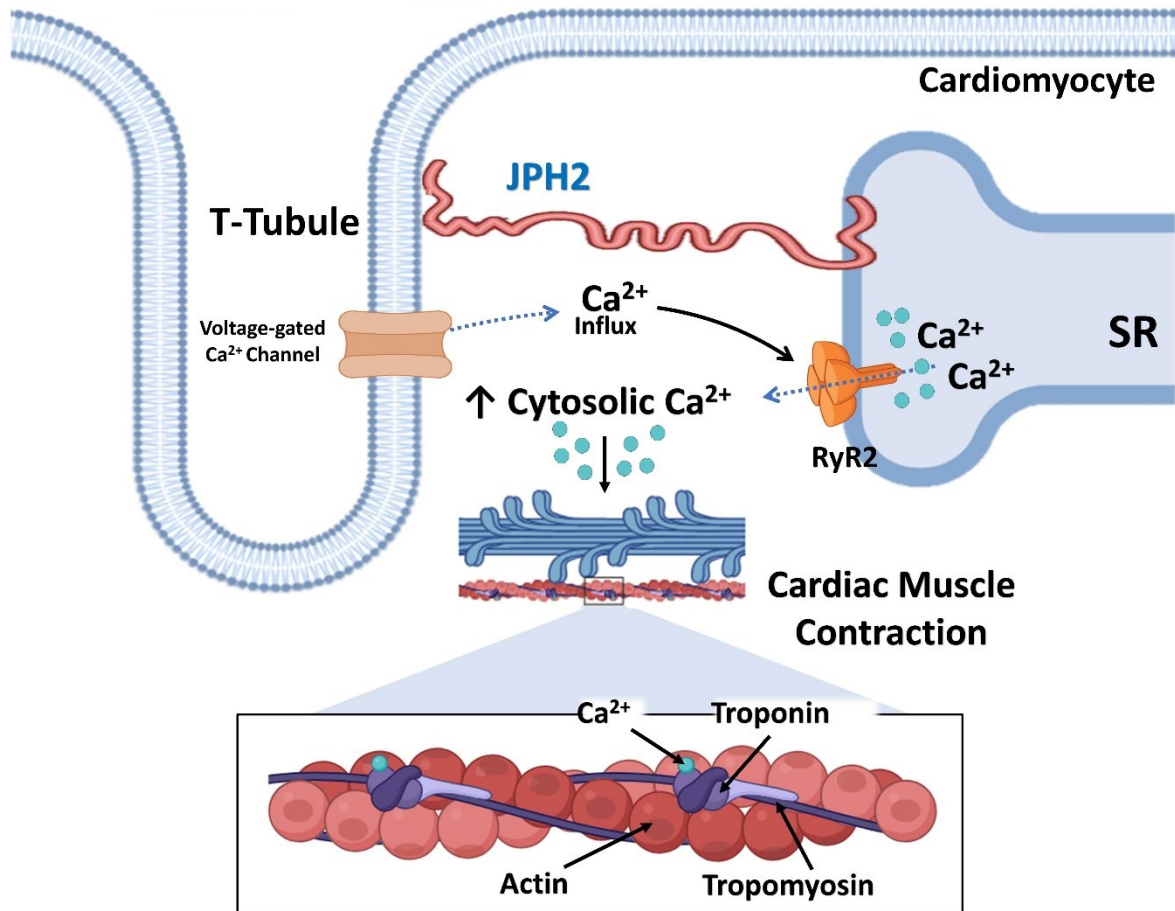


Figure 1.10. Mechanism of cardiac excitation-contraction coupling. Upon depolarization, the action potential propagates across the T-tubules and stimulates the voltage gated Ca^{2+} channels to open and induce Ca^{2+} influx, which in turn triggers Ca^{2+} -induced Ca^{2+} release from the SR via the RyR2, resulting in increased intracellular Ca^{2+} concentration. Ca^{2+} in turn binds to cardiac troponin to induce actin-myosin interaction and cardiac muscle contraction. JPH-2 anchors the T-tubule to the SR to stabilize the excitation-contraction coupling process. JPH-2, junctophilin-2; RyR2, type-2 ryanodine receptor; SR, sarcoplasmic reticulum (*Figure was created using BioRender*).

1.5.3.2. Effect of JPH-2 loss on cardiac contractile function

Loss of JPH-2 is known to disrupt the junctional interaction between T-tubules and the SR, which in turn impairs excitation-contraction coupling, reduces calcium-induced calcium release from the SR and eventually results in cardiac contractile dysfunction (**Figure 1.10**) [416]. This was evidenced in JPH-2 null mice which are embryonically lethal and exhibited irregular calcium transient and structural uncoupling between the dyad components [411]. Loss of JPH-2 is reported in different cardiac disease conditions including hypertrophic cardiomyopathy [417], dilated cardiomyopathy [418], and myocardial IR injury [70]. It was also observed during the progression from cardiac hypertrophy into heart failure in rats subjected to thoracic aortic banding and is implicated as an early event during the compensatory remodeling preceding the induction of heart failure [403]. This reduction in JPH-2 has been linked to the alteration in calcium homeostasis and impaired excitation-contraction coupling [417], as well as the disrupted junctional membrane complexes [419]. Following myocardial infarction, loss of JPH-2 and its reduced co-localization with type 2 ryanodine receptors were observed using live cell imaging microscopy [420].

Cardiac-specific knockout of JPH-2 in mouse hearts resulted in impaired T-tubule maturation and cardiac dysfunction [421, 422]. Although reported in limited cases, three JPH-2 mutations were identified in some individuals with hypertrophic cardiomyopathy at the N-terminus, the first MORN motif domain and the linker domain. These mutations were found to reduce calcium-induced calcium release in cardiomyocytes [423]. Two additional mutations were identified later in the linker region and the α -helical domain [424]. Taken together, preserving cardiac JPH-2 is critical for maintaining adequate contractile function and preventing the progression into disease conditions.

1.5.4. Impairment of excitation-contraction coupling and T-tubule distortion during DXR cardiotoxicity

DXR-induced cardiotoxicity is associated with T-tubule remodeling and impaired excitation-contraction coupling. DXR treatment in mice induced alterations in calcium handling as evidenced by the early reduction in calcium transient amplitude and its slower decay rate at 2 weeks of treatment preceding a late reduction in the SR calcium load [425]. In cardiomyocytes isolated from guinea pig hearts, DXR reduced calcium-induced calcium release from the SR [426]. This reduction in intracellular calcium is usually preceded by a transitory increase in calcium spark resulting from increased calcium leak from the SR as a compensation. However, with prolonged DXR treatment, intracellular calcium is reduced due to depletion of the SR calcium stores and reduced SERCA2a expression [425]. This means that the effect of DXR on calcium release from the SR is biphasic [427].

In hearts from rats treated with DXR, disrupted T-tubule organization was observed which, in part, contributed to the resulting left ventricular dysfunction [428]. DXR cardiotoxicity was also suggested to be associated with a reduction in T-tubule density and whole cell capacitance, which determines how fast the membrane potential responds to changes in current [429]. Transmission electron microscopy of cardiac tissues obtained from rats treated with DXR for 4 weeks revealed 30% reduction in T-tubule-SR junctional length and increased dyadic cleft distance, accompanied by a reduction in JPH-2 protein level [430]. DXR is also reported to decrease type 2 ryanodine receptor mRNA expression in cardiomyocytes, regardless of the changes in their activity [431, 432]. Collectively, this suggests a pivotal role of T-tubule-SR interaction, as well as the junctional calcium handling proteins, in the pathophysiology of DXR cardiotoxicity, which could be a

potential therapeutic target to protect against cardiac dysfunction accompanying anthracycline treatment.

1.5.5. MMP-2 association with T-tubule-SR junction and calcium transient

As mentioned earlier, MMP-2 was found in SR-enriched microsomes from cardiomyocytes where it induces degradation of SERCA2a, suggesting that MMP-2 may affect cardiac excitation-contraction coupling [69]. It was also found to target and cleave JPH-2 during myocardial IR injury [70]. MMP-2_{NTT76} is localized in discrete clusters along the Z-line of the sarcomere, which reflects its association with the T-tubules. Its cardiac-specific expression resulted in impaired calcium transient in cardiomyocytes [64]. Given the importance of cardiac dyad and excitation-contraction coupling in the pathophysiology of DXR cardiotoxicity, MMP-2, activated by DXR, may play a role in the disrupted T-tubule-SR organization, contributing to the resulting cardiac contractile dysfunction.

1.6. Thesis overview

1.6.1. Rationale

Since discovering the intracellular role of MMP-2 and how it contributes to the pathophysiology of several disorders, most previous studies have focused on investigating its role in the cytosol and the cardiac sarcomere. However, one of the important intercellular locales of MMP-2 is the interface between ER and mitochondria, known as the MAM. The role played by MMP-2 at this interface and how it affects mitochondrial and ER functions in pathology is not well investigated.

Both mitochondria and ER play significant roles in the regulation of several cellular processes and functions including cell death and survival, energy homeostasis and calcium regulation. In the present thesis, I focus on four main cellular processes regulated by the mitochondria or ER, particularly involved in the regulation of cardiac contractile function and myocardial cell death. These regulatory processes include: (a) the role of mitochondria in regulation of apoptotic cell death via the release and processing of AIF, (b) mitochondrial respiratory function and how the mitochondrial fusion protein Mfn-2 is affected during mitochondrial dysfunction, caused by oxidative stress during IR injury, that impairs ATP production and induces the inflammasome response, (c) the changes in ER homeostasis during cardiac injury, and how ER stress and the UPR contribute to the progression of myocardial cell death and, finally, (d) T-tubule-SR interaction which regulates the intracellular calcium level and the role of the junctional protein, JPH-2, in this process.

Using different cell and animal models, including STS-induced cytotoxicity in human fibrosarcoma (HT1080) cells, an *in vitro* mouse model of myocardial IR injury and an *in vivo*

mouse model of DXR-induced cytotoxicity, I investigate the role of MMP-2, activated in response to oxidative stress, in these cellular processes regulated by mitochondria and/or ER and how this contributes to the development of pathologies of cardiac diseases related to enhanced oxidative stress.

1.6.2. Overall hypothesis

I hypothesize that MMP-2, activated in response to oxidative stress, disrupts the regulation of mitochondrial function, ER homeostasis and T-tubule-SR interaction, by targeting and proteolyzing specific mitochondrial and ER/SR proteins localized at or near the MAM. This in turn results in impairment of the cellular processes and functions regulated by these subcellular organelles and induction of cell death pathways, leading to the development of pathological conditions including cardiac diseases. Therefore, inhibition of MMP-2 activity could be a potential therapeutic option to protect against such cellular dysfunction by preserving those targeted proteins at the MAM from proteolytic degradation.

1.6.3. Thesis objectives

1.6.3.1. Staurosporine-induced cleavage of apoptosis-inducing factor in human fibrosarcoma cells is independent of matrix metalloproteinase-2 (Chapter 3)

Mitochondrial AIF is cleaved and released into the cytosol in response to cellular stressors. As MMP-2 is localized to the MAM, I hypothesize that MMP-2 may exert a role in the processing and cleavage of AIF during STS-induced cytotoxicity. Using a human fibrosarcoma cell line I investigated whether:

- a) MMP-2 is activated during STS-induced cytotoxicity, and
- b) STS-induced cleavage and release of AIF is MMP-2-dependent

1.6.3.2. Matrix metalloproteinase-2 proteolyzes mitofusin-2 and impairs mitochondrial function during myocardial ischemia-reperfusion injury (Chapter 4)

During myocardial IR injury, MMP-2 is rapidly activated in response to oxidative stress. Oxidative stress also impairs mitochondrial function which is regulated by different proteins including Mfn-2 and induces the NLRP3 inflammasome. I hypothesize that MMP-2 proteolyzes Mfn-2 during IR injury and impairs mitochondrial function which contributes to contractile dysfunction. Using the *in vitro* mouse model of cardiac IR injury I investigated:

- a) the role of MMP-2 in mitochondrial dysfunction during IR injury,
- b) the role of MMP-2 in the inflammasome response during IR injury, and
- c) identified a potential mitochondrial proteolytic target of MMP-2

1.6.3.3. Matrix metalloproteinase-2 inhibition attenuates ER stress-mediated cell death during myocardial ischemia-reperfusion injury by preserving IRE1 α (Chapter 5)

ER stress is one of the major events accompanying myocardial IR injury. In response to ER stress, the UPR is activated through the stress sensor IRE1 α to restore protein folding. Failure of the UPR to reduce ER stress induces cellular dysfunction and apoptosis. As MMP-2 localizes to the MAM, I hypothesize that it proteolyzes IRE1 α during IR injury and stimulates the apoptotic response. Using the *in vitro* mouse model of cardiac IR injury I determined:

- a) the role of MMP-2 in ER stress and the UPR during IR injury,
- b) the role of MMP-2 in ER stress-mediated cell death during IR injury, and
- c) identified a potential proteolytic target of MMP-2 in the ER

1.6.3.4. Junctophilin-2 proteolysis and T-tubule remodeling are consequences of matrix metalloproteinase-2 activation during doxorubicin-induced cardiotoxicity (Chapter 6)

JPH-2 is reported to be a target of MMP-2 during IR injury in isolated hearts and both MMP-2 and JPH-2 colocalize at the Z-disk of the cardiac sarcomere. Loss of JPH-2 is also known to disrupt the T-tubule-SR interaction. I hypothesize that MMP-2 cleaves JPH-2 during DXR-cardiotoxicity resulting in T-tubule remodeling and cardiac contractile dysfunction. Using an *in vivo* mouse model of DXR-induced cardiotoxicity I:

- a) investigated whether JPH-2 is a proteolytic target of MMP-2,
- b) explored the effect of MMP-2 activation on T-tubule remodeling, and
- c) in neonatal rat ventricular cardiomyocytes treated with DXR, I investigated the role of MMP-2 in DXR-mediated changes in cytosolic calcium level

The overall goal is to fill in the gaps in our knowledge and provide a better understanding of the pathophysiological role of intracellular MMP-2 in cardiac pathologies, in order to provide a new therapeutic option to protect the heart with a potentially higher treatment success rate.

Chapter II

General Methods

This chapter contains detailed common methods used in several of the following study chapters (**III, IV, V, VI and appendix**). Methods used only for a particular study will be included in its specific chapter.

2.1. Animals

All animal studies were carried out using 3- 4 month-old male C57BL/6J mice weighing 25- 30 g. Mice were fed on a standard rodent chow diet ad libitum (fat 11.3%, fiber 4.6%, protein 21% w/w) and housed under conditions of constant temperature and humidity with a 12:12 h light-dark cycle. All animal experimental protocols were approved by the University of Alberta Health Sciences Welfare Committee (University of Alberta Animal Welfare, ACUC, study ID #AUP329, and AUP330) and conducted according to guidelines provided by the Guide to the Care and Use of Experimental Animals.

2.2. Isolated heart perfusion

Male C57BL/6J mice were anesthetized by an intraperitoneal injection of sodium pentobarbital (100 mg/kg). Following complete non-responsiveness to external stimuli, hearts were quickly excised and perfused *in vitro* at a constant pressure of 40 cmH₂O at 37°C in the Langendorff mode with Krebs–Henseleit solution (120 mM NaCl, 25 mM NaHCO₃, 10 mM dextrose, 1.75 mM CaCl₂, 1.2 mM MgSO₄, 1.2 mM KH₂PO₄, 4.7 mM KCl and 2 mM sodium pyruvate, pH 7.4) continuously aerated with 95% O₂ and 5% CO₂. The left atrium was then excised, and a pre-calibrated water-filled balloon made of polyvinylidene chloride (Saran[®]) wrap was inserted into the left ventricle through the mitral valve. The balloon was connected to a pressure transducer to measure the left ventricular developed pressure (LVDP) and heart rate (HR). Hearts with persistent arrhythmias, LVDP <80 cmH₂O, HR <300 min⁻¹, coronary flow <2 or >4

mL/min or time from excision to perfusion >2 min were excluded from the experiment. Following 40 min of baseline aerobic perfusion, hearts were subjected to 30 min of global, no-flow ischemia followed by 40 min of reperfusion and compared to hearts perfused aerobically for the same duration as controls. At the end of reperfusion, hearts were collected, the right atrium and aorta were cut off and the ventricles were kept, flash frozen in liquid nitrogen and stored at -80°C to be used later for preparation of ventricular extracts. To assess the changes in post-ischemic recovery of contractile function, cardiac contractile parameters including LVDP, HR, rates of contraction (dP/dt_{max}) and relaxation (dP/dt_{min}) were recorded and analyzed using ADI software (Holliston, MA, USA).

To test the effect of MMP-2 preferring inhibitors on cardiac post-ischemic recovery, mouse hearts were perfused with Krebs–Henseleit solution to which either ARP-100 (10 μ M, Cat#13321, Cayman Chemical), ONO-4817 (50 μ M, a gift from Ono Pharmaceutical, Osaka, Japan) or dimethyl sulfoxide (DMSO, vehicle, 0.1% v/v) were included, beginning 10 min prior to ischemia. This was done by replacing the Krebs–Henseleit solution in the fluid reservoir with another one containing the dissolved drug or vehicle. As the drugs or their vehicle were dissolved directly into the Krebs–Henseleit solution, the hearts were exposed to them also during the entire reperfusion phase. ARP-100 and ONO-4817 are MMP-2 preferring inhibitors with higher selectivity for MMP-2. The selectivity profile for ONO-4817 against MMPs in guinea pig joint cartilage is as follows: MMP-12 > -2 > -8 = -13 > -9 > -3 > -7 with inhibitory binding constant (K_i) values of 0.45, 0.73, 1.1, 1.1, 2.1, 42 and 2,500 nM respectively. The selectivity profile for ARP-100 against MMPs in HT1080 human fibrosarcoma cells is as follows: MMP-2 > -9 > -3 > -1 and -7 with IC_{50} values of 12, 200, 4,500, >50,000 and >50,000 nM respectively [94, 95]. The effect of the MMP-2 inhibitors on cardiac mechanical function was also evaluated under aerobic perfusion conditions in absence

of IR injury for the duration of the experiment. The experimental protocol for the different groups is shown in **Figure 2.1**.

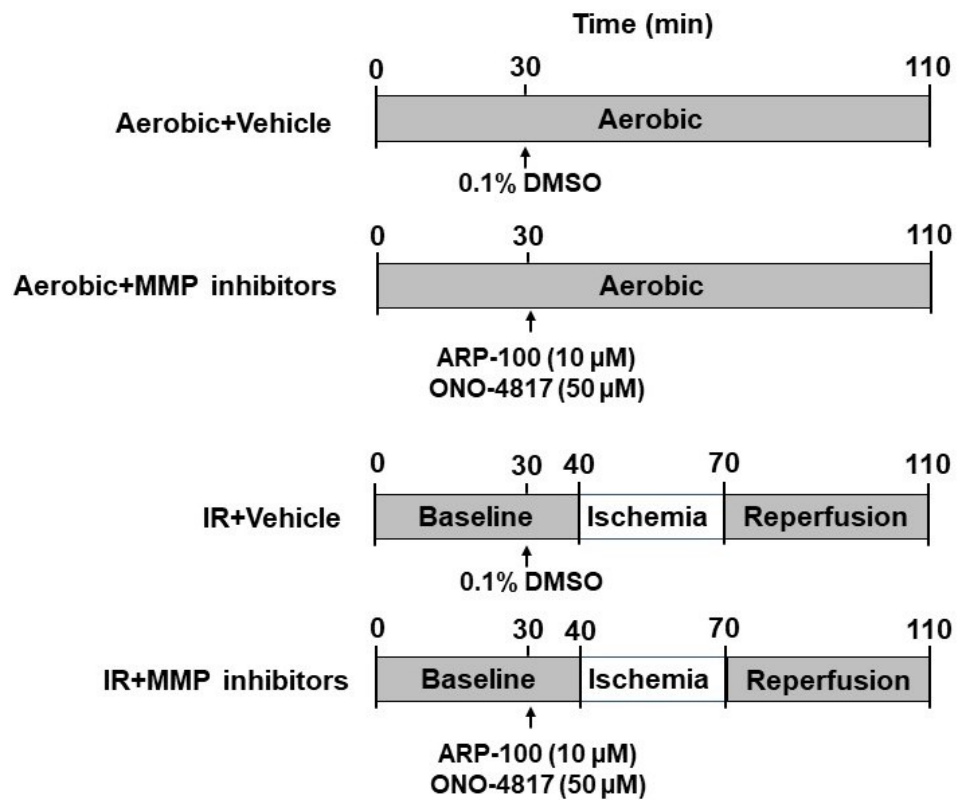


Figure 2.1. Schematic diagram of the experimental protocol of ischemia-reperfusion (IR) injury and the groups of isolated perfused mouse hearts.

2.3. Preparation of cellular or tissue extracts and subcellular fractionation

Frozen heart ventricles from the perfused mouse hearts were ground to a fine powder using a mortar and pestle cooled by liquid nitrogen and divided into three to four portions. To obtain a ventricular homogenate, one portion of the powdered heart ventricle was homogenized in ice cold radioimmunoprecipitation assay (RIPA) buffer (25 mM Tris-HCl, 150 mM NaCl, 1% w/v NP-40, 1% w/v sodium deoxycholate, 0.1% w/v sodium dodecyl sulfate (SDS), pH 7.6, 0.1% v/v proteinase inhibitor cocktail; Cat#P8340, Sigma-Aldrich) using a Dounce glass homogenizer (PYREX™) with 10-15 up and down strokes at 4°C, followed by centrifugation at 10,000 g for 10 min at 4°C to remove tissue debris. The supernatant was collected as ventricular homogenate, flash frozen in liquid nitrogen, and stored at -80°C. To obtain cellular lysate from human fibrosarcoma HT1080 cells or neonatal rat ventricular cardiomyocytes, the cells were lysed by rinsing twice with phosphate buffered saline (PBS) and incubating with RIPA buffer for 5 min at 4°C followed by scraping the lysed cells using 1.8 cm blade cell scraper (Falcon™). Lysed cells were then centrifuged at 10,000 g for 10 min at 4°C and the supernatant was kept as the cellular lysate.

To obtain cytosolic and mitochondria-enriched fractions from ground heart tissue, powdered heart ventricle was subjected to subcellular fractionation as previously described [433]. Ground tissue was homogenized in ice-cold homogenization buffer (20 mM Tris-HCl, 50 mM NaCl, 50 mM NaF, 5 mM sodium pyrophosphate, and 250 mM sucrose added on the day of the experiment, pH 7.0) using a Dounce glass homogenizer (PYREX™) with 10-15 up and down strokes at 4°C. Homogenized samples were centrifuged at 800 g for 10 min at 4°C to remove cellular debris. The supernatant was collected and centrifuged at 10,000 g for 20 min at 4°C. The pellet was resuspended in homogenization buffer to obtain the mitochondria-enriched fraction and the supernatant was ultra-centrifuged at 105,000 g for 60 min at 4°C. The subsequent supernatant

was used as the cytosolic fraction. The same procedure was used to obtain subcellular fractions from cell lysates obtained from human fibrosarcoma HT1080 cells or neonatal rat ventricular cardiomyocytes.

2.4. Measuring protein concentration

Protein concentrations in ventricular extracts or cellular lysates were measured using the bicinchoninic acid (BCA) assay. Samples were diluted in Milli-Q H₂O at a ratio of 1:2 for cellular lysates or 1:10 for ventricular extracts (ventricular homogenate or subcellular fraction) and 10 μ L were loaded per well in a clear, flat-bottom, polystyrene 96-well plate. Bovine serum albumin (BSA, ThermoFisher Scientific), diluted in H₂O, was used as a standard to generate a calibration curve with concentrations (31.25-1000 μ g/mL) of which 10 μ L were loaded per well. Then BCA solution (PierceTM BCA protein assay reagent A, ThermoFisher Scientific) was mixed with copper (II) sulfate solution (PierceTM BCA protein assay reagent B, ThermoFisher Scientific) at a ratio of 1:50, and 200 μ L of the reaction mixture was added to each well followed by incubation at 37°C for 30 min. Absorbance at 420 nm was measured using a UV_{max} kinetic microplate reader (Molecular Devices, San Jose, CA) and data was analyzed using SoftMax Pro (v 5.2C).

2.5. Gelatin zymography

To measure MMP-2 activity in cellular lysates, ventricular homogenates or subcellular fractions, the desired amount of protein in each sample was mixed in 6x non-reducing loading buffer (0.5 M Tris-HCl pH 6.8, 30% v/v glycerol, 10% w/v SDS, and 0.012% w/v bromophenol blue), and then separated on 8% polyacrylamide gels (see **Tables 2.1 and 2.2** for gel preparation details) co-polymerized with 2 mg/mL porcine gelatin (Cat#G8150, Sigma–Aldrich) by electrophoresis at 90 V for 2 h. The gels were then rinsed three times (20 min each) in 2.5% v/v

Triton X-100 in H₂O with gentle agitation to neutralize the SDS. The gels were then incubated in zymographic activity buffer (50 mM Tris-HCl, 150 mM NaCl, 5 mM CaCl₂·2H₂O, and 0.05% w/v NaN₃, pH 7.6) for 24- 48 h at 37°C. Subsequently gels were stained with Coomassie zymography staining solution (0.05% w/v Coomassie Brilliant Blue G-250, 25% v/v methanol, 10% v/v acetic acid) overnight followed by destaining three times (30 min each) in 4% v/v methanol and 8% v/v acetic acid solution. The gels were scanned using GS-800 densitometer (Bio-Rad, Hercules, CA) and quantified using ImageJ (Version 1.47v, NIH, USA). For MMP-2 and MMP-9 standards, conditioned serum-free medium from human fibrosarcoma HT1080 cells was used as a standard for MMP-2 and medium from cells stimulated with 100 ng/mL phorbol myristate acetate was used as a standard for MMP-9.

Table 2.1. Gelatin zymography 8% separating gel (prepares four 0.75 mm thick gels)

Solution	Volume (mL)
40% w/v Acrylamide/ 3.3% w/v bis-acrylamide	3.00
1.5 M Tris/ 0.4% w/v SDS. pH 8.8	3.75
Gelatin (20 mg/mL)	1.50
H ₂ O	6.75
10% w/v Ammonium Persulfate	0.05
Tetramethylethylenediamine	0.01

Table 2.2. Gelatin zymography stacking gel (prepares four 0.75 mm thick gels)

Solution	Volume (mL)
40% w/v Acrylamide/ 3.3% w/v bis-acrylamide	0.975
0.5 M Tris/ 0.4% w/v SDS. pH 6.8	2.500
H ₂ O	6.525
10% w/v Ammonium Persulfate	0.050
Tetramethylethylenediamine	0.010

2.6. Immunoblotting

To measure the level of a protein of interest in cellular lysates, ventricular homogenates or subcellular fractions, the desired amount of protein in each sample was mixed in 6x loading buffer (0.5 M Tris-HCl pH 6.8, 30% v/v glycerol, 10% w/v SDS, 0.012% w/v bromophenol blue, and 0.6 M dithiothreitol), and denatured at 95°C for 5 min, then separated on 4-15% SDS-polyacrylamide gels (Mini-PROTEAN TGX Precast Gels, Bio-Rad) by electrophoresis at 90 V for 90 min in 1x running buffer (25 mM Tris, 192 mM glycine, 0.1% w/v SDS, pH 8.3). BLUelf prestained protein ladder (Cat#PM008, FroggaBio) or PageRuler™ Plus prestained protein ladder (Cat#26619, ThermoFisher Scientific) were used as molecular weight markers. Proteins were transferred from the gels onto polyvinylidene difluoride (PVDF) membranes (0.2 µm pore size, Bio-Rad Laboratories, Hercules, CA, USA) at 100 V for 1 h at 4°C in 1x transfer buffer (25 mM Tris, 192 mM glycine, pH 8.3, 20% v/v methanol). Membranes were then blocked by incubating with 5% w/v BSA (Sigma-Aldrich) in Tris-buffered saline (0.1 M NaCl, 0.01 M Tris-base, pH 7.4) with 0.1% v/v Tween 20 (TBS-T) for 1 h at room temperature on a shaker. Membranes were then incubated with the desired primary antibody diluted in 5% w/v BSA in TBS-T overnight at 4°C on a shaker. Then membranes were washed five times (4 min each) with TBS-T at room temperature to remove unbound primary antibody followed by probing with horseradish peroxidase-conjugated goat anti-rabbit (1:2000, Cat#7074, Cell Signaling) or anti-mouse (1:2000, Cat#7076, Cell Signaling) secondary antibodies diluted in 5% w/v skim milk (Carnation, Markham, ON) for 1 h at room temperature on a shaker. Membranes were then washed three times (4 min each) with TBS-T to remove residual secondary antibody and protein bands were visualized with Clarity™ ECL chemiluminescent detection reagent (Bio-Rad) using ChemiDoc MP chemiluminescence imager (Bio-Rad). Relative band intensities were expressed as fold of the loading control band

intensity assessed using ImageJ software (Version 1.47v, NIH, USA). Glyceraldehyde 3-phosphate dehydrogenase (GAPDH) or α -tubulin were used as loading controls for cellular lysate, ventricular homogenate or cytosolic fraction, while VDAC was used as a loading control for mitochondria-enriched fraction.

2.7. Co-immunoprecipitation

To determine whether MMP-2 interacts with a protein of interest in the heart, ventricular homogenates (400 μ g total protein per sample) were diluted in RIPA buffer to a final volume of 200 μ L. Homogenates were first pre-cleared by incubation with Protein G Sepharose bead slurry (Cat#ab193259, Abcam) for 30 min at 4°C, followed by centrifugation at 3,000 g for 2 min at 4°C. After centrifugation, supernatants were incubated with rabbit MMP-2 antibody (1:100, Cat#ab92536, Abcam) or rabbit IgG isotype control (1:100, Cat#ab172730, Abcam) on a rotator overnight at 4°C. Then 50 μ L of Protein G Sepharose bead slurry was added to each sample and incubated under rotatory agitation overnight at 4°C. The suspension was then centrifuged at 3,000 g for 2 min at 4°C and the supernatant was transferred to another tube. The beads were then washed three times with wash buffer (150 mM NaCl, 10 mM Tris, 1 mM EDTA, 1 mM EGTA, 0.2 mM sodium orthovanadate, and 1% v/v Triton X-100, pH 7.4, 0.1% v/v proteinase inhibitor cocktail; Cat#P8340, Sigma-Aldrich), resuspended in 2 \times Laemmli buffer (40.125 M Tris-HCl, pH 6.8, 4% w/v SDS, 10% 2-mercaptoethanol, 20% v/v glycerol, and 0.004% w/v bromophenol blue), heat denatured at 95°C for 5 min, and split into two halves. Each was separated on 4-15% polyacrylamide gels for immunoblotting. After transfer, the PVDF membranes were probed with either MMP-2 antibody (1:500, Cat#ab92536, Abcam) or an antibody against the protein of interest to determine whether it is associated with MMP-2.

2.8. RNA isolation and qPCR

Total cellular RNA was extracted from heart ventricle using TRIzol reagent (Invitrogen, USA). Powdered tissue was homogenized in TRIzol (10 μ L per mg tissue) and kept for 10 min at room temperature. 150 μ L chloroform was then added to the suspension, vigorously shaken and incubated for 3 min at room temperature, followed by phase separation by centrifugation at 12,000 g for 15 min at 4°C. The upper aqueous layer containing the RNA was then precipitated by incubation with isopropanol (1:1 v/v) for 10 min at room temperature followed by centrifugation at 12,000 g for 15 min at 4°C to pellet the RNA. The pellet was then washed with 75% ethanol, air dried for 15 min, and solubilized by incubation in nuclease-free H₂O (ThermoFisher Scientific) for 15 min at 55°C. To eliminate genomic DNA contamination, RNA was digested with DNase I (Invitrogen, USA) for 30 min at 37°C. RNA was then quantified using a NanoDrop One spectrophotometer (ThermoFisher Scientific). Reverse transcription was then performed using high-capacity complementary DNA (cDNA) reverse transcription kit (Applied Biosystems, USA).

Primers were designed using the Integrated DNA Technologies Primer Quest Tool (IDT, Coralville, USA) and specificity was confirmed using Primer-BLAST (NCBI). cDNA samples were analyzed in duplicate by quantitative real-time polymerase chain reaction (qPCR) using the PowerTrack™ SYBR Green Master Mix (Applied Biosystems, USA) for 40 cycles (15 s denaturation, 45 s annealing, 60 s extension) in a QuantaStudio® 3 Real-Time PCR instrument (Applied Biosystems, USA). Cycle threshold (C_t) values and melt curves were analyzed with the QuantaStudio software (Applied Biosystems, USA). mRNA expression of each gene was calculated by first normalizing the C_t value of each sample to the reference gene *B2M* and then normalizing to the control group (sample from aerobic heart incubated in the same plate).

Chapter III

Staurosporine-Induced Cleavage of Apoptosis-Inducing Factor in Human Fibrosarcoma Cells Is Independent of Matrix Metalloproteinase-2

A version of this chapter has been published:

Wesam Bassiouni, John M. Seubert, Richard Schulz (2022). Staurosporine-induced cleavage of apoptosis-inducing factor in human fibrosarcoma cells is independent of matrix metalloproteinase-2. *Can J Physiol Pharmacol.* 100:184-91.

Abstract

Apoptosis-inducing factor (AIF) is a mitochondrial flavoprotein which mediates staurosporine (STS)-induced cell death. AIF cleavage and translocation to the cytosol is thought to be calpain-1-dependent as calpain inhibitors reduced AIF proteolysis. However, many calpain inhibitors also inhibit matrix metalloproteinase-2 (MMP-2) activity, an intracellular and extracellular protease implicated in apoptosis. Here I investigated whether MMP-2 activity is affected in response to STS and if contributes to AIF cleavage. Human fibrosarcoma HT1080 cells were treated with STS (0.1 μ M, 0.25-24 h). A significant increase in cellular MMP-2 activity was seen by gelatin zymography after 6 h STS treatment, prior to induction of cell necrosis. Immunoblotting showed the time-dependent appearance of two forms of AIF (~60 and 45 kDa) in the cytosol which were significantly increased at 6 h. Surprisingly, knocking down MMP-2 or inhibiting its activity with MMP-2 preferring inhibitors ARP-100 or ONO-4817, or inhibiting calpain activity with ALLM or PD150606, did not prevent the STS-induced increase in cytosolic AIF. These results show that although STS rapidly increases MMP-2 activity, the cytosolic release of AIF may be independent of the proteolytic activities of MMP-2 or calpain.

3.1. Introduction

AIF is a flavoprotein anchored to the mitochondrial inner membrane [281]. It binds to FAD to exert a NADH oxidase activity [282, 283]. Interestingly, AIF was revealed to induce apoptosis in a caspase-independent manner [281, 284]. It is synthesized as a 67 kDa protein with an N-terminal domain that contains a mitochondrial localization sequence. This targets it to the mitochondria where it is cleaved by a mitochondrial processing peptidase to a mature 62 kDa protein [286]. In mediating apoptosis, 62 kDa AIF is further cleaved and released into the cytosol in response to cellular stressors which induce calcium influx, or upon ER stress which induces calcium release from the ER, resulting in intracellular calcium overload. This process is known as the calcium-dependent mitochondrial permeability transition [287, 288].

Calpain-1, a calcium-dependent protease, is activated intracellularly by calcium influx and induces the cleavage of mitochondrial 62 kDa AIF into a 57 kDa form which is translocated to the cytosol and then to the nucleus where it induces DNA fragmentation and chromatin condensation resulting in cell death [289, 434]. Calpain-1-mediated AIF cleavage and release from the mitochondria occurs during STS-induced cell death [287]. STS is a potent protein kinase C inhibitor that induces apoptosis by the activation of caspase-3, as well as by the translocation of AIF to the nucleus [435, 436]. AIF cleavage may also occur via calcium-independent proteases such as cathepsin [292].

MMP-2 is a ubiquitously expressed member of the MMPs family of proteases which are best known to cleave extracellular matrix proteins during different physiological and disease conditions [2, 5, 437]. However, MMP-2 was also identified to exert intracellular effects by cleavage of selected intracellular proteins. For example in the heart undergoing oxidative stress

injury, it targets and cleaves cardiac contractile proteins such as TnI, α -actinin, myosin light chain-1 and titin resulting in cardiac contractile dysfunction (see [438] for review). MMP-2 is also reported to be localized to the MAM [64-66], and may induce ER stress by cleaving SERCA2a and JPH-2 [69, 70], and thus prevents calcium uptake to the ER, resulting in intracellular calcium overload [439]. However, whether MMP-2 activity is involved in STS-induced AIF cleavage and release from mitochondria is unknown.

3.2. Methods

3.2.1. Cell experiments

Human tumor fibrosarcoma cells (HT1080, ATCC), which robustly express MMP-2, were cultured in Dulbecco's Modified Eagle Medium (DMEM, Cat#11885-84, Gibco) containing 10% fetal bovine serum (FBS, Cat#12483-020, Gibco) and 1% penicillin-streptomycin (Cat#15070-063, Gibco). Experiments were performed on cell passages 5-12 obtained from a frozen cell stock. Independent experiments were performed using cells from different passages. The medium was exchanged for serum-free medium the day prior to treatments. Cells at a density of 2×10^5 cells/mL were treated with STS (0.1 μ M, Cat#ALX-380-014, Enzo Life Sciences) or its vehicle (0.1% *v/v* DMSO) for 0.25-24 h [440, 441]. Cell conditioned media were collected for the determination of cell cytotoxicity. Whole cell lysates and subcellular fractions were collected for MMP-2 activity, total protein level and distribution of AIF into cytosolic and mitochondria-enriched fractions. The cells were lysed by rinsing with PBS and incubating with RIPA buffer for 5 min at 4°C. Homogenates were centrifuged at 10,000 g for 10 min at 4°C and the supernatant was used as the cell lysate.

In order to determine protease-dependent AIF cleavage, cells were treated with either ONO-4817 (3, 10 or 30 μ M, a gift from Ono Pharmaceutical, Osaka, Japan) or ARP-100 (3, 10 or 30 μ M, Cat#13321, Cayman Chemical) as MMP-2 preferring inhibitors [94, 95], ALLM (10 or 30 μ M, Cat#15994, Cayman Chemical) as a selective calpain inhibitor [442, 443] or PD150606 (50, 100 or 200 μ M, Cat#513022, Calbiochem) as a nonselective MMP-2/calpain inhibitor [443] for 2 h followed by treatment with 0.1 μ M STS for 6 h. Drugs were dissolved in DMSO and diluted to give 0.1% v/v DMSO:H₂O as vehicle.

3.2.2. MMP-2 knockdown using siRNA

MMP-2 was knocked down in HT1080 cells using small interfering RNA (siRNA) according to the manufacturer's instructions. Briefly, cells were incubated with a 50:50 (% v/v) mixture of MMP-2 siRNA sequence (20 nM, Cat#4390824-s8851, ThermoFisher) and lipofectamine RNAiMAX transfection reagent (Cat#13778030, ThermoFisher) for 48 h. Control cells were incubated with siRNA negative control (Cat#4390843, ThermoFisher). MMP-2 knockdown was confirmed in cell lysates by gelatin zymography. Following the 48 h incubation period, cells were treated with STS 0.1 μ M for 6 h to determine the effect of MMP-2 knockdown on STS-induced AIF cleavage.

3.2.3. Subcellular fractionation

To obtain cytosolic and mitochondria-enriched subcellular fractions for determining the subcellular localization of AIF, cells were homogenized in ice-cold homogenization buffer and subjected to subcellular fractionation as described in **Chapter 2 (section 2.3)**.

3.2.4. Cytotoxicity determination

Aliquots of serum-free cell-conditioned media obtained following each treatment were used to determine cytotoxicity (LDH Assay Kit, Cat#ab65393, Abcam). Conditioned media were centrifuged at 250 g for 4 min to remove any residual cells. 50 μ L of the supernatant was then loaded onto a clear, flat-bottom 96-well plate (in triplicate) and incubated with 50 μ L reaction mixture (LDH substrate in assay buffer) for 30 min at room temperature, protected from light. Absorbance was measured at 490 nm using a UV_{max} kinetic microplate reader (Molecular Devices, San Jose, CA). The maximum lysis control value was obtained by incubating cells with lysis solution for 1 h to induce complete LDH release. The low control value was obtained by growing cells for the same duration of the experiment, in absence of STS or lysis solution. Percentage cytotoxicity for each sample was calculated using the following equation:

$$\% \text{ Cytotoxicity} = \frac{\text{test value} - \text{low control value}}{\text{maximum control value} - \text{low control value}} \times 100$$

3.2.5. Gelatin zymography

To measure MMP-2 activity in HT1080 cells, gelatin zymography was performed in whole cellular lysate using 15 μ g of sample protein as described in **Chapter 2 (section 2.5)**.

3.2.6. Immunoblotting

To measure the subcellular distribution of AIF in HT1080 cells, 20 or 50 μ g total protein from the mitochondria-enriched or cytosolic fractions, respectively, were separated on 4-15% polyacrylamide gels as described in **Chapter 2 (section 2.6)**.

The following monoclonal antibodies were used: anti-AIF (1:250, Cat#sc-13116, Santa Cruz Biotechnology), α -tubulin (1:2000, Cat#ab7750, Abcam) as a cytosolic fraction loading control and VDAC (1:1000, Cat#ab14734, Abcam) as a mitochondria-enriched fraction loading control.

3.2.7. Determination of the ability of MMP inhibitors to penetrate cells at an effective concentration

This experiment was designed to test whether the MMP inhibitors penetrated the cells to reach a concentration sufficient to block MMP-2 activity [444]. The hydrolysis of OmniMMP[®] fluorogenic substrate (Enzo Life Sciences, Farmingdale, NY; 25 μ M, prepared in 0.4% v/v DMSO) by recombinant human 64 kDa MMP-2 (Calbiochem, Billerica, MA; 0.5 nM in assay buffer consisting of 50 mM Tris-HCl, 150 mM NaCl, 5 mM CaCl₂·2H₂O, and 0.05% w/v NaN₃, pH 7.6) was measured at 37°C in presence of 30 μ L cell lysate prepared from cells treated with ARP-100, ONO-4817 or DMSO vehicle (8 h, 37°C), using a plate reader-based protocol. 30 μ L recombinant human 64 kDa MMP-2 in assay buffer and 60 μ L substrate were added to make a total volume of 120 μ L in black polystyrene half-area plates (Corning, NY). Fluorescence associated with the (7-meth-oxycoumarin-4-yl)acetyl-tagged cleavage product was measured in three replicate wells every 60 s for 1 h (λ_{ex} 328 nm, λ_{em} 393 nm) in a Synergy H1 fluorescence microplate reader (BioTek, Winooski, US).

3.2.8. *In silico* predicted cleavage sites of AIF by different proteases

The online cleavage prediction server Procleave was used to perform *in silico* prediction of AIF cleavage sites by different proteases [445]. This online tool suggests a number of potential target substrates and their corresponding cleavage sites by different proteases. The human AIF

FASTA sequence (UniProt ID-O95831) was entered into the Procleave query sequence section and proteases known to be active intracellularly were selected.

3.2.9. Statistics

Data are expressed as mean \pm standard error of the mean (SEM) (n=4-6, each n represents an independent experiment using a different cell passage). For multiple comparisons, one-way or two-way analysis of variance (ANOVA) followed by Dunnett's post-hoc test was used (GraphPad Prism 8, La Jolla, CA, USA). Statistical significance was considered at $p < 0.05$.

3.3. Results

3.3.1. STS induces activation of MMP-2 in HT1080 cells before induction of necrosis

The LDH cytotoxicity assay showed no significant cytotoxicity with up to 6 h 0.1 μ M STS treatment compared to vehicle, whereas 24 h treatment resulted in near 100% cytotoxicity (**Figure 3.1 A**). The MMP inhibitors, ARP-100 or ONO-4817 (10 μ M) or calpain inhibitors, ALLM (30 μ M) or PD150606 (100 μ M) did not significantly affect STS-induced cytotoxicity at 24 h nor did they cause any significant cell death on their own compared to vehicle (**Figure 3.2**).

The 6 h treatment was chosen for subsequent experiments. There was a significant increase in 72 kDa MMP-2 activity in cell lysates upon 6 h STS treatment as shown by gelatin zymography. There was no evidence for the induction of 92 kDa MMP-9 by STS (**Figure 3.1 B**).

3.3.2. STS induces the release of 60 and 45 kDa AIF fragments into the cytosol

Using immunoblotting, the 62 kDa form of AIF was detected in the mitochondria-enriched fraction with no significant change in its level over 6 h of STS treatment (**Figure 3.3 A**). In

contrast, two forms of AIF were detected in the cytosolic fraction. A band appearing at ~60 kDa (running at a slightly higher molecular weight than the reported 57 kDa for cytosolic AIF [282] and lower than the mitochondrial AIF band when both samples were run on the same gel) and another band at ~45 kDa were detected. There was a time-dependent significant increase in the levels of both cytosolic AIF forms following 6 h STS (**Figure 3.3 B**).

3.3.3. STS-induced cleavage of AIF is independent of MMP-2 or calpain activities

The ability of the MMP inhibitors to penetrate the cells and reach a concentration effective to inhibit MMP-2 activity was confirmed as shown by the ability of lysates prepared from cells treated with MMP-2 preferring inhibitors ARP-100 or ONO-4817 (10 μ M) to attenuate the cleavage of a fluorogenic MMP substrate by recombinant human MMP-2 (**Figure 3.4**).

The MMP-2 preferring inhibitors ARP-100 (3-30 μ M) or ONO-4817 (3-30 μ M) caused no significant change in 62 kDa AIF levels in the mitochondria-enriched fraction compared to STS alone (0.1 μ M, 6 h) (**Figures 3.5 A and C**). In the cytosolic fraction, neither of these inhibitors prevented the increase in the appearance and levels of both 60 and 45 kDa AIF forms compared to STS (0.1 μ M, 6 h) (**Figures 3.5 B and D**). This suggests that MMP-2 does not mediate the cleavage of AIF caused by STS. To confirm these results, endogenous MMP-2 in the cells was knocked down using siRNA which resulted in a complete loss in cell lysate MMP-2 activity (**Figure 3.6 A**). MMP-2 knockdown also did not prevent the STS-induced increase in 60 and 45 kDa AIF forms in the cytosolic fraction (**Figures 3.6 B and C**).

Neither the calpain inhibitor ALLM (10 and 30 μ M) nor the nonselective MMP-2/calpain inhibitor, PD150606 (50-200 μ M) caused any significant change in 62 kDa AIF levels in the mitochondria-enriched fraction or 60 and 45 kDa AIF levels in the cytosol compared to STS (0.1

μM , 6 h) (**Figures 3.7 A-D**). This suggests that STS-induced AIF cleavage is also independent of calpain.

3.3.4. *In silico* prediction of possible proteases that mediate AIF cleavage

I performed an *in silico* analysis using Procleave of the possible cleavage sites within AIF by different proteases. The cleavage sites which produce C- or N-terminal fragments of AIF of molecular weights close to 45 and 60 kDa were selected. Proteases known to be active only extracellularly were excluded from the analysis. A summary of the putative proteases cleaving AIF to such fragments is shown in **Table 3.1**. Based on this *in silico* analysis, AIF was found to possess amino acid sequences that could be targets of different isoforms of cathepsin, calpains, MMPs, proprotein convertase and others. The proteases which showed the top scores (>0.9) were MMP-2 and cathepsins-B, -D and -E.

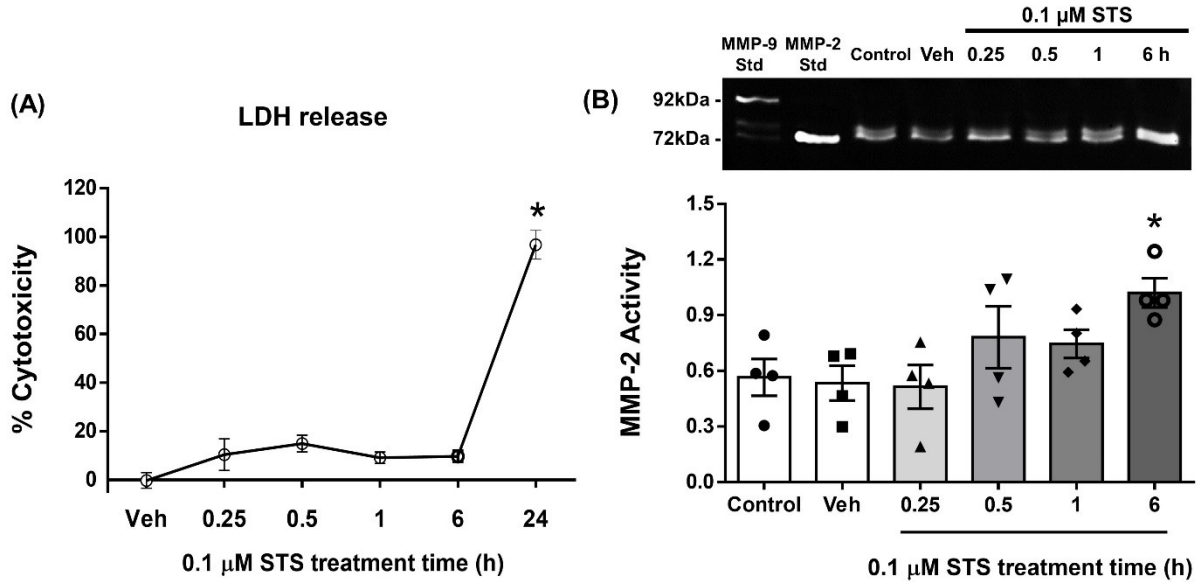


Figure 3.1. Staurosporine (STS) induces activation of MMP-2 in HT1080 cells. (A) Lactate dehydrogenase (LDH) assay showing time-dependent changes in 0.1 μM staurosporine (STS)-induced cytotoxicity in HT1080 cells compared to vehicle (n=5). (B) Upper panel: Representative gelatin zymogram showing time dependent changes of MMP-2 activity in cell lysates in response to 0.1 μM STS compared to vehicle (6 h) treatment. Lower panel: Quantification of 72 kDa MMP-2 activity normalized to MMP-2 standard (n=4 per group). *p<0.05 vs. vehicle by one-way ANOVA followed by Dunnett's post-hoc test.

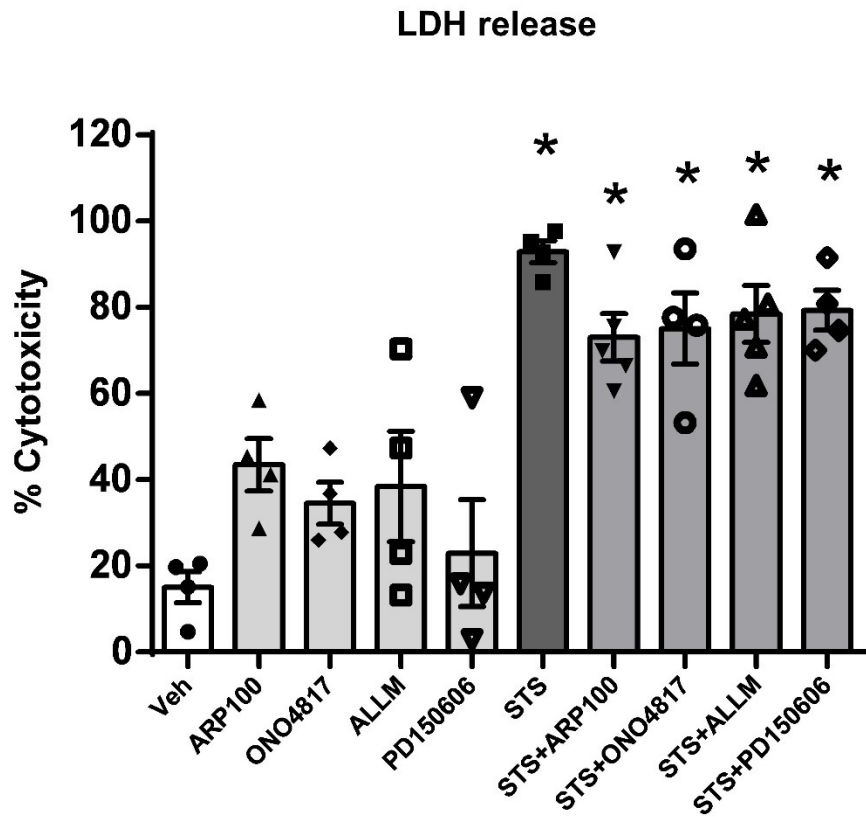


Figure 3.2. Effect of MMP-2 or calpain inhibitors on staurosporine (STS)-induced cytotoxicity in HT1080 cells. Effects of ARP-100 (10 μ M), ONO-4817 (10 μ M), ALLM (30 μ M) and PD150606 (100 μ M) in the presence or absence of STS (0.1 μ M, 24 h) on HT1080 cell cytotoxicity as measured by lactate dehydrogenase assay using serum-free cell conditioned media (n=4-5 per group). *p<0.05 vs. vehicle by one-way ANOVA followed by Dunnett's post-hoc test.

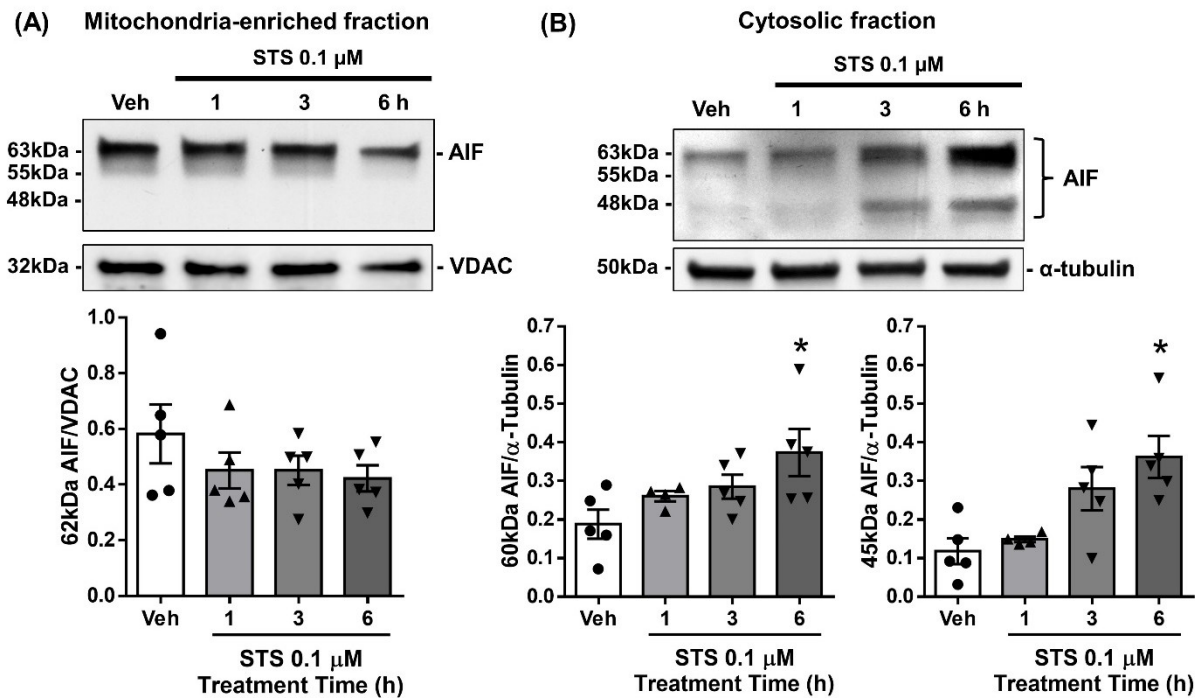


Figure 3.3. Staurosporine (STS) induces the cytosolic release and cleavage of apoptosis-inducing factor (AIF). Representative immunoblots (upper panel) and quantitative measurements (lower panel) of AIF levels in (A) mitochondria-enriched and (B) cytosolic fractions of HT1080 cells treated with STS 0.1 μ M for different times (n=4-5 per group). Position of molecular weight ladder proteins indicated on the left. *p<0.05 vs. vehicle by one-way ANOVA followed by Dunnett's post-hoc test.

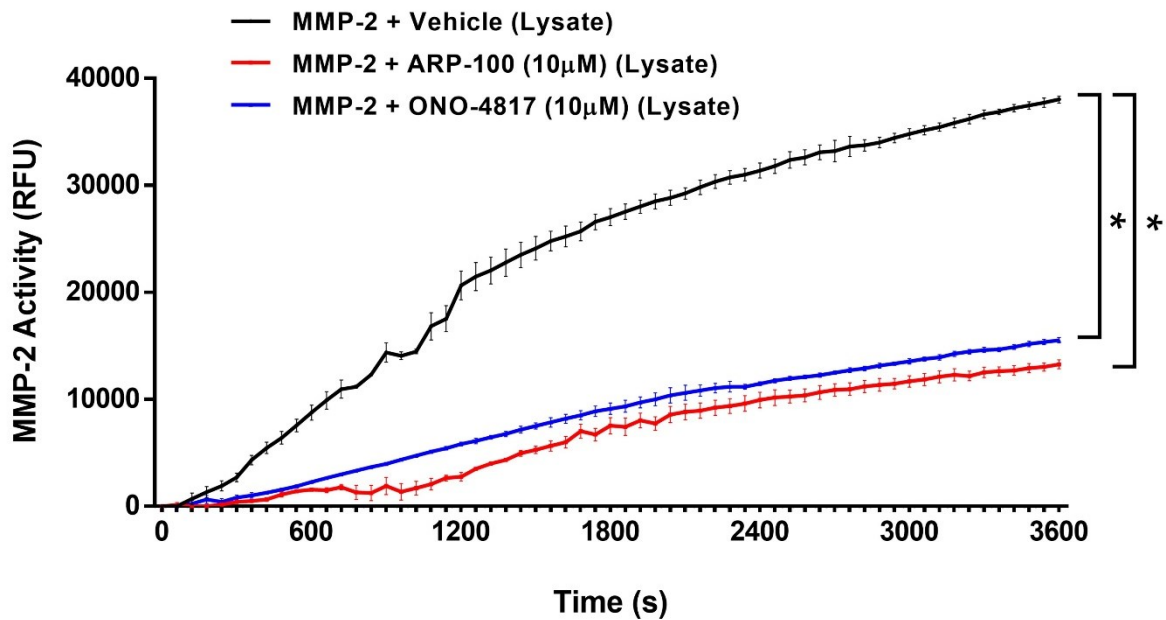


Figure 3.4. Changes in MMP-2 activity in HT1080 cell lysates by MMP-2 preferring inhibitors. Effect of cell lysates prepared from HT1080 cells treated (8 h) with ARP-100 (10 µM), ONO-4817 (10 µM) or DMSO vehicle on the ability of recombinant human MMP-2 to cleave Omni-MMP® fluorogenic substrate *in vitro* (n=3 per group). Values are presented as relative fluorescence unit (RFU). *p<0.05 vs. vehicle by two-way ANOVA followed by Dunnett's post-hoc test.

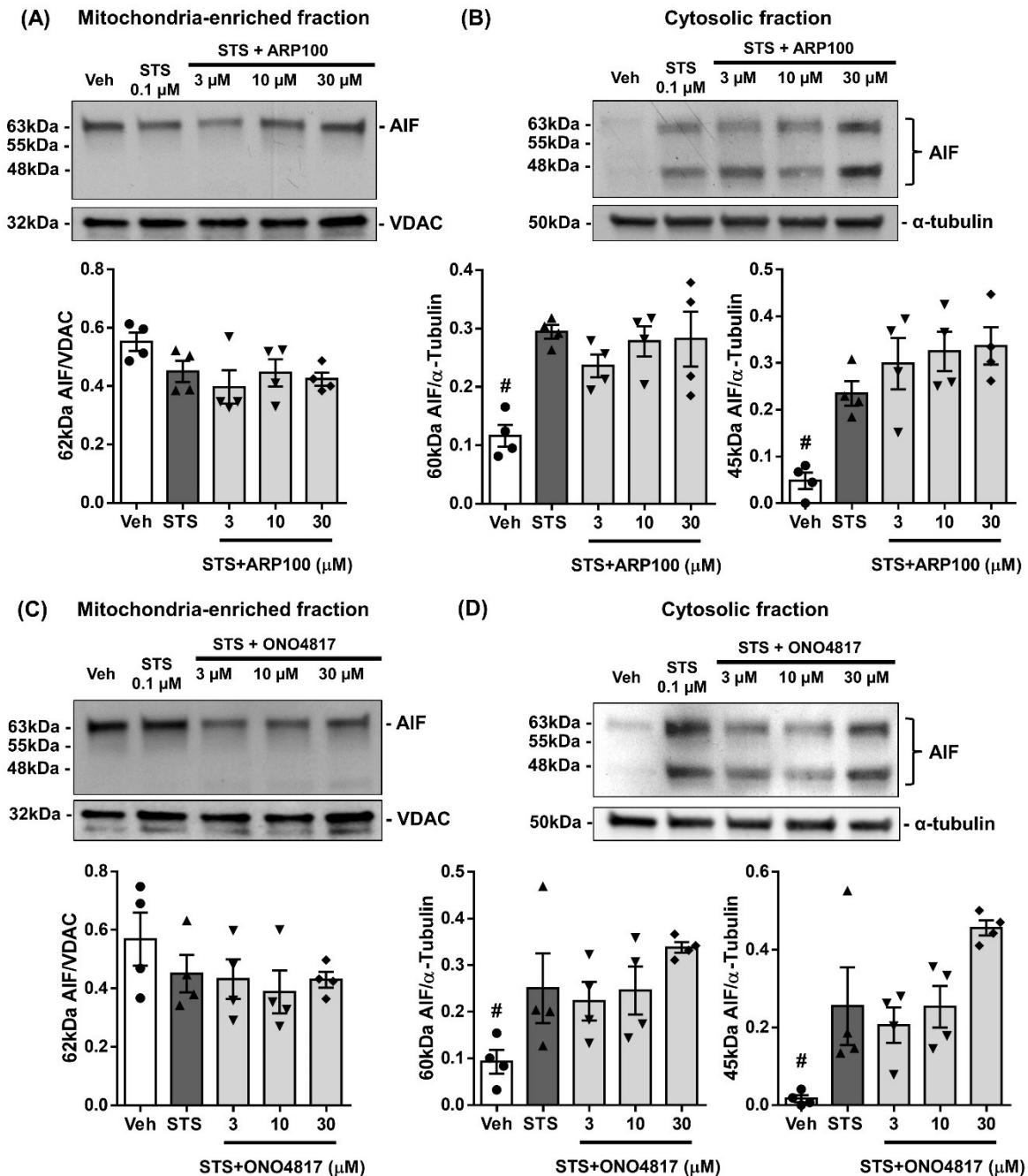


Figure 3.5. Effect of MMP-2 preferring inhibitors on staurosporine (STS)-induced apoptosis-inducing factor (AIF) cleavage. Representative immunoblots (upper panel) and quantitative measurements (lower panel) of AIF levels in (A) mitochondria-enriched and (B) cytosolic fractions of HT1080 cells treated with STS 0.1 μ M for 6 h with ARP-100 (3, 10 and 30 μ M). Representative immunoblots (upper panel) and quantitative measurements (lower panel) of AIF levels in (C) mitochondria-enriched and (D) cytosolic fractions of HT1080 cells treated with STS 0.1 μ M for 6 h with ONO-4817 (3, 10 and 30 μ M) (n=4 per group). Position of molecular weight ladder proteins indicated on the left. #p<0.05 vs. STS by one-way ANOVA followed by Dunnett's post-hoc test.

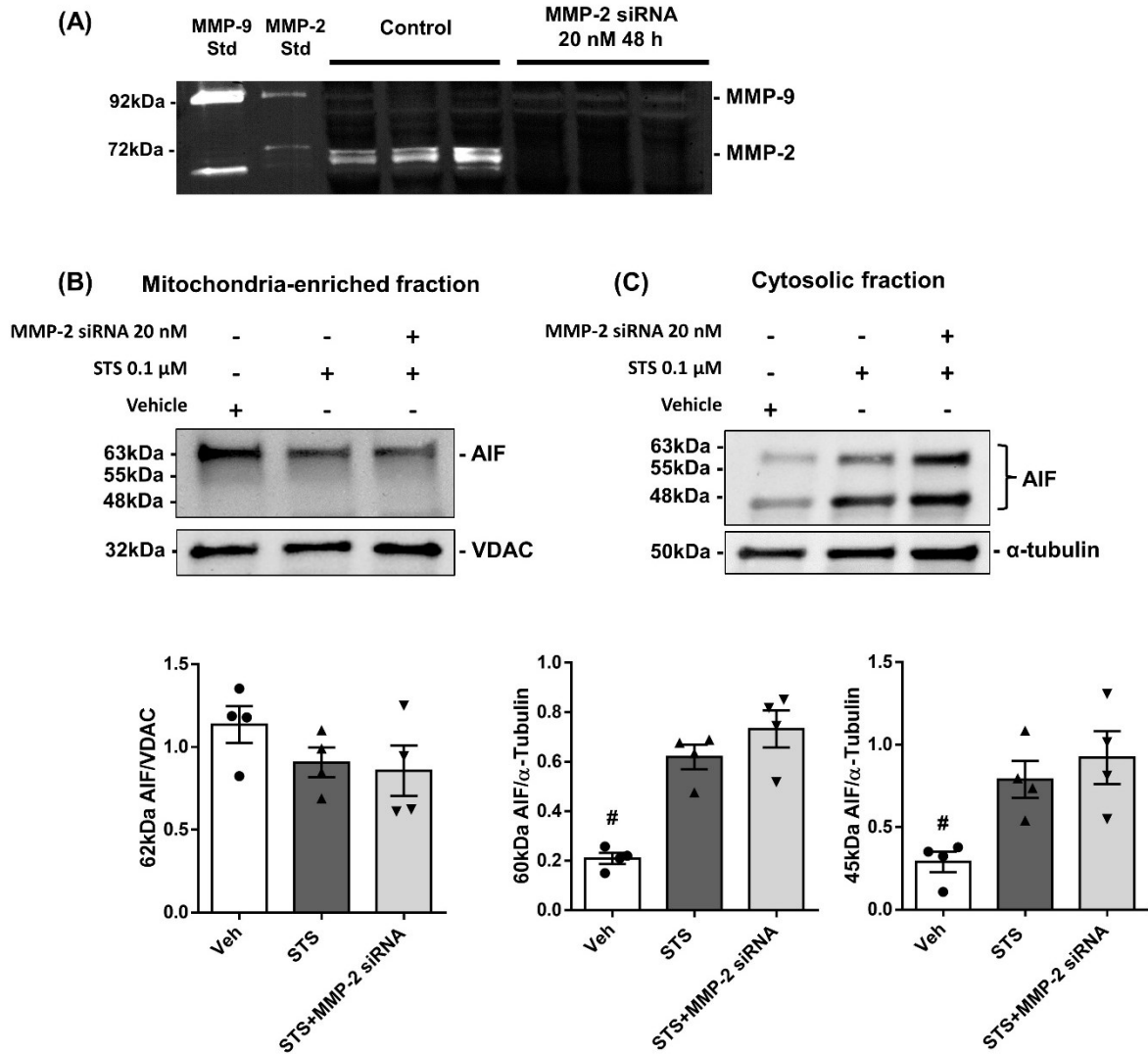


Figure 3.6. Effect of MMP-2 knockdown on staurosporine (STS)-induced apoptosis-inducing factor (AIF) cleavage. (A) Representative gelatin zymogram showing loss of matrix metalloproteinase-2 (MMP-2) gelatinolytic activity in HT1080 cells by knocking down MMP-2 using MMP-2 siRNA (20 nM) for 48 h compared to siRNA control. (B&C) Effect of MMP-2 knockdown on STS-induced AIF cleavage. Representative immunoblots (upper panel) and quantitative measurements (lower panel) of AIF levels in (B) mitochondria-enriched and (C) cytosolic fractions of HT1080 cells treated with STS 0.1 μ M for 6 h (n=4 per group). Position of molecular weight ladder proteins indicated on the left. #p<0.05 vs. STS by one-way ANOVA followed by Dunnett's post-hoc test.

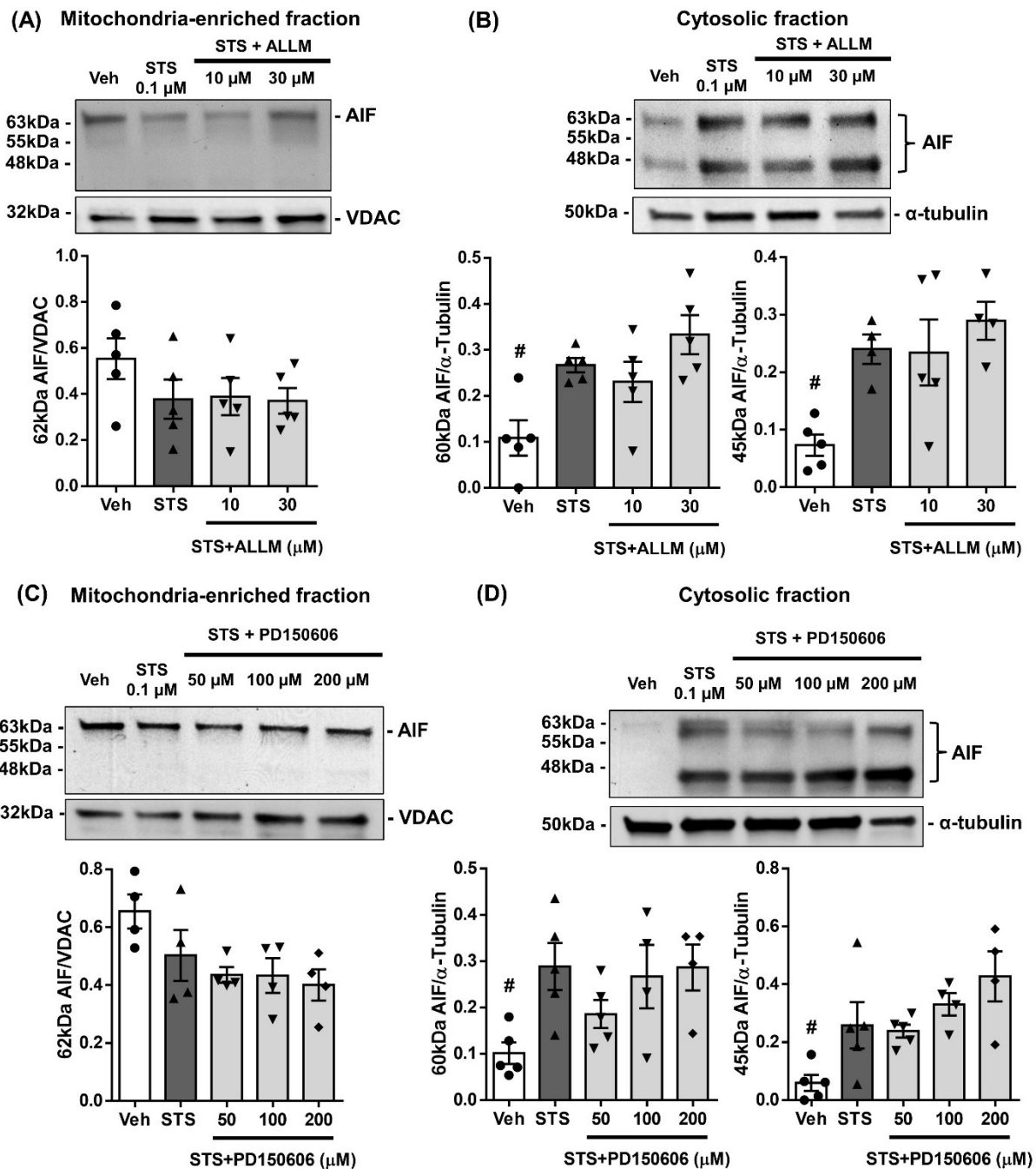


Figure 3.7. Effect of calpain inhibitors on staurosporine (STS)-induced apoptosis-inducing factor (AIF) cleavage. Representative immunoblots (upper panel) and quantitative measurements (lower panel) of AIF levels in (A) mitochondria-enriched and (B) cytosolic fractions of HT1080 cells treated with STS 0.1 μ M for 6 h with ALLM (10 and 30 μ M). Representative immunoblots (upper panel) and quantitative measurements (lower panel) of AIF levels in (C) mitochondria-enriched and (D) cytosolic fractions of HT1080 cells treated with STS 0.1 μ M for 6 h with PD150606 (50, 100 and 200 μ M) (n=4-5 per group). Position of molecular weight ladder proteins indicated on the left. #p<0.05 vs. STS by one-way ANOVA followed by Dunnett's post-hoc test.

Table 3.1. *In silico* predicted cleavage sites of human apoptosis-inducing factor (AIF) by different intracellular proteases listed in alphabetical order, according to Procleave.

The cleavage sites shown were selected on the basis that they produce C- or N-terminal fragments of AIF of molecular weights close to those seen in cytosolic fractions prepared from HT1080 cells treated with 0.1 μ M STS for 6 h (i.e. 45 and 60 kDa). Proteases known to be only active extracellularly (e.g. ADAMs, pepsin, astacin) were excluded from this analysis.

Protease	Position	Cleavage Site	N-Terminal Mass (kDa)	C-Terminal Mass (kDa)	Score (0-1)
Calpain-1	205	RSIY-FQPP	24.51	49.16	0.597
	104	SGLG-LTPE	12.64	61.04	0.552
	543	SEIT-IPPS	65.08	8.59	0.547
	206	SIYF-QPPS	24.66	49.01	0.538
	50	LELQ-MTRQ	6.05	67.63	0.538
	501	LVDS-SLPT	60.44	13.23	0.525
	546	TIPP-STPA	65.39	8.29	0.52
	109	TPEQ-KQKK	13.21	60.47	0.502
	472	NMTG-AAKP	56.87	16.8	0.495
Calpain-2	542	ASEI-TIPP	64.98	8.69	0.64
	205	RSIY-FQPP	24.51	49.16	0.598
	363	EGVK-VMPN	43.74	29.94	0.496
	509	VGVF-AKAT	61.36	12.32	0.482
	549	PSTP-AVPQ	65.68	8	0.471
	400	AAVG-LEPN	48.01	25.66	0.461
	104	SGLG-LTPE	12.64	61.04	0.451
	Cathepsin B	136	VPFL-LIGG	16.19	57.48
397		HIVA-AVGL	47.67	26	0.958
371		AIVQ-SVGV	44.59	29.08	0.956
72		VLVL-IVGL	8.6	65.08	0.942
260		CLIA-TGGT	31	42.67	0.915
137		PFLI-IGGG	16.31	57.37	0.906
259		KCLI-ATGG	30.93	42.74	0.847
Cathepsin D		72	VLVL-IVGL	8.6	65.08
	498	AIGL-VDSS	60.14	13.53	0.742
	258	EKCL-IATG	30.82	42.86	0.699
	407	NVEL-AKTG	48.81	24.87	0.69
	509	VGVF-AKAT	61.36	12.32	0.563
	70	NSVL-VLIV	8.39	65.29	0.562
	211	PPSF-YVSA	25.22	48.46	0.498
	Cathepsin E	72	VLVL-IVGL	8.6	65.08
258		EKCL-IATG	30.82	42.86	0.984
70		NSVL-VLIV	8.39	65.29	0.948

Protease	Position	Cleavage Site	N-Terminal Mass (kDa)	C-Terminal Mass (kDa)	Score (0-1)
	407	NVEL-AKTG	48.81	24.87	0.907
	137	PFLI-IGGG	16.31	57.37	0.866
	211	PPSF-YVSA	25.22	48.46	0.83
	243	RDNM-VKLN	29.01	44.66	0.794
Cathepsin G	349	PEYL-SNWT	41.92	31.75	0.491
	212	PSFY-VSAQ	25.38	48.3	0.407
	70	NSVL-VLIV	8.39	65.29	0.362
	103	ISGL-GLTP	12.47	61.21	0.338
	268	PRSL-SAID	32.01	41.67	0.33
	209	FQPP-SFYV	24.98	48.69	0.322
	480	YWHQ-SMFW	57.86	15.82	0.308
Cathepsin K	414	GGLE-IDSD	49.7	23.98	0.599
	210	QPPS-FYVS	25.07	48.61	0.561
	391	RKVE-TDHI	47.04	26.64	0.468
	480	YWHQ-SMFW	57.86	15.82	0.442
	247	VKLN-DGSQ	29.47	44.21	0.425
Cathepsin L	500	GLVD-SSLP	60.36	13.32	0.882
	138	FLLI-GGGT	16.42	57.25	0.878
	259	KCLI-ATGG	30.93	42.74	0.823
	213	SFYV-SAQD	25.48	48.2	0.769
	104	SGLG-LTPE	12.64	61.04	0.766
	80	STVG-AGAY	9.56	64.12	0.76
	146	AAFA-AARS	17.4	56.27	0.724
Cathepsin L3	401	AVGL-EPNV	48.13	25.55	0.634
	110	PEQK-QKKA	13.33	60.34	0.583
	552	PAVP-QAPV	65.94	7.73	0.564
	49	PLEL-QMTR	5.92	67.75	0.546
	218	AQDL-PHIE	25.99	47.68	0.54
	479	PYWH-QSMF	57.73	15.95	0.534
	349	PEYL-SNWT	41.92	31.75	0.528
Cathepsin S	259	KCLI-ATGG	30.93	42.74	0.897
	104	SGLG-LTPE	12.64	61.04	0.79
	117	AALS-ASEG	14.06	59.61	0.783
	552	PAVP-QAPV	65.94	7.73	0.747
	80	STVG-AGAY	9.56	64.12	0.726
	400	AAVG-LEPN	48.01	25.66	0.625
KPC2-type peptidase	530	TGIR-SESE	63.7	9.97	0.623
	344	MGKI-LPEY	41.31	32.37	0.561
	95	DEKR-YNER	11.42	62.26	0.523
	201	NGKE-RSIY	23.99	49.68	0.513

Protease	Position	Cleavage Site	N-Terminal Mass (kDa)	C-Terminal Mass (kDa)	Score (0-1)
	363	EGVK-VMPN	43.74	29.94	0.49
	202	GKER-SIYF	24.15	49.52	0.474
	233	TGKK-VVQL	27.84	45.83	0.474
MMP-1	497	EAIG-LVDS	60.03	13.65	0.594
	368	MPNA-IVQS	44.25	29.42	0.585
	348	LPEY-LSNW	41.81	31.87	0.545
	228	GVAV-LTGK	27.2	46.48	0.469
	267	TPRS-LSAI	31.89	41.78	0.46
MMP-2	267	TPRS-LSAI	31.89	41.78	0.999
	136	VPFL-LIGG	16.19	57.48	0.994
	211	PPSF-YVSA	25.22	48.46	0.988
	115	KKAA-LSAS	13.86	59.81	0.963
	368	MPNA-IVQS	44.25	29.42	0.941
	348	LPEY-LSNW	41.81	31.87	0.896
	228	GVAV-LTGK	27.2	46.48	0.868
MMP-3	228	GVAV-LTGK	27.2	46.48	0.829
	427	VNAE-LQAR	51.34	22.34	0.601
	86	AYAY-KTMK	10.27	63.4	0.56
	511	VFAK-ATAQ	61.56	12.12	0.501
	348	LPEY-LSNW	41.81	31.87	0.48
MMP-7	497	EAIG-LVDS	60.03	13.65	0.687
	228	GVAV-LTGK	27.2	46.48	0.663
	427	VNAE-LQAR	51.34	22.34	0.637
	236	KVVQ-LDVR	28.17	45.51	0.605
	217	SAQD-LPHI	25.88	47.79	0.579
MMP-8	267	TPRS-LSAI	31.89	41.78	0.767
	136	VPFL-LIGG	16.19	57.48	0.551
	427	VNAE-LQAR	51.34	22.34	0.523
	478	KPYW-HQSM	57.59	16.08	0.487
MMP-9	228	GVAV-LTGK	27.2	46.48	0.884
	136	VPFL-LIGG	16.19	57.48	0.831
	348	LPEY-LSNW	41.81	31.87	0.695
	211	PPSF-YVSA	25.22	48.46	0.69
	478	KPYW-HQSM	57.59	16.08	0.689
	267	TPRS-LSAI	31.89	41.78	0.666
	368	MPNA-IVQS	44.25	29.42	0.63
MMP-12	267	TPRS-LSAI	31.89	41.78	0.738
	136	VPFL-LIGG	16.19	57.48	0.648
	348	LPEY-LSNW	41.81	31.87	0.603

Protease	Position	Cleavage Site	N-Terminal Mass (kDa)	C-Terminal Mass (kDa)	Score (0-1)
	228	GVAV-LTGK	27.2	46.48	0.568
	257	YEKC-LIAT	30.71	42.97	0.511
	191	VTKT-LRFK	22.59	51.08	0.484
MMP-13	368	MPNA-IVQS	44.25	29.42	0.568
	267	TPRS-LSAI	31.89	41.78	0.533
	228	GVAV-LTGK	27.2	46.48	0.504
	497	EAIG-LVDS	60.03	13.65	0.467
	478	KPYW-HQSM	57.59	16.08	0.465
	188	DPNV-TKTL	22.26	51.41	0.458
	136	VPFL-LIGG	16.19	57.48	0.457
MMP-14	267	TPRS-LSAI	31.89	41.78	0.725
	69	DNSV-LVLI	8.28	65.4	0.493
	188	DPNV-TKTL	22.26	51.41	0.488
Meprin alpha subunit	206	SIYF-QPPS	24.66	49.01	0.74
	205	RSIY-FQPP	24.51	49.16	0.705
	391	RKVE-TDHI	47.04	26.64	0.608
	216	VSAQ-DLPH	25.77	47.91	0.581
	486	FWSD-LGPD	58.61	15.07	0.58
	184	WFSD-DPNV	21.84	51.84	0.54
	485	MFWS-DLGP	58.49	15.18	0.528
Meprin beta subunit	417	EIDS-DFGG	50.01	23.66	0.811
	184	WFSD-DPNV	21.84	51.84	0.739
	392	KVET-DHIV	47.14	26.54	0.699
	247	VKLN-DGSQ	29.47	44.21	0.671
	485	MFWS-DLGP	58.49	15.18	0.658
	240	LDVR-DNMV	28.65	45.02	0.627
Mitochondrial processing peptidase beta-subunit	267	TPRS-LSAI	31.89	41.78	0.822
	531	GIRS-ESET	63.79	9.88	0.617
	483	QSMF-WSDL	58.22	15.45	0.523
PCSK-1 peptidase	95	DEKR-YNER	11.42	62.26	0.732
	359	KVRR-EGVK	43.21	30.46	0.525
	530	TGIR-SESE	63.7	9.97	0.458
	344	MGKI-LPEY	41.31	32.37	0.443
	113	KQKK-AALS	13.72	59.96	0.443
	196	RFKQ-WNGK	23.26	50.41	0.436
PCSK-2 peptidase	95	DEKR-YNER	11.42	62.26	0.799
	196	RFKQ-WNGK	23.26	50.41	0.505
	266	GTPR-SLSA	31.81	41.87	0.455
	359	KVRR-EGVK	43.21	30.46	0.43

Protease	Position	Cleavage Site	N-Terminal Mass (kDa)	C-Terminal Mass (kDa)	Score (0-1)
	512	FAKA-TAQD	61.63	12.05	0.376
PCSK-4 peptidase	196	RFKQ-WNGK	23.26	50.41	0.562
PCSK-6 peptidase	196	RFKQ-WNGK	23.26	50.41	0.561
	266	GTPR-SLSA	31.81	41.87	0.492
	88	AYKT-MKED	10.5	63.18	0.492
PCSK-7 peptidase	196	RFKQ-WNGK	23.26	50.41	0.535
	269	RSLS-AIDR	32.09	41.58	0.459

3.4. Discussion

I investigated here whether MMP-2, known to have proteolytic effects on both intracellular and extracellular substrates, may be involved in the proteolytic processing and release of AIF into the cytosol from mitochondria in response to STS, a protein kinase C inhibitor which induces cell death. I reveal here for the first time that MMP-2 is activated by STS in HT1080 cells as an early event prior to induction of cell death. I also showed that STS stimulates the appearance of two cytosolic AIF forms at ~60 and 45 kDa without significantly affecting its mitochondrial levels. Finally, I suggest that the STS-induced release of mitochondrial AIF into the cytosol in HT1080 cells may be independent of the proteolytic activity of MMP-2 and calpain.

The intracellular localization and proteolytic targets of MMP-2 have rapidly expanded since the discovery of its critical role in proteolyzing cardiac TnI during IR injury (see [438] for review). The cellular events prior to STS-induced cell death were studied here. STS induces a rapid elevation of intracellular MMP-2 within 6 h. This enhanced MMP-2 activity can be explained by previous studies reporting that STS-mediated cell death involves induction of oxidative stress by elevation of RONS, including peroxynitrite, which contribute to the progression of apoptosis [446, 447]. Oxidative stress in turn activates MMP-2 intracellularly by the action of peroxynitrite which reacts with cellular glutathione to cause the S-glutathiolation of MMP-2 which induces conformational changes and exposes its catalytic site [43]. The association of MMP-2 with cell death pathways was previously reported as MMP-2 was shown to be localized to the nuclei of cells and cleaves PARP-1, a critical protein required for DNA repair [35]. Proteolysis of PARP-1 by MMP-2 inhibits DNA repair resulting in induction of apoptosis [36, 448]. However, the role of MMP-2 in AIF processing, an essential mitochondrial protein that mediates STS-induced cell death, has not been investigated.

MMP-2 may induce ER stress via its recently described ability to proteolyze SERCA2a and JPH-2 as shown in myocardial IR injury models [69, 70]. These proteins are localized at or near the MAM, where MMP-2 has also been localized [65]. In the current study, the mitochondrial 62 kDa form of AIF was detected in the mitochondria-enriched fraction of HT1080 cells. However, no significant changes in its level were observed upon STS challenge. On the other hand, two forms of AIF were detected in the cytosol at ~60 and ~45 kDa. The levels of both forms were significantly increased following 6 h STS. Otera et al. reported that detachment of AIF from the mitochondrial inner membrane space and release into the cytosol requires proteolytic processing of AIF, and that its 57 kDa cleaved form appears to be the apoptogenic one [286]. Our data suggests that there may be other cleavage products of AIF released into the cytosol following STS treatment, particularly that which I found at ~45 kDa. Whether the ~60 kDa form I found in the cytosol is an intermediate to the 57 kDa form, or has altered electrophoretic mobility due to post-translational modifications, remains to be studied.

Neither of the MMP-2 preferring inhibitors, ARP-100 or ONO-4817, significantly affected the levels of mitochondrial or cytosolic AIF forms. Similar results were obtained upon knocking down MMP-2 in HT1080 cells using MMP-2 siRNA prior to STS treatment. This suggests that MMP-2 may not be involved in the STS-induced processing of mitochondrial AIF and its release into the cytosol. Although MMP-2 activity was enhanced by STS treatment, it seems that MMP-2 may have a different role in STS-mediated pathological changes in HT1080 cells other than AIF proteolysis, at least at a time prior to any significant cell death.

Although calpain-1 was reported to mediate AIF release [287, 434], the selective calpain inhibitor ALLM [442, 443] did not show a significant change in the mitochondrial or cytosolic AIF levels. Similarly, the nonselective MMP-2/calpain inhibitor, PD150606 [443], did not cause

any significant effect on the levels of mitochondrial or cytosolic AIF. This suggests that the cleavage of mitochondrial AIF into 60 and 45 kDa cytosolic fragments may also be independent of calpain and may be mediated by other proteases. A protease that may mediate AIF cleavage is the calcium-independent cathepsin [292]. Based on the use of pharmacological inhibitors, calpain-1 and cathepsins-B, -L and -S were reported to mediate AIF cleavage in isolated mitochondria treated with atractyloside, a natural glycoside that is used to induce mitochondrial AIF release [292]. These reports are in line with our *in silico* analysis. Other than calpain and MMP-2, *in silico* analysis of AIF possible cleavage sites showed that it may be cleaved by different isoforms of cathepsins, MMPs and proprotein convertases with MMP-2 and cathepsins-B, -D and -E having the highest scores. As our results suggest that MMP-2 may not have a role in STS-induced AIF cleavage, the possible role of cathepsins in mediating AIF proteolysis merits further investigation.

In contrast to our results, Norberg et al. reported that AIF cleavage and release induced by STS is mediated via calpain-1, as they showed that PD150606, at a concentration of 200 μ M which significantly inhibits MMP-2 activity [287, 443], significantly abolished the STS-induced elevation in cytosolic AIF level in U1080 non-small cell lung carcinoma cells. However, they investigated a different cell line and used a higher STS concentration (0.2 μ M) and treatment duration (24 h) which would have caused 100% cytotoxicity of HT1080 cells used in our study. Another study also reported that calpain-1 mediates AIF release from mitochondria in primary cultures of hippocampal/cortical neurons. They showed that inhibition of calpain activity prevented AIF translocation to the nucleus and the transfected calpain-resistant AIF was not released to the nucleus following oxygen/glucose deprivation [449]. On the other hand, Joshi et al. reported results consistent with our findings, as they showed that PD150606 (50 μ M) or human erythrocyte calpastatin did not affect AIF release from rat liver mitochondria, while MDL-28170,

a cysteine protease inhibitor which inhibits cathepsin, decreased AIF release [291]. In PARP-1-dependent cell death, known as parthanatos, AIF was reported to be released into the cytosol uncleaved as a 62 kDa protein which is then translocated to the nucleus without the involvement of proteases including calpain. Parthanatos differs from apoptosis in being independent of caspase and includes large scale DNA fragmentation without formation of apoptotic bodies [450, 451]. This form of cell death occurs during STS-induced cytotoxicity of HeLa cells [452]. The results of this and previous studies suggest that the possible role of calpain in AIF cleavage requires further study, both *in vivo* and *in vitro*.

In conclusion, I showed that the activity of MMP-2, an important intracellular protease located in subcellular compartments where AIF is found, is elevated by STS as an early event prior to the induction of cell death. However, it and calpain appear not to be involved in the processing of AIF and its release into the cytosol under the conditions of our experiments. Further studies are required to reveal the role of MMP-2 in STS-induced cell injury.

Chapter IV

Matrix Metalloproteinase-2 Proteolyzes Mitofusin-2 and Impairs Mitochondrial Function During Myocardial Ischemia-Reperfusion Injury

A version of this chapter has been published:

Wesam Bassiouni, Robert Valencia, Zabed Mahmud, John M. Seubert, Richard Schulz (2023). Matrix metalloproteinase-2 proteolyzes mitofusin-2 and impairs mitochondrial function during myocardial ischemia-reperfusion injury. *Basic Res Cardiol.* 118:29.

Abstract

During myocardial ischemia-reperfusion (IR) injury matrix metalloproteinase-2 (MMP-2) is rapidly activated in response to oxidative stress. MMP-2 is a multifunctional protease that cleaves both extracellular and intracellular proteins. Oxidative stress also impairs mitochondrial function which is regulated by different proteins including mitofusin-2 (Mfn-2) which is lost in IR injury. Oxidative stress and mitochondrial dysfunction trigger the NLRP3 inflammasome and the innate immune response which invokes the *de novo* expression of an N-terminal truncated isoform of MMP-2 (MMP-2_{NTT76}) at or near mitochondria. I hypothesized that MMP-2 proteolyzes Mfn-2 during myocardial IR injury, impairing mitochondrial function and enhancing the inflammasome response. Isolated hearts from mice subjected to IR injury (30 min ischemia/40 min reperfusion) showed a significant reduction in left ventricular developed pressure (LVDP) compared to aerobically perfused hearts. IR injury increased MMP-2 activity as observed by gelatin zymography and increased degradation of troponin I, an intracellular MMP-2 target. MMP-2 preferring inhibitors, ARP-100 or ONO-4817, improved post-ischemic recovery of LVDP compared to vehicle perfused IR hearts. In muscle fibers isolated from IR hearts, the rates of mitochondrial oxygen consumption and ATP production were impaired compared to those from aerobic hearts, whereas ARP-100 or ONO-4817 attenuated these reductions. IR hearts showed higher levels of NLRP3, cleaved caspase-1 and interleukin-1 β in the cytosolic fraction, while the mitochondria-enriched fraction showed reduced levels of Mfn-2, compared to aerobic hearts. ARP-100 or ONO-4817 attenuated these changes. Co-immunoprecipitation showed that MMP-2 is associated with Mfn-2 in aerobic and IR hearts. ARP-100 or ONO-4817 also reduced infarct size and cell death in hearts subjected to 45 min ischemia/120 min reperfusion. Following myocardial IR injury, impaired contractile function and mitochondrial respiration and elevated

inflammasome response could be attributed, at least in part, to MMP-2 activation, which targets and cleaves mitochondrial Mfn-2. Inhibition of MMP-2 activity protects against cardiac contractile dysfunction in IR injury in part by preserving Mfn-2 and suppressing inflammation.

4.1. Introduction

Ischemic heart disease is a leading cause of death worldwide [115]. While restoration of blood flow to cardiac muscle by reperfusion is critical for heart survival, it also leads to further cardiac injury due to cellular changes in response to oxidative stress leading ultimately to myocardial cell death [119]. The pathophysiology of IR injury is not fully understood. As a result, preclinical studies have failed to translate into clinical practice [121]. We therefore need to understand the precise molecular mechanisms of IR injury to discover new therapeutic options for its treatment.

MMP-2 is a member of the MMPs family which is known to cleave extracellular matrix proteins under normal physiological conditions, such as angiogenesis and wound healing, as well as pathological conditions including inflammation, atherosclerosis, cancer metastasis and myocardial infarction [3-5, 7]. MMP-2 also exerts many effects by cleaving intracellular substrates during myocardial injury, which contributes to impaired contractile function during reperfusion [8, 9]. MMP-2 is localized to several intracellular organelles in cardiomyocytes including the sarcomere, cytoskeleton, nuclei, mitochondria and MAM [58]. Full length MMP-2 is rapidly activated during oxidative stress by peroxynitrite-induced S-glutathiolation [43]. Its proteolysis of sarcomeric proteins including TnI, titin, α -actinin and myosin light chain-1 contributes to contractile dysfunction [58]. An MMP-2_{NTT76}, lacking the first 76 amino acids, is induced by oxidative stress in cardiomyocytes and activates the innate immune response [66]. This isoform is enzymatically active and localizes in part to mitochondria [30, 64].

IR injury-induced oxidative stress disrupts the function of mitochondria by inducing mtDNA damage, altering calcium homeostasis and disrupting mitochondrial quality control

mechanisms that protect against cellular stress [453]. Among these are mitochondrial dynamics processes which include fusion and fission. Mitochondrial fusion includes the merging of the salvageable portions of two distinct, partially damaged mitochondria to maintain mitochondrial quality and morphology and prevent permanent loss of essential components including the mitochondrial proteins required for oxidative phosphorylation and ATP synthesis. This process is regulated by several proteins including Mfn-2 [233, 234]. Mitochondrial fission, on the other hand, divides injured mitochondria into two separate organelles. This process separates the injured mitochondrial segments which in turn are delivered to and degraded by lysosomes in a process known as mitophagy [234]. While enhanced mitochondrial fission is considered as an early marker of IR-induced mitochondrial damage [454], how factors regulating mitochondrial fusion change during IR injury is not well established [453].

Mfn-2 is localized to the MAM. It is responsible for the induction of outer mitochondrial membrane fusion, as well as tethering the mitochondria to the ER in order to regulate calcium transit at the MAM [195]. Loss of Mfn-2 during IR injury is observed, confirming the critical role of Mfn-2 in mitochondrial survival [253, 455]. However, increased Mfn-2 expression in cardiac myocytes is also seen depending upon the type of oxidative stress injury, which could be a part of an adaptive cardioprotective response [456]. Further research is required to reveal the exact role of Mfn-2 in IR injury.

The role of proteases and their targets in mitochondrial and contractile dysfunction of the heart in IR injury is emerging. Calpain inhibitors improve post-IR mitochondrial and contractile function [457], and prevent the cleavage of mitochondrial targets including Bid [458], and AIF [459]. Loss of Mfn-2 is associated with calpain activity in other organ injury models including glutamate-induced excitotoxicity [460], and acetaminophen-induced hepatotoxicity [461].

However, several calpain inhibitors used in these studies were shown to also inhibit MMP-2 activity [443]. Whether MMP-2 interacts with Mfn-2 and contributes to mitochondrial dysfunction in myocardial IR injury is unknown.

Oxidative stress also induces the activation of inflammasomes, multiprotein complexes which regulate the innate immune response and activate inflammation [462]. They are activated in response to mitochondrial damage, whereby they also affect mitochondrial function [312]. NLRP3, an inflammasome protein, localizes to the cytosol and ER and, when stimulated, assembles with the adaptor molecule containing caspase recruitment domain to form the inflammasome complex. This complex cleaves and activates caspase-1 and thereby IL-1 β . NLRP3 is one of the major components of the innate immune response [201]. Mitochondrial respiratory chain damage elevates the biosynthesis of RONS, resulting in the unfolding and activation of NLRP3 [312].

I investigated the relationship between MMP-2 and Mfn-2 during sterile inflammation in hearts subjected to IR injury. I show that MMP-2 activity is enhanced during myocardial IR injury with induction of MMP-2_{NTT76} expression as a part of the inflammasome response, impairing the mitochondrial respiratory chain and ultimately contractile function. Mfn-2 interacts with and is a proteolytic target of MMP-2. Pharmacological inhibition of MMP-2 activity attenuates the loss of Mfn-2 and inflammasome response, thereby preserving mitochondrial respiration and recovery of mechanical function following IR injury.

4.2. Methods

4.2.1. Isolated heart perfusion

Hearts from male C57BL/6J mice were isolated and subjected to *in vitro* IR injury in the Langendorff mode as described in **Chapter 2 (section 2.2)**.

Mice were assigned into 6 groups (n=5 per group) (Aerobic+Veh, Aerobic+ARP-100, Aerobic+ONO-4817, IR+Veh, IR+ARP-100, IR+ONO-4817). Due to the small size of the mouse heart, limited tissue available for biochemical analyses, and the need to use fresh and not frozen tissue for measuring mitochondrial respiration in muscle fibers [463], a separate series of heart perfusions (n=5 per group) was performed for the determination of mitochondrial oxygen consumption in permeabilized ventricular muscle fibers isolated immediately at the end of the isolated heart perfusion.

To evaluate the effect of MMP-2 inhibitors on irreversible injury (myocardial infarction), another series of isolated hearts (n=5 per group) was subjected to 45 min of global, no-flow ischemia followed by 120 min reperfusion and exposed to MMP-2 preferring inhibitors beginning 10 min prior to ischemia [464]. The coronary effluent was collected at 5, 10 and 15 min from the start of reperfusion and then every 15 min until the end of the reperfusion period for measuring LDH release. Hearts were then collected and stained for measuring infarct size (**see below**).

4.2.2. Preparation of ventricular extracts

Frozen heart ventricles were ground and homogenized as described in **Chapter 2 (section 2.3)**, to obtain whole tissue homogenate, cytosolic or mitochondria-enriched fractions.

4.2.3. Measurement of MMP-2 activity

MMP-2 activity in mouse hearts was determined by measuring the loss of TnI, a known intracellular substrate of MMP-2 in IR injury [9], in the cytosolic fraction using immunoblotting as described below. To confirm MMP-2 activation during IR injury, gelatin zymography was performed in both cytosolic and mitochondria-enriched fractions using 100 µg protein of each sample as described in **Chapter 2 (section 2.5)**.

4.2.4. Immunoblotting

To measure the level of a protein of interest in cytosolic or mitochondria-enriched fractions obtained from mouse heart ventricle, 30-35 µg total protein was separated on 4-15% SDS-polyacrylamide gels as described in **Chapter 2 (section 2.6)**.

Immunoblots were probed with two different monoclonal antibodies against Mfn-2: rabbit anti-Mfn-2 (1:1000, Cat#9482s, Cell Signaling) which binds to residues surrounding Val573, and mouse anti-Mfn-2 (1:1000, Cat#sc-100560, Santa Cruz Biotechnology) which binds to the C-terminal portion of Mfn-2. Other monoclonal antibodies used include: anti-MMP-2 (1:500, Cat#ab92536, Abcam), TnI (1:1000, Cat#MA-1040, IPOCdx), IL-1 β (1:500, Cat#ab9722, Abcam), caspase-1 (1:500, Cat#ab179515, Abcam), NLRP3 (1:500, Cat#15101s, Cell Signaling), α -tubulin (1:2000, Cat#ab7750, Abcam) as a cytosolic fraction loading control, or VDAC (1:1000, Cat#ab14734, Abcam) as a mitochondria-enriched fraction loading control.

4.2.5. Co-immunoprecipitation

To determine whether MMP-2 interacts with Mfn-2 in the heart, co-immunoprecipitation was performed in whole tissue homogenates obtained from aerobic or IR mouse hearts as described

in **Chapter 2 (section 2.7)**. Immunoblots were probed with either MMP-2 antibody (1:500, Cat#ab92536, Abcam) or Mfn-2 antibody (1:1000, Cat#9482s, Cell Signaling).

4.2.6. qPCR

Total cellular RNA was extracted from ventricular tissue and mRNA expression was measured as described in **Chapter 2 (section 2.8)**. qPCR primers for *B2M*, *FL-Mmp2* and *NTTMmp2* are shown in **Table 4.1**.

Table 4.1. Primer sequences used for qPCR.

Gene	Full Name	Sequence (5' to 3')	GeneBank ID	Product
<i>B2M</i>	beta-2-microglobulin	F: TGGTCTTTCTGGTGCTTGTCTC R: CCCGTTCTTCAGCATTTGGATTTC	NM_009735.3	170 bp
<i>Mmp2</i>	matrix metalloproteinase-2	F: GACCTCTGCGGGTTCTCTGC R: TTGCAACTCTCCTTGGGGCAGC	NM_008610.3	163 bp
<i>NTT-Mmp2</i>	N-terminal truncated <i>Mmp2</i>	F: GTGAATCACCCCACTGGTGGGTG R: TTGCAACTCTCCTTGGGGCAGC	N/A	229 bp

4.2.7. Mitochondrial respiration

Mitochondrial oxygen consumption in permeabilized mouse cardiac fibers was measured using a Clark electrode connected to an Oxygraph Plus recorder (Hansatech Instruments Ltd., Norfolk, England). Fresh cardiac muscle fibers were isolated from the left ventricles of the perfused hearts at the end of reperfusion as previously described [465]. Ventricular tissues were dissected under a dissecting microscope in ice-cold isolation buffer (2.77 mM CaK₂EGTA, 7.23 mM K₂EGTA, 20 mM imidazole, 20 mM taurine, 49 mM potassium methanesulfonate, 3 mM K₂HPO₄, 9.5 mM MgCl₂, 5.7 mM ATP, 1 μM leupeptin and 15 mM phosphocreatine). A 3-5 mm strip of the anterior left ventricle was isolated and dissected to remove fatty tissue and blood vessels. The myocardial strips were teased apart into bundles of 6-8 fibers each (1 mm wide, 3-4 mm long). Subsequently, fibers were permeabilized in isolation buffer containing 100 μg/mL saponin (Sigma-Aldrich) for 20 min, washed 3 times for 5 min in ice-cold respiration buffer (0.5 mM EGTA, 3 mM MgCl₂·6H₂O, 20 mM taurine, 10 mM KH₂PO₄, 20 mM HEPES, 1 g liter⁻¹ BSA, 60 mM potassium-lactobionate, 110 mM mannitol, 0.3 mM dithiothreitol), and immediately added to the respiration chamber containing 1.8 mL respiration buffer. All reagents used for preparing the isolation and respiration buffers were purchased from Sigma-Aldrich, except KH₂PO₄, HEPES and dithiothreitol, which were from ThermoFisher Scientific. One fiber strip was used for each single experiment. Glutamate (10 mM, Sigma-Aldrich) and malate (5 mM, Sigma-Aldrich) were added as substrates for complex I, while succinate (10 mM, Sigma-Aldrich) was used as a substrate for complex II and basal respiration was recorded. ADP (0.5 mM, Sigma-Aldrich) was then added to stimulate ATP-dependent respiration, which was subsequently inhibited using the ATP synthase inhibitor oligomycin (2.5 μM, Abcam). Maximal mitochondrial respiration was recorded by adding the mitochondrial oxidative phosphorylation

uncoupler (carbonyl cyanide p-trifluoro-methoxyphenyl hydrazone (FCCP), 4 μ M, Abcam). Finally, rotenone (2 μ M, Sigma-Aldrich) or antimycin A (5 μ M, Sigma-Aldrich) were used to inhibit complex I or II-mediated respiration respectively. The oxygen consumption rate (OCR) was measured following each step and normalized to the dry weight of each fiber (determined after overnight incubation in a drying oven). The respiratory control ratio (RCR) was calculated as the ratio between ATP-dependent and basal respiration rates to estimate mitochondrial respiratory efficiency.

Samples of the respiration buffer were collected after adding ADP and the level of ATP in each sample was measured using a fluorometric assay kit (Cat#ab83355, Abcam) by incubating samples with the reaction mixture for 30 min at room temperature while being protected from light. Fluorescence intensities were measured at excitation and emission wavelengths of 535 and 587 nm, respectively, using a fluorescence microplate reader (BioTek, Synergy H1, Winooski, US). ATP concentration was determined using a calibration curve obtained using the ATP standard and normalized to the dry weight of fibers.

4.2.8. Infarct size measurement

To evaluate the effect of MMP-2 inhibitors on infarct size, at the end of 120 min reperfusion, hearts were perfused through the aortic cannula with 1% w/v 2,3,5-triphenyltetrazolium chloride (Sigma-Aldrich) dissolved in Krebs-Henseleit solution for 15 min at 37°C. Then hearts were weighed and frozen overnight at -20°C. Hearts were then sectioned perpendicular to the long axis and the slices were incubated in 10% neutral formalin buffer for 1 h. Images were taken using a cell phone camera against a black background, and the area of infarction was quantified by measuring stained (red, live tissue) and unstained (white, necrotic) regions and

compared with total area of the slice. Percentage infarct size was calculated as an average of the different sections of each heart (5 sections per heart) using ImageJ software (Version 1.47v, NIH, USA).

4.2.9. LDH release measurement

To measure the extent of cell death during reperfusion, LDH activity was quantified in the coronary effluent using a CytoTox 96 Non-Radioactive Cytotoxicity Assay kit (Promega, United Kingdom). 50 μ L of the collected coronary effluents (in triplicates) were incubated with 50 μ L reaction mixture (LDH substrate in assay buffer) for 30 min at room temperature, protected from light. Absorbance was measured at 490 nm using microplate reader (BioTek, Synergy H1, Winooski, US). Standard LDH was used to generate a calibration curve with concentrations (0.005-0.32 U/mL) by incubating with the reaction mixture for the same duration. LDH activity was corrected for coronary flow and dry heart weight.

4.2.10. *In vitro* proteolysis of Mfn-2 by MMP-2

Mitochondria-enriched fractions (12 μ g total protein) prepared from the ventricles of aerobically perfused hearts were incubated with increasing concentrations of recombinant human 64 kDa MMP-2 (Sigma-Aldrich, 0.1, 1 or 10 ng) in the presence or absence of ARP-100 (30 μ M) for 1 h at 37°C in activity buffer (50 mM Tris-HCl, 150 mM NaCl, 5 mM CaCl₂·2H₂O, pH 7.6). An additional sample was kept at 4°C to rule out non-specific degradation of Mfn-2. The reaction was stopped by adding 6x SDS-containing sample buffer (0.5 M Tris-HCl pH 6.8, 30% v/v glycerol, 10% w/v SDS, 0.012% w/v bromophenol blue, and 0.6 M dithiothreitol). The reaction products were then separated on a 4-15% polyacrylamide gel, transferred, and immunoblotted with anti-Mfn-2 antibody (1:1000, Cat#9482s, Cell Signaling) as described above.

4.2.11. *In silico* analysis of Mfn-2 cleavage by MMP-2

The online cleavage prediction server Procleave was used to perform *in silico* prediction of Mfn-2 cleavage sites by MMP-2 [445]. This online tool suggests a number of potential target substrates and their corresponding cleavage sites by different proteases. The mouse Mfn-2 FASTA sequence (UniProt ID-Q80U63) was entered into the Procleave query sequence section and MMP-2 was selected as the protease of interest.

4.2.12. 3D crystal structure analysis

Amino acid sequences of human and mouse Mfn-2 were retrieved from Uniprot (<https://uniprot.org>). An X-Ray crystal structure (6JFK) of human nucleotide-free Mfn-2 was downloaded from the Protein Data Bank (PDB) (<https://www.rcsb.org/>) [466]. In PDB there are only three 3D structures of human Mfn-2 deposited, thus, a mouse Mfn-2 3D structure was created by homology modelling using SWISS-MODEL with the template 6JFK [467]. In the human Mfn-2 structure, residues 401–705 were deleted and replaced with the transmembrane domain residues 615–647. In the modelled structure of mouse Mfn-2 the missing residues 400-605 are part of the cytosolic domain predicted with SWISS-MODEL and AlphaFold (<https://alphafold.ebi.ac.uk/entry/O95140>) [468]. The structure was refined using the KoBaMIN webserver (<http://chopra-modules.science.purdue.edu>) and was evaluated for quality and validation by the Structural Analysis and Verification Server (SAVES) (<https://www.doe-mbi.ucla.edu/saves>). The top ten predicted cleavage sites of Mfn-2 by MMP-2 were drawn and visualized by PyMOL (v 2.1.1).

4.2.13. Statistics

Data are expressed as the mean \pm SEM of n independent experiments (where n represents an individual mouse heart sample). For multiple comparisons, one-way or two-way ANOVA followed by Dunnett's post-hoc test was used (GraphPad Prism version 8, La Jolla, CA, USA). Statistical significance was considered at $p < 0.05$.

4.3. Results

4.3.1. MMP-2 preferring inhibitors improve the recovery of contractile function after IR injury

Hearts subjected to IR injury (30 min ischemia, 40 min reperfusion) showed impaired contractile function as evidenced by a significant reduction in post-ischemic LVDP (**Figure 4.1 A**) and both dP/dt_{max} and dP/dt_{min} (**Figures 4.1 B and C**) compared to aerobically perfused hearts. These parameters were significantly improved post-IR injury by the MMP-2 preferring inhibitors, ARP-100 (10 μ M) or ONO-4817 (50 μ M) ($p < 0.05$). No significant change in HR was observed amongst the different groups (**Figure 4.2**). At these concentrations both ARP-100 and ONO-4817 did not significantly affect cardiac mechanical function under aerobic conditions in the absence of IR injury (**Figure 4.3**).

4.3.2. MMP-2 preferring inhibitors prevent impaired mitochondrial respiration in IR injury

Permeabilized cardiac fibers were isolated from hearts subjected to IR injury at the end of reperfusion. IR hearts exhibited impaired complex I and II-mediated mitochondrial respiration (**Figures 4.4 A and B**). There was a significant reduction in the RCR, ATP-dependent and

maximum mitochondrial OCR in fibers isolated from IR compared to aerobic hearts (**Figures 4.4 C-E**). All these changes were significantly attenuated in fibers isolated from IR+ARP-100 or IR+ONO-4817 hearts, suggesting that MMP-2 may have a role in the impairment of mitochondrial respiration caused by IR injury. There were no significant changes in basal, ATP-independent or non-mitochondrial respiration amongst the different groups (**Figures 4.4 F-H**). The ATP production rate was also significantly reduced in permeabilized fibers isolated from IR compared to aerobic hearts. Similarly, ARP-100 or ONO-4817 significantly attenuated this reduction ($p < 0.05$) (**Figure 4.4 I**). Neither ARP-100 nor ONO-4817 significantly affected mitochondrial respiratory parameters in fibers isolated from aerobic hearts (**Figure 4.5**).

4.3.3. MMP-2 is activated during myocardial IR injury

MMP-2 activation in the cytosolic fraction prepared from hearts at the end of reperfusion was determined by measuring the degradation of TnI, an intracellular MMP-2 target. Increased TnI degradation was observed in IR compared to aerobic hearts, as evidenced by the reduction in the ~30 kDa band and the appearance of an ~22 kDa fragment. ARP-100 or ONO-4817 attenuated the increase in TnI degradation ($p < 0.05$) (**Figure 4.6 A**). MMP-2 activity in cytosolic fractions was confirmed using gelatin zymography which showed that MMP-2 activity was significantly increased in IR injury compared to aerobic hearts ($p < 0.05$). Both ARP-100 and ONO-4817 significantly attenuated this increase in MMP-2 activity (**Figure 4.6 B**). The level of MMP-2 in purified cytosolic or mitochondria-enriched fractions across the different groups was not significantly changed (**Figure 4.7**).

The level of the mRNA for *NTT-Mmp2*, a driver of the innate immune response expressed as a result of oxidative stress [66, 174], was significantly increased by approximately 1.7 fold in

IR hearts and this increase was significantly reduced by ARP-100 or ONO-4817 ($p < 0.05$) (**Figure 4.8 A**). However, no significant change was observed in *FL-Mmp2* mRNA level in ventricular tissues from IR compared to aerobic hearts (**Figure 4.8 B**).

4.3.4. Inflammasome response is attenuated by MMP-2 preferring inhibitors

The levels of different markers of the inflammasome response were measured by immunoblotting. There was a significant increase in the level of NLRP3 in the cytosolic fraction from IR compared to aerobic hearts (**Figure 4.9 A**). This was accompanied by a reduction in procaspase-1 and pro-IL-1 β and a significant increase in the ratios of cleaved caspase-1 (P10)/procaspase-1 and IL-1 β /pro-IL-1 β in IR compared to aerobic hearts (**Figures 4.9 B and C**). These changes indicate the IR-induced induction of the inflammasome response with the subsequent cleavage of caspase-1 and activation of pro-inflammatory cytokines. All these changes were attenuated in IR+ARP-100 or IR+ONO-4817 groups ($p < 0.05$), suggesting that MMP-2 may be involved in the induction of the inflammasome response. Under aerobic conditions, both inhibitors did not significantly affect the levels of NLRP3, IL-1 β or caspase-1 in cytosolic fractions (**Figure 4.10**).

4.3.5. Mitochondrial Mfn-2 level is diminished after IR injury and preserved by MMP-2 preferring inhibitors

A significant reduction in the level of Mfn-2 in the mitochondria-enriched fraction in IR compared to aerobic hearts was seen using the Val573 epitope Mfn-2 antibody for immunoblotting. Both ARP-100 and ONO-4817 significantly attenuated this reduction, suggesting that the loss of Mfn-2 may be attributed to the proteolytic activity of MMP-2 (**Figure 4.11 A**). Similar results were obtained using an Mfn-2 antibody that binds to its C-terminus region (**Figure**

4.11 B). The mitochondrial level of Mfn-2 showed a significant correlation to cardiac mechanical function at the end of reperfusion when compared to LVDP, dP/dt_{\max} or dP/dt_{\min} ($p < 0.001$) (**Figures 4.11 C-E**). Aerobic hearts subjected to ARP-100 or ONO-4817 did not show significant change in Mfn-2 level (**Figure 4.12**).

I next determined whether MMP-2 interacts with Mfn-2 in heart tissue. Immunoprecipitation of ventricular extracts with anti-MMP-2 antibody followed by immunoblotting for Mfn-2 showed its presence in immunoprecipitates from both aerobic and IR hearts, suggesting a possible interaction between both proteins. No Mfn-2 bands were observed in immunoprecipitates from either aerobic or IR hearts using control IgG (**Figure 4.11 F**).

4.3.6. Mfn-2 is proteolyzed by MMP-2

Endogenous Mfn-2 in the mitochondria-enriched fraction of aerobic hearts was proteolyzed by incubation with MMP-2, as shown by the significant loss in 86 kDa Mfn-2 (**Figures 4.13 A and B**) along with the appearance of lower molecular weight fragments of ~ 60-75 kDa (**Figure 4.14**). The cleavage of Mfn-2 was prevented by ARP-100. Potential MMP-2 cleavage sites in mouse Mfn-2 were predicted using *in silico* analysis with Procleave along with their predicted amino acids sequences and the corresponding masses of both N- and C-terminal fragments. A summary of the top ten cleavage sites is shown in **Figure 4.13 C**. Positioning these predicted cleavage sites on the adapted 3D structure of mouse Mfn-2 shows a pronounced preference for MMP-2 proteolysis in the unstructured regions. Among the top ten cleavage sites, it was evident that MMP-2 prefers leucine in the P1' position as was demonstrated previously (**Figure 4.13 D**) [469]. *In silico* analysis showed that cleavage of Mfn-2 before amino acids 126 or 178 in the GTPase domain or before 579, 591 or 604 within the spacer between the first coiled-coil heptad

repeat domain and the transmembrane domain can produce lower molecular weight fragments of ~ 60-75 kDa, suggesting that these could be the potential cleavage sites by MMP-2 (**Figure 4.13 E**).

4.3.7. MMP-2 preferring inhibitors attenuate IR-induced myocardial infarction

A longer duration of 45 min ischemia and 120 min reperfusion was also investigated, allowing the measurement of myocardial infarct size and cell death estimated by the release of LDH activity into the coronary effluent (**Figure 4.15 A**). Hearts subjected to this more severe IR injury showed a greater reduction in post-IR LVDP compared to hearts subjected to 30 min ischemia and 40 min reperfusion (**Figure 4.1 A**). ARP-100 or ONO-4817 caused a significant improvement in post-IR LVDP compared to vehicle-perfused IR hearts (**Figure 4.15 B**). IR significantly increased infarct size compared to aerobic controls, which was attenuated by ARP-100 or ONO-4817 ($p < 0.05$) (**Figures 4.15 C and D**). LDH activity was also significantly higher in coronary effluent from IR hearts compared to aerobic ones, confirming myocardial cell death during IR injury, and peaked between 5-10 min from the start of reperfusion. Similarly, ARP-100 or ONO-4817 reduced LDH activity in coronary effluent ($p < 0.05$) (**Figure 4.15 E**), which was also observed when calculated as the total area under the curve (**Figure 4.15 F**).

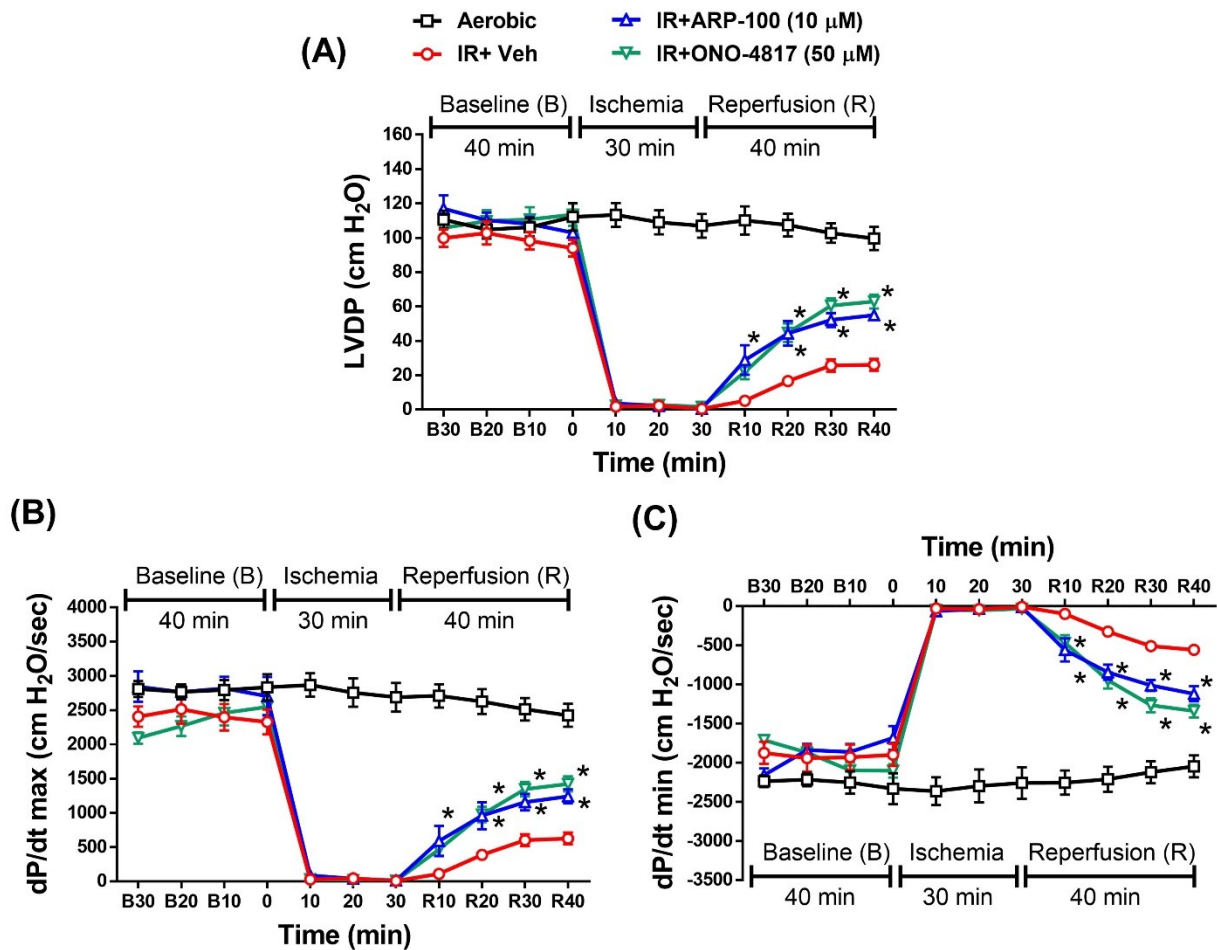


Figure 4.1. Hearts perfused with MMP-2 preferring inhibitors showed improved post-ischemic contractile function. Changes in (A) Left ventricular developed pressure (LVDP), (B) dP/dt_{max} or (C) dP/dt_{min} during IR injury in absence or presence of ARP-100 (ARP, 10 μ M), ONO-4817 (ONO, 50 μ M) or DMSO vehicle (Veh) compared to aerobic control (Aero) (n=5 per group). * $p < 0.05$ vs. IR+Veh by two-way ANOVA followed by Dunnett's post-hoc test.

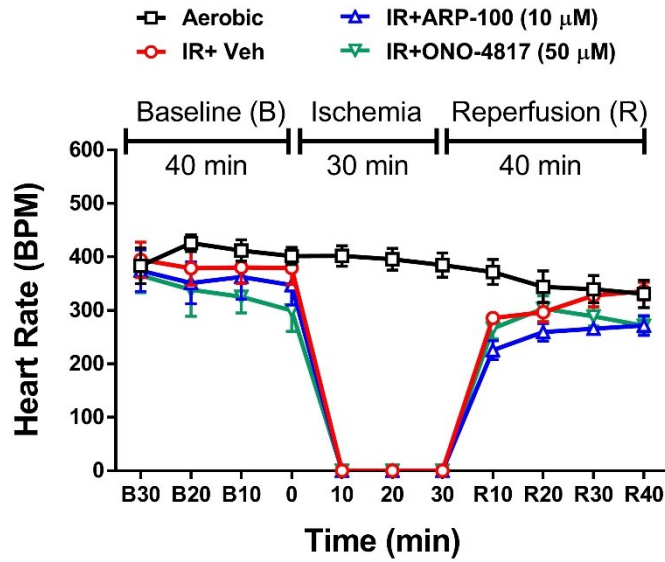


Figure 4.2. MMP-2 preferring inhibitors have no effect on post-ischemic heart rate during IR injury. Changes in heart rate in isolated mouse hearts subjected to IR injury in absence or presence of ARP-100 (ARP, 10 μM), ONO-4817 (ONO, 50 μM) or DMSO vehicle (Veh) compared to aerobic control (Aero) (n=5 per group).

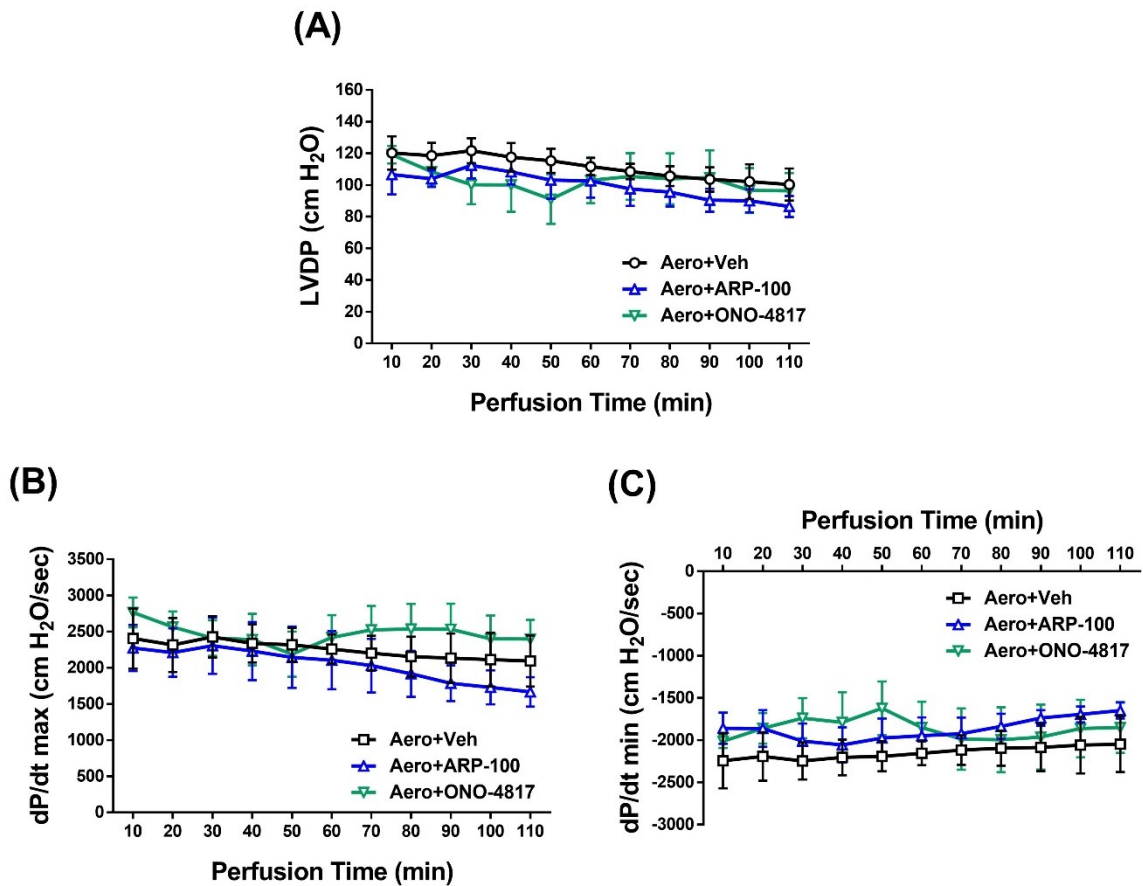


Figure 4.3. MMP-2 preferring inhibitors have no effect on cardiac contractile function under aerobic conditions. Changes in (A) left ventricular developed pressure (LVDP), (B) dP/dt_{max} or (C) dP/dt_{min} in aerobically perfused hearts in absence or presence of ARP-100 (ARP, 10 μ M), ONO-4817 (ONO, 50 μ M) or DMSO vehicle (Veh) ($n=5$ per group).

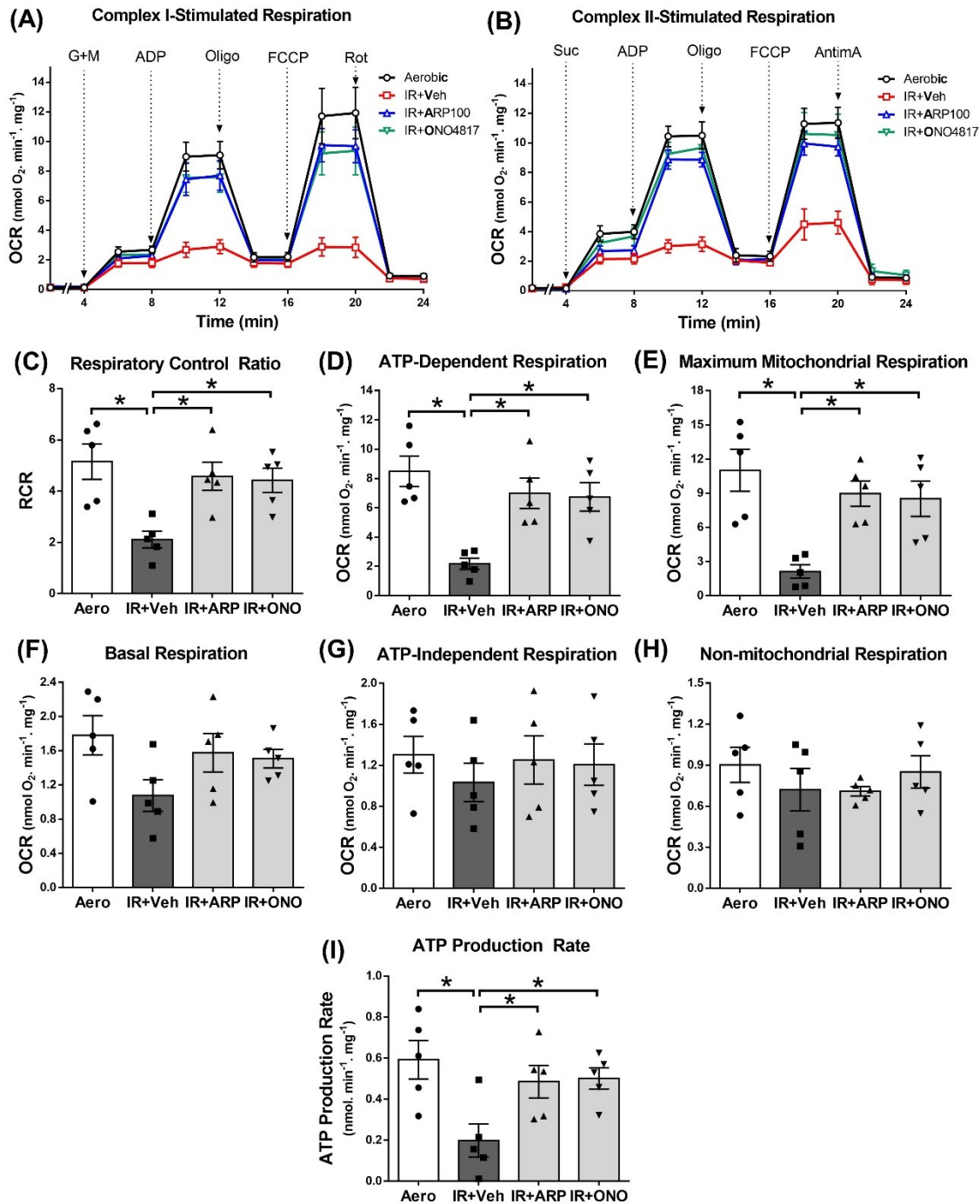


Figure 4.4. MMP-2 preferring inhibitors improve mitochondrial respiration in cardiac muscle fibers isolated from IR mouse hearts. (A) Complex I- and (B) complex II-stimulated mitochondrial oxygen consumption rate, (C) respiratory control ratio, (D) ATP-dependent respiration, (E) maximal mitochondrial respiration, (F) basal respiration, (G) ATP-independent respiration, (H) non-mitochondrial respiration and (I) ATP production rate in cardiac fibers isolated at the end of reperfusion from hearts subjected to IR injury in absence or presence of ARP-100 (ARP, 10 μ M), ONO-4817 (ONO, 50 μ M) or DMSO vehicle (Veh) compared to aerobic control (Aero) (n=5 per group). *p<0.05 by one-way ANOVA followed by Dunnett's post-hoc test.

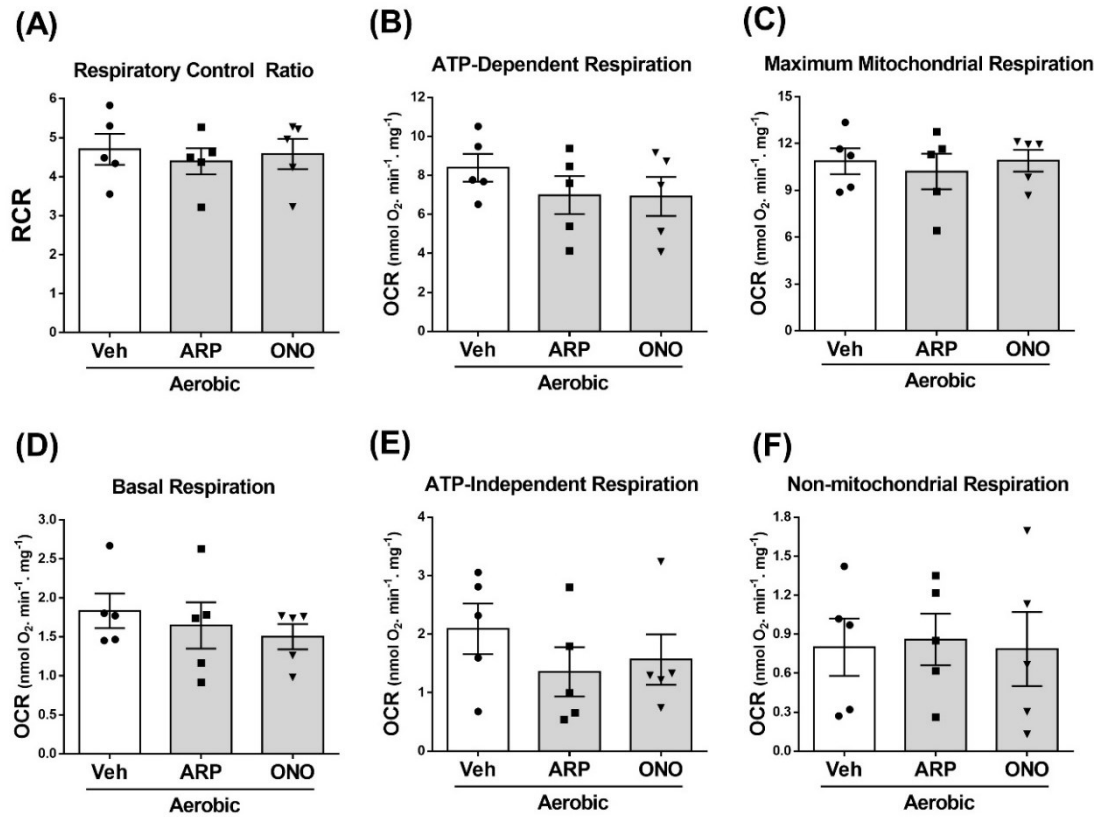


Figure 4.5. MMP-2 preferring inhibitors have no effect on mitochondrial respiration in cardiac muscle fibers isolated from aerobically perfused mouse hearts. (A) respiratory control ratio, (B) ATP-dependent respiration, (C) maximal mitochondrial respiration, (D) basal respiration, (E) ATP-independent respiration and (F) non-mitochondrial respiration in cardiac fibers isolated at the end of reperfusion from aerobically perfused hearts in absence or presence of ARP-100 (ARP, 10 μ M), ONO-4817 (ONO, 50 μ M) or DMSO vehicle (Veh) (n=5 per group).

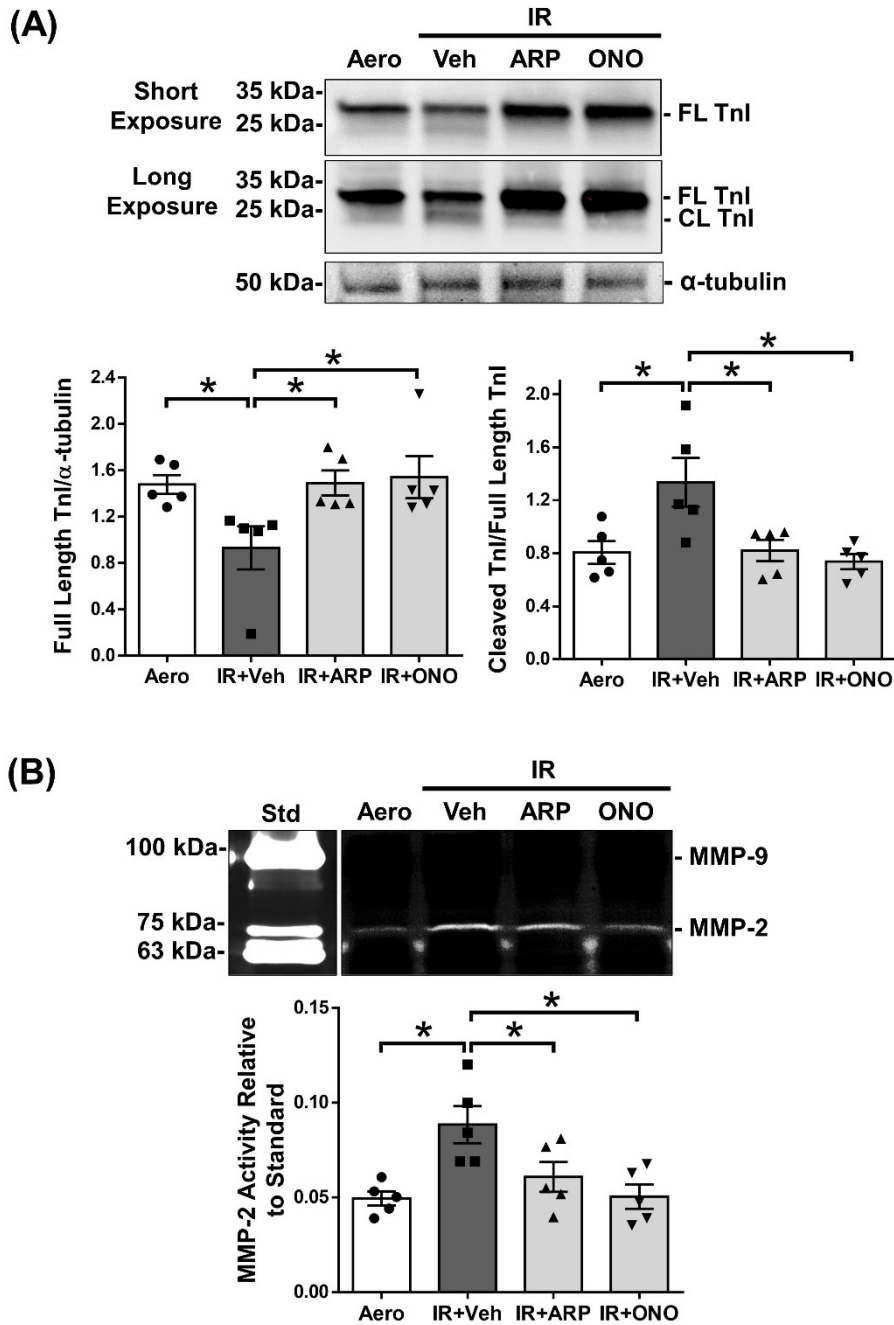


Figure 4.6. MMP-2 is activated in response to myocardial IR injury. (A) Representative immunoblots (upper panel) and quantitative measurements (lower panel) of full length (FL) and cleaved (CL) troponin I (TnI) levels in cytosolic fractions of IR hearts. (B) Representative gelatin zymogram (upper panel) and quantitative measurements (lower panel) of MMP-2 activity in cytosolic fractions of IR hearts in absence or presence of ARP-100 (ARP, 10 μ M), ONO-4817 (ONO, 50 μ M) or DMSO vehicle (Veh) compared to aerobic control (Aero). Bands are normalized to MMP-2 standard (Std) (n=5 per group). Std refers to conditioned medium from HT-1080 cells. Position of molecular weight ladder proteins indicated on the left. *p<0.05 by one-way ANOVA followed by Dunnett's post-hoc test.

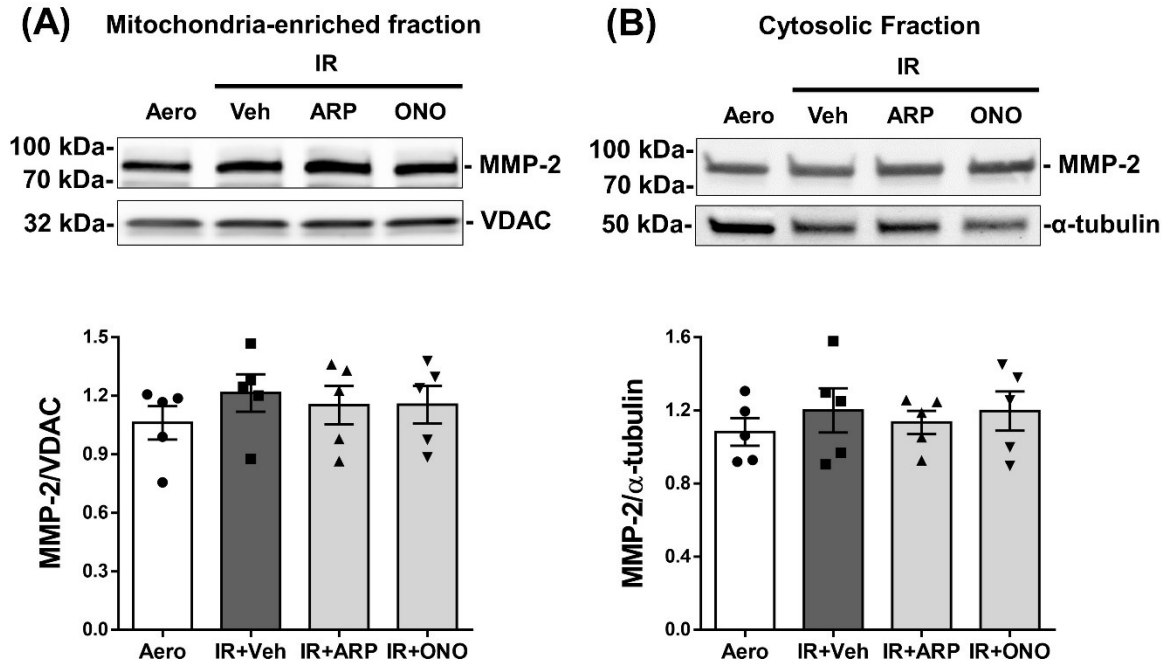


Figure 4.7. Mitochondrial or cytosolic MMP-2 protein levels are not affected by IR injury. Representative immunoblots (upper panels) and quantitative measurements (lower panels) of MMP-2 in (A) mitochondria-enriched or (B) cytosolic fractions of IR hearts in absence or presence of ARP-100 (ARP, 10 μ M), ONO-4817 (ONO, 50 μ M) or DMSO vehicle (Veh) compared to aerobic control (Aero) (n=5 per group). Position of molecular weight ladder proteins indicated on the left.

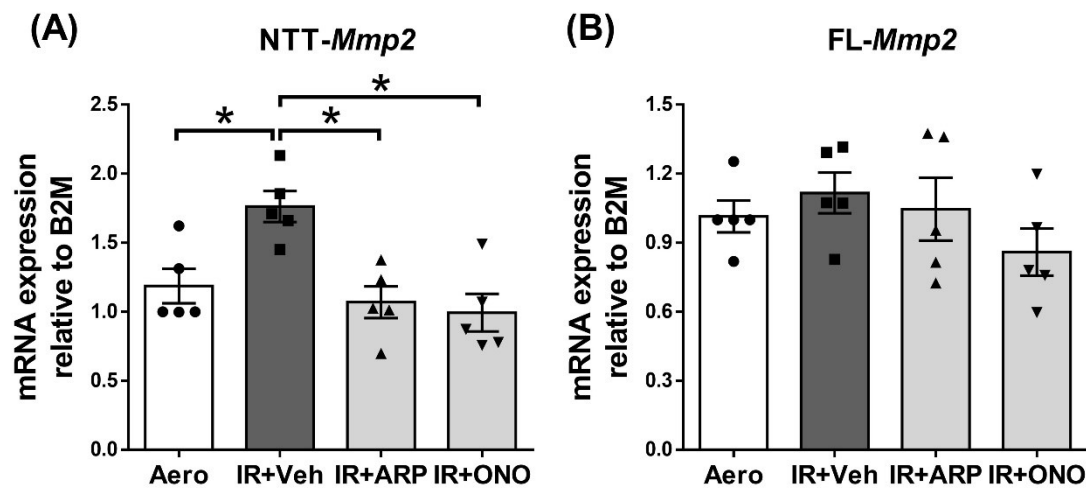


Figure 4.8. MMP-2 isoform expression in mouse hearts subjected to IR injury. mRNA expression of **(A)** N-terminal truncated (NTT)-*Mmp2* and **(B)** full length (FL)-*Mmp2* in IR heart in absence or presence of ARP-100 (ARP, 10 μ M), ONO-4817 (ONO, 50 μ M) or DMSO vehicle (Veh) compared to aerobic control (Aero) (n=5 per group). *p<0.05 by one-way ANOVA followed by Dunnett's post-hoc test.

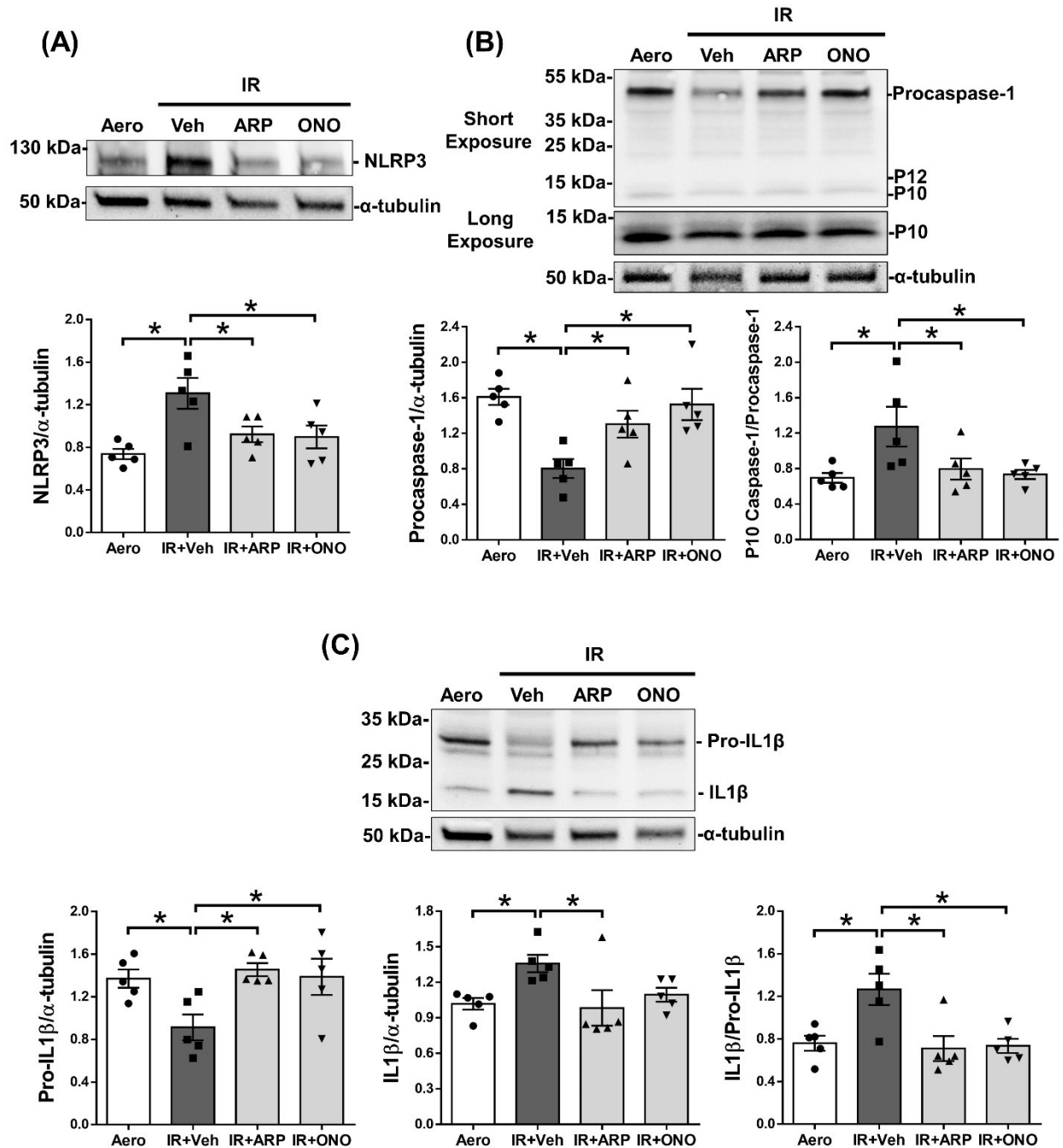


Figure 4.9. MMP-2 preferring inhibitors attenuate IR injury-induced increase in NLRP3 and active interleukin-1 β (IL-1 β) levels in the cytosolic fraction. Representative immunoblots (upper panels) and quantitative measurements (lower panels) of (A) NLRP3, (B) cleaved caspase-1 (P10)/procaspase-1 and (C) pro- and active IL-1 β in cytosolic fractions of IR hearts in absence or presence of ARP-100 (ARP, 10 μ M), ONO-4817 (ONO, 50 μ M) or DMSO vehicle (Veh) compared to aerobic control (Aero) (n=5 per group). Position of molecular weight ladder proteins indicated on the left. *p<0.05 by one-way ANOVA followed by Dunnett's post-hoc test.

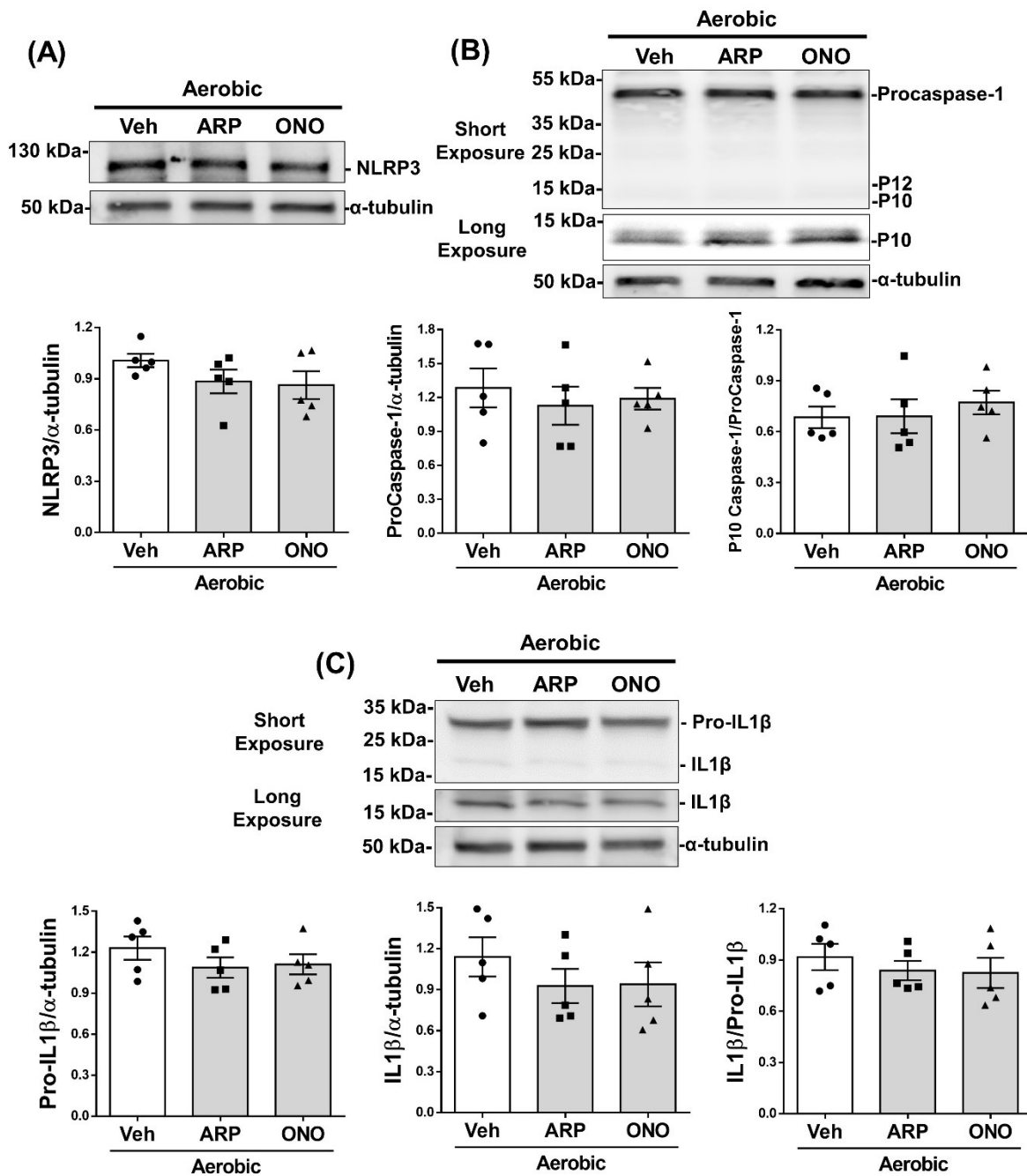


Figure 4.10. MMP-2 preferring inhibitors have no effect on inflammasome response in aerobically perfused hearts. Representative immunoblots (upper panels) and quantitative measurements (lower panels) of (A) NLRP3, (B) cleaved caspase-1 (P10)/procaspase-1 and (C) pro- and active IL-1 β in cytosolic fractions of aerobically perfused hearts in absence or presence of ARP-100 (ARP, 10 μ M), ONO-4817 (ONO, 50 μ M) or DMSO vehicle (Veh) (n=5 per group). Position of molecular weight ladder proteins indicated on the left.

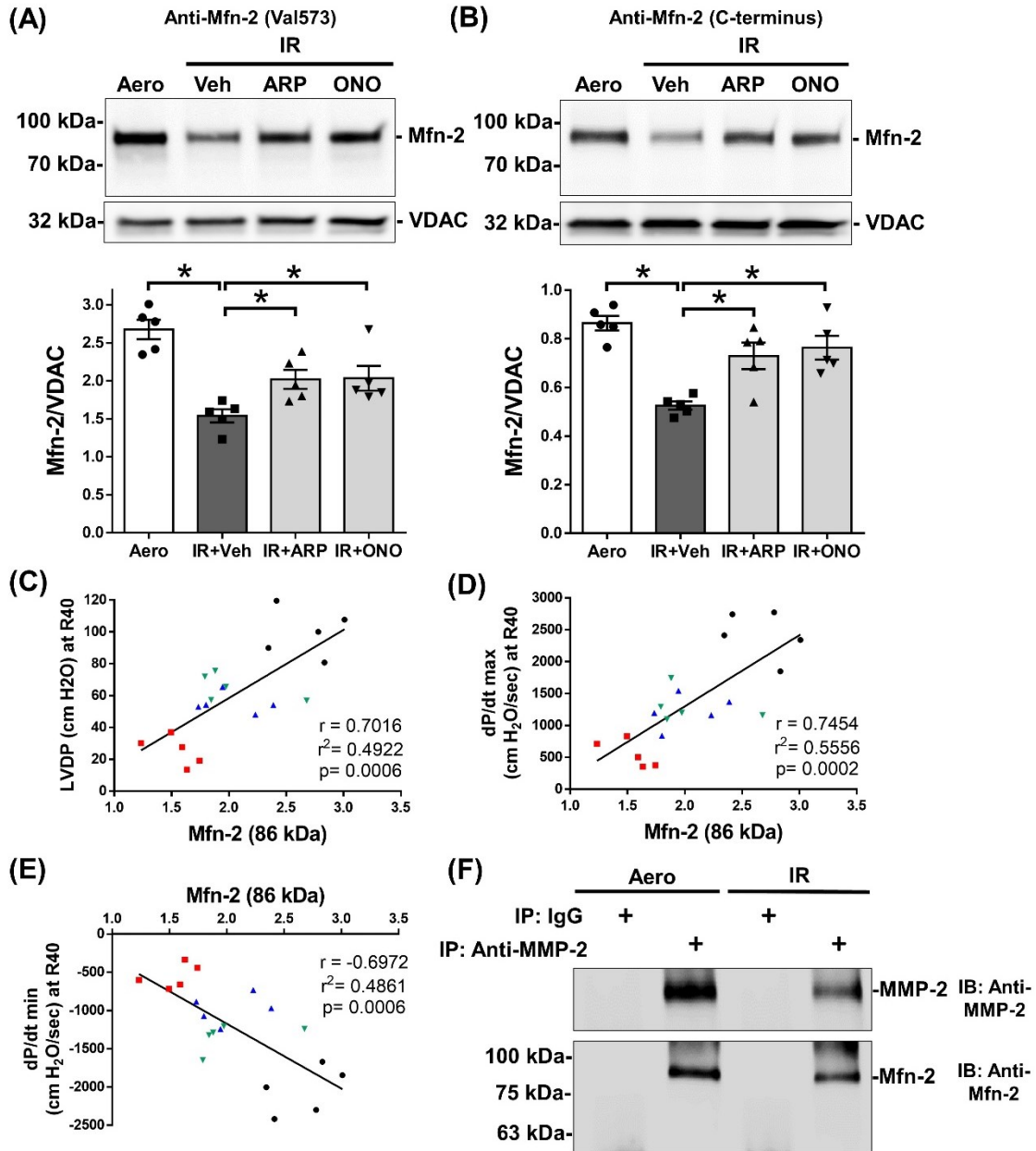


Figure 4.11. MMP-2 preferring inhibitors attenuate IR injury-induced reduction in Mfn-2 level in the mitochondria-enriched fraction. (A, B) Representative immunoblots (upper panels) and quantitative measurements (lower panels) of Mfn-2 level in IR hearts in absence or presence of ARP-100 (ARP, 10 μ M), ONO-4817 (ONO, 50 μ M) or DMSO vehicle (Veh) compared to aerobic control (Aero) using (A) anti-Mfn-2 (Val573) or (B) anti-Mfn-2 (C-terminus) antibody. (C-E) Correlation analysis of mitochondrial protein levels of Mfn-2 to (C) LVPD, (D) dP/dt_{max}, or (E) dP/dt_{min} at 40 min reperfusion (aerobic; black \bullet , IR+Veh; red \blacksquare , IR+ARP-100; blue \blacktriangle , IR+ONO-4817; green \blacktriangledown) (n=5 per group). (F) MMP-2 and Mfn-2 immunoblots using MMP-2 immunoprecipitates from aerobic and IR hearts showing an association between MMP-2 and Mfn-2, representative of four independent experiments. Position of molecular weight ladder proteins indicated on the left. *p<0.05 by one-way ANOVA followed by Dunnett's post-hoc test.

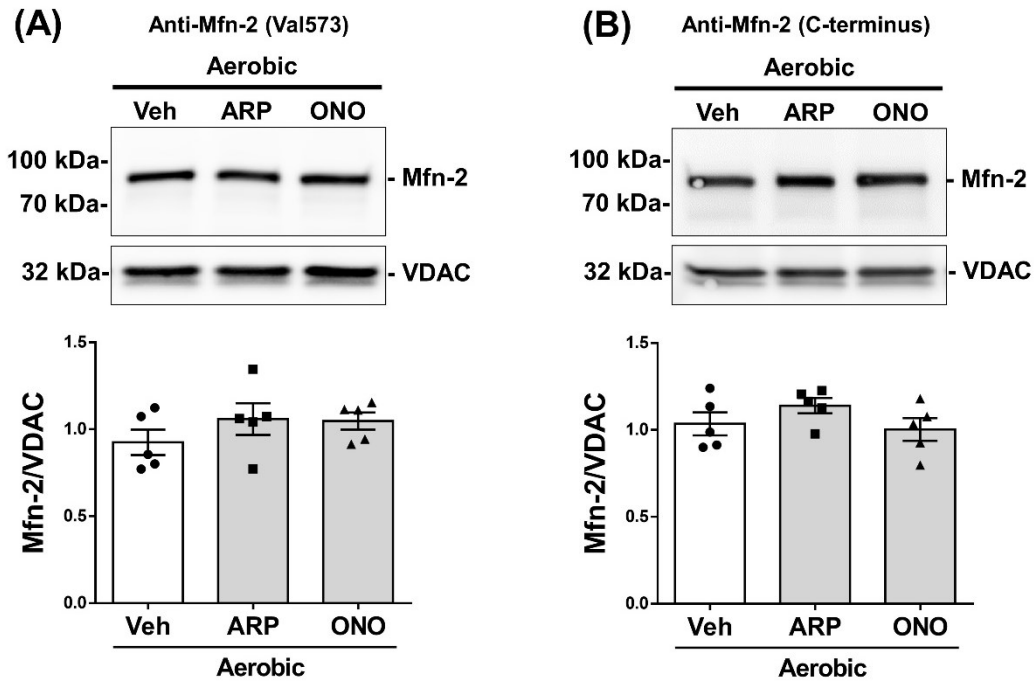


Figure 4.12. MMP-2 preferring inhibitors have no effect on Mfn-2 levels in the mitochondria-enriched fractions prepared from aerobically perfused hearts. (A, B) Representative immunoblots (upper panels) and quantitative measurements (lower panels) of Mfn-2 level in aerobically perfused hearts in absence or presence of ARP-100 (ARP, 10 μ M), ONO-4817 (ONO, 50 μ M) or DMSO vehicle (Veh) using (A) anti-Mfn-2 (Val573) or (B) anti-Mfn-2 (C-terminus) antibody (n=5 per group). Position of molecular weight ladder proteins indicated on the left.

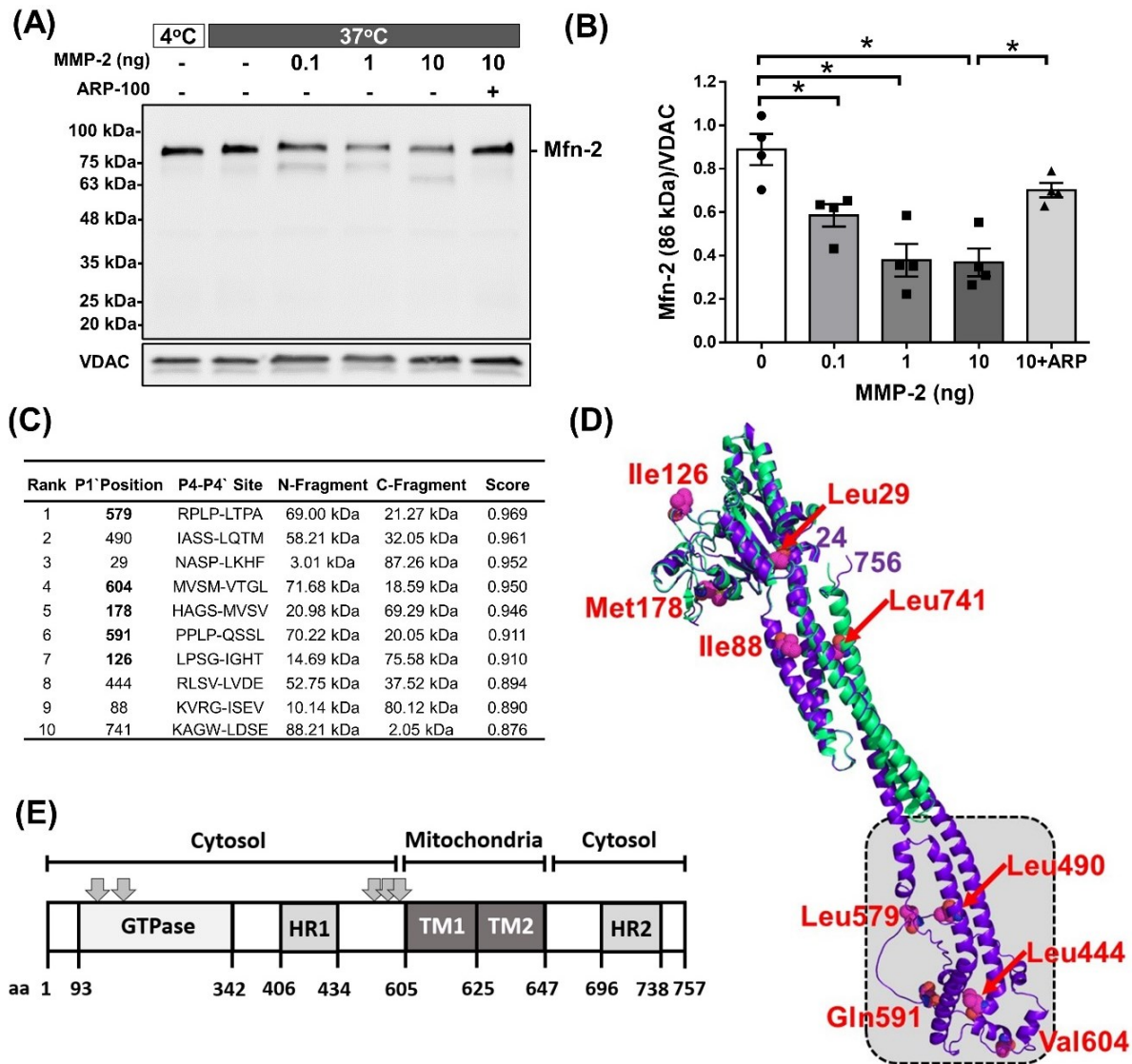


Figure 4.13. Mfn-2 is proteolyzed by MMP-2. (A) Immunoblot showing *in vitro* proteolysis of endogenous Mfn-2 in mitochondria-enriched fraction (12 μ g protein) from aerobic hearts incubated for 1 h at 37°C with MMP-2 (0.1, 1, 10 ng) in absence or presence of ARP-100 (30 μ M), representative of four different aerobic hearts showing similar results. Position of molecular weight ladder proteins indicated on the left. (B) Quantitative measurement of Mfn-2 (86 kDa) level relative to VDAC following proteolysis by MMP-2 (n=4). *p<0.05 by one-way ANOVA followed by Dunnett's post-hoc test. (C) *In silico* analysis of mouse Mfn-2 structure showing the top ten predicted cleavage sites of Mfn-2 by MMP-2 according to Procleave. (D) Structures of human Mfn-2 (PDB ID: 6JFK, green) and mouse Mfn-2 (predicted, purple) are superimposed together. Squiggles indicate unstructured regions. The top ten predicted cleavage sites are shown as ball and stick representations. The dashed box on the mouse Mfn-2 structure represents residues 400-605 which are missing in the crystal structure of human Mfn-2. (E) Representative Mfn-2 domain structure. Arrows denote the top five predicted cleavage sites by MMP-2 using Procleave *in silico* analysis which would result in Mfn-2 fragments of ~ 60-75 kDa as denoted in bold in (C).

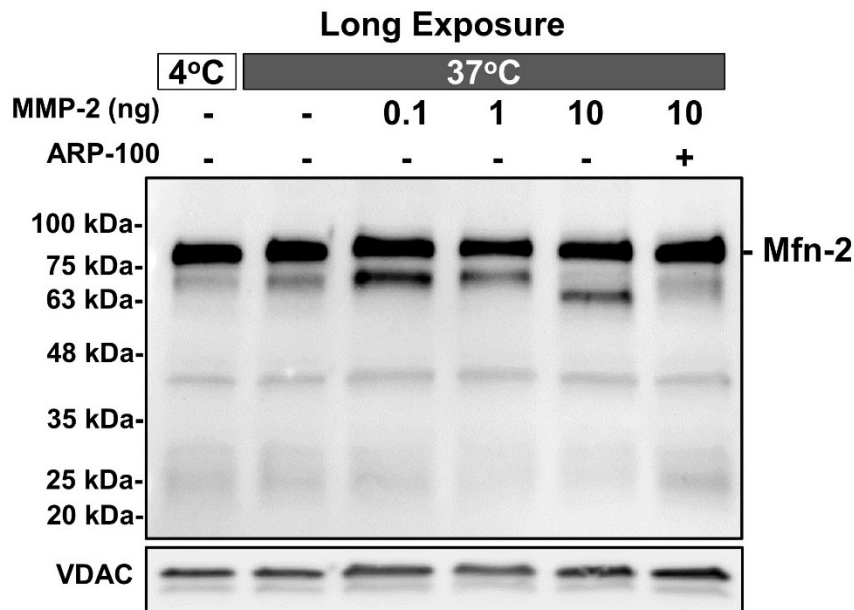


Figure 4.14. Long exposure of immunoblot in Figure 4.13A showing *in vitro* proteolysis of endogenous Mfn-2 in mitochondria-enriched fraction (12 μ g protein) from aerobic hearts incubated for 1 h at 37°C with MMP-2 (0.1, 1, 10 ng) in absence or presence of ARP-100 (30 μ M). The blot shows the appearance of lower molecular weight fragments (\sim 60-75 kDa) upon incubation with MMP-2, representative of four different aerobic hearts showing similar results. Position of molecular weight ladder proteins indicated on the left.

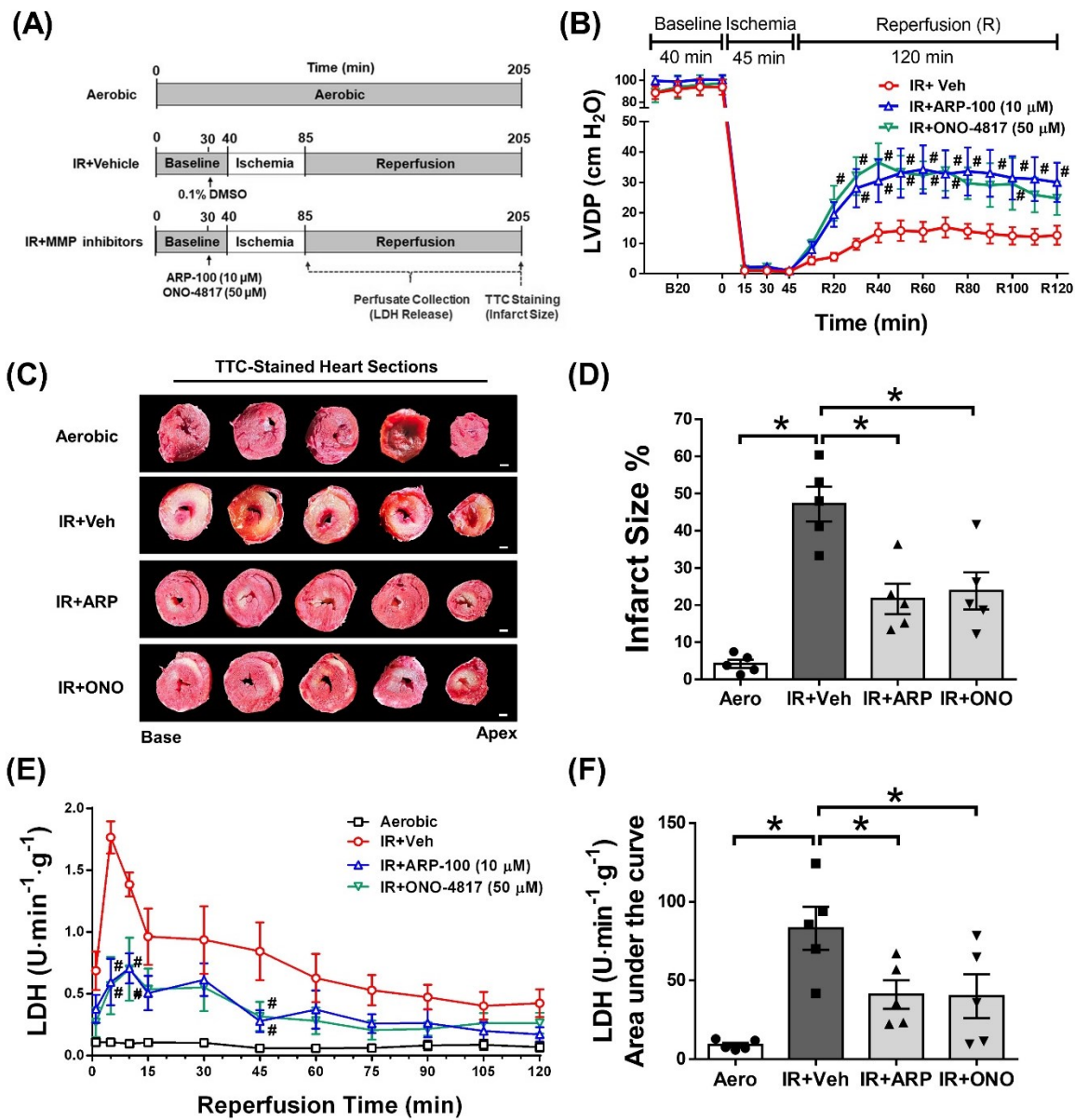


Figure 4.15. MMP-2 preferring inhibitors attenuate IR-induced myocardial infarction. (A) Schematic diagram of the experimental protocol and groups of isolated mouse hearts. **(B)** Changes in left ventricular developed pressure (LVDP) during more severe IR injury (45 min ischemia, 120 min reperfusion) in absence or presence of ARP-100 (ARP, 10 μM), ONO-4817 (ONO, 50 μM) or DMSO vehicle (Veh). **(C)** Representative images of 2,3,5-triphenyltetrazolium chloride (TTC)-stained heart slices showing viable (red) and necrotic (white) regions. Scale bar= 1 mm. **(D)** Quantification of infarct size expressed as the percentage of infarct to total area of the heart slice. **(E)** Changes in lactate dehydrogenase (LDH) activity in coronary effluent during reperfusion, and **(F)** quantification of the area under the curve among the different groups (n=5 per group). #p<0.05 vs. IR+Veh by two-way ANOVA followed by Dunnett's post-hoc test. *p<0.05 by one-way ANOVA followed by Dunnett's post-hoc test.

4.4. Discussion

I investigated whether mitochondrial Mfn-2 is affected by the proteolytic activity of MMP-2 during myocardial IR injury and how MMP-2 contributes to the impairment of mitochondrial function, induction of the inflammasome response and contractile dysfunction. Our study shows for the first time that Mfn-2 associates with and is a proteolytic target of MMP-2. I reveal that inhibition of MMP-2 activity protects against the loss of Mfn-2 during IR injury, improves mitochondrial respiration, attenuates the inflammasome response and thereby improves the post-IR recovery of contractile function. MMP-2 inhibitors also reduce myocardial infarct size and cell death when hearts are subjected to more severe IR injury. A schematic representation of this is shown in **Figure 4.16**.

MMP-2 is known to be activated during myocardial IR injury by peroxynitrite-induced S-glutathiolation [43, 44]. It was first identified to have an intracellular proteolytic activity by cleaving cardiac TnI in rat hearts subjected to IR injury [9]. MMP-2 was also activated in response to enhanced oxidative stress seen in hearts stimulated with pro-inflammatory cytokines [46], and in DXR-induced heart failure [60]. I show here that MMP-2 is activated in mouse hearts subjected to IR injury, indicated by the loss of TnI and increased gelatinolytic activity in heart tissue. The post-IR loss of mechanical function was significantly ameliorated with MMP-2 preferring inhibitors, ARP-100 or ONO-4817.

Cardiac muscle is rich in mitochondria to produce the ATP required for calcium-dependent contraction [470]. Mitochondria are also important for calcium-, metabolic- and apoptotic-signalling and the biosynthesis of amino acids and lipids [471]. Therefore, impairment of mitochondrial function would eventually result in cardiac contractile dysfunction, as encountered

during myocardial IR injury [472]. Preserving the integrity of mitochondrial regulatory proteins is thereby important to maintain mitochondrial function. MMP-2 is localized intracellularly to different subcellular compartments including mitochondria and the MAM [65]. The latter serves as the functional nexus between mitochondria and ER, playing a key role in calcium homeostasis, lipid metabolism, mitophagy and mitochondrial dynamics [473]. MMP-2_{NTT76}, which is not present under basal conditions but is expressed in response to oxidative stress, is reported to be localized to the subsarcolemmal mitochondria and possibly T-tubule-like structures [30]. It lacks the secretory signal sequence and the inhibitory pro-peptide of MMP-2, so it remains in the intracellular space and is enzymatically active [64, 66]. Our results show that *NTT-Mmp2* was significantly increased during IR along with the increase in MMP-2 proteolytic activity. The resultant MMP-2 activity may be a composite of both nascent MMP-2_{NTT76} as well as the oxidative stress-induced activation of MMP-2; approximately 50% of the latter is retained intracellularly due to its inefficient signal sequence [29]. This finding is supported by previous studies reporting induced myocardial *NTT-Mmp2* expression in response to oxidative stress in DXR-induced cardiotoxicity [60].

Reduction in mitochondrial respiratory chain complex-mediated oxygen consumption was reported following myocardial IR injury [224]. MMP-2 affects mitochondrial function, as transgenic mice with cardiac-specific overexpression of full length MMP-2 subjected to IR injury showed abnormalities in mitochondrial ultrastructure, impaired mitochondrial respiration and enhanced lipid peroxidation [63]. Hearts from cardiac-specific transgenic MMP-2_{NTT76} mice showed evidence of swollen mitochondria with less organized cristae and greater size heterogeneity. The hearts were also more susceptible to IR injury [30]. Hearts from mice undergoing DXR-induced cardiotoxicity, another type of oxidative stress injury, exhibited

mitochondrial fragmentation and cristae disruption amongst other cellular changes, while inhibiting MMP-2 activity preserved mitochondrial structure and morphology [60]. Our data shows an MMP-2-dependent contribution to the reduction in mitochondrial OCR following IR injury as ARP-100 or ONO-4817 attenuated the decreased RCR, ATP-dependent and maximal mitochondrial OCR and reduced ATP production rate in muscle fibers isolated from hearts subjected to IR injury. This reflects the ability of MMP-2 inhibitors to preserve a strong coupling between ATP synthesis and electron transport and help the mitochondria produce enough ATP to meet the demands of the cardiac muscle to maintain contractility.

Impairment of mitochondrial function results in the release of mitochondrial RONS, which in turn induce the NLRP3 inflammasome response [474]. This is consistent with our data showing the increased level of NLRP3, and cleaved caspase-1 and IL-1 β , indicating an induced inflammasome response and activated pro-inflammatory cascade. These changes may be attributed to MMP-2 activity, as they were attenuated by inhibition of MMP-2. NLRP3 regulates the innate immune response by sensing microbial infection, toxins or cellular damage via caspase-1 activation and the release of pro-inflammatory cytokines [475, 476]. In a mouse model of viral myocarditis, impaired cardiac and mitochondrial function was associated with increased NLRP3 level and induction of the inflammasome response [477]. Interestingly, MMP-2_{NTT76} is reported to be also involved in innate immunity. MMP-2_{NTT76} cleaves mitochondrial-associated inhibitor of kappa B-alpha in response to oxidative stress to release pro-inflammatory NF κ B to the nucleus, which results in mitochondrial-nuclear stress occurring as part of the innate immune response [66]. An association between MMP-2 and NLRP3 has been suggested. In aortic aneurysm, angiotensin II stimulated the release of mitochondrial RONS, activated NLRP3, and increased MMP-2 activity [478]. In vascular smooth muscle cells, MMP-2 expression was elevated by angiotensin II and

reduced by an NLRP3 inhibitor [479]. In cardiac fibroblasts cocultured with M1 macrophages, NLRP3 activation was associated with the upregulation of MMP-2 [480]. There appears to be an important crosstalk between MMP-2 and NLRP3 also in cardiac myocytes which likely involves the effect of both on mitochondrial function.

To elucidate how MMP-2 impairs mitochondrial function and induces the inflammasome response, I aimed to identify potential proteolytic substrates of MMP-2 in mitochondria. One of the key mitochondrial proteins that are essential for their function is Mfn-2. Mfn-2 plays a major role in mitochondrial fusion and is also localized to the MAM [195]. It also possesses a cytosolic GTPase domain, making it accessible to intracellular MMP-2. Several studies reported Mfn-2 loss in hearts subjected to *in vivo* or *in vitro* IR injury, in cell models of hypoxia-reoxygenation injury [455, 481, 482], and in the cardiac cell response to aortic constriction [483], or high glucose [484]. In contrast, the observed upregulation of Mfn-2 in IR injury and in response to oxidative stress could be an adaptive mechanism to protect the heart, as cardiac-specific deletion of Mfn-2 in mice resulted in impaired mitochondrial respiration and cardiac dysfunction [253, 456]. In HL-1 cells and neonatal rat ventricular cardiomyocytes subjected to hypoxia and reoxygenation, overexpression of Mfn-2 protected against cell death [481, 485]. By the use of co-immunoprecipitation I revealed that MMP-2 is associated with Mfn-2 in the heart. MMP-2 was able to cleave Mfn-2 *in vitro* and *in silico* analysis predicted that the cut sites lie particularly in unstructured regions in its cytosolic domain. This supports our data showing that the loss in mitochondrial Mfn-2 during IR was attenuated by MMP-2 inhibition. Furthermore, the level of Mfn-2 in the mitochondria-enriched fraction showed a positive correlation to the recovery of contractile function post-IR injury.

MMP-2-mediated loss of Mfn-2 during IR injury could be linked to the observed impairment in mitochondrial function. Mfn-2 is essential for mitochondria-ER tethering and calcium transit between both organelles. This tethering was reduced upon deletion of Mfn-2 in mouse embryonic fibroblasts which showed disrupted ER morphology [195]. Mfn-2 deletion decreased mitochondrial calcium uptake through a reduction in cardiomyocyte SR-mitochondrial contact in isolated mitochondria [255]. Furthermore, deletion of Mfn-2 in different animal and cell models resulted in mitochondrial fragmentation, impaired mitochondrial respiration and reduced ATP production [253, 254]. Mice with cardiac-specific double knockout of Mfn-1/Mfn-2 developed dilated cardiomyopathy with impaired cardiac function, mitochondrial structural abnormalities and diminished survival [250]. Similarly, deletion of Mfn-1/Mfn-2 in adult mouse hearts induced mitochondrial fragmentation, mitochondrial respiratory dysfunction and a progression to dilated cardiomyopathy [486]. Mfn-2, but not Mfn-1, knockout mice also exhibited impaired oxygen consumption and mitochondrial respiration [251]. This suggests that MMP-2-mediated impairment of mitochondrial respiratory function could be attributed to its ability to proteolyze Mfn-2. This could be attributed to Mfn-2 being required for the uptake of calcium by mitochondria from ER which is in turn needed for the function of the electron transport chain and oxidative phosphorylation. Thus loss of Mfn-2 will result in impaired calcium uptake by mitochondria and reduced ATP production [251, 487].

Several Mfn-2-dependent processes are associated with changes in mitochondrial dynamics. Mfn-2, as an outer mitochondrial membrane fusion protein, mediates the docking and fusion of mitochondria through the oligomerization of the GTPase domains of different Mfn-2 proteins [488]. Tethering of ER and mitochondria, which requires Mfn-2, is also required for the homeostasis of mitochondrial dynamics, as many key regulatory proteins of mitochondrial

dynamics are present in the MAM and require efficient calcium transit for their activity [196, 489]. Therefore, loss of Mfn-2 would indeed disrupt mitochondrial dynamics and function during IR injury.

MMP-2 activation during IR injury may also contribute to the development of myocardial cell death and infarction when hearts are subjected to longer durations of ischemia and reperfusion that induce necrotic rather than stunning injury. Our data shows that MMP-2 inhibition also reduced myocardial cell death as evidenced by the reduction in infarct size and LDH release. This is supported by a previous study showing that MMP-2 activity is higher in the infarct zone and area at risk in rat hearts subjected to *in vivo* IR injury with 90 min ischemia followed by 60 min reperfusion [140]. Ilomastat, a nonselective MMP inhibitor, reduced infarct size in rat hearts subjected to *in vivo* IR injury [149]. This protective effect of MMP inhibitors against myocardial infarction could be attributed to their ability to protect mitochondrial function and subsequently attenuate the inflammasome response as shown in our study. Activation of the NLRP3 inflammasome response induces pyroptosis which worsens cardiac injury and increases the extent of myocardial infarction [490].

In conclusion, MMP-2 activation during myocardial IR injury may impair mitochondrial respiration by proteolysis of Mfn-2 and induction of the inflammasome response, contributing to impaired mechanical function. Inhibition of MMP-2 could be a potential therapeutic option to protect against mitochondrial and cardiac contractile dysfunction in part by preserving Mfn-2, attenuating myocardial cell death and reducing both innate immune response and inflammasome activation and thereby sterile inflammation.

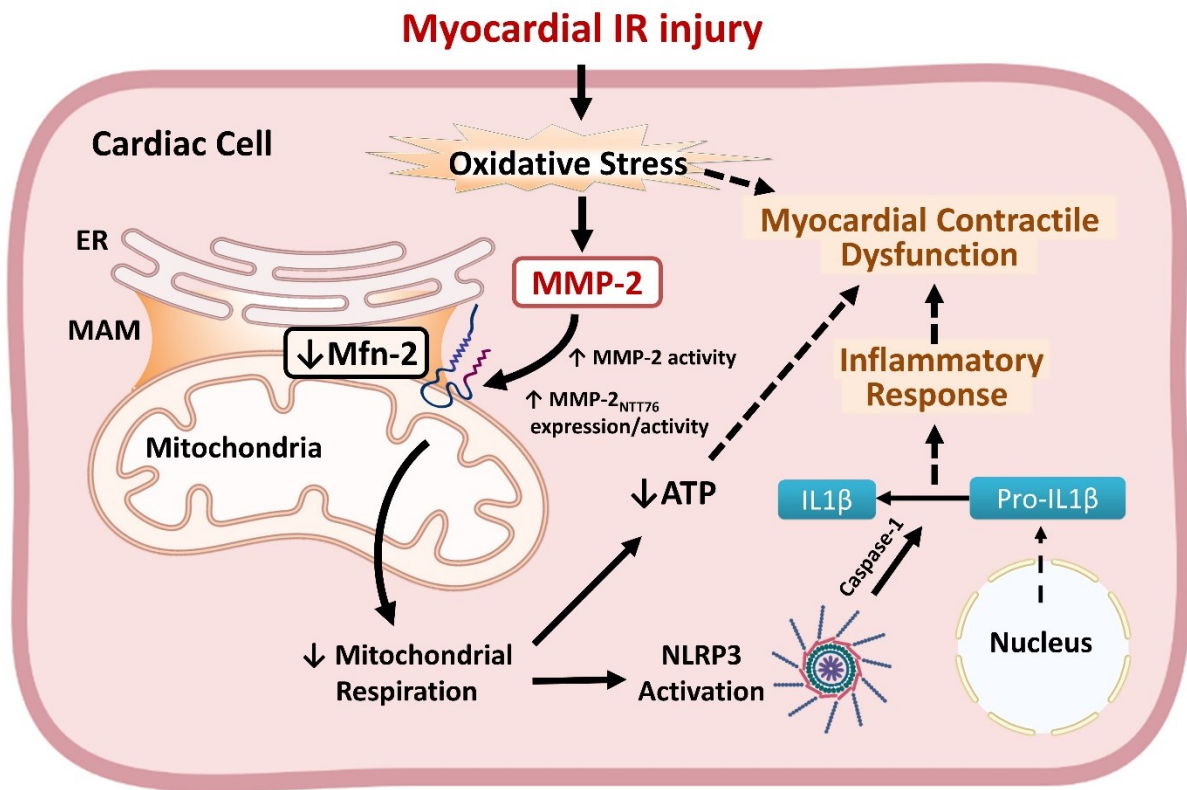


Figure 4.16. Schematic diagram showing the potential role of MMP-2 in mitochondrial dysfunction and inflammasome activation during myocardial ischemia-reperfusion (IR) injury. MMP-2 activated intracellularly in response to oxidative stress during IR injury with induced expression of MMP-2_{NTT76} targets and cleaves the mitochondrial fusion protein Mfn-2 to impair mitochondrial respiration and reduce ATP production, as our data shows, which, as reported, could be consequences of Mfn-2 loss [253]. Mitochondrial dysfunction induces the NLRP3 inflammasome response with subsequent activation of the pro-inflammatory cytokine IL-1β [474]. Collectively, these cellular changes lead to cardiac contractile dysfunction. Inhibition of MMP-2 activity, as our data show, attenuates these changes and improves mitochondrial respiration and contractile function after IR injury. Solid arrows denote pathways analyzed in the current study. Dotted arrows denote literature-based pathways (*Figure was created using BioRender*).

Chapter V

MMP-2 Inhibition Attenuates ER Stress-Mediated Cell Death During Myocardial Ischemia-Reperfusion Injury by Preserving IRE1 α

A part of this chapter has been submitted as a manuscript to the Journal of Molecular and Cellular Cardiology:

Wesam Bassiouni, Zabed Mahmud, Thomas Simmen, John M. Seubert, Richard Schulz. MMP-2 inhibition attenuates ER stress-mediated cell death during myocardial ischemia-reperfusion injury by preserving IRE1 α .

Abstract

Endoplasmic reticulum (ER) stress is one of the major events accompanying myocardial ischemia-reperfusion (IR) injury, as oxidative stress disrupts protein folding in the ER. As a result, the unfolded protein response (UPR) is activated through different ER stress sensors including inositol-requiring enzyme 1 α (IRE1 α) and protein kinase R-like ER kinase (PERK), which help restore protein folding. Failure of the UPR to reduce ER stress induces cellular dysfunction and apoptosis. Matrix metalloproteinase-2 (MMP-2) is a ubiquitous protease that is activated intracellularly in response to oxidative stress during myocardial IR injury. MMP-2 partially localizes to the mitochondrial-ER-associated membrane which regulates ER homeostasis. However, the role of MMP-2 in ER homeostasis is unknown. I hypothesized that MMP-2 may be involved in the regulation of the UPR and ER stress-mediated apoptotic response during IR injury. Isolated mouse hearts subjected to IR injury showed a significant reduction in left ventricular developed pressure compared to aerobically perfused controls. Ventricular extracts obtained from IR hearts had higher levels of 78 kDa glucose-regulated protein and protein disulfide isomerase compared to aerobic controls, indicating the induction of ER stress. Lower levels of IRE1 α and PERK were also observed. MMP-2 preferring inhibitors, ARP-100 or ONO-4817, given 10 min prior to ischemia, improved post-ischemic recovery of left ventricular developed pressure and preserved the level of IRE1 α . IR hearts also exhibited higher levels of CHOP and mitochondrial Bax and increased caspase-3 and -9 activities, indicating induction of ER stress-mediated apoptosis during IR, all of which were attenuated by MMP-2 inhibitors. Ventricular extracts from ischemic hearts prior to reperfusion also had lower levels of IRE1 α that were preserved by MMP-2 preferring inhibitors. However, only CHOP was upregulated in these ischemic hearts with no other evidence of apoptotic cell death. Immunoprecipitation studies showed an association between

MMP-2 and IRE1 α in aerobic and IR hearts. Incubation of mouse heart extract with exogenous MMP-2 showed evidence of IRE1 α proteolysis. During myocardial IR injury MMP-2 is not involved in the induction of ER stress, however, it may impair the UPR and induce apoptosis by proteolysis of IRE1 α . Inhibition of MMP-2 activity protects against cardiac contractile dysfunction in part by preserving IRE1 α and preventing the progression to myocardial cell death.

5.1. Introduction

The ER serves several cellular functions including protein synthesis, folding and translocation as well as calcium homeostasis and lipid biosynthesis [324, 325]. Therefore, maintenance of ER homeostasis is important for proper protein folding, and any physiological or pathological stimuli that disrupt this process will result in the accumulation of misfolded proteins, a process known as ER stress [323]. ER stress is one of the major events accompanying myocardial IR injury [379]. Reperfusion injury results from the cellular damage that occurs in response to enhanced oxidative stress which ultimately leads to myocardial cell death [119]. Lack of oxygen during ischemia and increased production of RONS upon reperfusion can trigger ER stress by inducing improper protein folding in the ER [380-382]. The pathophysiology of IR injury is not fully understood and identifying how ER stress signalling contributes to myocardial cell death during IR injury could be helpful in providing new therapeutic options for its management.

ER stress is sensed by ER-resident chaperones such as protein disulfide isomerase (PDI), which promotes oxidative protein folding, and GRP78, a chaperone which controls the UPR. GRP78 binds to the UPR signalling molecules and keeps them inactive in unstressed cells, and releases them in response to ER stress [344, 491]. The UPR is an adaptive response that occurs in response to ER stress to prevent the accumulation of misfolded proteins [492]. It works by lowering the number of proteins that need to be folded by transcriptional downregulation of secretory protein synthesis, increasing the folding capability of the ER or increasing the removal of misfolded proteins [339]. The UPR process is regulated by the induction of three main proteins: ATF6, PERK and IRE1 α [342]. IRE1 α is the most conserved UPR protein amongst different species [493]. Upon activation, it induces splicing of the mRNA encoding transcription factor XBP1. The encoded XBP1s in turn translocates to the nucleus and induces the transcription of

UPR target genes and folding enzymes to correct for protein misfolding [341, 345]. Thus, UPR activation is essential to protect against ER stress-mediated cellular damage [494].

Overactivation or failure of the UPR can result in the induction of apoptotic cell death mediated by ER stress, signalling the transition from an adaptive to a maladaptive response, which leads to disease progression [356, 360]. One of the mechanisms that regulate this apoptotic response is the transcriptional upregulation of CHOP, triggered by IRE1 α and PERK [365]. CHOP, subsequently, inhibits the anti-apoptotic Bcl-2 and induces upregulation and translocation of the pro-apoptotic Bax from the cytosol to the mitochondria to induce cytochrome C release, which in turn induces a caspase cascade and apoptosis [367, 368]. Induction of ER stress-mediated apoptosis is reported as one of the main features associated with myocardial IR injury in response to prolonged, unresolved ER stress, as evidenced by CHOP upregulation during reperfusion in mice subjected to IR injury *in vivo* [384]. Therefore, keeping a precise balance of UPR components is critical for cell survival during IR injury.

Several proteases are reported to be activated during myocardial IR injury and contribute to the resulting cardiac contractile dysfunction, among them is matrix MMP-2 [9]. MMP-2 is a multifunctional protease that is implicated in the pathophysiology of different disease conditions including ischemic heart disease, by mediating the proteolysis of several extracellular and intracellular proteins [8, 10]. It is activated intracellularly by the action of peroxynitrite-induced cysteine S-glutathiolation in response to oxidative stress [43]. MMP-2 is localized to several intracellular compartments, among them is the interface between the ER and mitochondria, known as the MAM [65]. MAM maintenance prevents the induction of ER stress [495]. Given that MMP-2 induces proteolytic degradation of different proteins known to be localized to the MAM such as Mfn-2 and calreticulin [65, 496], it might play a role in the dysregulation of ER homeostasis in

cardiac diseases. Whether MMP-2 is involved in the progression of the ER stress response and its associated cell death during IR injury is unknown.

I investigated whether MMP-2 activation during IR injury is involved in the ER stress response and ER stress-mediated apoptosis. I show that MMP-2, activated during IR, is not involved in the induction of ER stress or the process of protein misfolding. However, MMP-2 contributes to ER stress-mediated apoptotic cell death during IR in part by proteolysis of IRE1 α , which is initiated during ischemia. Pharmacological inhibition of MMP-2 preserves IRE1 α and attenuates ER stress-mediated apoptosis during IR injury, thereby protecting against myocardial contractile dysfunction.

5.2. Methods

5.2.1. Isolated heart perfusion

Hearts from male C57BL/6J mice were isolated and subjected to *in vitro* IR injury in the Langendorff mode as described in **Chapter 2 (section 2.2)**.

The heart perfusion groups included ones subjected only to ischemia or to IR in absence or presence of MMP-2 preferring inhibitors. Following 40 min of baseline aerobic perfusion, IR hearts were subjected to 30 min of global, no-flow ischemia followed by 40 min of reperfusion. The ischemic heart group was subjected to 30 min ischemia without reperfusion. Each group was compared to time-matched aerobically perfused hearts. Groups were assigned as follows: Aerobic 110 min, IR+Veh, IR+ARP-100, IR+ONO-4817, Aerobic 70 min, Ischemia+Veh, Ischemia+ARP-100 and Ischemia+ONO-4817.

5.2.2. Preparation of ventricular extracts

Frozen heart ventricles were finely ground and homogenized as described in **Chapter 2 (section 2.3)**, to obtain ventricular homogenates, cytosolic or mitochondria-enriched fractions. For caspase activity assay, ground tissue was prepared for cytosolic fraction isolation in the absence of protease inhibitors (see **section 5.10**).

5.2.3. Immunoblotting

To measure the level of proteins of interest in ventricular homogenates, cytosolic or mitochondria-enriched fractions obtained from mouse heart ventricle, 30-35 μ g total protein was separated on 4-15% SDS-polyacrylamide gels as described in **Chapter 2 (section 2.6)**.

The following primary antibodies were used (all from Cell Signaling): anti-IRE1 α (1:1000, Cat#3294), PERK (1:1000, cat#3192), PDI (1:1000, cat#3501), GRP78 (1:1000, Cat#3177), XBP1s (1:1000, Cat#83418), CHOP (1:1000, Cat#2895), Bax (1:1000, Cat#2772), caspase-3 (1:1000, Cat#9665), caspase-9 (1:1000, Cat#9506), GAPDH (1:2000, Cat#2118) as a ventricular homogenate or cytosolic fraction loading control, and VDAC (1:1000, Cat#ab14734, Abcam) as a mitochondria-enriched fraction loading control.

5.2.4. Co-immunoprecipitation

To determine whether MMP-2 interacts with IRE1 α in the heart, co-immunoprecipitation was performed in ventricular homogenates obtained from aerobic or IR mouse hearts as described in **Chapter 2 (section 2.7)**. Immunoblots were probed with either MMP-2 antibody (1:500, Cat#ab92536, Abcam) or IRE1 α antibody (1:1000, Cat#3294, Cell Signaling).

5.2.5. qPCR

Total cellular RNA was extracted from ventricular tissue and mRNA expression was measured as described in **Chapter 2 (section 2.8)**. qPCR primers for *B2M*, *IRE1 α* , *PERK*, *PDI*, *GRP78* and *XBPIs* are shown in **Table 5.1**.

Table 5.1. Primer sequences used for qPCR.

Gene	Full Name	Sequence (5' to 3')	GeneBank ID	Product
<i>B2M</i>	beta-2-microglobulin	F: TGGTCTTTCTGGTGCTTGTCTC R: CCCGTTCTTCAGCATTTGGATTTC	NM_009735.3	170 bp
<i>XBPIs</i>	spliced x box-binding protein 1	F: TGCTGAGTCCGCAGCAGGTG R: ACAGGGTCCAACCTTGTCCAG	NM_001271730.1	132 bp
<i>GRP78</i>	78 kDa-glucose regulated protein	F: TGCAGCAGGACATCAAGTTC R: TTTCTTCTGGGGCAAATGTC	NM_001163434.1	111 bp
<i>IRE1α</i>	inositol-requiring enzyme 1 α	F: ACGGTGGACATCTTTTCTGC R: TGGGGATCCATAGCAATCAT	NM_023913.2	194 bp
<i>PDI</i>	protein disulfide isomerase	F: AACGGGAGAAGCCATTGTA R: AGGTGTCATCCGTCAGCTCT	NM_027959.4	155 bp
<i>PERK</i>	protein kinase R-like ER kinase	F: GGGTGGAAACAAAGAAGAC R: CAATCAGCAACGGAAACT	NM_010121.3	96 bp

5.2.6. *In vitro* proteolysis of IRE1 α by MMP-2

Ventricular homogenates (15 μ g total protein) prepared from the ventricles of aerobically perfused hearts were incubated with increasing concentrations of recombinant human 64 kDa MMP-2 (Sigma-Aldrich, 1, 10 or 100 ng) in the presence or absence of ARP-100 (30 μ M) for 1 h at 37°C in activity buffer (50 mM Tris-HCl, 150 mM NaCl, 5 mM CaCl₂·2H₂O, pH 7.6). An additional sample was kept at 4°C to rule out non-specific degradation of IRE1 α . The reaction was stopped by adding SDS-containing sample buffer. The reaction products were then separated on a 4-15% polyacrylamide gel, transferred, and immunoblotted with anti-IRE1 α antibody (Cat#3294, Cell Signaling) as described above.

5.2.7. *In silico* analysis of IRE1 α cleavage by MMP-2

The online cleavage prediction server Procleave was used to perform *in silico* prediction of IRE1 α cleavage sites by MMP-2 [445]. Procleave is an online tool that suggests potential substrates that could be targeted by different proteases and their corresponding cleavage sites. The mouse IRE1 α FASTA sequence (UniProt ID-Q9EQY0) was entered into the Procleave query sequence section and MMP-2 was selected as the protease of interest.

5.2.8. 3D crystal structure analysis

Amino acid sequences of mouse IRE1 α were retrieved from Uniprot (<https://uniprot.org>). X-Ray crystal structures (4PL3/4PL4/4PL5) of murine IRE1 α were downloaded from the PDB (<https://www.rcsb.org/>) [466, 497]. All three X-ray crystal structures are similar and solved for the cytoplasmic domain (550-977 residues) of the mouse IRE1 α except they are in complex with three different inhibitors, MKC9989/OICR464/ OICR573 [497]. In the mouse IRE1 α crystal structures, residues 1-549 containing luminal, disordered, and transmembrane helical regions are missing. AlphaFold (<https://alphafold.ebi.ac.uk/entry/Q9EQY0>) [468] was used to predict those regions of the IRE1 α . The modelled full-length IRE1 α structure was refined using the KoBaMIN webserver (<http://chopra-modules.science.purdue.edu>) and was evaluated for quality and validation by SAVES (<https://www.doe-mpi.ucla.edu/saves>). The top ten predicted cleavage sites of IRE1 α by MMP-2 were drawn and visualized by PyMOL (v 2.1.1).

5.2.9. Measurement of caspase activity

Caspases-3 and -9 activities were measured in cytosolic fractions obtained from heart ventricle using fluorometric enzyme assays. A caspase peptide substrate was diluted in 2x reaction

buffer (20 mM HEPES, 40 mM NaCl, 0.2% CHAPS, 0.4 mM EDTA, 4% glycerol, 4 mM dithiothreitol, pH 7.4). Caspase-3 activity was quantified as the rate of production of the fluorogenic 7-amino-4-methylcoumarin (AMC, Cat#257370, Sigma-Aldrich) following the cleavage of the caspase-3 substrate, Ac-DEVD-AMC (Cat#ALX-260-031-M005, Enzo Life Sciences), while caspase-9 activity was determined as the rate of production of the fluorogenic 7-amino-4-(trifluoromethyl)coumarin (AFC, Cat#248924, Sigma-Aldrich) following the cleavage of the caspase-9 substrate, Ac-LEHC-AFC (Cat#ALX-260-116-M005, Enzo Life Sciences). The fluorescence intensities were measured at excitation and emission wavelengths of 380 and 460 nm, respectively, following 1 h incubation at 37°C with the corresponding substrate using a fluorescence microplate reader (BioTek, Synergy H1, Winooski, US). The activity was then calculated using a linear standard curve created with AMC or AFC standards for caspase-3 or -9, respectively, and normalized to the protein concentration in each sample.

5.2.10. Thioflavin T binding assay

To confirm the induction of ER stress during IR injury, the extent of protein aggregation was measured in insoluble fractions obtained from heart extracts using the thioflavin T (ThT) binding assay [498]. For insoluble protein extraction, the pellet obtained from the first step of the subcellular fractionation was resuspended in aqueous buffer (20 mM Tris, 100 mM NaCl, 0.1% proteinase inhibitor cocktail; Cat#P8340, Sigma-Aldrich) and centrifuged at 20,000 g for 20 min at 4°C. Then the pellet was carefully resuspended in detergent buffer (20 mM Tris-HCl, 100 mM NaCl, 0.1% SDS, 1% sodium deoxycholate, 1% Igepal, 0.1% proteinase inhibitor cocktail, pH 7.6) and incubated with benzonase nuclease (65 units/mL, Sigma-Aldrich) for 5 min to remove nucleic acids that may interfere with ThT, followed by centrifugation at 20,000 g for 20 min at 4°C. The detergent-insoluble pellet was washed two times with aqueous buffer to remove any residual

detergent that may interfere with the assay. Finally, the pellet was resuspended in aqueous buffer and used as the insoluble protein fraction.

The extent of protein aggregation in heart extracts was determined by measuring the ability of ThT to bind to aggregated proteins using a fluorometric assay. ThT is a small molecule which selectively binds to protein aggregates to give a fluorescent signal. The insoluble protein fractions obtained from heart ventricles were incubated with 10 μ M ThT (Cat#T3516, Sigma-Aldrich) prepared in assay buffer (10 mM Tris, 150 mM NaCl, pH 7.4), for 30 min followed by measuring the fluorescence signal at excitation and emission wavelengths of 440 and 490 nm, respectively, using a fluorescence microplate reader (BioTek, Synergy H1, Winooski, US). The fluorescence intensity was presented as relative fluorescence units (RFU) and normalized to the protein concentration of each sample.

5.2.11. Statistics

Data are expressed as the mean \pm SEM of n independent experiments (where n represents an individual mouse heart). For multiple comparisons, one-way or two-way ANOVA followed by Dunnett's post-hoc test was used (GraphPad Prism version 8, La Jolla, CA, USA). Statistical significance was considered at $p < 0.05$.

5.3. Results

5.3.1. MMP-2 preferring inhibitors protect against IR-induced cardiac contractile dysfunction

Hearts subjected to IR injury showed a significant reduction in post-ischemic LVDP (**Figure 5.1 A**) and the rates of contraction (dp/dt_{max}) and relaxation (dp/dt_{min}) (**Figures 5.1 B and**

C) compared to aerobically perfused hearts, indicating impaired contractile function resulting from IR. The MMP-2 preferring inhibitors, ARP-100 (10 μ M) or ONO-4817 (50 μ M), significantly attenuated the reduction in these contractile parameters ($p < 0.05$).

5.3.2. MMP-2 is not involved in the induction of ER stress response during IR injury

To confirm the induction of ER stress response during IR, changes in the mRNA and protein levels of ER stress markers, GRP78 and PDI, were measured in heart extracts. The mRNA and protein levels of both GRP78 and PDI in ventricular extracts were significantly higher in hearts subjected to IR compared to aerobic controls, confirming the induction of ER stress during IR. ARP-100 or ONO-4817 did not significantly affect the increase in GRP78 or PDI, suggesting that IR-mediated induction of ER stress is independent of MMP-2 (**Figures 5.2 A-D**). Aerobic hearts subjected to ARP-100 or ONO-4817 did not show significant changes in GRP78 or PDI protein levels (**Figures 5.4 A and B**). The extent of protein aggregation was also measured as an indication of ER stress using the ThT fluorometric binding assay in insoluble fractions from heart extracts. The insoluble fraction from IR hearts exhibited higher ThT fluorescence intensity compared to aerobic controls ($p < 0.05$), indicating the accumulation of misfolded protein aggregates during IR. However, ARP-100 or ONO-4817 did not significantly affect this increase (**Figure 5.2 E**).

5.3.3. MMP-2 preferring inhibitors preserve IRE1 α protein level after IR injury

To investigate how the UPR is affected in response to ER stress, I measured the changes in two UPR markers, IRE1 α and PERK. Under our experimental conditions, the protein levels of both markers were significantly reduced in ventricular extracts from IR hearts compared to aerobic controls (**Figures 5.3 A and B**). ARP-100 or ONO-4817 significantly attenuated the reduction in IRE1 α protein levels compared to IR hearts. However, they did not significantly affect the IR-

mediated reduction in PERK protein levels (**Figures 5.3 A and B**), suggesting that the loss in IRE1 α , but not PERK, may be attributed to the proteolytic activity of MMP-2. IR significantly increased the mRNA levels of both IRE1 α and PERK compared to aerobic controls, and this was not reduced by the MMP-2 inhibitors (**Figures 5.3 C and D**).

MMP-2-mediated proteolysis of IRE1 α would require their interaction. Therefore, I tested this possibility using immunoprecipitation. Ventricular extracts from aerobic or IR hearts were first immunoprecipitated with anti-MMP-2 antibody, followed by immunoblotting for IRE1 α . This showed an interaction between these proteins in the heart. Immunoblotting of these immunoprecipitates with anti-IRE1 α antibody showed both intact 130 kDa IRE1 α and a lower molecular weight band of \sim 100-110 kDa, which could be a proteolytic fragment of IRE1 α . No IRE1 α bands were observed in immunoprecipitates from either aerobic or IR hearts using control IgG (**Figure 5.3 E**).

IR also significantly increased the mRNA levels of XBP1s compared to aerobic controls, regardless of MMP-2 inhibition. However, no significant change in XBP1s protein levels in ventricular extracts was observed amongst the different groups (**Figures 5.5 A and B**). ARP-100 or ONO-4817 did not cause any change in IRE1 α , PERK or XBP1s protein levels in ventricular extracts from aerobic hearts (**Figures 5.4 C and D and 5.5 C**).

The protein levels of both IRE1 α and PERK in ventricular extracts from hearts at the end of reperfusion showed significant linear correlation to cardiac contractile parameters, including LVDP, dP/dt_{\max} or dP/dt_{\min} ($p < 0.01$ for IRE1 α and < 0.05 for PERK) (**Figure 5.6**).

5.3.4. MMP-2 preferring inhibitors attenuate ER stress-mediated apoptosis during IR injury

Changes in different regulators of ER stress-mediated apoptosis were measured in subcellular fractions obtained from hearts subjected to IR injury in order to evaluate the extent of apoptotic cell death. There was a significant increase in the level of CHOP in the cytosolic fraction obtained from IR hearts compared to aerobic controls. This increase in CHOP was abolished by ARP-100 or ONO-4817 ($p < 0.05$) (**Figure 5.7 A**). The level of Bax was also significantly higher in the mitochondria-enriched fraction obtained from IR hearts compared to aerobic controls, while ARP-100 or ONO-4817 attenuated this increase. There was no change in the cytosolic level of Bax amongst the different groups (**Figures 5.7 B and C**). The activities of both caspases-3 and -9 were higher in the cytosolic fractions obtained from IR hearts compared to aerobic ones, indicating an induction of apoptotic signalling, while ARP-100 or ONO-4817 significantly attenuated the increase in their activities (**Figures 5.7 D and E**). This was confirmed using immunoblotting, where both MMP inhibitors prevented the increase in caspase-3 or -9 cleavage compared to IR hearts, evidenced by the significant reduction in the ratios of cleaved caspase-3/procaspase-3 and cleaved caspase-9/procaspase-9 by ARP-100 or ONO-4817 (**Figures 5.8 A and B**). Under aerobic conditions, neither inhibitor caused significant changes in the levels of CHOP, Bax, caspase-3 or -9 (**Figures 5.8 C and D and 5.9**).

5.3.5. IRE1 α is proteolyzed by MMP-2

To investigate the ability of MMP-2 to proteolyze IRE1 α , an *in vitro* proteolysis assay was performed by incubating ventricular extracts from aerobic hearts with increasing concentrations of human recombinant MMP-2. This resulted in a significant reduction in the level of endogenous

IRE1 α which was prevented by ARP-100 (**Figures 5.10 A and B**), indicating that the loss in IRE1 α could be attributed to the proteolytic activity of MMP-2. No lower molecular weight products were observed using immunoblotting. *In silico* analysis was used to predict the potential MMP-2 cleavage sites in mouse IRE1 α using Procleave. The predicted amino acids sequences and the corresponding masses of both N- and C-terminal fragments were also analyzed. A summary of the top ten cleavage sites is shown in **Figure 5.10 C**. Positioning these predicted cleavage sites on the 3D structure of mouse IRE1 α shows that, among the top ten cleavage sites, MMP-2 can target three cleavage sites in the N-terminal luminal region and six cleavage sites in the C-terminal cytoplasmic region of IRE1 α . Many of these cleavage sites have leucine or isoleucine in the P1' position which are favored for MMP-2 cleavage as previously reported (**Figure 5.10 D**) [469]. Cleavage of IRE1 α before amino acids 228 in the luminal region or 743 or 786 in the cytoplasmic region can produce lower molecular weight fragments close to 100 kDa, which is similar to the detected lower molecular weight band of approximately 100-110 kDa observed in the immunoprecipitates from ventricular extracts.

5.3.6. MMP-2 preferring inhibitors preserve IRE1 α during ischemia prior to progression into myocardial cell death

Similar to IR injury, induction of ER stress was observed in mouse hearts subjected only to ischemia without reperfusion, as evidenced by the increased level of GRP78 in ventricular extracts compared to aerobic controls. Similarly, ARP-100 or ONO-4817 did not significantly affect this increase in GRP78 (**Figure 5.11 A**). However, no significant change in PDI level was observed amongst the different groups (**Figure 5.11 B**). ThT assay also showed no significant difference in fluorescence intensity amongst the different groups, suggesting no detectable misfolded protein accumulation during ischemia (**Figure 5.11 C**). On the other hand, the level of

IRE1 α was also significantly reduced in ischemic hearts compared to aerobic controls. Both ARP-100 and ONO-4817 attenuated this reduction ($p < 0.05$) (**Figure 5.12 A**). No significant changes in the levels of PERK or XBP1s in ventricular extracts were observed amongst the different groups (**Figures 5.12 B and C**).

ER stress-mediated apoptotic markers were also measured in mouse hearts subjected to ischemia. The level of CHOP, an early marker of ER stress-mediated apoptosis, in the cytosolic fraction was significantly higher in ischemic hearts compared to aerobic ones. This increase was prevented by ARP-100 or ONO-4817 ($p < 0.05$) (**Figure 5.13 A**). On the other hand, no significant changes were observed in Bax level in mitochondria-enriched or cytosolic fractions amongst the different groups (**Figures 5.13 B and C**). The activities of both caspases-3 and -9 as well as their protein levels did not significantly change in the cytosolic fractions amongst the different groups (**Figures 5.13 D and E and 5.14**), indicating that the degree of injury during ischemia is not enough to trigger apoptotic cell death.

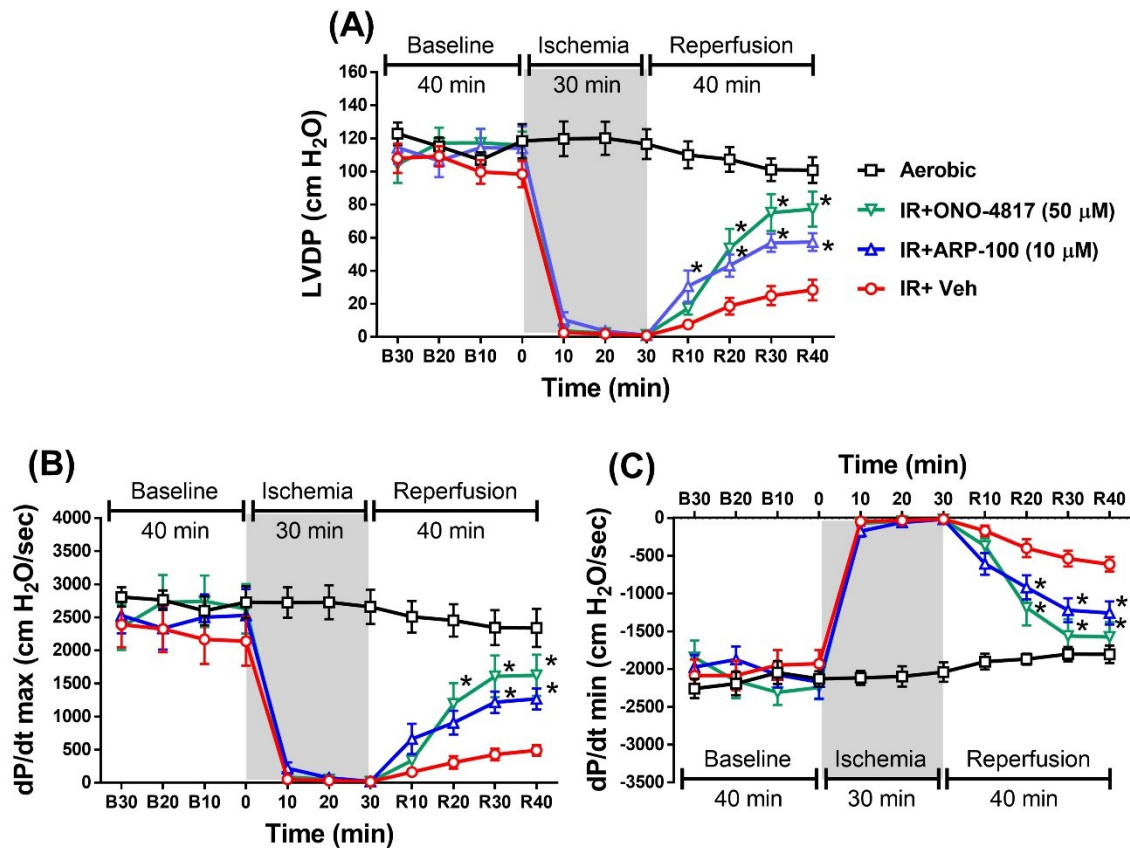


Figure 5.1. MMP-2 preferring inhibitors improve post-ischemic contractile function in isolated mouse hearts subjected to IR injury. Changes in (A) left ventricular developed pressure (LVDP), (B) dP/dt_{max} or (C) dP/dt_{min} during IR injury in absence or presence of ARP-100 (ARP, 10 μM), ONO-4817 (ONO, 50 μM) or DMSO vehicle (Veh) compared to aerobic control (Aero) (n=5 hearts per group). *p<0.05 vs. IR+Veh by two-way ANOVA followed by Dunnett's post-hoc test.

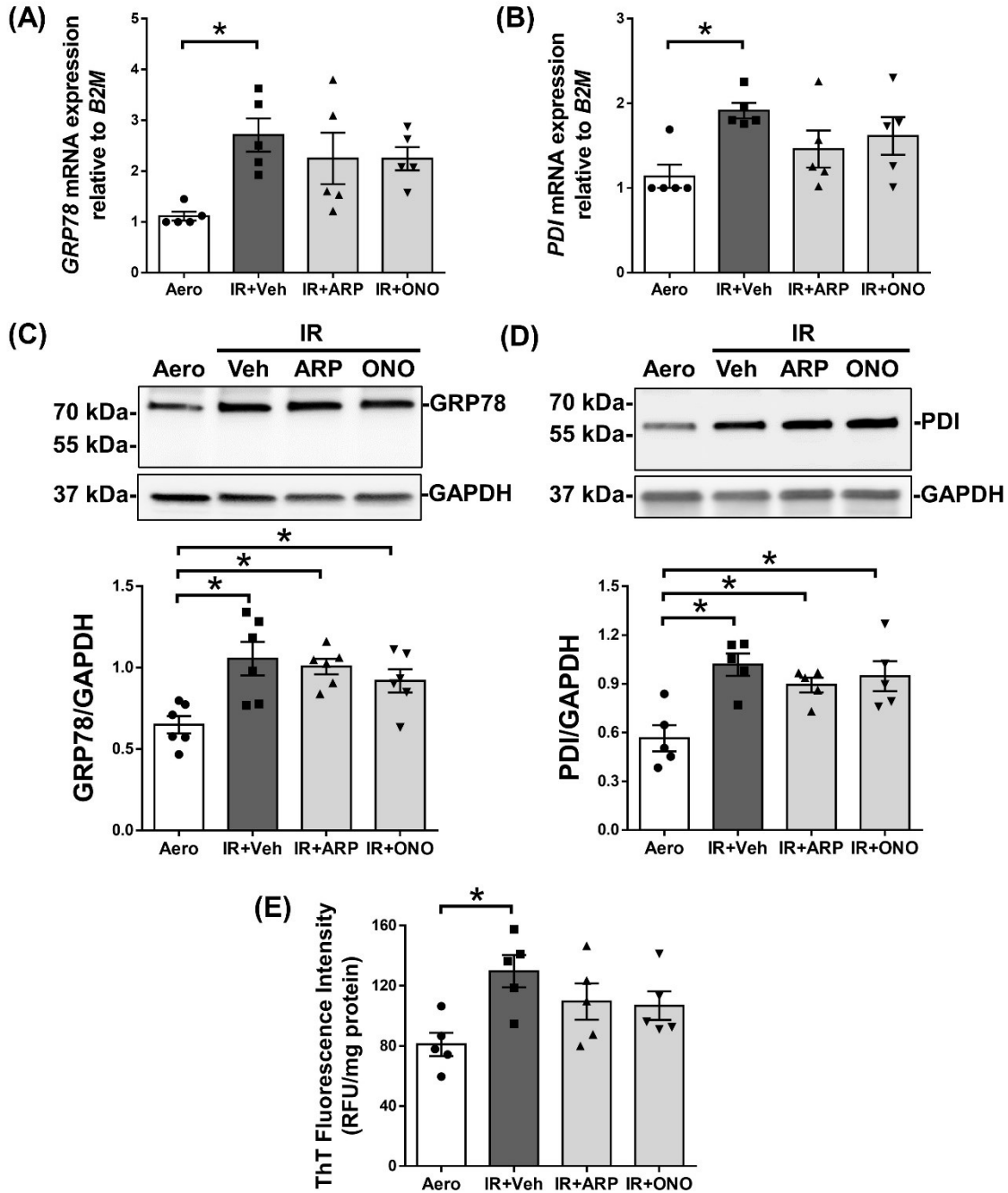


Figure 5.2. Myocardial IR injury is associated with ER stress response. (A&B) mRNA expression of **(A)** *GRP78* and **(B)** *PDI* in IR hearts. **(C&D)** Representative immunoblots (upper panels) and quantitative measurements (lower panels) of **(C)** *GRP78* and **(D)** *PDI* protein levels in ventricular extracts from IR hearts. Position of molecular weight ladder proteins indicated on the left. **(E)** Thioflavin T (ThT) fluorescence intensities in the insoluble fractions obtained from IR hearts in absence or presence of ARP-100 (ARP, 10 μ M), ONO-4817 (ONO, 50 μ M) or DMSO vehicle (Veh) compared to aerobic control (Aero). Values are presented as relative fluorescence unit (RFU) normalized to protein concentration (n=5 hearts per group). *p<0.05 by one-way ANOVA followed by Dunnett's post-hoc test.

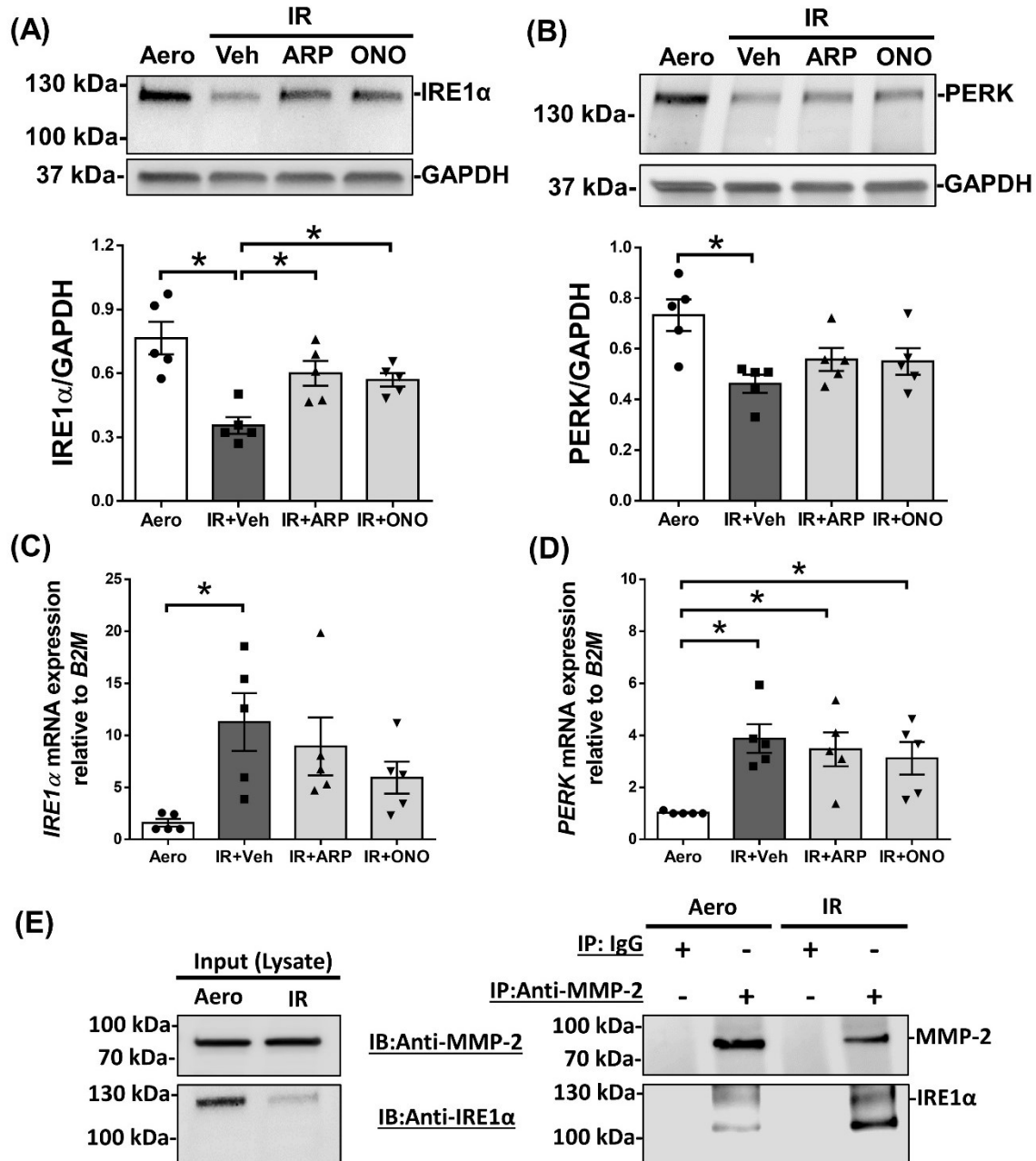


Figure 5.3. MMP-2 preferring inhibitors prevent IRE1 α loss during IR injury. (A&B) Representative immunoblots (upper panels) and quantitative measurements (lower panels) of (A) IRE1 α and (B) PERK protein levels in ventricular extracts from IR hearts. (C&D) mRNA expression of (C) IRE1 α and (D) PERK in IR hearts in absence or presence of ARP-100 (ARP, 10 μ M), ONO-4817 (ONO, 50 μ M) or DMSO vehicle (Veh) compared to aerobic control (Aero) (n=5 hearts per group). (E) MMP-2 and IRE1 α immunoblots using ventricular extracts containing total protein lysate (input, left panel) or MMP-2 immunoprecipitates (right panel) from aerobic and IR hearts showing an association between MMP-2 and IRE1 α , representative of three independent experiments with similar results. Position of molecular weight ladder proteins indicated on the left. *p<0.05 by one-way ANOVA followed by Dunnett's post-hoc test.

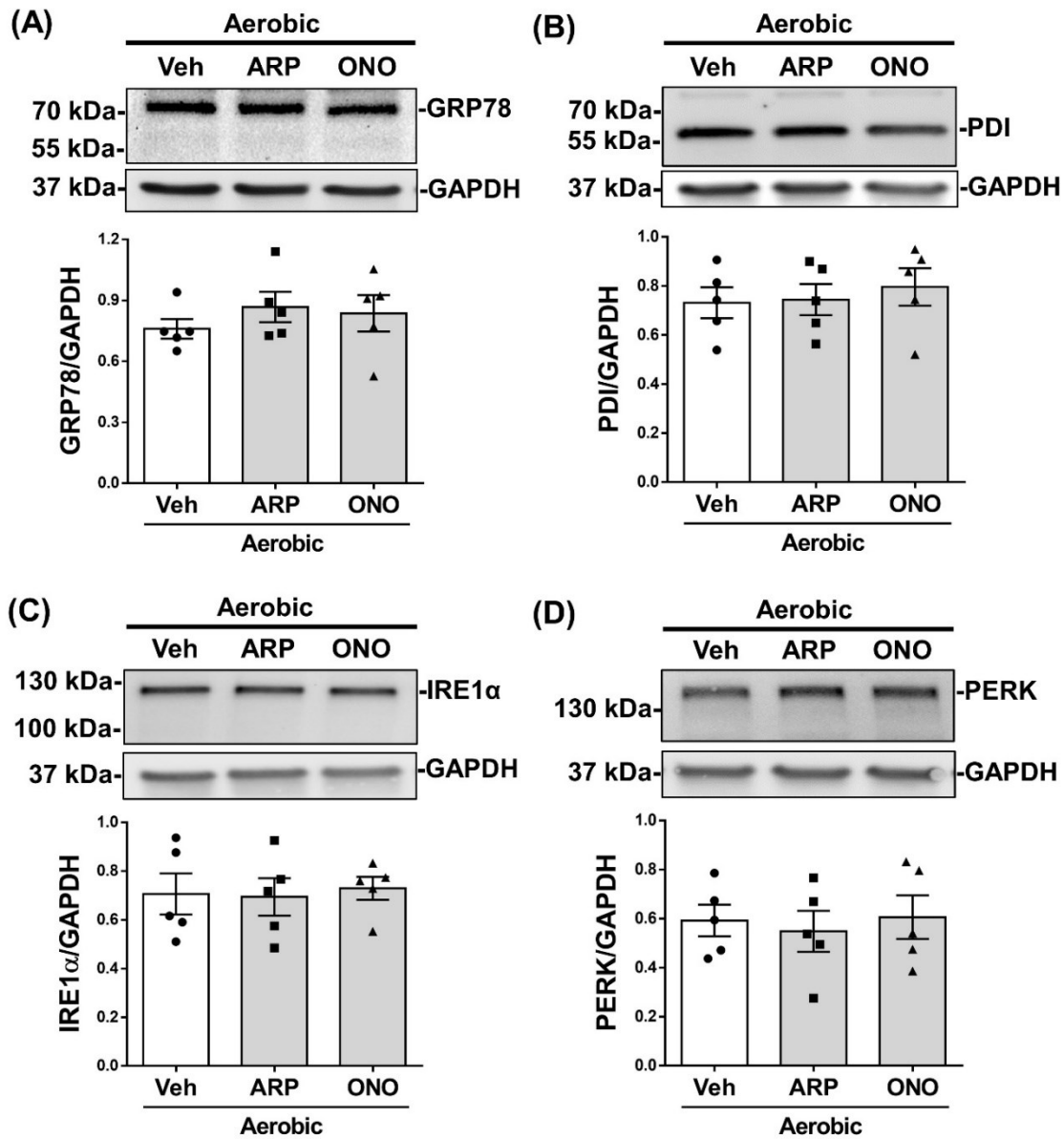


Figure 5.4. MMP-2 preferring inhibitors have no effect on ER stress or UPR markers in aerobically perfused hearts. Representative immunoblots (upper panels) and quantitative measurements (lower panels) of (A) GRP78, (B) PDI, (C) IRE1 α or (D) PERK levels in ventricular extracts from aerobically perfused hearts in absence or presence of ARP-100 (ARP, 10 μ M), ONO-4817 (ONO, 50 μ M) or DMSO vehicle (Veh) (n=5 hearts per group). Position of molecular weight ladder proteins indicated on the left.

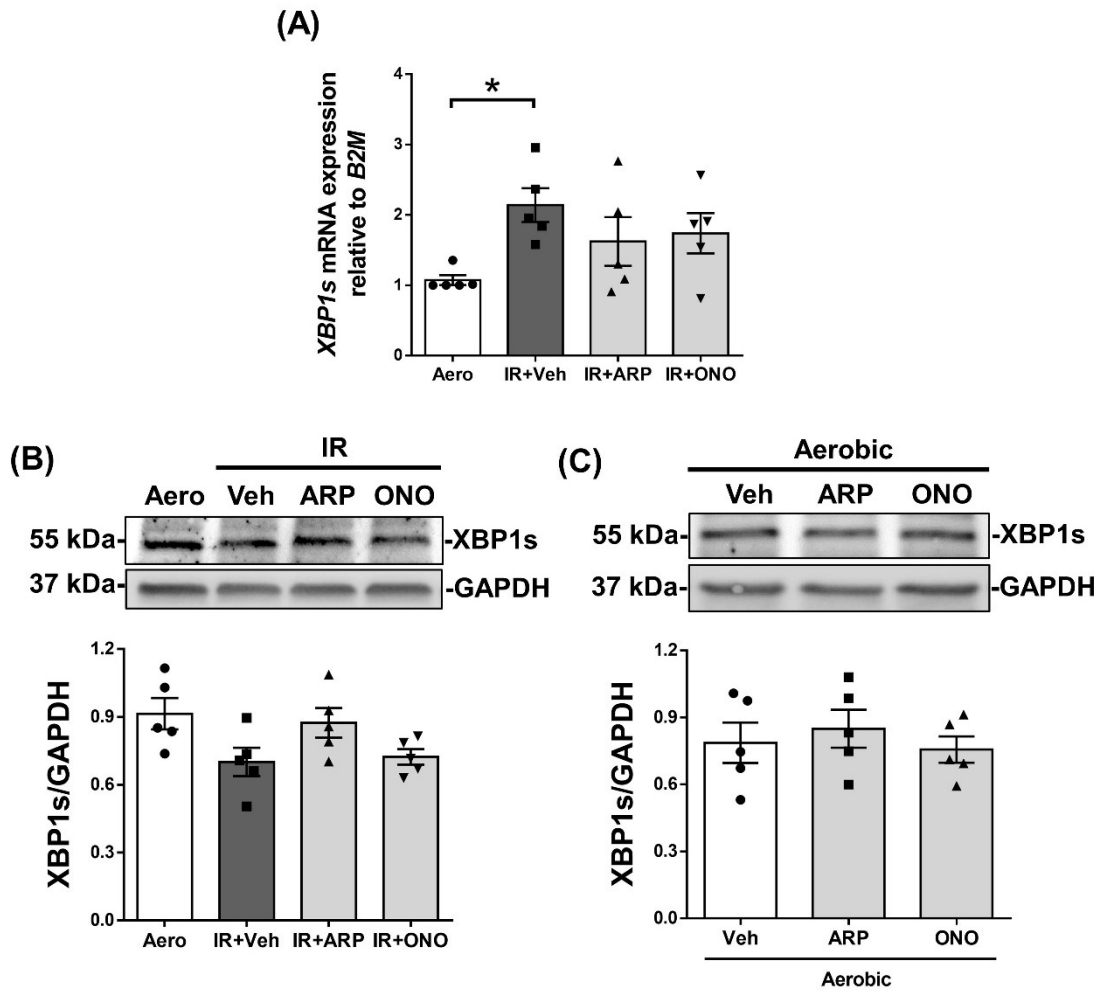


Figure 5.5. Changes in XBP1s in hearts subjected to IR injury. (A) mRNA expression of *XBP1s* in IR hearts. (B&C) Representative immunoblots (upper panels) and quantitative measurements (lower panels) of XBP1s protein levels in ventricular extracts from (B) IR or (C) aerobic hearts in absence or presence of ARP-100 (ARP, 10 μ M), ONO-4817 (ONO, 50 μ M) or DMSO vehicle (Veh) (n=5 hearts per group). Position of molecular weight ladder proteins indicated on the left. *p<0.05 by one-way ANOVA followed by Dunnett's post-hoc test.

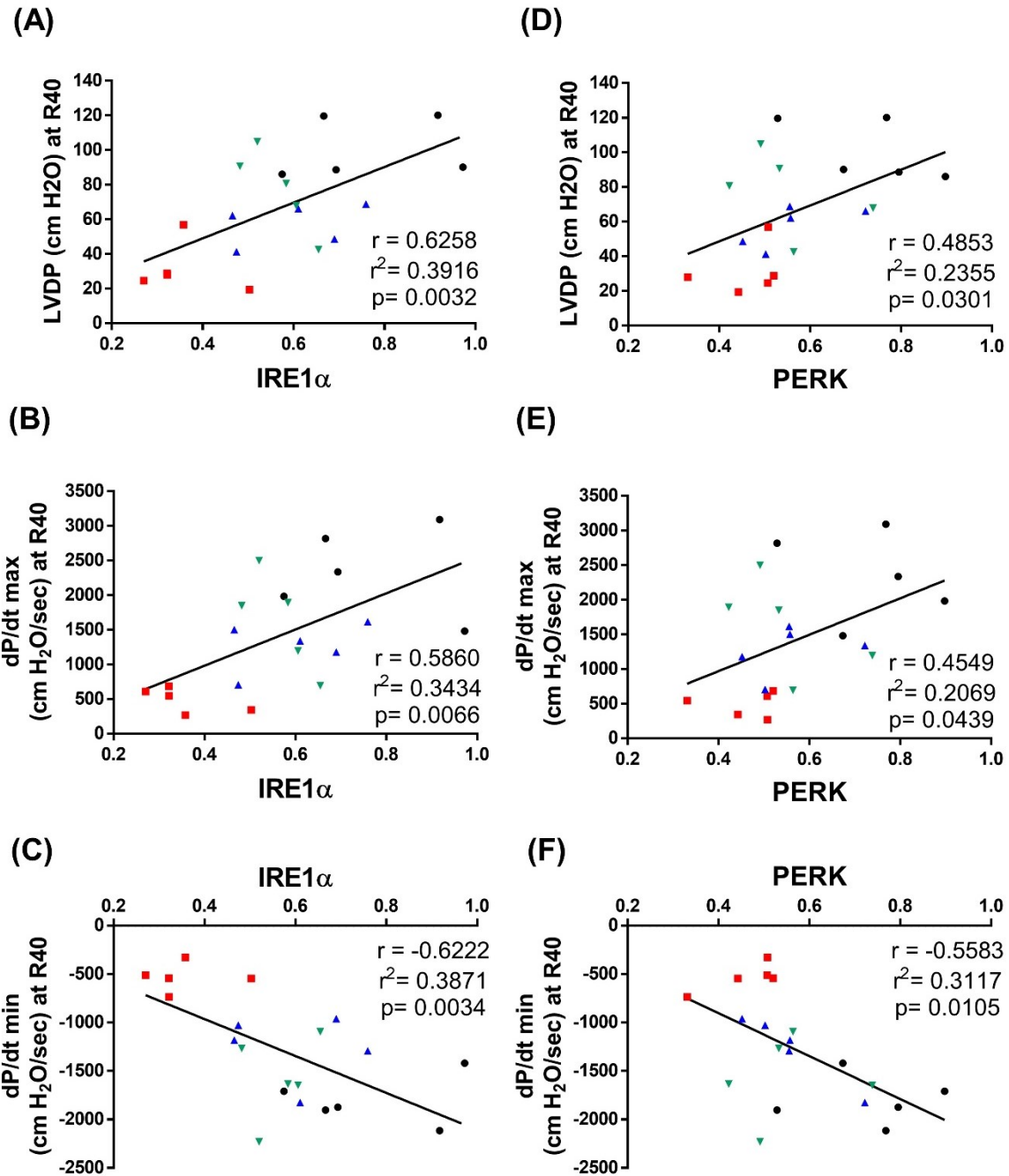


Figure 5.6. IRE1 α and PERK protein levels correlate with cardiac mechanical function. Correlation analysis of (A-C) IRE1 α or (D-F) PERK protein levels in ventricular extracts to LVDP, dP/dt_{max}, or dP/dt_{min} at 40 min reperfusion (aerobic; black ●, IR+Veh; red ■, IR+ARP-100; blue ▲, IR+ONO-4817; green ▼) (n=5 hearts per group).

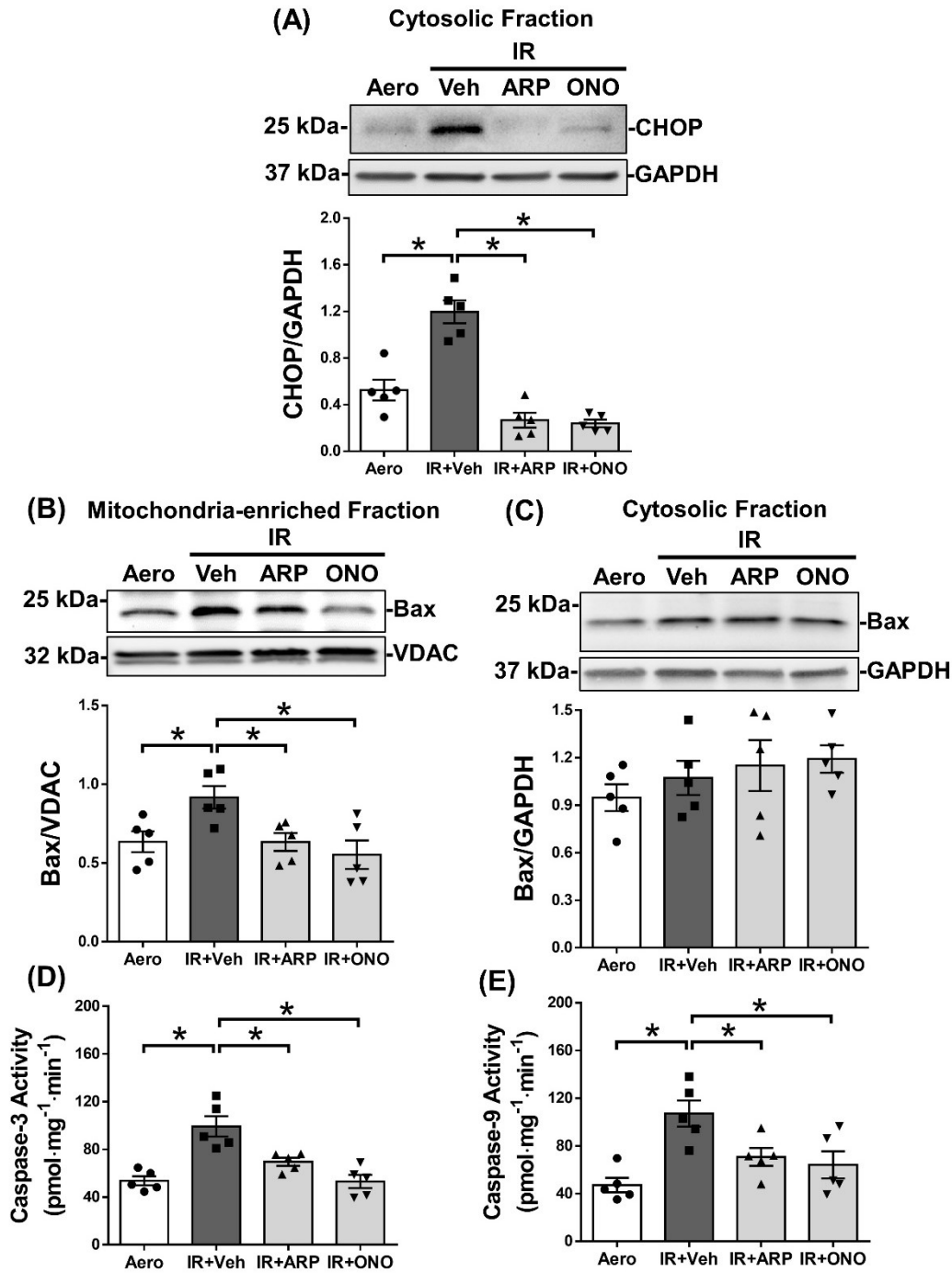


Figure 5.7. MMP-2 preferring inhibitors attenuate ER stress-mediated apoptosis during IR injury. Representative immunoblots (upper panels) and quantitative measurements (lower panels) of the levels of (A) CHOP in cytosolic fraction, (B) Bax in mitochondria-enriched fraction or (C) Bax in cytosolic fraction from IR hearts. Position of molecular weight ladder proteins indicated on the left. Changes in (D) caspase-3 or (E) caspase-9 activities in cytosolic fractions from IR hearts in absence or presence of ARP-100 (ARP, 10 μM), ONO-4817 (ONO, 50 μM) or DMSO vehicle (Veh) compared to aerobic control (Aero) ($n=5$ hearts per group). * $p<0.05$ by one-way ANOVA followed by Dunnett's post-hoc test.

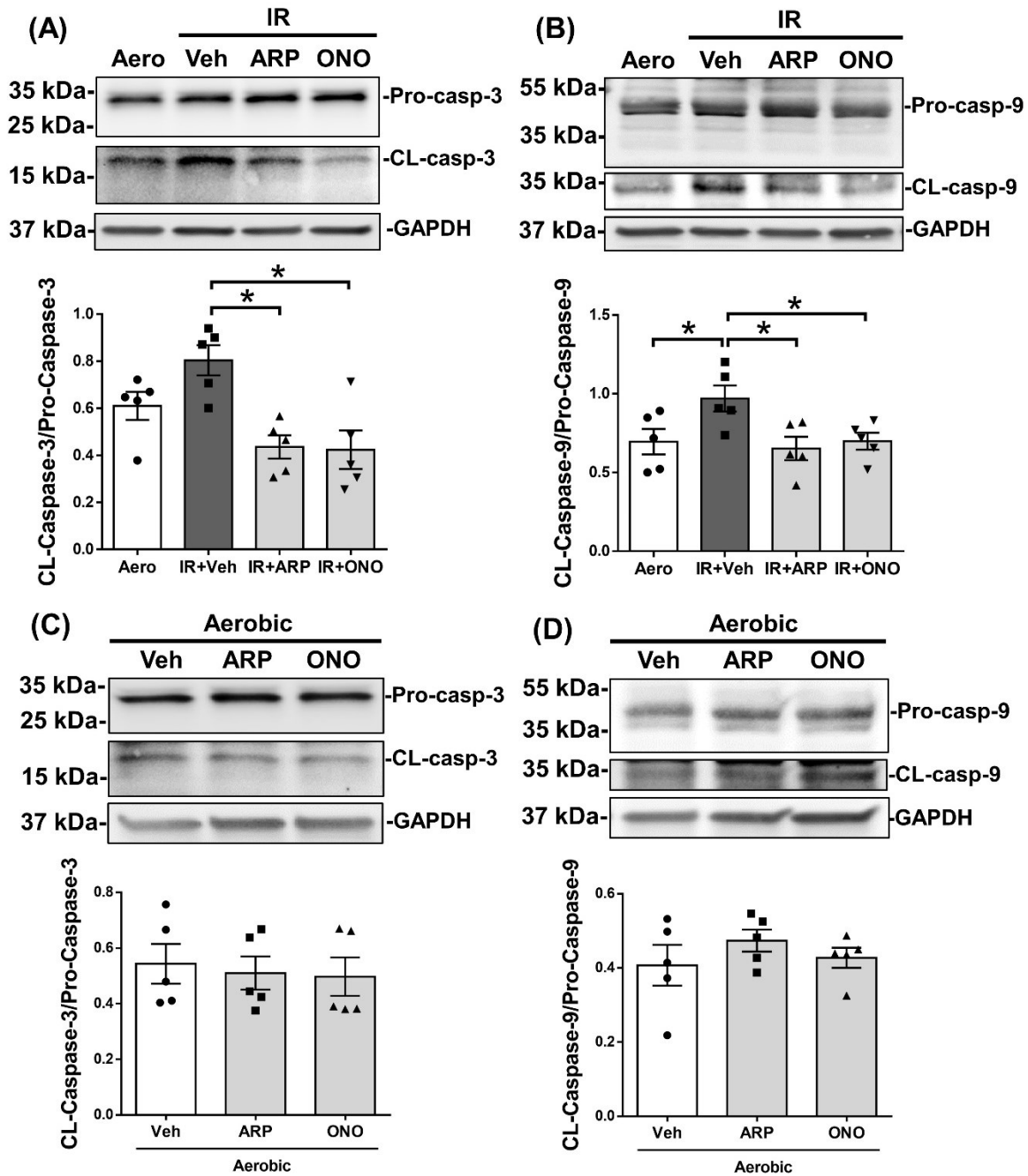


Figure 5.8. MMP-2 preferring inhibitors attenuate the IR-induced increase in caspases-3 and -9 cleavage. Representative immunoblots (upper panels) and quantitative measurements (lower panels) of (A) pro- and cleaved caspase-3 or (B) pro- and cleaved caspase-9 levels in cytosolic fraction from IR hearts and (C) pro- and cleaved caspase-3 or (D) pro- and cleaved caspase-9 levels in cytosolic fraction from aerobic hearts in absence or presence of ARP-100 (ARP, 10 μ M), ONO-4817 (ONO, 50 μ M) or DMSO vehicle (Veh) (n=5 hearts per group). Position of molecular weight ladder proteins indicated on the left. *p<0.05 by one-way ANOVA followed by Dunnett's post-hoc test.

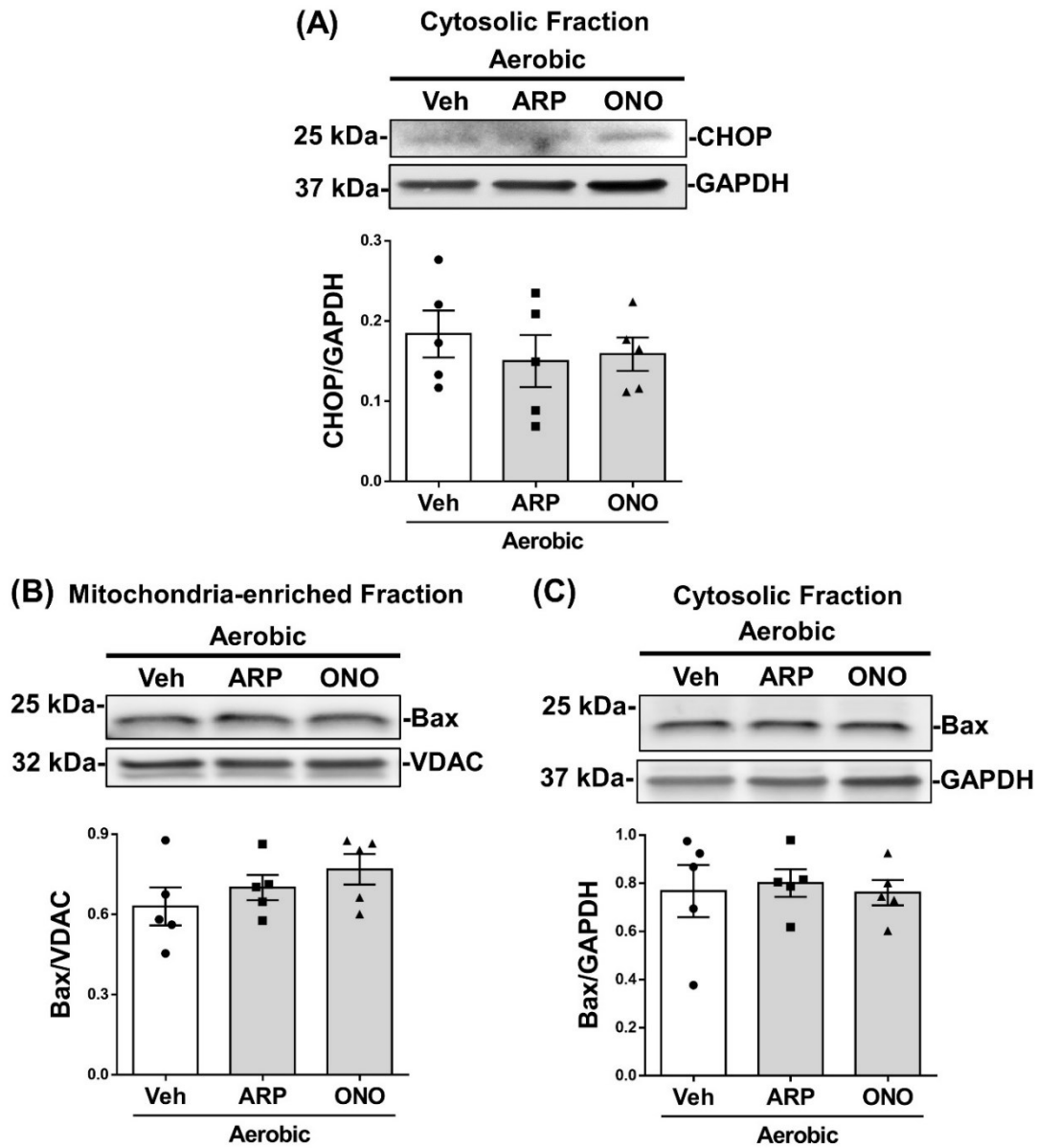


Figure 5.9. MMP-2 preferring inhibitors have no effect on CHOP or Bax in aerobically perfused hearts. Representative immunoblots (upper panels) and quantitative measurements (lower panels) of the levels of **(A)** CHOP in cytosolic fraction, **(B)** Bax in mitochondria-enriched fraction or **(C)** Bax in cytosolic fraction from aerobically perfused hearts in absence or presence of ARP-100 (ARP, 10 μ M), ONO-4817 (ONO, 50 μ M) or DMSO vehicle (Veh) (n=5 hearts per group). Position of molecular weight ladder proteins indicated on the left.

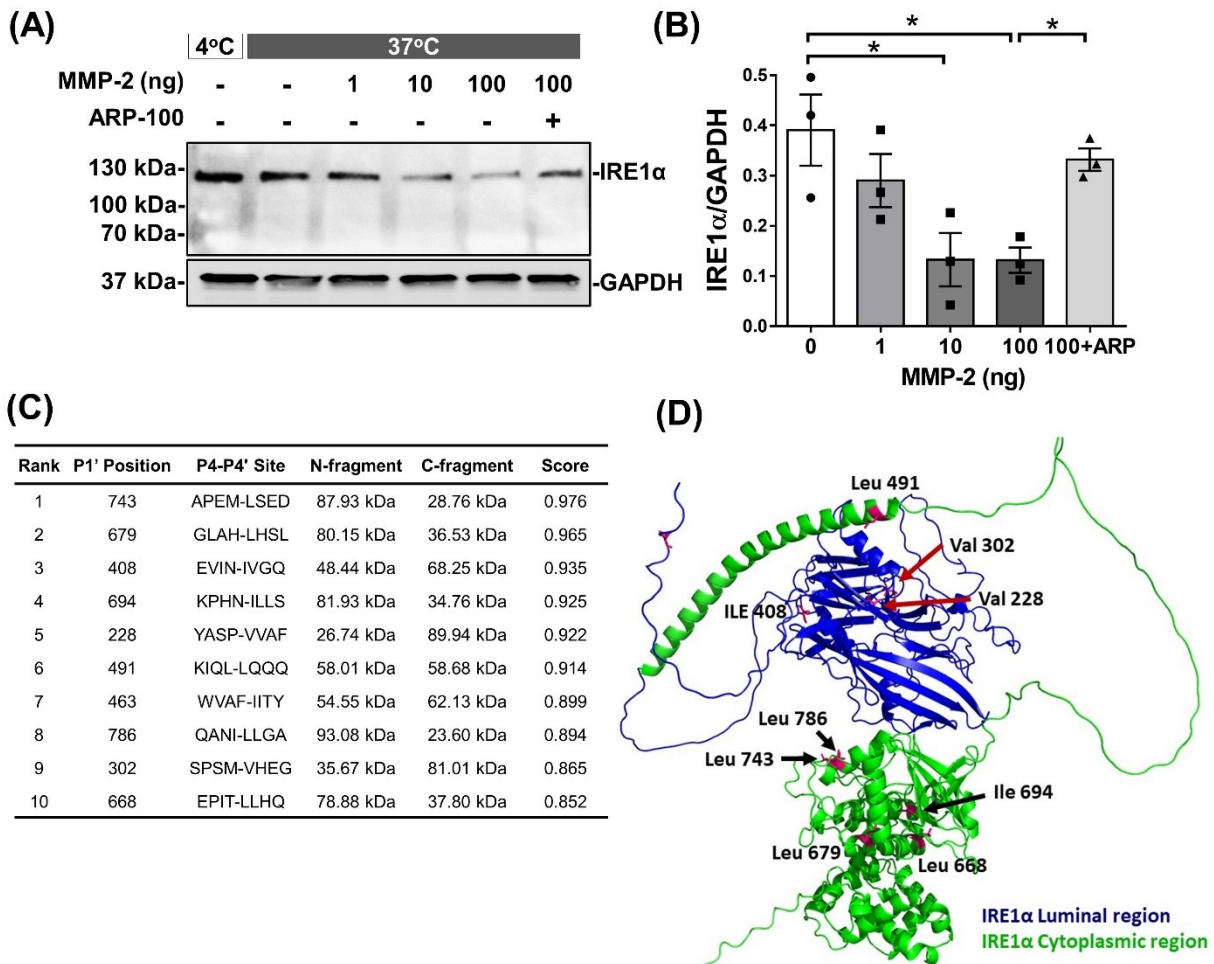


Figure 5.10. IRE1 α is proteolyzed by MMP-2. (A) Immunoblot showing *in vitro* proteolysis of endogenous IRE1 α in ventricular extracts (15 μ g protein) from aerobic hearts incubated for 1 h at 37°C with MMP-2 in absence or presence of ARP-100 (30 μ M), representative of three different aerobic hearts showing similar results. (B) Quantitative measurement of IRE1 α levels relative to GAPDH following proteolysis by MMP-2 (n=3 hearts). *p<0.05 by one-way ANOVA followed by Dunnett's post-hoc test. (C) *In silico* analysis of mouse IRE1 α structure showing the top ten predicted cleavage sites of IRE1 α by MMP-2 according to Procleave. (D) 3D structure of modelled mouse IRE1 α . Squiggles indicate unstructured regions. The blue represents the IRE1 α luminal region and the green represents the IRE1 α cytoplasmic region. The top ten predicted cleavage sites are shown as purple stick representations.

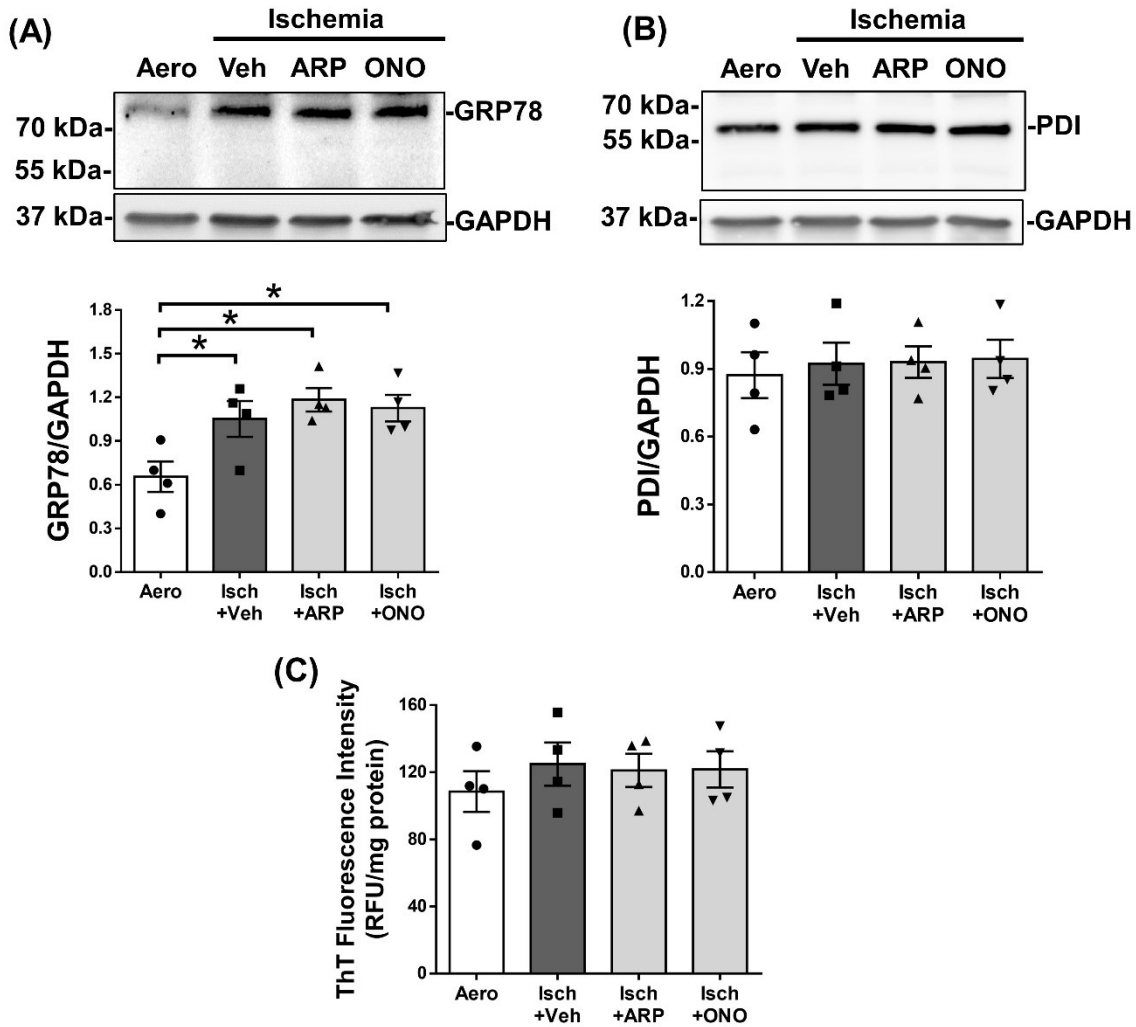


Figure 5.11. GRP78 is upregulated during myocardial ischemia. (A&B) Representative immunoblots (upper panels) and quantitative measurements (lower panels) of **(A)** GRP78 and **(B)** PDI protein levels in ventricular extracts from ischemic hearts. Position of molecular weight ladder proteins indicated on the left. **(C)** Thioflavin T (ThT) fluorescence intensities in the insoluble fractions obtained from ischemic hearts in absence or presence of ARP-100 (ARP, 10 μ M), ONO-4817 (ONO, 50 μ M) or DMSO vehicle (Veh) compared to aerobic control (Aero). Values are presented as relative fluorescence unit (RFU) normalized to protein concentration (n=4 hearts per group). *p<0.05 by one-way ANOVA followed by Dunnett's post-hoc test.

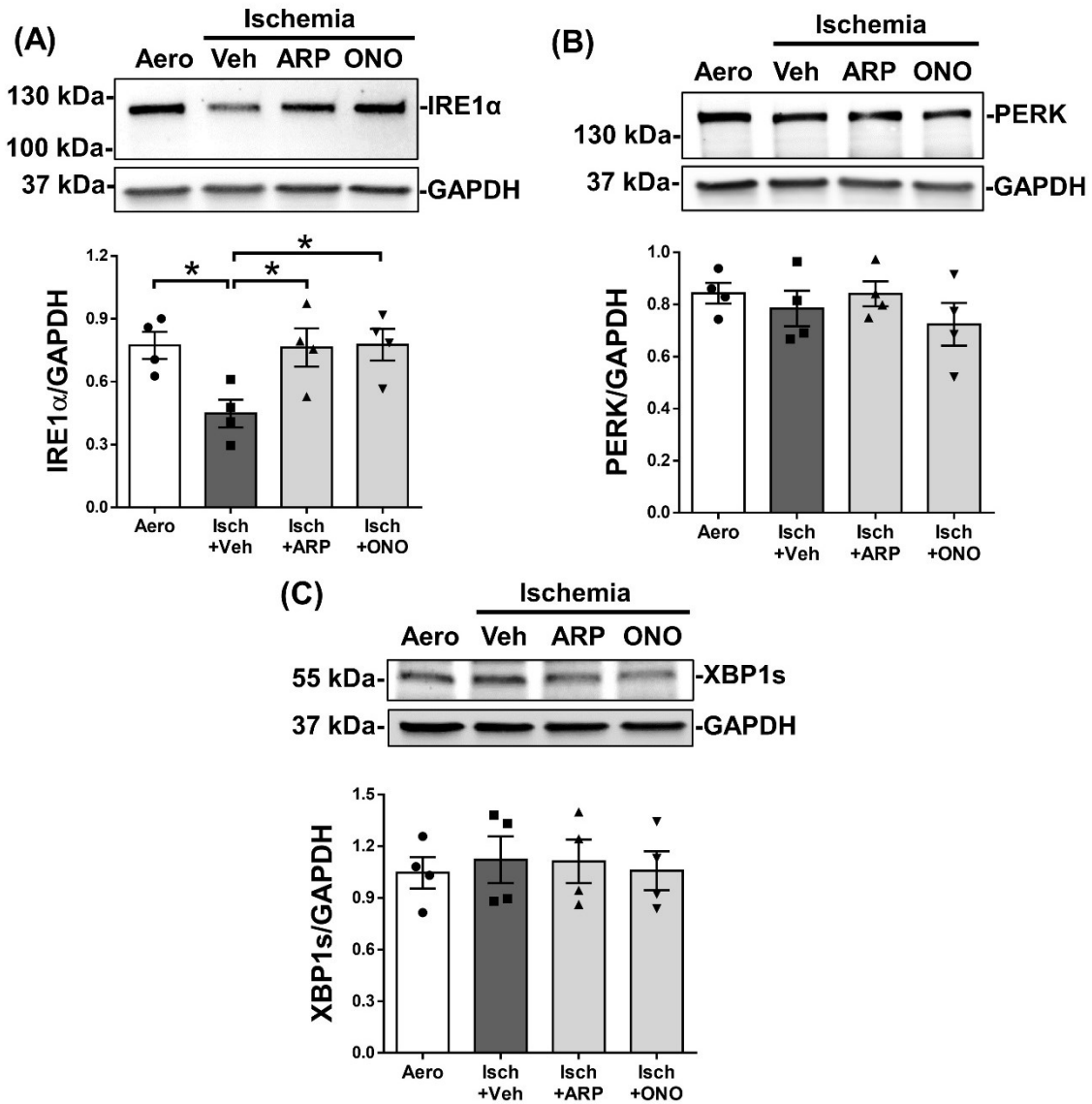


Figure 5.12. MMP-2 preferring inhibitors prevent IRE1 α loss during myocardial ischemia. Representative immunoblots (upper panels) and quantitative measurements (lower panels) of (A) IRE1 α , (B) PERK or (C) XBP1s protein levels in ventricular extracts from IR hearts in absence or presence of ARP-100 (ARP, 10 μ M), ONO-4817 (ONO, 50 μ M) or DMSO vehicle (Veh) compared to aerobic control (Aero) (n=4 hearts per group). Position of molecular weight ladder proteins indicated on the left. *p<0.05 by one-way ANOVA followed by Dunnett's post-hoc test.

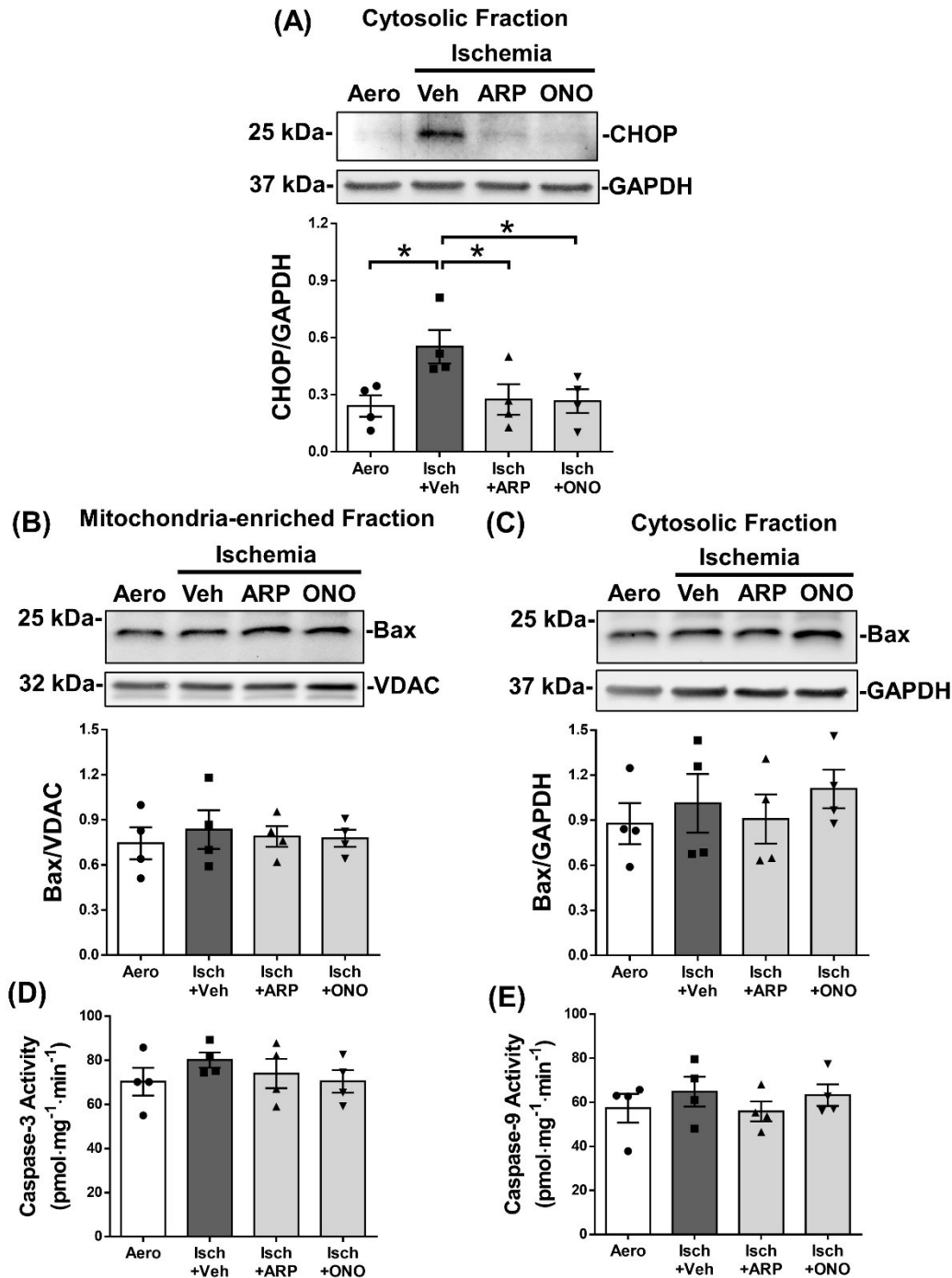


Figure 5.13. ER stress-mediated apoptosis is not developed during myocardial ischemia. Representative immunoblots (upper panels) and quantitative measurements (lower panels) of the levels of (A) CHOP in cytosolic fraction, (B) Bax in mitochondria-enriched fraction or (C) Bax in cytosolic fraction from ischemic hearts. Position of molecular weight ladder proteins indicated on the left. Changes in (D) caspase-3 or (E) caspase-9 activities in cytosolic fractions from ischemic hearts in absence or presence of ARP-100 (ARP, 10 μM), ONO-4817 (ONO, 50 μM) or DMSO vehicle (Veh) compared to aerobic control (Aero) ($n=4$ hearts per group). * $p<0.05$ by one-way ANOVA followed by Dunnett's post-hoc test.

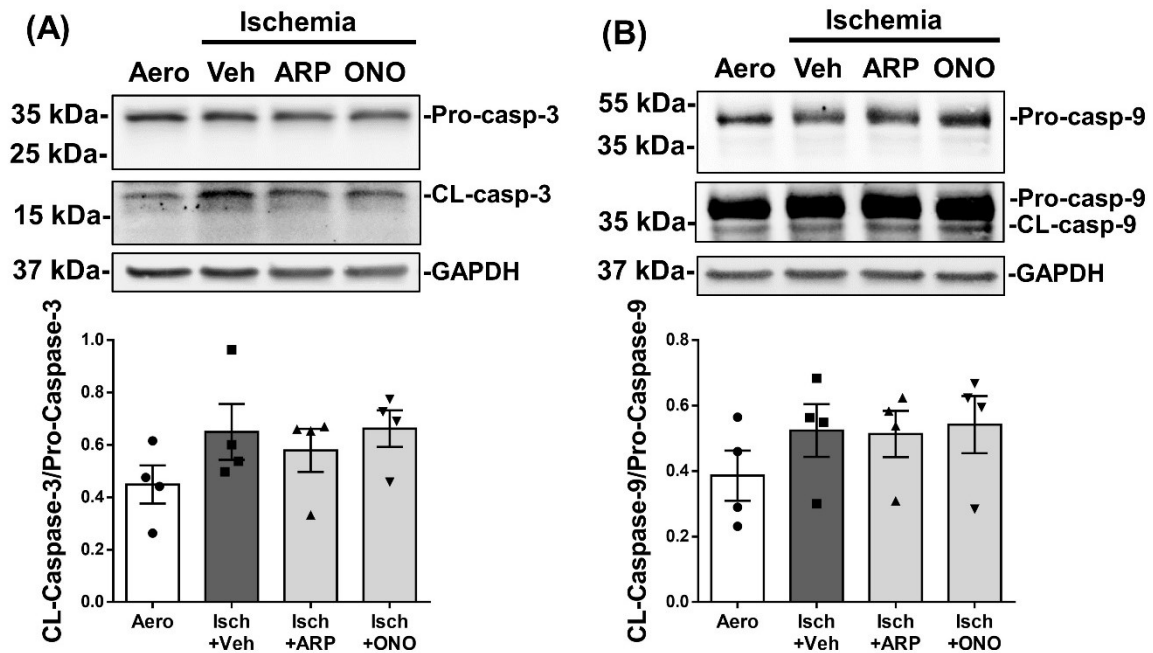


Figure 5.14. Changes in caspases-3 and -9 protein levels during myocardial ischemia. Representative immunoblots (upper panels) and quantitative measurements (lower panels) of (A) pro- and cleaved caspase-3 or (B) pro- and cleaved caspase-9 levels in cytosolic fraction from ischemic hearts in absence or presence of ARP-100 (ARP, 10 μ M), ONO-4817 (ONO, 50 μ M) or DMSO vehicle (Veh) compared to aerobic control (Aero) (n=4 hearts per group). Position of molecular weight ladder proteins indicated on the left.

5.4. Discussion

I investigated the relationship between MMP-2 activation during myocardial IR injury and the induction of markers of ER stress-mediated apoptotic cell death and how MMP-2 affects the UPR proteins, IRE1 α and PERK, in this setting. Our data shows that both IRE1 α and PERK are downregulated during IR, while only IRE1 α is downregulated during ischemia alone. The loss in IRE1 α but not PERK during IR could be attributed to the proteolytic activity of MMP-2. Although MMP-2 seems not to be involved in the induction of ER stress response or misfolded protein aggregation during IR, MMP-2 contributes to the progression of apoptosis resulting from persistent ER stress which can be linked to the reduction in IRE1 α . I reveal that inhibition of MMP-2 activity preserves IRE1 α level, attenuates ER stress-mediated cell death and thereby improves the recovery of cardiac contractile function post-IR. A schematic representation of this is shown in **Figure 5.15**.

It is well established that MMP-2 is activated during myocardial IR injury. MMP-2 is expressed in its zymogen form inside the cell as it possesses a pro-peptide domain which binds to the catalytic zinc in its active site, rendering it inactive [19]. In response to enhanced oxidative stress during IR injury, MMP-2 gets activated by the action of peroxynitrite-induced cysteine S-glutathiolation which induces conformational changes that expose its active site [43, 44]. I previously showed that MMP-2 is activated in isolated mouse hearts subjected to IR injury under the same experimental conditions I used in this study [496]. Consistent with previous reports [8, 9], our data showed that MMP-2 contributes to the resulting cardiac contractile dysfunction during IR, as the MMP-2 preferring inhibitors, ARP-100 or ONO-4817, improved the post-ischemic recovery of cardiac contractile parameters that deteriorated in response to IR. As reported, this is attributed to MMP-2-associated proteolysis of several intracellular proteins that are vital for cardiac contractile function such as TnI, titin and myosin light chain 1/MYL3, among others [58].

In the present study, I focused on how MMP-2 activation during IR affects ER stress and UPR signalling, considering that MMP-2 is localized near the ER [65]. There is a crosstalk between ER stress and oxidative stress as both accentuate each other, which raises the question whether MMP-2 plays a role in the induction of ER stress response and its progression into apoptosis during IR injury. The process of protein folding depends on the redox status of the ER. Oxidative stress during IR can trigger protein misfolding and the ER stress response due to an altered ER redox state [381, 382]. Meanwhile, during ER stress, dysregulation of the disulfide bonds between cysteine amino acids of polypeptides, results in enhanced oxidative stress via the biosynthesis of RONS, as the disulfide bond formation is highly sensitive to the redox balance in the ER. RONS are formed as byproducts due to the electron transfer from the peptide sulfhydryl group to molecular oxygen. ER stress also induces mitochondrial dysfunction which itself increases mitochondrial RONS production [499].

Myocardial IR injury is known to be associated with ER stress [384, 500]. Our data showed that IR increased the mRNA and protein levels of the ER chaperones GRP78 and PDI, which act as ER stress sensors, indicating that ER stress was induced. This is consistent with previous studies reporting increased expression of GRP78 in neonatal rat ventricular cardiomyocytes subjected to hypoxia and reoxygenation [501], as well as in isolated perfused mouse hearts subjected to IR injury [388]. PDI was also reported to be upregulated in infarcted mouse hearts caused by permanent occlusion of the left anterior descending coronary artery [502]. Using the ThT binding assay, I found a significant increase in protein aggregation following IR injury, which results from enhanced oxidative stress, and in turn triggers the ER stress response. However, MMP-2 inhibitors were unable to attenuate the increases in GRP78 or PDI mRNA or protein levels during IR. They also did not affect the IR-induced aggregation of misfolded proteins, suggesting that, although

MMP-2 gets activated during IR, it is not involved in the induction of ER stress response per se or the process of protein misfolding.

In response to ER stress, the UPR is activated to correct for protein misfolding [492]. This is known to be accompanied by the increased expression and activation of UPR proteins including IRE1 α and PERK [341]. Surprisingly, our data showed a profound reduction in both PERK and IRE1 α protein levels in extracts from mouse hearts subjected to IR injury. However, I found significant increases in the mRNA levels of PERK, IRE1 α and its downstream transcription factor, XBP1s, in IR hearts, suggesting that the reductions in these markers occur at the protein rather than the transcriptional level. The changes in IRE1 α and PERK may be also dependent on the duration and degree of IR injury. Although MMP-2 inhibitors did not affect the IR-induced reduction in the protein level of PERK, they significantly attenuated the loss in IRE1 α . This suggests that MMP-2 plays a role in the loss in IRE1 α , but not PERK. Although IR increased the mRNA level of XBP1s, its protein level was not significantly different from aerobic controls, indicating a disruption of UPR signalling during IR which could be due to the reduction in IRE1 α . Using immunoprecipitation I revealed that MMP-2 is associated with IRE1 α in extracts from aerobic control or IR hearts. Our data also showed that MMP-2 can proteolyze endogenous IRE1 α in ventricular extracts. This was also supported by *in silico* and 3D crystal structure analyses which revealed several potential sites in mouse IRE1 α that could be targeted by MMP-2, both in its luminal and cytosolic domains. Cleavage of IRE1 α within the cytoplasmic linker region is reported to be mediated by caspase in hematopoietic cells in response to ER stress, where the pan-caspase inhibitor z-VAD-FMK prevented IRE1 α proteolysis [503]. Interestingly, z-VAD-FMK was reported to exhibit significant MMP-2 inhibitory activity at concentrations commonly used to inhibit caspase activity [504].

The duration of ischemia and degree of ER stress could affect the changes in IRE1 α . Studies showed that although IRE1 α signalling is enhanced in response to the ER stress inducers, tunicamycin or thapsigargin, prolonged exposure to these agents resulted in a reduction in IRE1 α signalling and disassembly of its clusters [360, 505]. Cardiac-specific knockout of XBP1s in mouse hearts exacerbated the impairment in contractile function and increased infarct size caused by IR injury, while its overexpression reversed these changes [387]. Cardiac-specific overexpression of IRE1 α in mouse hearts subjected to transverse aortic constriction also improved cardiac contractile function [506]. This is consistent with our data showing that the changes in IRE1 α protein level are significantly correlated to cardiac contractile function. This highlights the critical importance of maintaining a balanced UPR, particularly in the level of IRE1 α , to preserve contractile function during IR injury.

Persistent ER stress and failure of the UPR to prevent the accumulation of misfolded proteins induces the transition from an adaptive to a maladaptive UPR which induces apoptotic cell death [354]. Our data showed that IR injury is associated with the upregulation of CHOP, increased translocation of Bax from the cytosol to the mitochondria and increased activation of caspases-3 and -9. These changes during IR indicate the induction of ER stress-mediated apoptosis. This is consistent with a previous study reporting increased CHOP expression and apoptotic signalling during IR injury [384]. The induction of apoptosis during IR seems to be MMP-2-dependent, as MMP-2 inhibitors attenuated all these changes in apoptotic markers. This could be also linked to the MMP-2-mediated reduction in IRE1 α in response to IR. Lugea et al. reported that XBP1 deficiency triggers CHOP upregulation and the apoptotic response due to the failure of UPR to resolve misfolded protein accumulation [371]. Another study also showed that genetic knockdown of IRE1 α in neuronal cancer cells increases CHOP expression and triggers apoptosis

by mediating mitochondrial dysfunction [353]. Propagation of ER stress-mediated apoptosis could be contributing to the resulting cardiac dysfunction as several studies reported the association between CHOP-mediated apoptosis and the development of cardiac diseases including dilated cardiomyopathy [374], and pressure overload-induced heart failure [373]. Therefore, preventing ER stress-mediated apoptosis could be another mechanism for the cardioprotective effect of MMP-2 inhibitors.

As ER stress is reported to be initiated during ischemia even before the start of reperfusion [380], I investigated the changes in ER stress and apoptotic markers in hearts subjected to ischemia without reperfusion and how MMP-2 inhibition affects this. Similar to IR, our data shows that ischemia per se induces an ER stress response, evidenced by the upregulation of GRP78 in ischemic hearts. However, no significant change was observed in PDI level, suggesting that the degree of ER stress during ischemia is less prominent compared to IR injury. No significant difference in protein aggregation was observed between ischemic and aerobic hearts. The increase in GRP78 during ischemia was also not affected by MMP-2 inhibition, indicating that MMP-2 may not be involved in the induction of ER stress during ischemia. Another similar observation was the reduction in IRE1 α during ischemia which was also reversed by MMP-2 inhibitors, giving more evidence of a potential MMP-2-mediated proteolytic degradation of IRE1 α . Several studies reported that MMP-2 activity is elevated not only in response to reperfusion by also during myocardial ischemia [140], skeletal muscle ischemia [507], as well as in pulmonary endothelial cells subjected to hypoxia [508]. Although it is not clear how MMP-2 is activated during ischemia, Cadete et al. suggested that this could be attributed to the mild increase in RONS production during ischemia [140, 509]. Yet, MMP-2 activation and its role in ischemic injury need further investigation.

The principal difference in ER stress signalling between IR and ischemia alone was the progression of the apoptotic response. Although ER stress-mediated apoptosis was observed in our model of IR injury, mouse hearts subjected to ischemia without reperfusion had only higher levels of CHOP compared to aerobic ones, while there were no differences in Bax levels or caspases-3 or -9 activities between ischemic and aerobic hearts, despite the reduction in IRE1 α . This suggests that the extent of injury during ischemia is not sufficient to trigger apoptosis. This is also consistent with our finding that ischemia does not exhibit a noticeable aggregation of misfolded proteins. However, CHOP, an early apoptotic marker, was still upregulated in ischemic hearts, meaning that it is highly sensitive to the changes in IRE1 α , although this is not reflected in the other apoptotic markers. This is consistent with previous studies reporting that the changes in CHOP occur faster than the subsequent changes in caspases and other apoptotic markers considering that CHOP regulates their expression at the transcriptional level [510, 511].

In conclusion, myocardial IR injury is associated with the induction of the ER stress response and the UPR. The action of MMP-2 does not involve the induction of the ER stress response but the proteolysis of the UPR protein IRE1 α , which is initiated during ischemia. This results in the disruption of the UPR and progression of ER stress-mediated apoptotic cell death as a result of persistent ER stress during IR, eventually leading to contractile dysfunction of the heart. Inhibiting MMP-2 activity could be a potential therapeutic option to preserve cardiac function and protect against myocardial cell death in part by preserving IRE1 α and preventing the transition from adaptive to maladaptive response during ER stress.

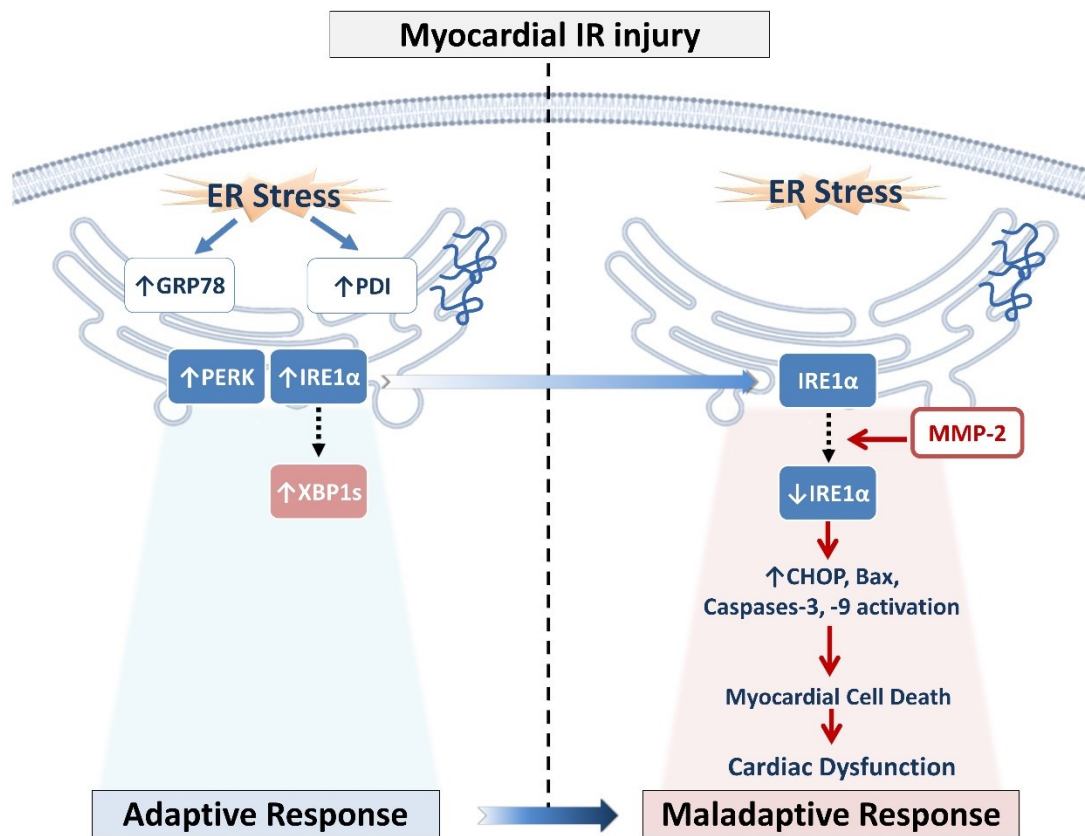


Figure 5.15. Schematic diagram showing the potential role of MMP-2 in ER stress-mediated cell death during myocardial IR injury. During IR injury, ER stress signalling is initiated with the upregulation of PDI and GRP78 to induce the UPR evidenced by increased mRNA expression of *PERK*, *IRE1α* and *XBP1s*. However, MMP-2 activated during IR targets and cleaves the UPR protein *IRE1α* resulting in disruption of UPR and triggering the upregulation of CHOP with subsequent translocation of Bax to mitochondria and activation of caspases-3 and -9 to induce apoptotic cell death, which eventually leads to contractile dysfunction of the heart (*Figure was created using BioRender*).

Chapter VI

Junctophilin-2 Proteolysis and T-Tubule Remodeling Are Consequences of Matrix Metalloproteinase-2 Activation During Doxorubicin-Induced Cardiotoxicity

A version of this chapter is under revision in the Journal of Physiology:

Wesam Bassiouni, Brandon Y.H. Chan, Andrej Roczkowsky, Zabed Mahmud, Woo Jung Cho, Richard Schulz. Junctophilin-2 proteolysis and T-tubule remodeling are consequences of matrix metalloproteinase-2 activation during doxorubicin-induced cardiotoxicity

Abstract

Treatment of cancer patients with anthracyclines is known to cause dose-dependent cardiotoxicity through several mechanisms including oxidative stress. The Schulz lab previously showed that matrix metalloproteinase-2 (MMP-2) is activated during, and contributes to, anthracycline-induced cardiotoxicity. An important feature of doxorubicin (DXR)-induced cardiotoxicity is defective excitation-contraction coupling which is associated with loss of cardiac junctophilin-2 (JPH-2). JPH-2 is a membrane protein that tethers T-tubules to the sarcoplasmic reticulum, allowing for calcium-induced calcium release in cardiomyocytes. Here I investigated the mechanism of JPH-2 loss in DXR cardiotoxicity and demonstrated the effect of MMP inhibition on JPH-2 cleavage and T-tubule remodeling. C57BL/6J mice were treated with DXR for 4 weeks with or without the MMP inhibitor (doxycycline) or MMP-2 preferring inhibitor (ONO-4817). Both inhibitors attenuated DXR-induced cardiac dysfunction. Using electron microscopy, myocytes in hearts from DXR-treated mice showed abnormally swollen T-tubules and mitochondria. This was accompanied by JPH-2 cleavage as evidenced by immunoblotting. MMP inhibitors preserved normal T-tubule and mitochondria structure and prevented JPH-2 proteolysis shown by the reduction in its 63 and 25 kDa cleavage products. Loss of JPH-2 and impaired calcium transients were also observed in neonatal rat ventricular cardiomyocytes treated with DXR, while ONO-4817 attenuated these changes. To understand why the electrophoretic mobility of JPH-2 is slower than its molecular weight, heart extracts were N-deglycosylated with PNGase F to better resolve it and its cleavage fragments. N-deglycosylation significantly increased the 75 kDa JPH-2 band from DXR hearts. *In silico* analysis predicted cleavage sites between JPH-2 MORN repeats and within its unstructured region. These results reveal that JPH-2 proteolysis is

a consequence of MMP-2 activation and highlight a mechanism of the beneficial prophylactic action of MMP inhibitors in preventing DXR-induced cardiotoxicity.

6.1. Introduction

Anthracyclines, which include DXR, are a family of chemotherapeutic agents that have been used since the 1960s for the treatment of different types of tumors such as leukemia, lymphoma, lung and breast cancers and multiple myeloma [150, 151]. However, their efficacy has been limited by dose-dependent development of severe, irreversible cardiotoxicity including left ventricular dysfunction and heart failure, with significant morbidity and mortality [152]. Several mechanisms underlying DXR-induced cardiotoxicity are proposed, including enhanced oxidative stress, altered iron metabolism, dysregulation of calcium homeostasis, as well as degradation of sarcomeric proteins and activation of apoptotic pathways [160]. Although antioxidants, angiotensin-converting enzyme inhibitors, angiotensin II receptor antagonists, beta-blockers or alpha-1 receptor agonists have been proposed as cardioprotective agents against DXR-induced cardiotoxicity, no specific treatment for mitigating myocardial injury has been developed and long-term cardiac remodeling remains persistent [160, 170]. This necessitates the development of better therapy for management of DXR-cardiotoxicity.

MMPs are a family of zinc-dependent endopeptidases which were first shown to cleave extracellular matrix proteins under physiological conditions such as angiogenesis and wound healing as well as pathological conditions including atherosclerosis, cancer metastasis and myocardial infarction [4, 5, 7]. MMP-2 is ubiquitous and is now recognized to also proteolyze intracellular proteins during myocardial injury [9]. MMP-2 and its proteolytic targets are found in several intracellular organelles in cardiomyocytes including the sarcomere, cytoskeleton, nuclei, mitochondria and the MAM [58]. It is rapidly activated during oxidative stress by the action of peroxynitrite-induced S-glutathiolation [43], and proteolyzes specific cardiac contractile and regulatory proteins such as titin, α -actinin, TnI and myosin light chain 1, resulting in myocardial

contractile dysfunction [58]. It was shown that MMP-2 is stimulated in cardiomyocytes as a result of DXR-induced oxidative stress, which also induces the de novo expression of an MMP-2_{NTT76} [174].

An essential process that controls the contractile function of the heart is excitation-contraction coupling. Upon depolarization, voltage-gated calcium channels in the plasma membrane open and allow the influx of extracellular calcium which in turn activates calcium efflux from the SR via type 2 ryanodine receptors [391, 395]. This calcium-induced calcium release depends on the action of a family of junctional membrane proteins known as junctophilins (JPH) which anchor the T-tubules to the terminal cisternae of the SR [411, 412]. The predominant isoform expressed in cardiomyocytes is JPH-2 [411]. It is localized in close proximity to the Z-disc region of the sarcomere where MMP-2 is also localized [59], as well as type 2 ryanodine receptors [413]. Loss of JPH-2 has been reported to be involved in the induction of heart failure in mice by disrupting junctional membrane complexes and impairing cardiac contractility [419]. Moreover, JPH-2 levels were also lower in patients with hypertrophic cardiomyopathy, which in turn results in altered calcium homeostasis and impaired excitation-contraction coupling [417]. The Schulz lab identified JPH-2 as a proteolytic target of MMP-2 during IR injury in isolated rat hearts [70].

The predicted molecular weight of JPH-2 is 75 kDa while it demonstrates an electrophoretic mobility of approximately 100 kDa in gel electrophoresis [70, 512]. This difference could be due to post-translational modifications such as N-glycosylation, which targets membrane-bound proteins [513]. N-glycosylation is reported to have more effects on protein dynamics than on tertiary structure. It decreases protein conformational and allosteric changes and increases protein stability by acting as a molecular glue that holds peptide residues together [514].

Glycosylation also reduces the susceptibility of proteins to proteolytic degradation [515]. Reduced N-glycosylation is reported to contribute to the progression of dilated cardiomyopathy into heart failure in mice [516]. It is unknown whether JPH-2 is N-glycosylated and if this could affect its cleavage by MMP-2.

I investigated whether JPH-2 is proteolytically cleaved by MMP-2 during DXR-induced cardiotoxicity. I show that MMP-2, activated in hearts from DXR-treated mice, proteolyzes JPH-2 which contributes to the resulting cardiac contractile dysfunction. I also found that JPH-2 is N-glycosylated and that MMP-2-mediated cleavage of JPH-2 is independent of its N-glycosylation. I also show that MMP-2 participates in the DXR-induced abnormalities in T-tubule and mitochondrial structure in cardiomyocytes as pharmacological inhibition of MMP-2 attenuates JPH-2 cleavage and preserves their structure during DXR-induced cardiotoxicity.

6.2. Methods

6.2.1. Induction of DXR cardiotoxicity

C57BL/6J mice were injected with DXR (6 mg/kg/wk, i.p., cumulative dose of 24 mg/kg, Sigma-Aldrich, St. Louis, MO, USA) once per week for 4 weeks. Using this dose, DXR reaches a plasma concentration of 0.05 μ M by 24 h which is seen during its clinical use [517, 518]. Mice were randomly assigned into control, DXR+Vehicle, DXR+Doxycycline or DXR+ONO-4817 groups. Starting on day 1, both control and DXR-groups were treated daily by oral gavage, for 28 days, with saline or the MMP inhibitor (Doxycycline, 15 mg/kg, Sigma-Aldrich, St. Louis, MO, USA) or the MMP-2 preferring inhibitor (ONO-4817, 60 mg/kg, Ono Pharmaceutical Co., Osaka, Japan), prepared in 2% carboxymethyl cellulose. Following that, changes in systolic and diastolic

function were recorded using echocardiography. These MMP inhibitors showed no adverse effects when tested in rodents at the same doses in different disease models [110, 519, 520].

6.2.2. Echocardiography

Mice were anesthetized by inhalation of 1.5% *v/v* isoflurane. Measurements were taken by transthoracic 2D/M-mode echocardiography using a Vevo 770 high-resolution imaging system with a 30 MHz transducer (VisualSonics, Toronto, ON, Canada). Left ventricular posterior wall and interventricular septum thicknesses were measured by obtaining M-mode images. Following echocardiography, mice were anesthetized by *i.p.* injection of 240 mg/kg sodium pentobarbital (Bimeda-MTC Animal Health Inc., Cambridge, ON, Canada). Mice were then euthanized by bilateral thoracotomy and hearts were rapidly excised and exsanguinated with PBS for further experiments.

6.2.3. Preparation of ventricular extracts and N-deglycosylation of glycoproteins

Hearts were isolated and frozen at the end of experiment, and the frozen ventricles were pulverized under liquid nitrogen, weighed and homogenized in 1:10 (*w/v*) RIPA buffer (Sigma-Aldrich) containing 0.1% protease inhibitor cocktail by sonication using a microtip equipped Sonifier 250 (Branson Ultrasonics, Danbury, CT) for 2 min (in cycles of 15 s on, 15 s off) at 4°C. The homogenate was centrifuged at 10,000 g for 10 min at 4°C and the supernatant, designated as the ventricular extract, was collected and stored at -80°C. Following that, the total protein concentration in each sample was measured by BCA assay using BSA as a standard.

In order to test the effect of N-glycosylation on JPH-2 electrophoretic mobility, ventricular extracts were divided into two halves and one half was subjected to an N-deglycosylation protocol

using PNGase F (New England Biolab) under denaturing conditions as described by the manufacturer. Briefly, 15 µg of sample protein was treated with 10X glycoprotein denaturing buffer (1 µl) and denatured by heating at 100°C for 10 min. Then the following components were added to the reaction mixture: 10X glyco-buffer (2 µl), 10% NP-40 (2 µl) and PNGase F (2 µl) and incubated at 37°C for 1 h before being analyzed by immunoblotting.

6.2.4. Isolation and culture of neonatal rat ventricular cardiomyocytes

To investigate the effect of DXR and MMP-2 inhibition on calcium transients, primary cultures of ventricular cardiomyocytes from neonatal rat hearts were used. Hearts from 2-4 day-old neonatal Sprague-Dawley rat pups were isolated and placed in ice-cold PBS. The hearts were rinsed twice, the atria were removed, and then the ventricles were finely minced with scissors. The minced tissue was washed three times in ice-cold PBS solution and placed in a T25 tissue culture flask containing ice-cold PBS, collagenase (0.10% *w/v*), DNase (0.025% *w/v*), and trypsin (0.05% *w/v*), followed by digestion on rotary shaker at 37°C for 30 min. Then digested tissue was transferred to a 50 mL tube containing 20 mL DMEM/F12 medium supplemented with 20% FBS and 1% penicillin-streptomycin, followed by centrifugation at 140 g for 1 min at 4°C and the supernatant was discarded. Digestions were repeated two more times, while collecting the supernatant fractions. After the final digestion, digested tissue and supernatant fractions were pooled and centrifuged at 300 g for 7 min at 4°C. The pellet was resuspended in 12 ml of plating medium (DMEM/F12 medium supplemented with 10% horse serum, 5% FBS and 1% penicillin-streptomycin) and passed through a 70 µm pore size nylon mesh strainer. Cells were plated on cell culture dishes pre-coated with laminin 24 h prior to plating (Sigma-Aldrich, Oakville, ON, Canada) at a density of 5×10^5 cells/mL. Cultured cardiomyocytes were allowed to adhere for 48 h

prior to the experiment. Cell culture confluency (~80%) and cardiomyocyte beating were confirmed using a phase-contrast light microscope.

On the day of the experiment, the culture medium was replaced with serum-free medium and the cells were treated with different concentrations of DXR (0.1-3 μM , Sigma-Aldrich) or DMSO (vehicle, 0.1% v/v) and incubated for 24 h at 37°C and 5% CO₂. Then aliquots of the conditioned media were collected to measure LDH release. A concentration of 0.3 μM DXR was chosen for the subsequent experiments where cells were treated with the MMP-2 preferring inhibitor, ONO-4817 (1 μM) for 2 h followed by treatment with 0.3 μM DXR for 24 h. After rinsing with PBS, the cells were lysed by incubating with RIPA buffer for 5 min at 4°C. Homogenates were centrifuged at 10,000 g for 10 min at 4°C and the supernatant was used as the cell lysate.

6.2.5. Cytotoxicity determination

Aliquots of serum-free cell-conditioned media (in triplicate) were used to determine cytotoxicity by measuring LDH release using a CytoTox 96 Non-Radioactive Cytotoxicity Assay kit (Promega, United Kingdom) as described in **Chapter 3 (section 3.2.4)**.

6.2.6. Measurement of cytosolic calcium using fluorescent microscopy

To measure the changes in cytosolic calcium, neonatal rat ventricular cardiomyocytes were plated in a 35 mm glass petri dish (MatTek, Ashland, MA, USA) in plating medium. Following 24 h DXR treatment in absence or presence of ONO-4817 in serum-free medium, cardiomyocytes were treated with Fluo-4 AM (5 μM , Cat#F14201, Invitrogen) for 30 min at 37°C to measure cytosolic calcium and Hoechst 33342 dye (1 μM , Cat#H3570, Invitrogen) for 10 min at 37°C to

stain nuclei. Microscopy was performed in phenol-free medium, and recordings were observed at 37°C using a Zeiss Axio Observer Z1 inverted epifluorescence microscope (63x oil objective lens) and analyzed using Zeiss Zen software. Five fields of cardiomyocytes were randomly selected to acquire the images from each group. Using time-series image acquisition with 0.5 s intervals, calcium transients were monitored and recorded as the change in fluorescence intensities (ΔF) relative to the minimum fluorescence intensity (F_0) and analyzed using ImageJ software (Version 1.47v, NIH, USA).

6.2.7. Immunoblotting

For measurement of JPH-2 levels in both PNGase F treated and untreated heart extracts as well as in lysates obtained from neonatal rat ventricular cardiomyocytes, 15 μg total protein of heart extracts or 10 μg total protein of cellular lysates was separated on 10% polyacrylamide gels by electrophoresis as described in **Chapter 2 (section 2.6)**.

The following primary antibodies were used: anti-JPH-2 (1:2000, Cat#40-5300, ThermoFisher Scientific, Waltham, MA, USA) and GAPDH (1:2000, Cat#2118, Cell Signaling Technology, Danvers, MA, USA) as a loading control.

6.2.8. Transmission electron microscopy

For conventional transmission electron microscopy, left ventricular tissue was pre-fixed in a 2.5% glutaraldehyde in 0.1 M sodium cacodylate buffer, pH 7.4 (Electron Microscopy Sciences, Hatfield, PA, USA) overnight at 4°C followed by post-fixation in a mixture of 2% osmium tetroxide and 1.5% potassium ferrocyanide in 0.1 M sodium cacodylate buffer for 2 h at room temperature. The fixed tissue was contrasted by 2% uranyl acetate for 1 h at room temperature and

Walton's lead aspartate for 30 min at 60°C. The fixed and contrasted tissue was dehydrated in ascending ethanol series (30, 50, 70, 80, 95, and 100%), embedded in Spurr's resin (Electron Microscopy Sciences, Hatfield, PA, USA), and thermally polymerized for 72 h at 70°C. The polymerized tissue was longitudinally trimmed along the myofilaments and cut using an ultramicrotome with a diamond knife (DiATOME, Hatfield, PA, USA). 70 nm ultrathin sections were obtained and transferred to a 200-mesh bare copper grid. The sections were observed with a JEOL JEM-1400 Plus transmission electron microscope (JEOL USA, Peabody, MA, USA) at 70 KeV with an AMT NanoSprint 12-megapixel CMOS camera (Advanced Microscope Technique, Woburn, MA, USA). Changes in T-tubule number and surface area, as well as mitochondria surface area, were quantified using ImageJ software (Version 1.47v, NIH, USA).

6.2.9. *In silico* analysis of JPH-2 cleavage by MMP-2

An online tool, CleavPredict, was used to predict mouse JPH-2 cleavage sites by MMP-2 [521]. This online tool is optimized for MMPs and predicts substrate cleavage sites for 11 MMPs including MMP-2 by using a position weight matrix algorithm. The mouse JPH-2 FASTA sequence (UniProt ID-Q9ET78) was entered into the CleavPredict query sequence section and MMP-2 was selected as the protease. The datasets from CleavPredict result from a high-throughput proteomics technique and proteome identification of preferred protease cleavage sites was used to determine the substrate specificity profile of MMP-2.

6.2.10. 3D crystal structure analysis

The amino acid sequence of mouse JPH-2 was retrieved from Uniprot (<https://uniprot.org>). An X-Ray crystal structure (7RXQ) of N-terminal (1-327) JPH-2 in complex with a CaV1.1 peptide was downloaded from the PDB (<https://www.rcsb.org/>) [466]. In PDB, only the 3D

structure of human JPH-2 is deposited, thus, a mouse JPH-2 3D structure was created by homology modelling using SWISS-MODEL with the 7RXQ template [467]. The missing transmembrane domain (residues 675-696) was modelled by AlphaFold (<https://alphafold.ebi.ac.uk/entry/O95140>) [468], with per-residue confidence score between 70 and 90. The intrinsically disordered regions were modeled as squiggles by AlphaFold with very low pLDDT scores of < 50. The structure was then refined using the KoBaMIN webserver [522] and was evaluated for quality and validation by SAVES [523]. The top ten predicted cleavage sites of JPH-2 by MMP-2 were drawn and visualized by PyMOL (v 2.1.1).

6.2.11. Statistics

Data are expressed as mean \pm SEM (n hearts per group). For multiple comparisons, one-way ANOVA was used followed by Sidak's post hoc test using GraphPad Prism 8 (GraphPad Software, La Jolla, CA, USA). Statistical significance was considered at p values < 0.05.

6.3. Results

6.3.1. MMP inhibitors attenuate DXR-induced systolic and diastolic dysfunction

As shown in **Table 6.1**, DXR induced both systolic and diastolic dysfunction in the mouse hearts as evidenced by a significant reduction in ejection fraction, fractional shortening, cardiac output and E/A ratio. Doxycycline or ONO-4817 significantly improved ejection fraction and fractional shortening. ONO-4817 significantly improved cardiac output, whereas doxycycline improved the E/A ratio. This indicates that MMP inhibition attenuates both systolic and diastolic dysfunction induced by DXR. Doxycycline, but not ONO-4817, also attenuated DXR-induced cardiac remodeling as seen by preventing the increase in left ventricular internal diameter as well as the left ventricular posterior wall and interventricular septum thicknesses during systole.

Table 6.1. Cardiac function and morphology in control and doxorubicin (DXR)-treated mice with or without doxycycline (Doxy) or ONO-4817 (ONO) following 28 days of treatment.

Measures	Control (n=6)	DXR (n=5)	DXR + Doxy (n=5)	DXR + ONO (n=6)
Heart Rate (beat/min)	447±14	419±15	454±18	461±10
Body Weight (g)	25.4±0.6	20.9±0.8*	21.4±0.7	23.5±0.2 [#]
Systolic Function				
Ejection Fraction (%)	60.7±2.6	47.5±3.3*	58.1±2.8 [#]	58.3±1.8 [#]
Fractional Shortening (%)	32.1±1.8	23.5±2.0*	30.2±1.9 [#]	30.2±1.2 [#]
Cardiac Output (mL/min)	18.3±0.8	11.4±1.6*	14.9±1.0	16.3±1.0 [#]
Stroke Volume (mL)	40.9±1.8	29.5±3.6*	33.1±2.7	35.6±1.7
LV End-systolic Volume (mL)	24.5±2.4	33.8±3.6*	23.7±1.8 [#]	25.0±1.7
LV End-diastolic Volume Diastole (mL)	68.1±4.3	59.0±5.3	56.8±2.8	60.3±2.7
Diastolic Function				
E/A	1.08±0.04	0.84±0.07*	1.11±0.10 [#]	0.90±0.03
Mitral A Velocity (mm/s)	351±31	265±19	290±57	312±37
Mitral E Velocity (mm/s)	501±45	430±32	432±74	453±57
Deceleration Time (ms)	20.9±2.5	23.3±2.3	21.5±2.9	19.1±1.8
E/E'	-29.0±1.8	-28.6±3.0	-28.2±5.9	-33.8±3.2
Isovolumetric Contraction Time (ms)	11.7±0.6	17.4±1.3*	15.2±1.1	11.5±1.4 [#]
Isovolumetric Relaxation Time (ms)	20.0±0.7	20.8±1.1	19.1±0.9	18.3±1.4
TEI Index	0.78±0.04	0.82±0.04	0.86±0.01	0.72±0.04
Morphology				
LV Internal Diameter Systole (mm)	2.55±0.08	2.94±0.13*	2.55±0.12 [#]	2.60±0.07
LV Internal Diameter Diastole (mm)	3.96±0.11	3.70±0.15	3.66±0.08	3.75±0.07
LV Posterior Wall Thickness Systole (mm)	1.17±0.03	0.96±0.05*	1.14±0.06 [#]	1.07±0.03
LV Posterior Wall Thickness Diastole (mm)	0.74±0.02	0.71±0.03	0.79±0.07	0.74±0.02
Interventricular Septum Thickness Systole (mm)	1.28±0.06	0.94±0.08*	1.27±0.09 [#]	1.05±0.08
Interventricular Septum Thickness Diastole (mm)	0.79±0.02	0.69±0.04	0.79±0.05	0.70±0.05

*p<0.05 vs control, [#]p<0.05 vs DXR by one-way ANOVA followed by Sidak's post-hoc test. LV= left ventricular.

6.3.2. MMP inhibitors prevent the cleavage of JPH-2 during DXR-induced cardiotoxicity

Immunoblots for JPH-2 from heart extracts showed no changes in the 100 kDa band corresponding to full length JPH-2 (**Figures 6.1 A and B**). Three bands corresponding to putative lower molecular weight fragments of JPH-2 were observed at 75, 63 and 25 kDa. While there were no differences in the ratio of the 75 kDa fragment to full length 100 kDa JPH-2 amongst the different groups (**Figure 6.1 C**), DXR significantly increased the ratio of both the 63 and 25 kDa fragments to full length 100 kDa JPH-2 compared to control (**Figures 6.1 D and E**). The MMP inhibitors, doxycycline or ONO-4817, prevented the DXR-induced increase in the ratios of 63 and 25 kDa JPH-2 fragments to 100 kDa JPH-2 (**Figures 6.1 D and E**).

Correlation analysis of the levels of the putative JPH-2 cleavage products and echocardiographic parameters showed significant negative correlations between the ratios of the 63 or 25 kDa band to 100 kDa band intensities with ejection fraction, fractional shortening, cardiac output and E/A ratio (**Figure 6.2**). In contrast, there was no significant correlation between these echocardiographic parameters and the JPH-2 75 kDa to 100 kDa band intensity ratio.

6.3.3. MMP-2 favors the cleavage of JPH-2 at the joining region between its MORN repeats

Using CleavPredict, along with the predicted secondary structure of JPH-2, I identified 26 potential cleavage sites in the murine JPH-2 sequence by MMP-2 and calculated the corresponding masses of both its N- and C-terminal cleavage fragments. I tabulated the ten cleavage sites with the highest position weight matrix score (**Figures 6.3 A and B**). Among these, it is evident that MMP-2 has a preference for leucine in the P1' position, as previously demonstrated [469] (**Figure**

6.3 A). As intact JPH-2 in mouse heart extracts runs in gel electrophoresis at higher molecular weight than expected, the resultant cleavage products of JPH-2 may also appear at molecular weights higher than calculated. Cleavage before amino acids L213, L223 or L242 would produce C-terminal fragments approximately corresponding to the apparent molecular weight of 63 kDa, while cleavage before amino acid S495 can produce a C-terminal fragment approximately corresponding to the apparent molecular weight of 25 kDa (considering that the cleavage fragments may also run slower than expected). Positioning cleavage sites on the 3D structure of mouse JPH-2 shows a preference for MMP-2 proteolysis in its unstructured regions (**Figure 6.3 C**).

6.3.4. JPH-2 is N-glycosylated

Being a membrane-associated protein [411], JPH-2 may undergo post-translational modifications such as N-glycosylation that could affect its electrophoretic mobility. I wished to better understand the disparity between the predicted and the apparent molecular weight of JPH-2 in electrophoresis, and determine whether removal of this post-translational modification would allow for the detection of JPH-2 cleavage products measured by immunoblotting. In this regard, N-glycosylation of JPH-2 was tested using PNGase F which deglycosylates proteins. Deglycosylation with PNGase F revealed a partial mobility shift of JPH-2 from 100 kDa to its predicted molecular weight of 75 kDa (**Figure 6.4 A**). There were no significant changes in the 100 kDa JPH-2/GAPDH ratios across all groups, whether glycosylated or deglycosylated (**Figure 6.4 B**). PNGase F treatment significantly increased the ratio of the 75 kDa band to full length 100 kDa JPH-2 in the DXR-treated groups (**Figure 6.4 C**). Deglycosylation did not affect the ratios of the 63 or 25 kDa fragments to 100 kDa JPH-2 (**Figures 6.4 D and E**). As such, the ratio of the 63 or 25 kDa fragments to 100 kDa JPH-2 remained elevated in the DXR group and were reduced in

the doxycycline or ONO-4817 groups, whether glycosylated or deglycosylated (**Figures 6.4 D and E**).

6.3.5. MMP inhibitors preserve T-tubule shape and size and mitochondria size in hearts from DXR-treated mice

Transmission electron micrographs of T-tubules in the left ventricular cardiomyocytes from control hearts revealed normal T-tubules which are distributed along the Z-lines or perpendicular to them (**Figure 6.5 A**). Amongst pronounced derangements in sarcomere and mitochondria ultrastructure [60], DXR hearts also showed the appearance of abnormally large, swollen T-tubules compared to control, along with T-tubules having normal appearance (**Figures 6.5 A and C**). The abnormal T-tubule structure was attenuated by doxycycline or ONO-4817, which revealed normal T-tubules in both shape and size (**Figures 6.5 A and C**). No noticeable difference in the total number of T-tubules was observed amongst the different groups (**Figure 6.5 B**). DXR hearts also exhibited abnormally swollen mitochondria evidenced by the increase in mitochondria surface area, compared to control, while doxycycline or ONO-4817 preserved normal mitochondrial size (**Figures 6.5 A and D**).

6.3.6. MMP inhibition attenuates DXR-induced reduction in JPH-2 and altered calcium transients in neonatal rat ventricular cardiomyocytes

Neonatal rat ventricular cardiomyocytes treated with DXR for 24 h showed significant cytotoxicity evidenced by an increase in LDH release at higher DXR concentrations (1 and 3 μM) and no significant cell death at low DXR concentrations (0.1 and 0.3 μM) (**Figure 6.6 A**). Therefore, a concentration of 0.3 μM DXR was used for the subsequent experiments as the highest concentration that did not show significant cell death. Treatment with DXR (0.3 μM) caused a

significant reduction in the 100 kDa JPH-2 band in neonatal rat ventricular cardiomyocytes compared to control. Two lower molecular weight fragments appeared at 75 and 25 kDa with significant increases in their ratios to full length 100 kDa JPH-2 in DXR-treated cells compared to control. The MMP-2 preferring inhibitor ONO-4817 prevented the DXR-induced reduction in the 100 kDa JPH-2 as well as the increase in the ratios of 75 and 25 kDa JPH-2 fragments to 100 kDa JPH-2 (**Figures 6.6 B-E**).

Cytosolic calcium transients were measured in neonatal rat ventricular cardiomyocytes treated with 0.3 μ M DXR for 24 h. In non-treated myocytes, a rise in cytosolic calcium transients was observed evidenced by the increase in the peak fluorescence intensity ratio ($\Delta F/F_0$) calculated as the difference between the maximum (F) and minimum (F_0) fluorescence intensities relative to the minimum fluorescence intensity (F_0). DXR significantly reduced the peak $\Delta F/F_0$ compared to control, while ONO-4817 attenuated this reduction ($p < 0.05$) (**Figure 6.7**).

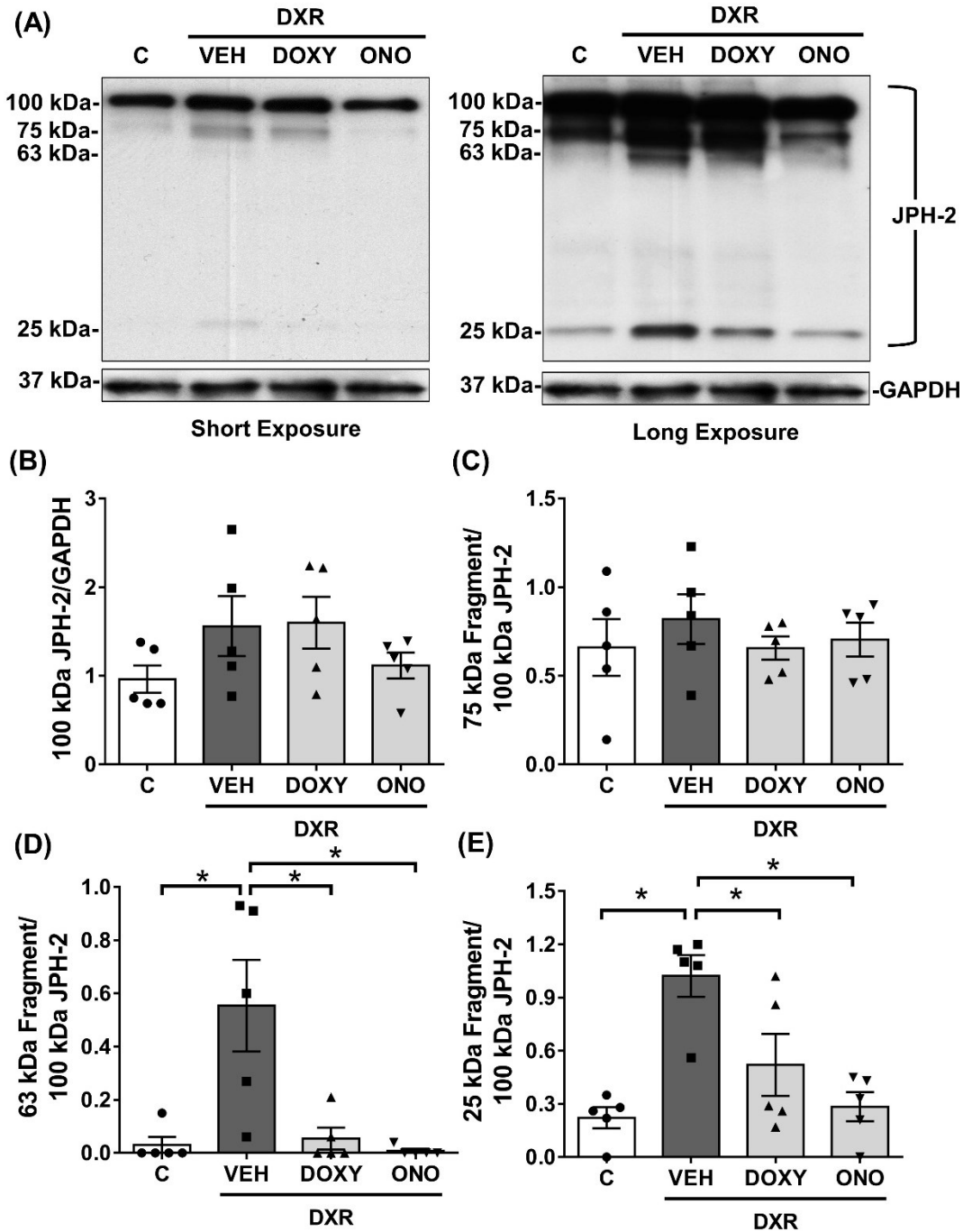


Figure 6.1. MMP inhibitors attenuate JPH-2 cleavage in hearts from DXR-treated mice. (A) Representative immunoblot showing levels of JPH-2 and its putative cleavage products in ventricular extracts from mice treated with DXR in absence and presence of doxycycline (DOXY), ONO-4817 (ONO) or vehicle (VEH). Quantitative measurements of JPH-2 levels are shown for 100 kDa full length JPH-2 (B) or 75 kDa (C), 63 kDa (D) and 25 kDa fragments (E). The 100 kDa band is normalized to GAPDH and 75, 63 and 25 kDa bands are normalized to 100 kDa JPH-2 (n=5 per group). Position of molecular weight ladder proteins indicated on the left. *p<0.05 by one-way ANOVA followed by Sidak's post-hoc test.

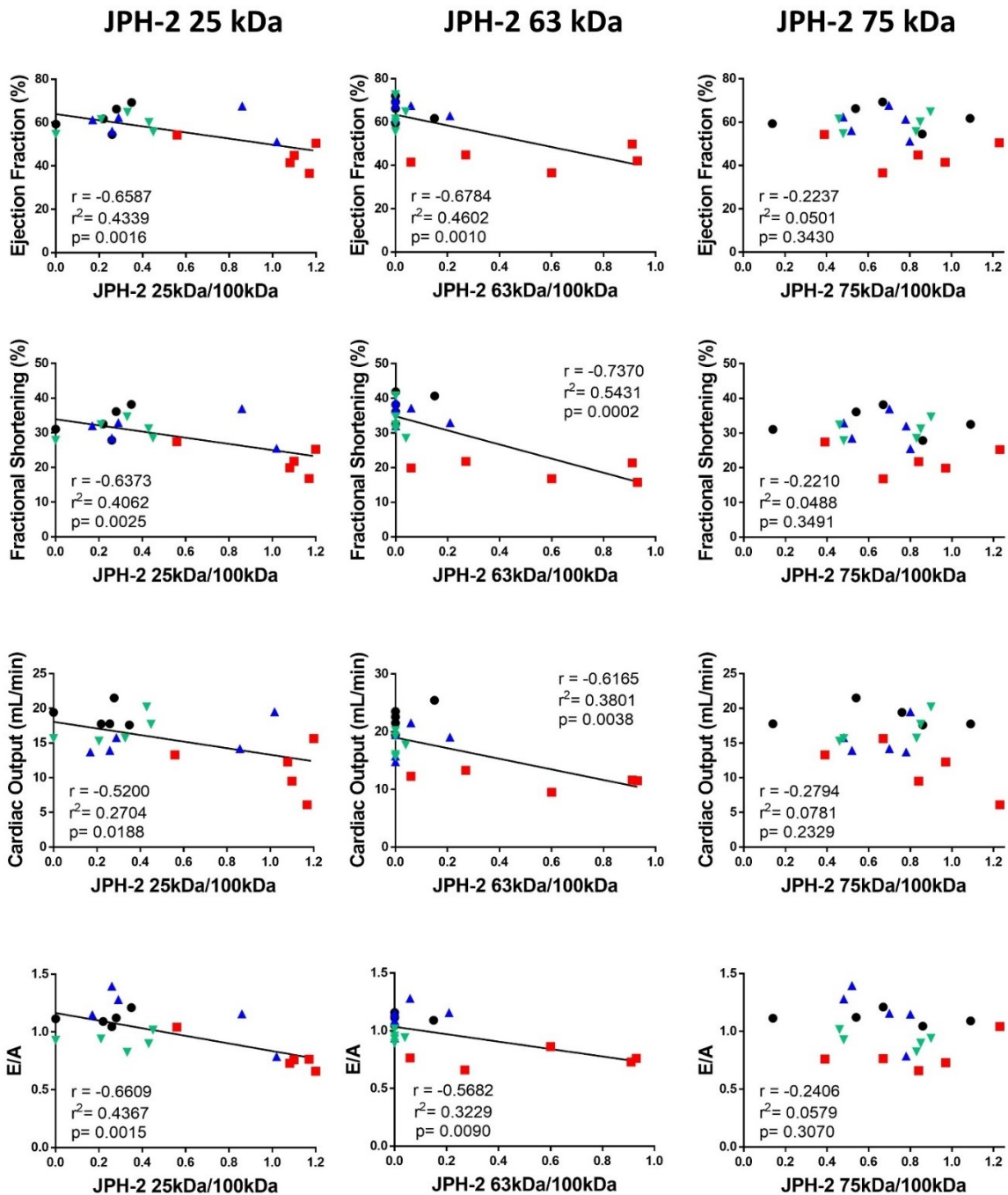


Figure 6.2. The levels of JPH-2 63 and 25 kDa fragments in hearts from DXR-treated mice are negatively correlated to cardiac functional parameters. Correlation analysis of the levels of JPH-2 cleavage fragments (75, 63 and 25 kDa) to cardiac echocardiographic parameters (ejection fraction, fractional shortening, cardiac output and E/A ratio) in hearts from DXR-treated mice in presence of vehicle (red ■), doxycycline (blue ▲), or ONO-4817 (green ▼) compared to control mice (black ●) (n=5 per group). p<0.05 denotes significant correlation.

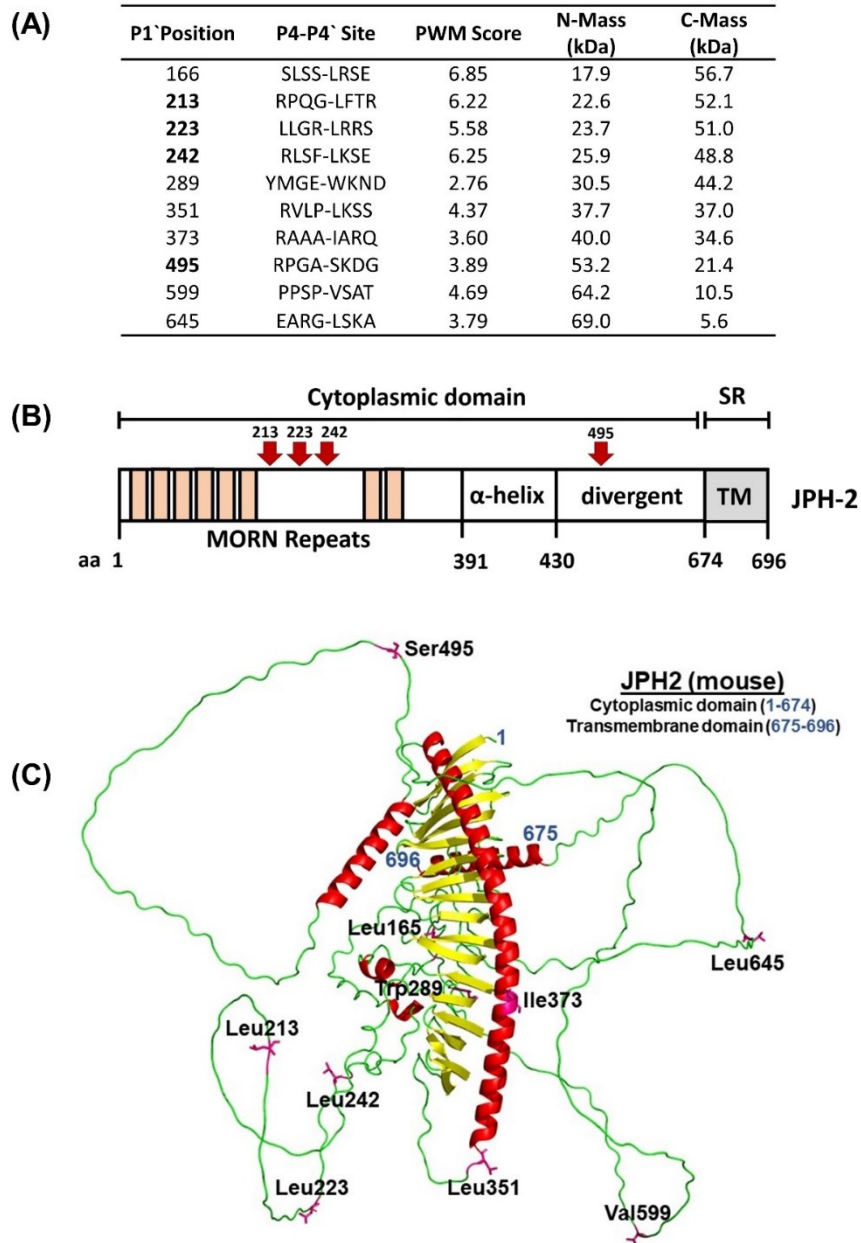


Figure 6.3. *In silico* analysis of the predicted cleavage sites within JPH-2 by MMP-2. (A) Top ten positional weight matrix (PWM) score for MMP-2 cleavage sites within the cytoplasmic domain of mouse JPH-2 according to CleavPredict. (B) Representative sequence organization of JPH-2 structure showing 8 MORN repeats interrupted by a joining region along with α -helix domain, divergent region and C-terminal transmembrane domain. Cleavage sites at P1' 213, 223, 242 and 495 (red arrows in panel B, bold in panel A) were predicted to produce cleavage fragments with a similar molecular weight observed in DXR hearts by gel electrophoresis. (C) Structure of mouse JPH-2 (model based on human JPH-2 PDB ID:7RXQ, α -helix: red, β -sheet: yellow and disordered regions: green). Predicted cleavage sites are shown as pink sticks.

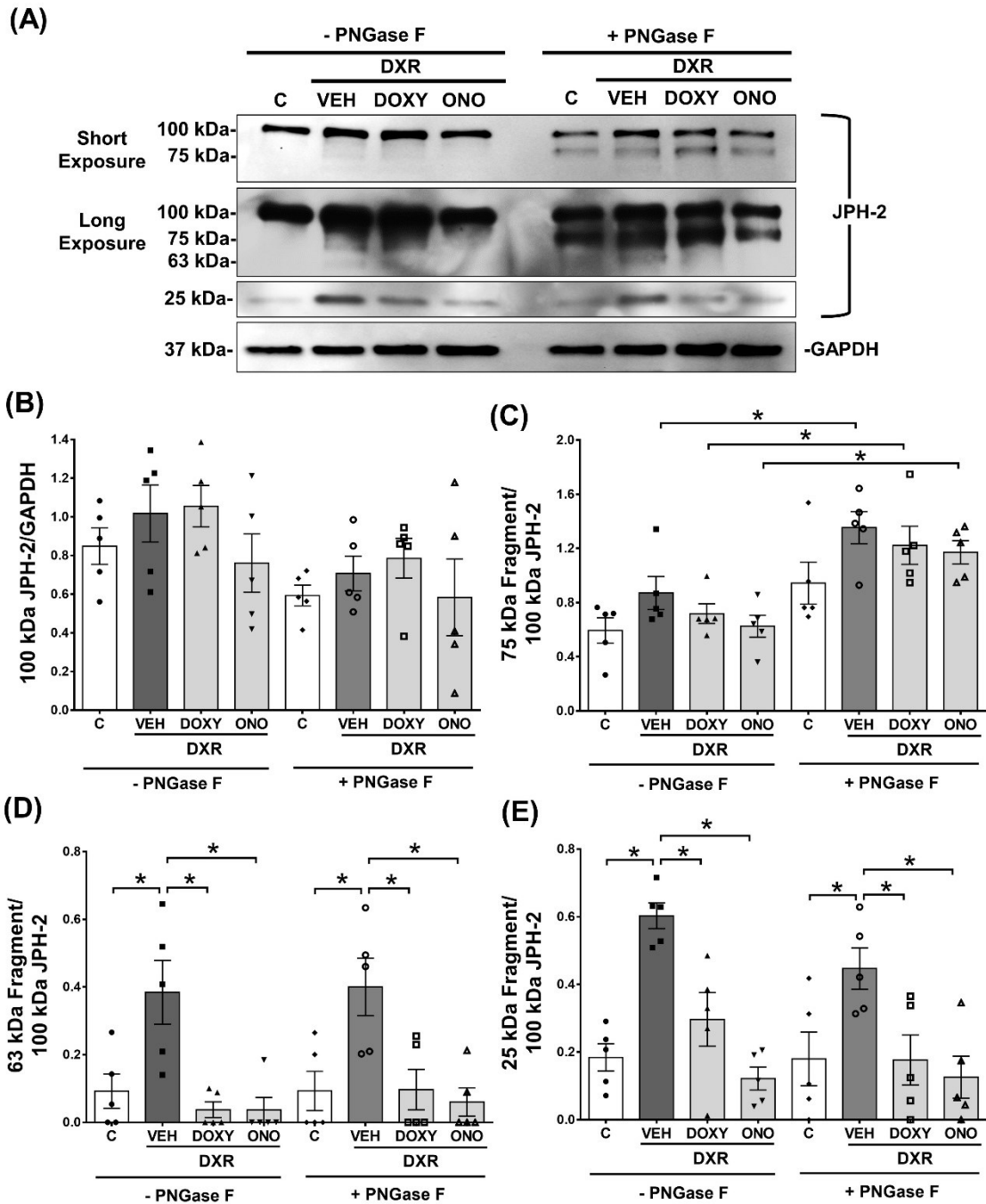


Figure 6.4. JPH-2 is N-glycosylated in mouse hearts. (A) Representative immunoblot showing levels of JPH-2 and its putative cleavage products in ventricular extracts from mice treated with DXR in absence and presence of doxycycline (DOXY), ONO-4817 (ONO) or vehicle (VEH) followed by *in vitro* treatment with PNGase F. Quantitative measurements of JPH-2 levels are shown for 100 kDa full length JPH-2 (B) or 75 kDa (C), 63 kDa (D) and 25 kDa fragments (E). The 100 kDa band is normalized to GAPDH and 75, 63 and 25 kDa bands are normalized to 100 kDa JPH-2 (n=5 per group). Position of molecular weight ladder proteins indicated on the left. *p<0.05 by one-way ANOVA followed by Sidak's post-hoc test.

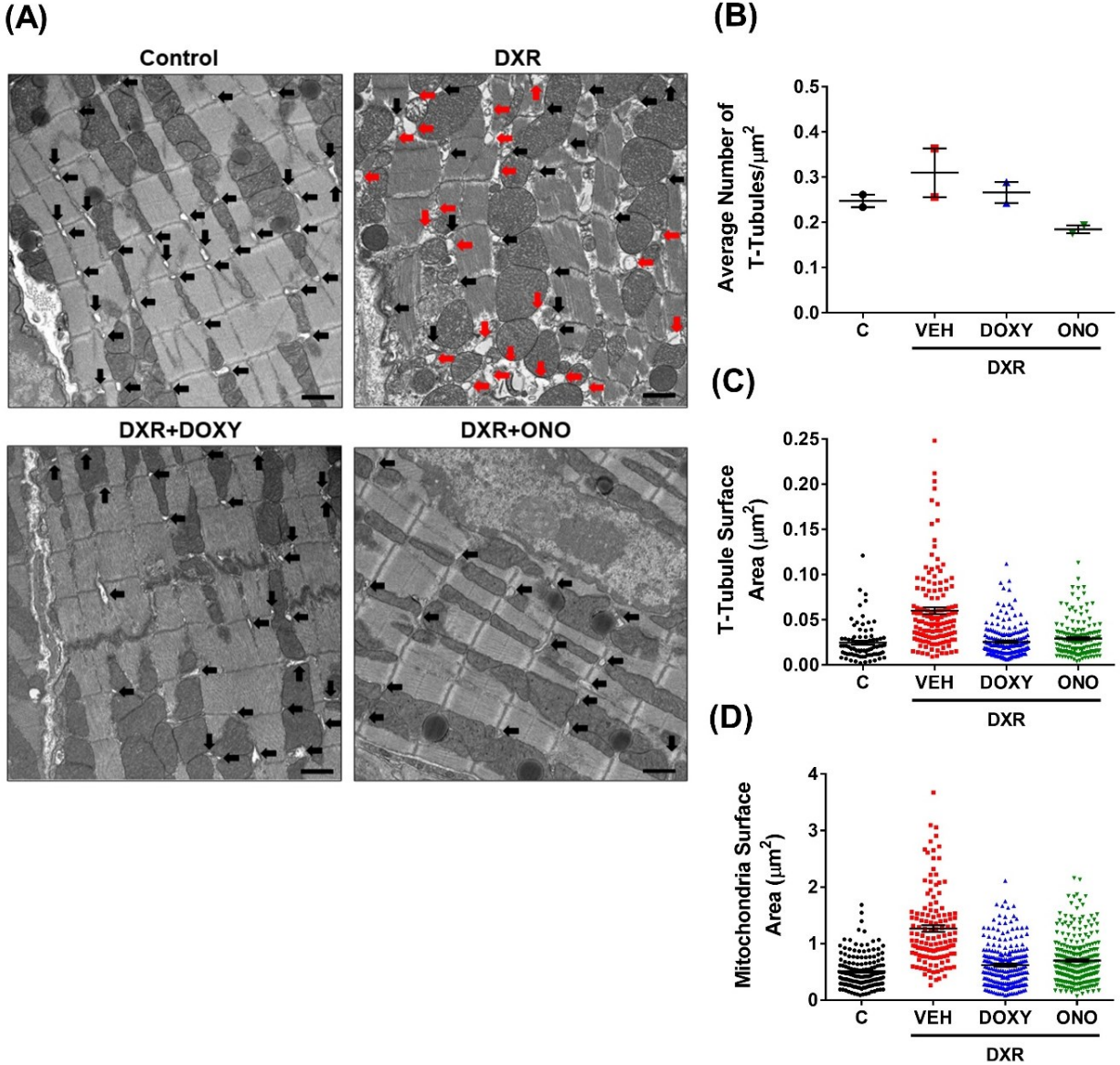


Figure 6.5. MMP inhibitors prevent T-tubule and mitochondria derangements in cardiac myocytes in hearts from DXR-treated mice. (A) Representative transmission electron micrographs of T-tubules in the left ventricular cardiomyocytes of control and DXR-treated mice in absence and presence of doxycycline (DOXY) or ONO-4817 (ONO). Representative of more than 50 images from each group (two different hearts per group). Scale bar = 1 μm . (B-D) Quantitative measurements of the average number of T-tubules per μm^2 (B), T-tubule surface area (C), or mitochondria surface area (D) in hearts from control and DXR-treated mice in absence and presence of doxycycline (DOXY) or ONO-4817 (ONO). The dots in panels C and D are technical replicates from images obtained from two different hearts per group. No statistical analysis was done on these images due to the low number of biological replicates.

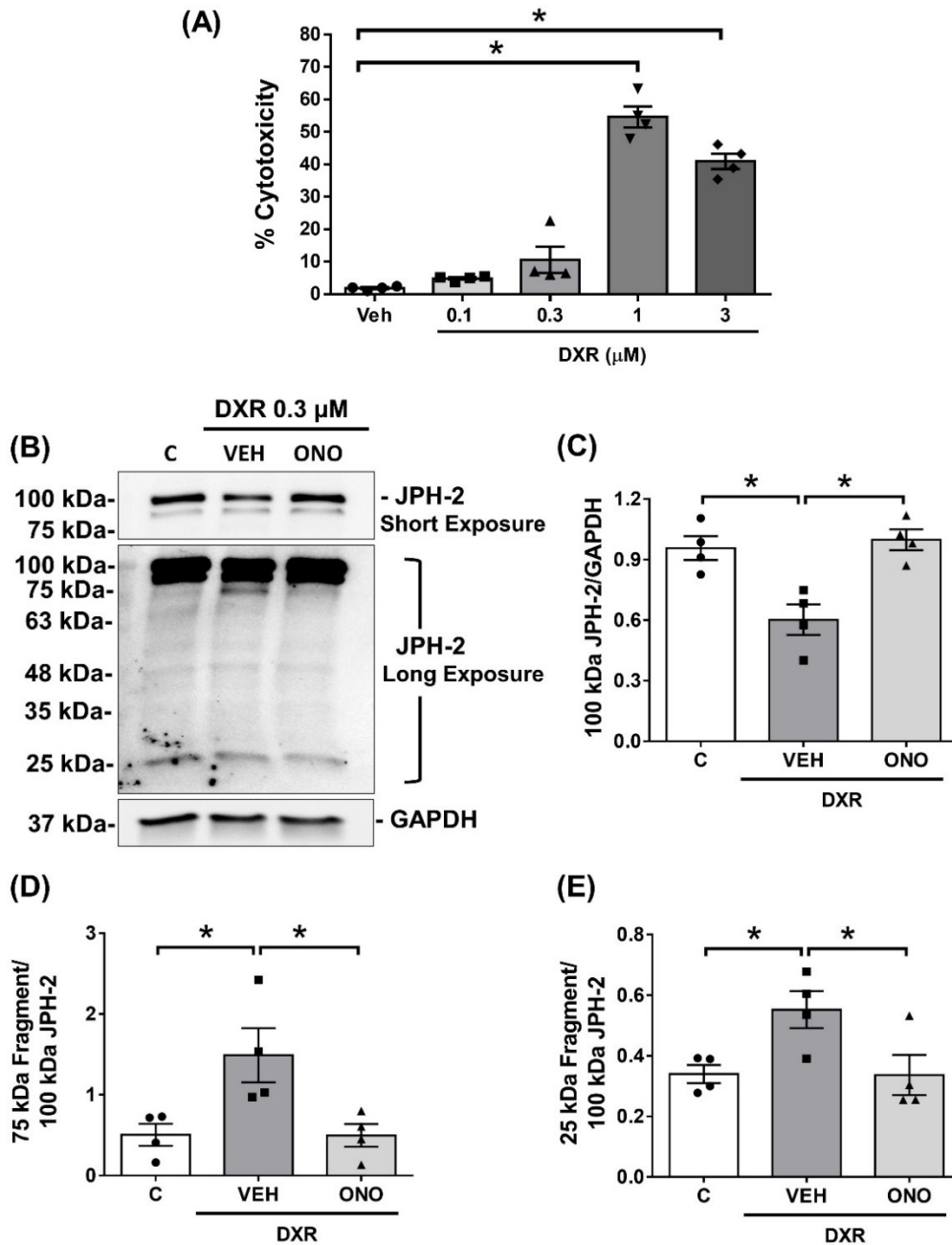


Figure 6.6. MMP-2 inhibition attenuates JPH-2 cleavage in DXR-treated neonatal rat ventricular cardiomyocytes. (A) Lactate dehydrogenase (LDH) assay showing percentage cytotoxicity in neonatal rat ventricular cardiomyocytes treated with DXR (0.1-3 μM) for 24 h. (B) Representative immunoblot showing levels of JPH-2 and its putative cleavage products in neonatal rat ventricular cardiomyocytes treated with 0.3 μM DXR in absence and presence of ONO-4817 (ONO). Quantitative measurements of JPH-2 levels are shown for 100 kDa full length JPH-2 (C) or 75 kDa (D), and 25 kDa fragments (E). The 100 kDa band is normalized to GAPDH and 75 and 25 kDa bands are normalized to 100 kDa JPH-2 (n=4 per group). Position of molecular weight ladder proteins indicated on the left. *p<0.05 by one-way ANOVA followed by Sidak's post-hoc test.

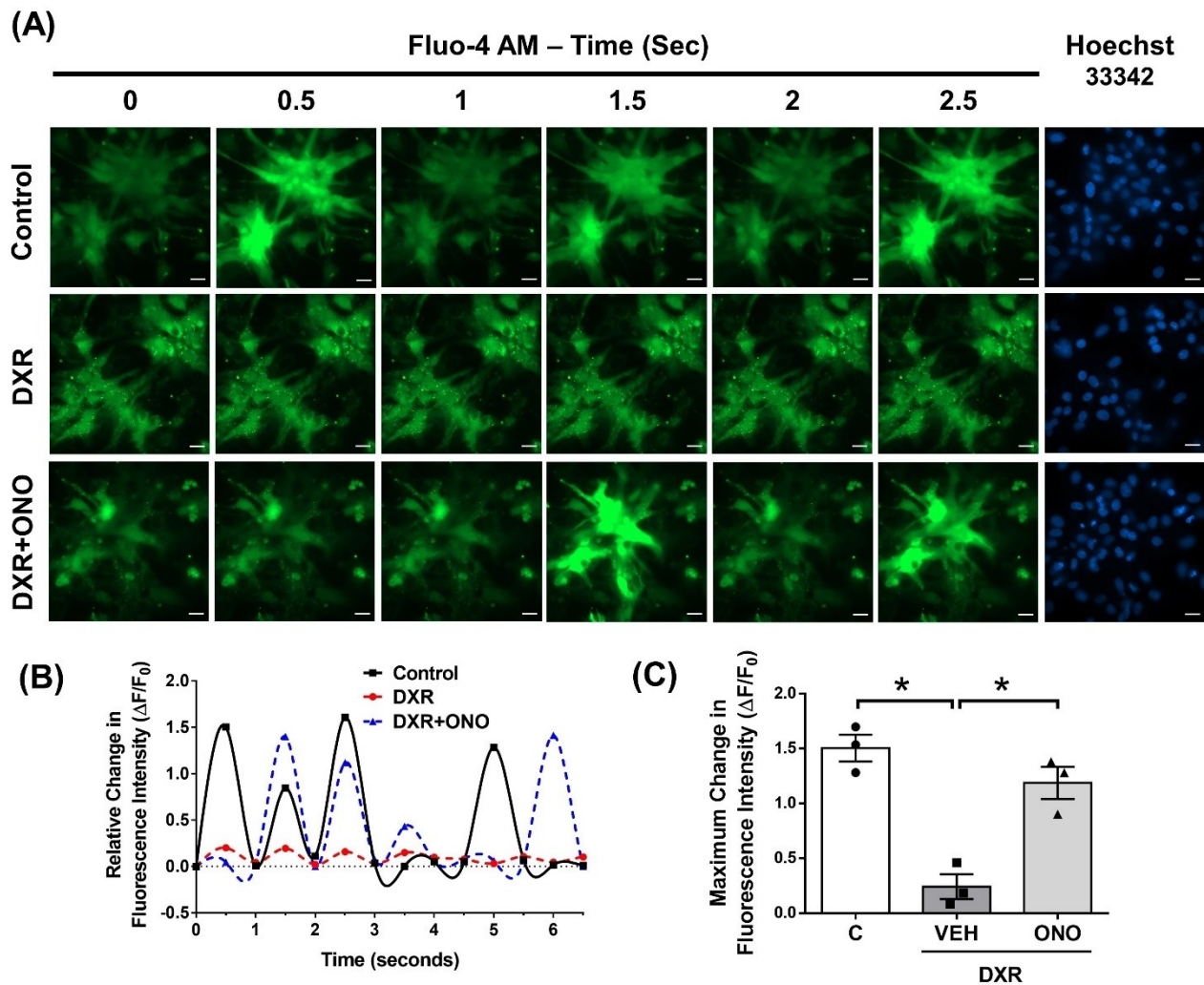


Figure 6.7. MMP-2 inhibition improves cytosolic calcium transients in DXR-treated neonatal rat ventricular cardiomyocytes. (A) Representative images of neonatal rat ventricular cardiomyocytes stained with Fluo-4 AM (for cytosolic calcium, green) and Hoechst 33342 (for nuclei, blue) after 24 h DXR treatment in absence or presence of ONO-4817 (ONO). Scale bar = 20 μm . (B) Representative quantitative measurements of the changes in Fluo-4 fluorescence intensity (ΔF) in time-series images acquired every 0.5 s relative to the minimum fluorescence intensity (F_0). (C) Quantitative measurements of the peak changes in Fluo-4 fluorescence intensity (maximum ΔF) relative to the minimum fluorescence intensity (F_0) ($n=3$ per group, 5 fields each). * $p<0.05$ by one-way ANOVA followed by Sidak's post-hoc test.

6.4. Discussion

I investigated whether JPH-2 is proteolyzed by MMP-2 during DXR-induced cardiotoxicity and how this contributes to the associated cardiac dysfunction. Here I show that MMP-2, activated during DXR-cardiotoxicity, cleaves cardiac JPH-2, which anchors the T-tubule to the SR, into lower molecular weight C-terminal fragments of ~ 63 and 25 kDa which negatively correlate with parameters of cardiac contractile function. JPH-2 is also found to be partially N-glycosylated which affects its electrophoretic mobility and results in its appearance higher than its calculated molecular weight during gel electrophoresis. I also show that DXR-mediated abnormalities in T-tubule and mitochondria structure as well as cytosolic calcium transients are attenuated by MMP inhibition. A schematic representation of the speculated role of MMP-2 in JPH-2 cleavage during DXR-induced cardiotoxicity is shown in **Figure 6.8**.

MMP-2 plays a dominant role in the pathophysiology of DXR-induced cardiotoxicity. As the Schulz lab previously showed [60], DXR-induced cardiac dysfunction was attenuated by the MMP inhibitors doxycycline or ONO-4817. I show here that this effect could be in part attributed to preserving JPH-2 from proteolytic cleavage. JPH-2 is a membrane-bound protein which is essential for the tethering between T-tubules and the SR which facilitates excitation-contraction coupling in cardiomyocytes [416]. This role of JPH-2 was demonstrated in previous studies as mice with cardiac-specific knockout of JPH-2 exhibited cardiac dysfunction, while its overexpression restored normal cardiac function in response to pressure overload [421]. JPH-2 protein level was lower in patients with hypertrophic cardiomyopathy and JPH-2 knockdown in HL-1 cardiomyocytes resulted in impaired excitation-contraction coupling [417], indicating the importance of JPH-2 for proper cardiac function. In our study, DXR induced the cleavage of mouse cardiac JPH-2 into putative lower molecular weight fragments of 75, 63 and 25 kDa. MMP-2 may

be responsible for the cleavage of JPH-2 into the 63 and 25 kDa, but not the 75 kDa fragment, as the increase in the 63 and 25 kDa fragments in hearts from DXR-treated mice was abolished by the MMP inhibitor doxycycline as well as MMP-2 preferring inhibitor ONO-4817. The potential relevance of the 63 and 25 kDa fragments in cardiac dysfunction was emphasized by their significant negative correlation to several echocardiographic parameters. These findings suggest that the protective effect of MMP inhibition may be in part attributed to preserving JPH-2 level in cardiomyocytes. MMP-2-mediated JPH-2 proteolysis was also confirmed in DXR-treated neonatal rat ventricular cardiomyocytes. MMP-2 was previously reported to be activated by DXR in neonatal rat ventricular cardiomyocytes [174]. Our data shows that MMP inhibition preserves JPH-2 protein level in DXR-treated neonatal rat ventricular cardiomyocytes and reduces the increase in the ratios of 75 and 25 kDa fragments to 100 kDa JPH-2. However, there were some discrepancies between mouse hearts and neonatal rat ventricular cardiomyocytes, as the increase in the 75 kDa fragment observed in neonatal rat ventricular cardiomyocytes was not observed in mouse hearts, and the 63 kDa fragment detected in mouse hearts was not observed in immunoblots from neonatal rat ventricular cardiomyocytes. These discrepancies could be due to the species difference, molecular weight shifts that occur as a result of post-translational modifications such as N-glycosylation, or the incomplete development of the contractile machinery in neonatal rat ventricular cardiomyocytes [524].

The cleavage of JPH-2 into a 25 kDa fragment was observed in mice subjected to transverse aortic constriction-induced pressure overload, with calpain-2 being suggested to be responsible for its cleavage as this was accompanied by an increase in calpain-2 protein level [525]. Calpain is suggested to mediate JPH-2 cleavage in mouse hearts subjected to *in vitro* or *in vivo* IR injury as the loss of JPH-2 was prevented by the calpain inhibitor, MDL-28170, or transgenic

overexpression of the endogenous calpain inhibitor, calpastatin [526]. However, the role of MMP-2 in JPH-2 proteolysis cannot be ruled out, as the calpain inhibitors, calpastatin and MDL-28170, used in these studies were also shown to inhibit MMP-2 activity [443, 527].

In silico and crystal structure analysis of mouse JPH-2 cleavage sites by MMP-2 predicted that MMP-2 may cleave JPH-2 between G212 and L213, R222 and L223, or F241 and L242 to produce C-terminal fragments of approximately 63 kDa, and between A494 and S495 to produce a C-terminal fragment of approximately 25 kDa. These sites lie in the unstructured region of JPH-2, which is particularly susceptible to proteolytic attack, and three of them have leucine in the P1' position, which is favored by MMP-2 for cleavage [469]. Using Uniprot sequence align, a sequence similarity of 97.1% was found between mouse and rat JPH-2. Seven of the top ten predicted mouse JPH-2 cleavage sites by MMP-2 are also found in rat JPH-2 as shown by *in silico* analysis [70].

I also show for the first time that JPH-2 may undergo N-glycosylation in mouse hearts which affects its mobility during gel electrophoresis, causing it to run slower than its calculated molecular weight. N-glycosylation occurs as a post-translational modification of membrane-associated proteins to enhance their stability [514]. Our results show that N-deglycosylation of JPH-2 by PNGase F significantly increased the ratio of the 75, but not the 63 nor 25 kDa, fragments to 100 kDa JPH-2 in samples from DXR-treated mouse hearts. This suggests that the 75 kDa band is likely full length JPH-2 that appeared following its N-deglycosylation, considering that the predicted molecular weight of JPH-2 is 75 kDa. Therefore, removal of the N-glycan revealed a partial mobility shift of JPH-2 from 100 kDa to its predicted molecular weight of 75 kDa. This increase in the 75 kDa band intensity following PNGase F treatment was not reversed by the MMP inhibitors, confirming that it is not a proteolytic product of MMP-2. On the other hand, the DXR-

mediated increase in both 63 and 25 kDa fragments can be attributed to the proteolytic activity of MMP-2, and was not affected by PNGase treatment.

JPH-2 loss is known to induce disruption of the T-tubule-SR interface, which in turn attenuates excitation-contraction coupling in cardiomyocytes and induces cardiac contractile dysfunction [419, 528]. Therefore, I investigated the changes in T-tubule structure in response to DXR-cardiotoxicity. Our data shows that hearts from DXR-treated mice exhibited T-tubule distension as evidenced by the appearance of abnormally large, swollen T-tubules compared to control hearts, while inhibition of MMP-2 activity preserved normal T-tubule structure. This suggests that these changes could be attributed to MMP-2 activation in the heart. This highlights the beneficial effect of MMP inhibition in improving T-tubule integrity and preventing DXR-induced cardiac dysfunction. This could be also linked to MMP-2-mediated cleavage of JPH-2 as cardiac-specific deletion of JPH-2 in mice is reported to impair T-tubule maturation [422, 529]. In mouse models of hypertrophic or dilated cardiomyopathy, loss of JPH-2 was associated with impaired systolic function and progressive T-tubule remodeling [418]. Similar results were observed *in vitro*, as knockdown of JPH-2 in cultured cardiomyocytes compromised T-tubule structural integrity and reduced the junctional T-tubule/SR surface area [403, 530]. DXR treatment is also known to be associated with mitochondrial damage and dysfunction [531, 532]. Interestingly, hearts from mice with cardiac-specific expression of MMP-2_{NTT76} exhibited swollen mitochondria with less organized cristae [30]. Our data shows that MMP-2 activation during DXR-cardiotoxicity contributes to the associated mitochondrial swelling as MMP inhibition preserved normal mitochondrial structure. This could be also linked to MMP-2-mediated loss in JPH-2 as JPH-2 is reported in an unreviewed preprint to regulate mitochondrial metabolism and JPH-2

knockdown in stem cell-derived cardiomyocytes resulted in Mfn-2 downregulation, disruption of mitochondrial cristae structure, biogenesis and oxidative capacity [533].

DXR-induced cardiotoxicity is known to be associated with impaired excitation-contraction coupling and calcium transients. DXR treatment of mice resulted in an early reduction in calcium transient amplitude and a slower calcium decay rate at 2 weeks of treatment, followed by a late reduction in SR calcium load [425]. Using whole-cell voltage clamp to measure calcium transients and voltage-gated calcium channel current in cardiomyocytes isolated from adult guinea pig hearts, DXR treatment for 1 h was reported to reduce calcium-induced calcium release from the SR [426]. Our data shows that DXR causes a profound reduction in cytosolic calcium transients in neonatal rat ventricular cardiomyocytes. This reduction was attenuated by ONO-4817, suggesting that MMP-2 activation by DXR contributes to the impaired calcium signalling. This reduction in calcium transients by DXR can be partially linked to MMP-2-mediated JPH-2 proteolysis, as JPH-2 is essential for T-tubule-SR interaction and excitation contraction coupling [414]. Cardiomyocytes from JPH-2 null mice exhibited impaired calcium transients and structural uncoupling between T-tubule and SR [411]. Similarly, JPH-2 knockdown in HL-1 cardiomyocytes resulted in reduced intracellular calcium transients [417]. This confirms that MMP-2-mediated proteolysis of JPH-2 is a major contributor to the DXR-associated impairment in calcium transients and T-tubule remodeling, eventually resulting in cardiac contractile dysfunction.

In conclusion, our findings reveal a novel mechanism by which MMP inhibitors protect against DXR-induced cardiotoxicity by preventing the proteolysis of JPH-2. I show that JPH-2 is N-glycosylated which affects its electrophoretic mobility, and MMP-2, activated in mouse hearts by DXR, proteolyzes JPH-2 into lower molecular weight fragments of 63 and 25 kDa, which negatively correlate to cardiac function. I also show that MMP inhibition preserves normal T-

tubule and mitochondrial structure in DXR hearts as well as calcium transients in neonatal rat ventricular cardiomyocytes. Our data provides further insight into the cardioprotective mechanisms of MMP inhibitors and suggests new possible therapeutic options for the treatment of DXR-induced cardiotoxicity.

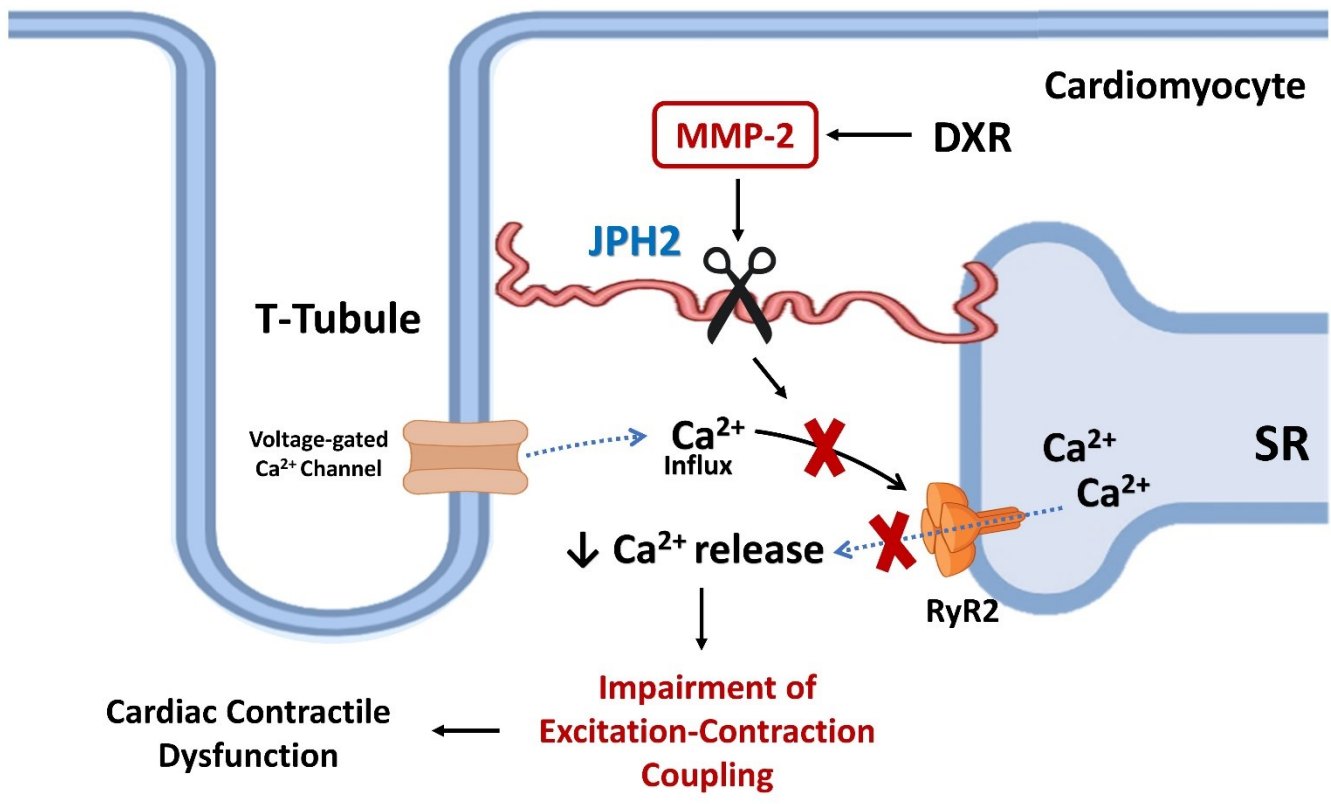


Figure 6.8. Schematic representation of the role of MMP-2 in JPH-2 cleavage during DXR-induced cardiotoxicity. MMP-2 activation results in proteolysis of JPH-2 which is essential for the close association between the T-tubule and sarcoplasmic reticulum (SR). Cleavage of JPH-2 reduces calcium release from the SR and subsequently impairs excitation-contraction coupling that eventually leads to cardiac contractile dysfunction.

Chapter VII

Conclusions

7.1. Conclusions

I discovered, in the present thesis, novel mechanisms of MMP-2-mediated cardiac contractile dysfunction during two critical cardiac conditions: myocardial IR injury and DXR-induced cardiotoxicity. These mechanisms involve targeting and proteolyzing specific proteins localized at the interface between the ER and mitochondria known as the MAM. As a part of the pathophysiological role of MMP-2, I introduced new potential MMP-2 proteolytic targets including Mfn-2 in the mitochondria and IRE1 α in the ER. MMP-2-mediated loss in these proteins during IR injury resulted in mitochondrial dysfunction, impaired UPR and ER homeostasis, induction of the inflammasome response as well as an enhanced ER stress-mediated apoptotic response, which ultimately led to myocardial cell death and cardiac contractile dysfunction. I also revealed that JPH-2, which is known to be a proteolytic target of MMP-2 in IR injury, is also cleaved by MMP-2 during DXR-cardiotoxicity, resulting in T-tubule remodeling, impaired calcium handling and cardiac contractile dysfunction.

Cardiac diseases comprise the first leading cause of death worldwide [115]. Myocardial IR injury and anthracycline-induced cardiotoxicity are two major cardiac pathologies, and the pathophysiology of these conditions is not well understood. Despite the numerous studies that provide potential therapeutic options for the management of these conditions in the past decades, most of the pre-clinical trials failed to be translated into clinical practice, as many of the provided therapies act mainly via alleviating the symptoms or targeting a single pathway that contributes to the disease progression [121, 534]. That is why understanding the precise molecular mechanisms that contribute to the pathophysiology of these cardiac conditions is critical to provide new and effective therapy and limit the morbidity and mortality associated with them.

MMP-2 has been revealed to be an important downstream mediator of the pathophysiological changes occurring during myocardial IR injury and DXR-induced cardiotoxicity [58, 60], being activated intracellularly in response to oxidative stress [43, 44]. Additionally, the constitutively active intracellular isoform of MMP-2, MMP-2_{NTT76}, is known to be transcriptionally upregulated in these cardiac disorders [30, 60]. Full length MMP-2 is reported to be localized to the MAM [65], while MMP-2_{NTT76} is reported to be found in the intermembranous space of mitochondria [30, 64], which suggests a potential role of MMP-2 and/or MMP-2_{NTT76} in the dysregulation of mitochondrial and ER/SR functions during oxidative stress and cardiac injury. Therefore my main focus, in the present work, is to understand the role of MMP-2 in mitochondrial and ER/SR dysregulation.

As mitochondria play a fundamental role in regulating apoptosis via AIF processing and release [282], the role of MMP-2 in AIF cleavage was investigated in human tumor fibrosarcoma cells as an MMP-2 expressing cell line. I showed that MMP-2 is activated during STS-induced cytotoxicity as an early event prior to the induction of cell death. However, under our experimental conditions, MMP-2 does not seem to be involved in STS-mediated release and cleavage of mitochondrial AIF which mediates caspase-independent apoptosis. Our data also showed that STS-induced AIF cleavage is calpain-independent. The precise role of MMP-2 during STS-induced cytotoxicity and the actual protease responsible for AIF cleavage remain to be investigated.

Although MMP-2 is not involved in mitochondrial AIF processing, it plays other roles in the regulation of mitochondrial function and homeostasis. I showed that MMP-2 is involved in the pathophysiology of mitochondrial dysfunction during myocardial IR injury. A proposed mechanism is by targeting and proteolyzing Mfn-2, an important mitochondrial protein that

regulates their function, which is localized at the MAM [195], where MMP-2 is also found. Mfn-2 is essential for mitochondrial fusion and tethering of the ER to mitochondria which in turn is required for regulation of calcium transit from the ER to mitochondria and the function of the electron transport chain [195]. I showed that MMP-2-mediated loss in Mfn-2 contributes to the associated mitochondrial respiratory dysfunction, impaired ATP production and the induction of the inflammasome response which eventually led to cardiac contractile dysfunction during IR injury. Mitochondrial dysfunction and inflammation can also trigger myocardial cell death and the progression into myocardial infarction. Therefore, inhibiting MMP-2 activity can protect against mitochondrial dysfunction, attenuate the inflammasome activation and reduce the degree of infarction and cell death during IR injury, in part by preserving mitochondrial Mfn-2. Collectively, these novel mechanisms contribute to the protective effect of MMP-2 inhibitors against cardiac dysfunction during IR injury.

Another novel finding of our study is that MMP-2 activation during IR injury can affect ER homeostasis, the second major function of the MAM, which is required for several cellular processes in cardiac cells, particularly protein synthesis and folding, when disrupted will trigger the ER stress response [323]. Although I showed that MMP-2 is not involved in the ER stress response itself during IR, it can target and cleave the UPR protein IRE1 α , being a distinctive ER stress sensor that is essential for restoring proper protein folding. This in turn impairs the UPR and enhances ER stress-mediated apoptotic cell death, contributing eventually to the resulting cardiac contractile dysfunction and myocardial cell death. Therefore, inhibiting MMP-2 activity can protect against cardiac injury during IR, in part, by preserving IRE1 α protein level and attenuating ER stress-mediated apoptotic response, subsequently preventing the transition from an adaptive to a maladaptive response.

Another critical cardiac condition that was investigated in our study is DXR-induced cardiotoxicity, as MMP-2 is also known to contribute to the cardiotoxic complications associated with DXR treatment for cancer [60]. I revealed a new mechanism of this pathophysiological role of MMP-2, particularly by targeting and cleaving the junctional protein, JPH-2, which tethers the T-tubules to SR. JPH-2 is reported to be targeted by MMP-2 during IR injury [70]. Here I showed that it is also cleaved by MMP-2 in hearts from DXR-treated mice as well as in neonatal rat ventricular cardiomyocytes treated with DXR. This in turn resulted in induction of T-tubule remodeling and mitochondrial swelling. Loss in JPH-2 also impaired cytosolic calcium signalling which in turn results in cardiac contractile dysfunction. Therefore, inhibiting MMP-2 activity can preserve JPH-2 protein level, maintain normal T-tubule structure and improve cytosolic calcium transient which eventually protects against the cardiac contractile dysfunction associated with DXR treatment.

Previous studies reported that many pharmacological approaches targeting a single molecule or organelle are not effective for several reasons when tested clinically. These include age, comorbidities and concurrent medications that may affect mitochondrial function (for review see [535]). Involvement of other heart cell types such as endothelial cells, fibroblasts and inflammatory cells as well as other contributors such as oxidative stress and calcium overload in the pathophysiology of cardiac injury is another factor for the clinical failure of these approaches [536, 537]. Most of the known current treatments for myocardial IR injury or DXR-induced cardiotoxicity are reported to exert their cardioprotective effect via acting as antioxidants or through other mechanisms that are different from their known mechanisms of action such as reducing apoptosis or inflammation [170, 538, 539]. This means there could be a major player in the pathophysiology of these cardiac pathologies that is involved in the downstream pathway of

these therapies and is not uncovered yet. This unique player could be MMP-2. Here I show that MMP-2 inhibition could protect the mitochondria, attenuate the inflammasome response, reduce the ER stress-mediated myocardial cell death and preserve normal T-tubule structure and calcium signalling among several mechanisms for its cardioprotective effect against cardiac injury as reported in previous studies [58]. As full length MMP-2 is directly and rapidly activated by oxidative stress and MMP-2_{NTT76} is translated as an active protease in response to oxidative stress, MMP-2 can be considered as an early effector of oxidative stress, making it an attractive pharmacological target. MMP-2 affects several intracellular organelles including the sarcomere, cytoskeleton, nuclei and mitochondria [58]. Many of the proteolytic targets of MMP-2 in these organelles are essential for cardiac function. Therefore, MMP-2 inhibition favors cardioprotection on different downstream effectors that may confer more efficient translational results when using MMP-2 inhibitors as adjunct therapy. Indeed ONO-4817 was developed as an orally available MMP-2 preferring inhibitor [94], and is effective not only in IR injury [59] but also in anthracycline-induced cardiotoxicity [60], which would facilitate its use in clinical trials. Yet further studies are required to validate the efficacy of ONO-4817 or other MMP-2 inhibitors in other more relevant models of co-morbid ischemic heart disease and/or anthracycline cardiotoxicity.

In summary, MMP-2 targets and proteolyzes critical proteins at the MAM including Mfn-2 and IRE1 α during IR injury and JPH-2 during DXR-induced cardiotoxicity. Loss in any of these proteins contributes to the resulting cardiac contractile dysfunction by impairing the homeostatic functions of the MAM. Therefore, the use of MMP-2 inhibitors as adjunct therapy during reperfusion in patients suffering from ischemic heart disease or in cancer patients under DXR therapy could be promising in protecting against cardiac dysfunction.

7.2. Limitations

7.2.1. Limitations of Chapter 3

I provided in **Chapter 3** evidence of MMP-2 activation in response to STS treatment in HT1080 cells and that STS-induced mitochondrial AIF release and cleavage is independent of MMP-2 or calpain. I also used different concentrations of the MMP-2 and/or calpain pharmacological inhibitors as well as siRNA to knock down MMP-2. Some limitations of this chapter include the sole use of the STS-treated human tumor HT1080 cells as a model of AIF cleavage. I did not include primary cells such as cardiomyocytes or other cancer cell lines to get a better understanding of how AIF is processed. Investigating the involvement of MMP-2 in AIF cleavage in other models such as myocardial IR injury [540] is warranted. To genetically silence MMP-2, I used MMP-2 siRNA which only reduces gene expression at the mRNA level and may induce silencing of off-target mRNAs with complementary sequences. Other approaches such as CRISPER/Cas9 which completely silences the gene expression at the DNA level would be more robust [541].

Our data shows that neither MMP-2 nor calpain play a role in STS-induced AIF cleavage. Although it was not the focus of the study, I did not investigate the involvement of other proteases such as cathepsins, particularly cathepsins-B, -D and -E which showed high scores in proteolyzing AIF using *in silico* analysis. Cathepsins were also reported to mediate AIF cleavage in isolated mitochondria treated with atractyloside, as discussed earlier [292]. The exact role of MMP-2 in STS-induced cytotoxicity also remains to be investigated. Furthermore, the identity of the 60 and 45 kDa cytosolic AIF fragment needs to be confirmed using mass spectrometry.

7.2.2. Limitations of Chapter 4

Some limitations of **Chapter 4** include the use of an *in vitro* mouse heart model of IR injury rather than an *in vivo* model. Although this allows for assessment of contractile function without the interference of external factors, it excludes the effect of essential regulators of cardiac function such as hormonal and neuronal modulators [542]. The Krebs-Henseleit solution used in Langendorff mouse heart perfusion has limited oxygen-carrying capacity and low oncotic pressure compared to the use of whole blood for perfusion. Therefore it does not completely simulate the blood-perfused heart [139]. Although the use of constant pressure Langendorff perfusion does not override the autoregulatory mechanisms of the heart, it is also difficult to achieve a controlled flow rate while using this mode. This mode does not allow for the study of the effect of low-flow ischemia on cardiac function [543]. The method of excising the heart and cannulating the aorta increases the vulnerability of the heart to injury and the possibility of preconditioning and may cause additional stress to the heart [544].

I only used male mice for the whole study which obviates the assessment of sex-related differences in cardiac injury and how this could affect the role of MMP-2 in mitochondrial function, considering that some pathological phenotypes are developed in male but not in female mice, particularly when subjected to IR injury [545]. Hearts from female rats are reported to be more resistant to damage following oxygen deprivation and develop smaller infarct size following IR injury compared to males [546, 547]. I did not include female mice in the study because this will increase the cost required for breeding and maintaining them. Additionally, the age of the mice will need to be considered as estrogen is reported to have a protective effect against myocardial IR injury. Therefore, women before menopause are protected against myocardial ischemia [548, 549].

Another limitation is the sole use of pharmacological MMP-2 inhibitors rather than genetic models. Follow-up studies using transgenic mice with cardiac-specific expression of MMP-2_{NTT76} [64] and full length MMP-2 [63] or their knockout mice are necessary to confirm these results. The use of cardiac-specific Mfn-2 knockout mice would also be helpful to confirm whether the cardioprotective effect of the MMP-2 inhibitors depends, in part, on preserving Mfn-2 function, by showing that their cardioprotective effect is lost or impaired in Mfn-2 knockout mice.

Although measuring protein level using immunoblotting is widely used, it relies on the specificity of the antibody used which detects only a specific epitope in the protein structure. Therefore some proteolytic products of the cleaved protein may be missed when detected by immunoblotting. To overcome this problem, I used two different monoclonal antibodies against Mfn-2, one which binds to residues surrounding Val573, and another one which binds to the C-terminal portion of Mfn-2. However, no cleavage products were detected, despite observing lower molecular weight bands with *in vitro* proteolysis. This could be due to the specificity of the antibody, or those proteolytic products may undergo further cleavage by MMP-2 itself or other endogenous proteases. The identity of the putative bands observed with *in vitro* proteolysis still needs to be confirmed using mass spectrometry. Additionally, to confirm the precise MMP-2 cleavage site in Mfn-2 structure proposed by *in silico* analysis, a mouse model of mutant Mfn-2 is required. However, this was not done in the present work due to the high cost of breeding and maintenance. Due to the absence of a commercially available antibody against MMP-2_{NTT76}, I relied on measuring its mRNA level using qPCR, which overlooks the effects of any post-translational modifications occurring in response to IR injury.

As shown in the **Appendix**, I measured the changes in Drp-1 protein level in mitochondria-enriched and cytosolic fractions obtained from IR hearts. However, a fuller understanding of

mitochondrial dynamics would also include measuring Drp-1 phosphorylation and its post-translational modifications in myocardial IR injury [550].

7.2.3. Limitations of Chapter 5

As discussed in **section 7.2.2**, similar to **Chapter 4**, the sole use of male mice, the use of an *in vitro* model of IR injury rather than an *in vivo* model, as well as the use of only pharmacological inhibitors rather than genetic models, are also considered limitations for **Chapter 5**.

Some other limitations of **Chapter 5** include not using a genetic model of IRE1 α knockout mice which would provide more evidence of its involvement in the cardioprotective effect of the MMP-2 inhibitors, by showing that their cardioprotective effect is lost or impaired in IRE1 α knockout mice. I measured the changes in the mRNA and protein levels of the UPR proteins IRE1 α and PERK, however, I did not measure the changes in the other UPR protein, ATF6, due to the difficulty in detecting its level because of it being translocated from the ER to the Golgi and undergoing proteolytic cleavage in response to ER stress [348]. Measuring the changes in ATF6 would provide a better idea about how UPR is affected during IR injury. Although I found significant difference in IRE1 α and PERK protein levels during IR injury, I did not evaluate the changes in their activities which require deep investigation of their dependent signalling pathways such as the changes in the transcription factors XBP1s, eIF2 α and ATF4 and their localization to different subcellular compartments, particularly to the nuclear fraction [346, 347, 551]. This would provide a better understanding of how MMP-2 modulates ER stress and UPR during IR injury.

Although I found a significant reduction in the IRE1 α mother band in IRE1 α immunoblots prepared using extracts from IR hearts, or upon incubation with exogenous MMP-2, I did not detect

lower molecular weight bands. This could be due to the specificity of the antibody, or those proteolytic products may undergo further cleavage by MMP-2 itself or other endogenous proteases. Additionally, the identity of the 100 kDa band observed in MMP-2 immunoprecipitates needs to be confirmed using mass spectrometry.

Measuring ThT binding to aggregated proteins as an indication of ER stress is more robust when performed by staining living cells or sliced tissue sections compared to *in vitro* ThT binding assay which is done using frozen samples and requires isolation of the insoluble proteins [552]. This was not done in the present study as it requires more heart samples or additional experiments with cultured cardiomyocytes. More reliable, but sophisticated, methods for measuring ER stress are by measuring ER dilation in tissue using electron microscopy or by ER real-time redox measurement using ER-targeted redox-sensitive green fluorescent protein [553].

7.2.4. Limitations of Chapter 6

In **Chapter 6**, I studied the role of MMP-2 in DXR-induced cardiotoxicity using both *in vivo* animal model of DXR-treated mice as well as cell model of neonatal rat ventricular cardiomyocytes treated with DXR. However, a limitation of the use of DXR-treated mice is that mouse hearts become smaller when treated with DXR instead of developing hypertrophy compared to what is observed clinically, as cancer patients are known to suffer from dilated cardiomyopathy as a side effect of anthracycline treatment [554, 555]. The use of neonatal rat ventricular cardiomyocytes to study DXR toxicity and measure calcium signalling is widely used. However, compared to neonatal rat cardiomyocytes, the differentiation cycle in adult rat cardiomyocytes is accompanied by re-expression of the fetal gene program, which means a fetal-like transcriptional state in response to stress. This in turn mimics the pathological changes

occurring in human cardiomyopathies [556]. They were not used in the present study as, in their isolated state, the adult cardiomyocytes are fragile and show significantly high rates of death within already 24 h of culture. Healthy cardiomyocytes do not beat and the ones which do are already partially damaged [557].

Other limitations of **Chapter 6** include the examination of only male mice which limits the assessment of sex-related differences in DXR-induced cardiotoxicity. The difference in outcomes and sensitivities of males and females to DXR treatment is well documented [558]. I also did not include genetic models with MMP-2 or JPH-2 knockout to confirm the role of MMP-2-mediated cleavage of JPH-2 in DXR-induced cardiotoxicity, by showing that the cardioprotective effect of the MMP-2 inhibitors is impaired in JPH-2 knockout mice. Follow-up studies are also required to confirm the identity of the putative proteolytic products of JPH-2 in both mouse heart and neonatal rat ventricular cardiomyocytes using mass spectrometry. Upon N-deglycosylation of the ventricular extracts, a partial mobility shift of JPH-2 from 100 kDa to its predicted molecular weight of 75 kDa is observed. However, the protein is incompletely N-deglycosylated as a strong 100 kDa band is still detected. This does not allow a full interpretation of the effect of N-glycosylation on MMP-2-mediated cleavage pattern of JPH-2. Adding more PNGase F or longer incubation time with the extracts may be required to obtain complete N-deglycosylation.

The changes in mitochondria and T-tubule surface areas, which are quantified in images obtained using transmission electron microscopy from serial thin sections, are acquired using 2D images which do not fully reconstitute the 3D nature of these organelles. Therefore some changes in their structures may be not observed with traditional electron microscopy. Although it is more expensive and requires a qualified technician to operate, quantifying the area of these organelles using 3D scanning electron microscopy would be more informative [559, 560]. I was also unable

to quantify the distance between the T-tubules and SR in the obtained images as the gap between them is too small (12-15 nm in depth) [561]. Measuring this distance would provide more information about the effect of JPH-2 loss on the structure of the junctional dyad.

7.3. Future directions

The current thesis provides a potential adjunct therapy to protect against cardiac dysfunction during ischemic heart disease, particularly myocardial IR injury, as well as during anticancer therapy with anthracyclines. The data presented in this thesis is obtained using *in vitro* and *in vivo* animal experiments and *in vitro* cell experiments. The main focus of the thesis is to uncover new mechanisms contributing to the pathophysiological role of MMP-2 in these cardiac pathologies and propose novel proteolytic targets of MMP-2 which need to be preserved to protect the cardiac function, specifically at the MAM. Further studies and future experiments are still required. Some are summarized in the following points:

- 7.3.1. Investigate how the mitochondrial quality control proteins other than Mfn-2 are affected by MMP-2 activation during IR injury. Changes in the expression, activity and localization of the mitochondrial fission protein, Drp-1, and mitophagy proteins, PINK1 and parkin, need to be assessed to get a better understanding of mitochondrial regulation during IR.
- 7.3.2. Investigate the changes in mitochondrial biogenesis in response to MMP-2 activation during IR, being a crucial regulator of mitochondrial homeostasis. This includes the assessment of mtDNA and mitobiogenesis proteins.
- 7.3.3. Study the changes in cardiac metabolism, including glycolysis and fatty acid oxidation during IR and the involvement of MMP-2 in their regulation using a model of mouse

working heart perfusion, to get a better understanding of how MMP-2 affects cardiac energy metabolism.

- 7.3.4. Apply *in silico* screening with the use of computational modeling and molecular docking to provide more reliable information about MMP-2 targeted cleavage sites in the proposed mitochondrial and ER proteolytic substrates.
- 7.3.5. The use of genetic models of Mfn-2, IRE1 α or JPH-2 knockout mice to confirm their role in the cardioprotective effect of MMP-2 inhibitors during IR injury and/or DXR-induced cardiotoxicity, by showing that their cardioprotective effect is inhibited by knocking out these genes.
- 7.3.6. The use of point mutation to provide additional information about the exact sites targeted for proteolysis in the protein of interest and whether the targeted amino acid sequence can be substituted to protect this protein from proteolytic cleavage by MMP-2 without affecting its function.
- 7.3.7. Apply the same experimental approaches used in the current study using transgenic mice with cardiac-specific expression of MMP-2_{NTT76}.
- 7.3.8. Apply the same experimental approaches using female and/or aged mice, to allow studying the effect of sex and aging, respectively, on MMP-2 pathophysiological role in cardiac injury.
- 7.3.9. Study the changes in mitochondrial quality control proteins during ischemia prior to reperfusion and whether MMP-2 inhibition can protect against these changes.
- 7.3.10. Investigate the effect of MMP-2 activation on mitochondrial dynamics using 3D scanning electron microscopy.

To allow better interpretation of these new pre-clinical findings and translating them into clinical settings, applying similar experimental approaches in other models of cardiac injury, and in *in vivo* models and studies in humans are necessary. This can be achieved via a series of future experiments as follows:

- 7.3.11. Investigate the role of MMP-2 in mitochondrial and ER dysfunctions using an *in vivo* model of myocardial IR injury, such as left anterior descending coronary artery ligation in mice with the oral administration of the MMP-2 inhibitors.
- 7.3.12. Measure the changes in MMP-2 activity and expression as well as the changes in mitochondrial and UPR protein levels in samples from patients suffering from myocardial infarction, using blood samples, atrial appendages or other cardiac tissue biopsies following heart transplantation.
- 7.3.13. Investigate the effect of MMP-2-mediated cleavage of JPH-2 on calcium signalling in other models such as IR injury and how the other calcium handling proteins, such as mitochondrial calcium uniporter, type-2 ryanodine receptors and Na⁺/Ca²⁺ exchanger, are affected.
- 7.3.14. Study the interaction of MMP-2 and inflammasomes in an *in vivo* animal model of inflammation such as with lipopolysaccharide-treated mice, with the use of an inflammasome inhibitor such as MCC950 to evaluate its effect on MMP-2 activity.
- 7.3.15. Assess the rate of mitochondrial oxygen consumption in cardiac muscle fibers isolated from human infarct hearts with the introduction of MMP-2 inhibitors.

References

1. Gross J and Lapiere CM (1962). Collagenolytic activity in amphibian tissues: a tissue culture assay. *Proc Natl Acad Sci U S A* 48, 1014-1022.
2. Iyer RP, Patterson NL, Fields GB and Lindsey ML (2012). The history of matrix metalloproteinases: milestones, myths, and misperceptions. *Am J Physiol Heart Circ Physiol* 303, H919-930.
3. Bräuninger H, Krüger S, Bacmeister L, Nyström A, Eyerich K, Westermann D and Lindner D (2023). Matrix metalloproteinases in coronary artery disease and myocardial infarction. *Basic Res Cardiol* 118, 18.
4. Hu J, Van den Steen PE, Sang QX and Opdenakker G (2007). Matrix metalloproteinase inhibitors as therapy for inflammatory and vascular diseases. *Nat Rev Drug Discov* 6, 480-498.
5. Page-McCaw A, Ewald AJ and Werb Z (2007). Matrix metalloproteinases and the regulation of tissue remodelling. *Nat Rev Mol Cell Biol* 8, 221-233.
6. Vacek TP, Rehman S, Neamtu D, Yu S, Givimani S and Tyagi SC (2015). Matrix metalloproteinases in atherosclerosis: role of nitric oxide, hydrogen sulfide, homocysteine, and polymorphisms. *Vasc Health Risk Manag* 11, 173-183.
7. DeLeon-Pennell KY, Meschiari CA, Jung M and Lindsey ML (2017). Matrix metalloproteinases in myocardial infarction and heart failure. *Prog Mol Biol Transl Sci* 147, 75-100.
8. Cheung PY, Sawicki G, Wozniak M, Wang W, Radomski MW and Schulz R (2000). Matrix metalloproteinase-2 contributes to ischemia-reperfusion injury in the heart. *Circulation* 101, 1833-1839.
9. Wang W, Schulze CJ, Suarez-Pinzon WL, Dyck JR, Sawicki G and Schulz R (2002). Intracellular action of matrix metalloproteinase-2 accounts for acute myocardial ischemia and reperfusion injury. *Circulation* 106, 1543-1549.
10. Schulz R (2007). Intracellular targets of matrix metalloproteinase-2 in cardiac disease: rationale and therapeutic approaches. *Annu Rev Pharmacol Toxicol* 47, 211-242.
11. Murphy G and Nagase H (2008). Progress in matrix metalloproteinase research. *Mol Aspects Med* 29, 290-308.
12. Si-Tayeb K, Monvoisin A, Mazzocco C, Lepreux S, Decossas M, Cubel G, Taras D, Blanc JF, Robinson DR and Rosenbaum J (2006). Matrix metalloproteinase 3 is present in the cell nucleus and is involved in apoptosis. *Am J Pathol* 169, 1390-1401.
13. Rouet-Benzineb P, Buhler JM, Dreyfus P, Delcourt A, Dorent R, Perennec J, Crozatier B, Harf A and Lafuma C (1999). Altered balance between matrix gelatinases (MMP-2 and MMP-9) and their tissue inhibitors in human dilated cardiomyopathy: potential role of MMP-9 in myosin-heavy chain degradation. *Eur J Heart Fail* 1, 337-352.

14. Miller JP, Holcomb J, Al-Ramahi I, de Haro M, Gafni J, Zhang N, Kim E, Sanhueza M, Torcassi C, Kwak S, Botas J, Hughes RE and Ellerby LM (2010). Matrix metalloproteinases are modifiers of huntingtin proteolysis and toxicity in Huntington's disease. *Neuron* 67, 199-212.
15. Marchant DJ, Bellac CL, Moraes TJ, Wadsworth SJ, Dufour A, Butler GS, Bilawchuk LM, Hendry RG, Robertson AG, Cheung CT, Ng J, Ang L, Luo Z, Heilbron K, Norris MJ, Duan W, Bucyk T, Karpov A, Devel L, Georgiadis D, Hegele RG, Luo H, Granville DJ, Dive V, McManus BM and Overall CM (2014). A new transcriptional role for matrix metalloproteinase-12 in antiviral immunity. *Nat Med* 20, 493-502.
16. Shimizu-Hirota R, Xiong W, Baxter BT, Kunkel SL, Maillard I, Chen XW, Sabeh F, Liu R, Li XY and Weiss SJ (2012). MT1-MMP regulates the PI3K δ -Mi-2/NuRD-dependent control of macrophage immune function. *Genes Dev* 26, 395-413.
17. Cauwe B and Opdenakker G (2010). Intracellular substrate cleavage: a novel dimension in the biochemistry, biology and pathology of matrix metalloproteinases. *Crit Rev Biochem Mol Biol* 45, 351-423.
18. Cui N, Hu M and Khalil RA (2017). Biochemical and biological attributes of matrix metalloproteinases. *Prog Mol Biol Transl Sci* 147, 1-73.
19. Nagase H, Visse R and Murphy G (2006). Structure and function of matrix metalloproteinases and TIMPs. *Cardiovasc Res* 69, 562-573.
20. Visse R and Nagase H (2003). Matrix metalloproteinases and tissue inhibitors of metalloproteinases: structure, function, and biochemistry. *Circ Res* 92, 827-839.
21. Bigg HF, Rowan AD, Barker MD and Cawston TE (2007). Activity of matrix metalloproteinase-9 against native collagen types I and III. *Febs J* 274, 1246-1255.
22. Shimokawa K, Katayama M, Matsuda Y, Takahashi H, Hara I, Sato H and Kaneko S (2002). Matrix metalloproteinase (MMP)-2 and MMP-9 activities in human seminal plasma. *Mol Hum Reprod* 8, 32-36.
23. Suzuki K, Enghild JJ, Morodomi T, Salvesen G and Nagase H (1990). Mechanisms of activation of tissue procollagenase by matrix metalloproteinase 3 (stromelysin). *Biochemistry* 29, 10261-10270.
24. Uría JA and López-Otín C (2000). Matrilysin-2, a new matrix metalloproteinase expressed in human tumors and showing the minimal domain organization required for secretion, latency, and activity. *Cancer Res* 60, 4745-4751.
25. Caterina JJ, Skobe Z, Shi J, Ding Y, Simmer JP, Birkedal-Hansen H and Bartlett JD (2002). Enamelysin (matrix metalloproteinase 20)-deficient mice display an amelogenesis imperfecta phenotype. *J Biol Chem* 277, 49598-49604.

26. Kerkelä E, Böhling T, Herva R, Uria JA and Saarialho-Kere U (2001). Human macrophage metalloelastase (MMP-12) expression is induced in chondrocytes during fetal development and malignant transformation. *Bone* 29, 487-493.
27. Dufour A, Sampson NS, Zucker S and Cao J (2008). Role of the hemopexin domain of matrix metalloproteinases in cell migration. *J Cell Physiol* 217, 643-651.
28. Hegde RS and Bernstein HD (2006). The surprising complexity of signal sequences. *Trends Biochem Sci* 31, 563-571.
29. Ali MA, Chow AK, Kandasamy AD, Fan X, West LJ, Crawford BD, Simmen T and Schulz R (2012). Mechanisms of cytosolic targeting of matrix metalloproteinase-2. *J Cell Physiol* 227, 3397-3404.
30. Lovett DH, Mahimkar R, Raffai RL, Cape L, Zhu BQ, Jin ZQ, Baker AJ and Karliner JS (2013). N-terminal truncated intracellular matrix metalloproteinase-2 induces cardiomyocyte hypertrophy, inflammation and systolic heart failure. *PLoS One* 8, e68154.
31. Yang Z, Strickland DK and Bornstein P (2001). Extracellular matrix metalloproteinase 2 levels are regulated by the low density lipoprotein-related scavenger receptor and thrombospondin 2. *J Biol Chem* 276, 8403-8408.
32. Chow AK, Cena J, El-Yazbi AF, Crawford BD, Holt A, Cho WJ, Daniel EE and Schulz R (2007). Caveolin-1 inhibits matrix metalloproteinase-2 activity in the heart. *J Mol Cell Cardiol* 42, 896-901.
33. Cho WJ, Chow AK, Schulz R and Daniel EE (2007). Matrix metalloproteinase-2, caveolins, focal adhesion kinase and c-Kit in cells of the mouse myocardium. *J Cell Mol Med* 11, 1069-1086.
34. Mannello F and Medda V (2012). Nuclear localization of matrix metalloproteinases. *Prog Histochem Cytochem* 47, 27-58.
35. Kwan JA, Schulze CJ, Wang W, Leon H, Sariahmetoglu M, Sung M, Sawicka J, Sims DE, Sawicki G and Schulz R (2004). Matrix metalloproteinase-2 (MMP-2) is present in the nucleus of cardiac myocytes and is capable of cleaving poly (ADP-ribose) polymerase (PARP) in vitro. *Faseb J* 18, 690-692.
36. Xie Y, Mustafa A, Yerzhan A, Merzhakupova D, Yerlan P, A NO, Wang X, Huang Y and Miao L (2017). Nuclear matrix metalloproteinases: functions resemble the evolution from the intracellular to the extracellular compartment. *Cell Death Discov* 3, 17036.
37. Sinha SK, Asotra K, Uzui H, Nagwani S, Mishra V and Rajavashisth TB (2014). Nuclear localization of catalytically active MMP-2 in endothelial cells and neurons. *Am J Transl Res* 6, 155-162.

38. Nagase H, Enghild JJ, Suzuki K and Salvesen G (1990). Stepwise activation mechanisms of the precursor of matrix metalloproteinase 3 (stromelysin) by proteinases and (4-aminophenyl)mercuric acetate. *Biochemistry* 29, 5783-5789.
39. Van Wart HE and Birkedal-Hansen H (1990). The cysteine switch: a principle of regulation of metalloproteinase activity with potential applicability to the entire matrix metalloproteinase gene family. *Proc Natl Acad Sci U S A* 87, 5578-5582.
40. Ip YC, Cheung ST and Fan ST (2007). Atypical localization of membrane type 1-matrix metalloproteinase in the nucleus is associated with aggressive features of hepatocellular carcinoma. *Mol Carcinog* 46, 225-230.
41. Okamoto T, Akaike T, Sawa T, Miyamoto Y, van der Vliet A and Maeda H (2001). Activation of matrix metalloproteinases by peroxynitrite-induced protein S-glutathiolation via disulfide S-oxide formation. *J Biol Chem* 276, 29596-29602.
42. Castro MM, Cena J, Cho WJ, Walsh MP and Schulz R (2012). Matrix metalloproteinase-2 proteolysis of calponin-1 contributes to vascular hypocontractility in endotoxemic rats. *Arterioscler Thromb Vasc Biol* 32, 662-668.
43. Viappiani S, Nicolescu AC, Holt A, Sawicki G, Crawford BD, León H, van Mulligen T and Schulz R (2009). Activation and modulation of 72kDa matrix metalloproteinase-2 by peroxynitrite and glutathione. *Biochem Pharmacol* 77, 826-834.
44. Wang W, Sawicki G and Schulz R (2002). Peroxynitrite-induced myocardial injury is mediated through matrix metalloproteinase-2. *Cardiovasc Res* 53, 165-174.
45. Yasmin W, Strynadka KD and Schulz R (1997). Generation of peroxynitrite contributes to ischemia-reperfusion injury in isolated rat hearts. *Cardiovasc Res* 33, 422-432.
46. Gao CQ, Sawicki G, Suarez-Pinzon WL, Csont T, Wozniak M, Ferdinandy P and Schulz R (2003). Matrix metalloproteinase-2 mediates cytokine-induced myocardial contractile dysfunction. *Cardiovasc Res* 57, 426-433.
47. Ferdinandy P, Danial H, Ambrus I, Rothery RA and Schulz R (2000). Peroxynitrite is a major contributor to cytokine-induced myocardial contractile failure. *Circ Res* 87, 241-247.
48. Ali MA, Fan X and Schulz R (2011). Cardiac sarcomeric proteins: novel intracellular targets of matrix metalloproteinase-2 in heart disease. *Trends Cardiovasc Med* 21, 112-118.
49. Sariahmetoglu M, Crawford BD, Leon H, Sawicka J, Li L, Ballermann BJ, Holmes C, Berthiaume LG, Holt A, Sawicki G and Schulz R (2007). Regulation of matrix metalloproteinase-2 (MMP-2) activity by phosphorylation. *Faseb J* 21, 2486-2495.

50. Sung MM, Schulz CG, Wang W, Sawicki G, Bautista-López NL and Schulz R (2007). Matrix metalloproteinase-2 degrades the cytoskeletal protein alpha-actinin in peroxynitrite mediated myocardial injury. *J Mol Cell Cardiol* 43, 429-436.
51. Schulze CJ, Wang W, Suarez-Pinzon WL, Sawicka J, Sawicki G and Schulz R (2003). Imbalance between tissue inhibitor of metalloproteinase-4 and matrix metalloproteinases during acute myocardial [correction of myoctardial] ischemia-reperfusion injury. *Circulation* 107, 2487-2492.
52. Kandasamy AD and Schulz R (2009). Glycogen synthase kinase-3beta is activated by matrix metalloproteinase-2 mediated proteolysis in cardiomyoblasts. *Cardiovasc Res* 83, 698-706.
53. Jurasz P, Chung AW, Radomski A and Radomski MW (2002). Nonremodeling properties of matrix metalloproteinases: the platelet connection. *Circ Res* 90, 1041-1043.
54. Galt SW, Lindemann S, Allen L, Medd DJ, Falk JM, McIntyre TM, Prescott SM, Kraiss LW, Zimmerman GA and Weyrich AS (2002). Outside-in signals delivered by matrix metalloproteinase-1 regulate platelet function. *Circ Res* 90, 1093-1099.
55. Sheu JR, Fong TH, Liu CM, Shen MY, Chen TL, Chang Y, Lu MS and Hsiao G (2004). Expression of matrix metalloproteinase-9 in human platelets: regulation of platelet activation in in vitro and in vivo studies. *Br J Pharmacol* 143, 193-201.
56. Sawicki G, Salas E, Murat J, Miszta-Lane H and Radomski MW (1997). Release of gelatinase A during platelet activation mediates aggregation. *Nature* 386, 616-619.
57. Soslau G, Mason C, Lynch S, Benjamin J, Ashak D, Prakash JM, Moore A, Bagsiyao P, Albert T, Mathew LM and Jost M (2014). Intracellular matrix metalloproteinase-2 (MMP-2) regulates human platelet activation via hydrolysis of talin. *Thromb Haemost* 111, 140-153.
58. Hughes BG and Schulz R (2014). Targeting MMP-2 to treat ischemic heart injury. *Basic Res Cardiol* 109, 424.
59. Ali MA, Cho WJ, Hudson B, Kassiri Z, Granzier H and Schulz R (2010). Titin is a target of matrix metalloproteinase-2: implications in myocardial ischemia/reperfusion injury. *Circulation* 122, 2039-2047.
60. Chan BYH, Roczkowsky A, Cho WJ, Poirier M, Sergi C, Keschrums V, Churko JM, Granzier H and Schulz R (2021). MMP inhibitors attenuate doxorubicin cardiotoxicity by preventing intracellular and extracellular matrix remodelling. *Cardiovasc Res* 117, 188-200.
61. Sawicki G, Leon H, Sawicka J, Sariahmetoglu M, Schulze CJ, Scott PG, Szczesna-Cordary D and Schulz R (2005). Degradation of myosin light chain in isolated rat hearts subjected to ischemia-reperfusion injury: a new intracellular target for matrix metalloproteinase-2. *Circulation* 112, 544-552.

62. Brown DA (2013). Lipid rafts. Encyclopedia of biological chemistry (second edition). Lennarz WJ and Lane MD. Waltham, *Academic Press*, 741-744.
63. Zhou HZ, Ma X, Gray MO, Zhu BQ, Nguyen AP, Baker AJ, Simonis U, Cecchini G, Lovett DH and Karliner JS (2007). Transgenic MMP-2 expression induces latent cardiac mitochondrial dysfunction. *Biochem Biophys Res Commun* 358, 189-195.
64. Lovett DH, Chu C, Wang G, Ratcliffe MB and Baker AJ (2014). A N-terminal truncated intracellular isoform of matrix metalloproteinase-2 impairs contractility of mouse myocardium. *Front Physiol* 5, 363.
65. Hughes BG, Fan X, Cho WJ and Schulz R (2014). MMP-2 is localized to the mitochondria-associated membrane of the heart. *Am J Physiol Heart Circ Physiol* 306, H764-770.
66. Lovett DH, Mahimkar R, Raffai RL, Cape L, Maklashina E, Cecchini G and Karliner JS (2012). A novel intracellular isoform of matrix metalloproteinase-2 induced by oxidative stress activates innate immunity. *PLoS One* 7, e34177.
67. Lin HB, Sharma K, Bialy D, Wawrzynska M, Purves R, Cayabyab FS, Wozniak M and Sawicki G (2014). Inhibition of MMP-2 expression affects metabolic enzyme expression levels: proteomic analysis of rat cardiomyocytes. *J Proteomics* 106, 74-85.
68. Mohammad G and Kowluru RA (2011). Novel role of mitochondrial matrix metalloproteinase-2 in the development of diabetic retinopathy. *Invest Ophthalmol Vis Sci* 52, 3832-3841.
69. Roczkowsky A, Chan BYH, Lee TYT, Mahmud Z, Hartley B, Julien O, Armanious G, Young HS and Schulz R (2020). Myocardial MMP-2 contributes to SERCA2a proteolysis during cardiac ischaemia-reperfusion injury. *Cardiovasc Res* 116, 1021-1031.
70. Chan BYH, Roczkowsky A, Cho WJ, Poirier M, Lee TYT, Mahmud Z and Schulz R (2019). Junctophilin-2 is a target of matrix metalloproteinase-2 in myocardial ischemia-reperfusion injury. *Basic Res Cardiol* 114, 42.
71. Aldonyte R, Brantly M, Block E, Patel J and Zhang J (2009). Nuclear localization of active matrix metalloproteinase-2 in cigarette smoke-exposed apoptotic endothelial cells. *Exp Lung Res* 35, 59-75.
72. Hill JW, Poddar R, Thompson JF, Rosenberg GA and Yang Y (2012). Intranuclear matrix metalloproteinases promote DNA damage and apoptosis induced by oxygen-glucose deprivation in neurons. *Neuroscience* 220, 277-290.
73. Ali MAM, Garcia-Vilas JA, Cromwell CR, Hubbard BP, Hendzel MJ and Schulz R (2021). Matrix metalloproteinase-2 mediates ribosomal RNA transcription by cleaving nucleolar histones. *Febs J* 288, 6736-6751.

74. Sawicki G, Sanders EJ, Salas E, Wozniak M, Rodrigo J and Radomski MW (1998). Localization and translocation of MMP-2 during aggregation of human platelets. *Thromb Haemost* 80, 836-839.
75. Malara A, Ligi D, Di Buduo CA, Mannello F and Balduini A (2018). Sub-cellular localization of metalloproteinases in megakaryocytes. *Cells* 7, 80.
76. Lee AY, Akers KT, Collier M, Li L, Eisen AZ and Seltzer JL (1997). Intracellular activation of gelatinase A (72-kDa type IV collagenase) by normal fibroblasts. *Proc Natl Acad Sci U S A* 94, 4424-4429.
77. Murphy G (2011). Tissue inhibitors of metalloproteinases. *Genome Biol* 12, 233.
78. Shiomi T, Lemaître V, D'Armiento J and Okada Y (2010). Matrix metalloproteinases, a disintegrin and metalloproteinases, and a disintegrin and metalloproteinases with thrombospondin motifs in non-neoplastic diseases. *Pathol Int* 60, 477-496.
79. Brew K and Nagase H (2010). The tissue inhibitors of metalloproteinases (TIMPs): an ancient family with structural and functional diversity. *Biochim Biophys Acta* 1803, 55-71.
80. Baker AH, Edwards DR and Murphy G (2002). Metalloproteinase inhibitors: biological actions and therapeutic opportunities. *J Cell Sci* 115, 3719-3727.
81. Mocchegiani E, Costarelli L, Giacconi R, Cipriano C, Muti E and Malavolta M (2006). Zinc-binding proteins (metallothionein and alpha-2 macroglobulin) and immunosenescence. *Exp Gerontol* 41, 1094-1107.
82. Starkey PM and Barrett AJ (1982). Evolution of alpha 2-macroglobulin. The demonstration in a variety of vertebrate species of a protein resembling human alpha 2-macroglobulin. *Biochem J* 205, 91-95.
83. Chu CT, Howard GC, Misra UK and Pizzo SV (1994). Alpha 2-macroglobulin: a sensor for proteolysis. *Ann N Y Acad Sci* 737, 291-307.
84. Strickland DK, Ashcom JD, Williams S, Burgess WH, Migliorini M and Argraves WS (1990). Sequence identity between the alpha 2-macroglobulin receptor and low density lipoprotein receptor-related protein suggests that this molecule is a multifunctional receptor. *J Biol Chem* 265, 17401-17404.
85. Kang J, Lemaire HG, Unterbeck A, Salbaum JM, Masters CL, Grzeschik KH, Multhaup G, Beyreuther K and Müller-Hill B (1987). The precursor of Alzheimer's disease amyloid A4 protein resembles a cell-surface receptor. *Nature* 325, 733-736.
86. Hashimoto H, Takeuchi T, Komatsu K, Miyazaki K, Sato M and Higashi S (2011). Structural basis for matrix metalloproteinase-2 (MMP-2)-selective inhibitory action of β -amyloid precursor protein-derived inhibitor. *J Biol Chem* 286, 33236-33243.

87. Higashi S and Miyazaki K (2008). Identification of amino acid residues of the matrix metalloproteinase-2 essential for its selective inhibition by beta-amyloid precursor protein-derived inhibitor. *J Biol Chem* 283, 10068-10078.
88. Sparano JA, Bernardo P, Stephenson P, Gradishar WJ, Ingle JN, Zucker S and Davidson NE (2004). Randomized phase III trial of marimastat versus placebo in patients with metastatic breast cancer who have responding or stable disease after first-line chemotherapy: Eastern Cooperative Oncology Group trial E2196. *J Clin Oncol* 22, 4683-4690.
89. Peterson JT (2004). Matrix metalloproteinase inhibitor development and the remodeling of drug discovery. *Heart Fail Rev* 9, 63-79.
90. Golub LM, Lee HM, Lehrer G, Nemiroff A, McNamara TF, Kaplan R and Ramamurthy NS (1983). Minocycline reduces gingival collagenolytic activity during diabetes. Preliminary observations and a proposed new mechanism of action. *J Periodontal Res* 18, 516-526.
91. Golub LM, Goodson JM, Lee HM, Vidal AM, McNamara TF and Ramamurthy NS (1985). Tetracyclines inhibit tissue collagenases: effects of ingested low-dose and local delivery systems. *J Periodontol* 56 Suppl 11S, 93-97.
92. Cerisano G, Buonamici P, Valenti R, Sciagrà R, Raspanti S, Santini A, Carrabba N, Dovellini EV, Romito R, Pupi A, Colonna P and Antoniucci D (2014). Early short-term doxycycline therapy in patients with acute myocardial infarction and left ventricular dysfunction to prevent the ominous progression to adverse remodelling: the TIPTOP trial. *Eur Heart J* 35, 184-191.
93. Golub LM, McNamara TF, D'Angelo G, Greenwald RA and Ramamurthy NS (1987). A non-antibacterial chemically-modified tetracycline inhibits mammalian collagenase activity. *J Dent Res* 66, 1310-1314.
94. Yamada A, Uegaki A, Nakamura T and Ogawa K (2000). ONO-4817, an orally active matrix metalloproteinase inhibitor, prevents lipopolysaccharide-induced proteoglycan release from the joint cartilage in guinea pigs. *Inflamm Res* 49, 144-146.
95. Rossello A, Nuti E, Orlandini E, Carelli P, Rapposelli S, Macchia M, Minutolo F, Carbonaro L, Albini A, Benelli R, Cercignani G, Murphy G and Balsamo A (2004). New N-arylsulfonyl-N-alkoxyaminoacetohydroxamic acids as selective inhibitors of gelatinase A (MMP-2). *Bioorg Med Chem* 12, 2441-2450.
96. Novak MJ, Johns LP, Miller RC and Bradshaw MH (2002). Adjunctive benefits of subantimicrobial dose doxycycline in the management of severe, generalized, chronic periodontitis. *J Periodontol* 73, 762-769.
97. Valentín S, Morales A, Sánchez JL and Rivera A (2009). Safety and efficacy of doxycycline in the treatment of rosacea. *Clin Cosmet Investig Dermatol* 2, 129-140.

98. Ceron CS, Baligand C, Joshi S, Wanga S, Cowley PM, Walker JP, Song SH, Mahimkar R, Baker AJ, Raffai RL, Wang ZJ and Lovett DH (2017). An intracellular matrix metalloproteinase-2 isoform induces tubular regulated necrosis: implications for acute kidney injury. *Am J Physiol Renal Physiol* 312, F1166-f1183.
99. Fernandez-Patron C, Kassiri Z and Leung D (2016). Modulation of systemic metabolism by MMP-2: from MMP-2 deficiency in mice to MMP-2 deficiency in patients. *Compr Physiol* 6, 1935-1949.
100. Berry E, Hernandez-Anzaldo S, Ghomashchi F, Lehner R, Murakami M, Gelb MH, Kassiri Z, Wang X and Fernandez-Patron C (2015). Matrix metalloproteinase-2 negatively regulates cardiac secreted phospholipase A2 to modulate inflammation and fever. *J Am Heart Assoc* 4, e001868.
101. Hernandez-Anzaldo S, Berry E, Brglez V, Leung D, Yun TJ, Lee JS, Filep JG, Kassiri Z, Cheong C, Lambeau G, Lehner R and Fernandez-Patron C (2015). Identification of a novel heart-liver axis: matrix metalloproteinase-2 negatively regulates cardiac secreted phospholipase A2 to modulate lipid metabolism and inflammation in the liver. *J Am Heart Assoc* 4, e002553.
102. Gonzalez-Villasana V, Fuentes-Mattei E, Ivan C, Dalton HJ, Rodriguez-Aguayo C, Fernandez-de Thomas RJ, Aslan B, Del CMP, Velazquez-Torres G, Previs RA, Pradeep S, Kahraman N, Wang H, Kanlikilicer P, Ozpolat B, Calin G, Sood AK and Lopez-Berestein G (2015). Rac1/Pak1/p38/MMP-2 axis regulates angiogenesis in ovarian cancer. *Clin Cancer Res* 21, 2127-2137.
103. Zhang Y and Chen Q (2017). Relationship between matrix metalloproteinases and the occurrence and development of ovarian cancer. *Braz J Med Biol Res* 50, e6104.
104. Mann DL and Spinale FG (1998). Activation of matrix metalloproteinases in the failing human heart: breaking the tie that binds. *Circulation* 98, 1699-1702.
105. Bergman MR, Teerlink JR, Mahimkar R, Li L, Zhu BQ, Nguyen A, Dahi S, Karlner JS and Lovett DH (2007). Cardiac matrix metalloproteinase-2 expression independently induces marked ventricular remodeling and systolic dysfunction. *Am J Physiol Heart Circ Physiol* 292, H1847-1860.
106. Wang GY, Bergman MR, Nguyen AP, Turcato S, Swigart PM, Rodrigo MC, Simpson PC, Karlner JS, Lovett DH and Baker AJ (2006). Cardiac transgenic matrix metalloproteinase-2 expression directly induces impaired contractility. *Cardiovasc Res* 69, 688-696.
107. Barhoumi T, Fraulob-Aquino JC, Mian MOR, Ouerd S, Idris-Khodja N, Huo KG, Rehman A, Caillon A, Dancose-Giambattisto B, Ebrahimian T, Lehoux S, Paradis P and Schiffrin EL (2017). Matrix metalloproteinase-2 knockout prevents angiotensin II-induced vascular injury. *Cardiovasc Res* 113, 1753-1762.

108. Lalu MM, Cena J, Chowdhury R, Lam A and Schulz R (2006). Matrix metalloproteinases contribute to endotoxin and interleukin-1beta induced vascular dysfunction. *Br J Pharmacol* 149, 31-42.
109. Lee HW, Lee SJ, Lee MY, Park MW, Kim SS and Shin N (2019). Enhanced cardiac expression of two isoforms of matrix metalloproteinase-2 in experimental diabetes mellitus. *PLoS One* 14, e0221798.
110. Yaras N, Sariahmetoglu M, Bilginoglu A, Aydemir-Koksoy A, Onay-Besikci A, Turan B and Schulz R (2008). Protective action of doxycycline against diabetic cardiomyopathy in rats. *Br J Pharmacol* 155, 1174-1184.
111. Heusch G (2019). Myocardial ischemia: lack of coronary blood flow, myocardial oxygen supply-demand imbalance, or what? *Am J Physiol Heart Circ Physiol* 316, H1439-h1446.
112. Ibanez B, James S, Agewall S, Antunes MJ, Bucciarelli-Ducci C, Bueno H, Caforio ALP, Crea F, Goudevenos JA, Halvorsen S, Hindricks G, Kastrati A, Lenzen MJ, Prescott E, Roffi M, Valgimigli M, Varenhorst C, Vranckx P and Widimský P (2018). 2017 ESC guidelines for the management of acute myocardial infarction in patients presenting with ST-segment elevation: the task force for the management of acute myocardial infarction in patients presenting with ST-segment elevation of the European Society of Cardiology (ESC). *Eur Heart J* 39, 119-177.
113. Heidenreich PA, Bozkurt B, Aguilar D, Allen LA, Byun JJ, Colvin MM, Deswal A, Drazner MH, Dunlay SM, Evers LR, Fang JC, Fedson SE, Fonarow GC, Hayek SS, Hernandez AF, Khazanie P, Kittleson MM, Lee CS, Link MS, Milano CA, Nwacheta LC, Sandhu AT, Stevenson LW, Vardeny O, Vest AR and Yancy CW (2022). 2022 AHA/ACC/HFSA guideline for the management of heart failure: executive summary: a report of the American College of Cardiology/American Heart Association Joint Committee on clinical practice guidelines. *J Am Coll Cardiol* 79, 1757-1780.
114. Foundation HaS (2022). Report on the health of Canadians. Heart and Stroke Foundation Ottawa, Canada, *Heart and Stroke Foundation*
115. Tsao CW, Aday AW, Almarzooq ZI, Alonso A, Beaton AZ, Bittencourt MS, Boehme AK, Buxton AE, Carson AP, Commodore-Mensah Y, Elkind MSV, Evenson KR, Eze-Nliam C, Ferguson JF, Generoso G, Ho JE, Kalani R, Khan SS, Kissela BM, Knutson KL, Levine DA, Lewis TT, Liu J, Loop MS, Ma J, Mussolino ME, Navaneethan SD, Perak AM, Poudel R, Rezk-Hanna M, Roth GA, Schroeder EB, Shah SH, Thacker EL, VanWagner LB, Virani SS, Voecks JH, Wang NY, Yaffe K and Martin SS (2022). Heart disease and stroke statistics-2022 update: a report from the American Heart Association. *Circulation* 145, e153-639.
116. Topol EJ (1998). Toward a new frontier in myocardial reperfusion therapy: emerging platelet preeminence. *Circulation* 97, 211-218.

117. Verma S, Fedak PW, Weisel RD, Butany J, Rao V, Maitland A, Li RK, Dhillon B and Yau TM (2002). Fundamentals of reperfusion injury for the clinical cardiologist. *Circulation* 105, 2332-2336.
118. Ibáñez B, Heusch G, Ovize M and Van de Werf F (2015). Evolving therapies for myocardial ischemia/reperfusion injury. *J Am Coll Cardiol* 65, 1454-1471.
119. Braunwald E and Kloner RA (1985). Myocardial reperfusion: a double-edged sword? *J Clin Invest* 76, 1713-1719.
120. Kalogeris T, Baines CP, Krenz M and Korthuis RJ (2016). Ischemia/reperfusion. *Compr Physiol* 7, 113-170.
121. Hausenloy DJ, Botker HE, Engstrom T, Erlinge D, Heusch G, Ibanez B, Kloner RA, Ovize M, Yellon DM and Garcia-Dorado D (2017). Targeting reperfusion injury in patients with ST-segment elevation myocardial infarction: trials and tribulations. *Eur Heart J* 38, 935-941.
122. Krijnen PA, Nijmeijer R, Meijer CJ, Visser CA, Hack CE and Niessen HW (2002). Apoptosis in myocardial ischaemia and infarction. *J Clin Pathol* 55, 801-811.
123. Kubasiak LA, Hernandez OM, Bishopric NH and Webster KA (2002). Hypoxia and acidosis activate cardiac myocyte death through the Bcl-2 family protein BNIP3. *Proc Natl Acad Sci U S A* 99, 12825-12830.
124. Tani M and Neely JR (1989). Role of intracellular Na⁺ in Ca²⁺ overload and depressed recovery of ventricular function of reperfused ischemic rat hearts. Possible involvement of H⁺-Na⁺ and Na⁺-Ca²⁺ exchange. *Circ Res* 65, 1045-1056.
125. Zorov DB, Juhaszova M and Sollott SJ (2014). Mitochondrial reactive oxygen species (ROS) and ROS-induced ROS release. *Physiol Rev* 94, 909-950.
126. Piper HM, Meuter K and Schäfer C (2003). Cellular mechanisms of ischemia-reperfusion injury. *Ann Thorac Surg* 75, S644-648.
127. Tissier R, Ghaleh B, Cohen MV, Downey JM and Berdeaux A (2012). Myocardial protection with mild hypothermia. *Cardiovasc Res* 94, 217-225.
128. Heusch G (2017). Vagal cardioprotection in reperfused acute myocardial infarction. *JACC Cardiovasc Interv* 10, 1521-1522.
129. García-Ruiz JM, Fernández-Jiménez R, García-Alvarez A, Pizarro G, Galán-Arriola C, Fernández-Friera L, Mateos A, Nuno-Ayala M, Agüero J, Sánchez-González J, García-Prieto J, López-Melgar B, Martínez-Tenorio P, López-Martín GJ, Macías A, Pérez-Asenjo B, Cabrera JA, Fernández-Ortiz A, Fuster V and Ibáñez B (2016). Impact of the timing of metoprolol administration during STEMI on infarct size and ventricular function. *J Am Coll Cardiol* 67, 2093-2104.

130. Tomai F, Crea F, Chiariello L and Giofrè PA (1999). Ischemic preconditioning in humans: models, mediators, and clinical relevance. *Circulation* 100, 559-563.
131. Xi L, Hess ML and Kukreja RC (1998). Ischemic preconditioning in isolated perfused mouse heart: reduction in infarct size without improvement of post-ischemic ventricular function. *Mol Cell Biochem* 186, 69-77.
132. Gross GJ and Peart JN (2003). KATP channels and myocardial preconditioning: an update. *Am J Physiol Heart Circ Physiol* 285, H921-930.
133. Anselmi A, Abbate A, Girola F, Nasso G, Biondi-Zoccai GG, Possati G and Gaudino M (2004). Myocardial ischemia, stunning, inflammation, and apoptosis during cardiac surgery: a review of evidence. *Eur J Cardiothorac Surg* 25, 304-311.
134. Braunwald E and Kloner RA (1982). The stunned myocardium: prolonged, postischemic ventricular dysfunction. *Circulation* 66, 1146-1149.
135. Bolli R (1990). Mechanism of myocardial "stunning". *Circulation* 82, 723-738.
136. Kloner RA (2020). Stunned and hibernating myocardium: where are we nearly 4 decades later? *J Am Heart Assoc* 9, e015502.
137. Frangogiannis NG (2012). Regulation of the inflammatory response in cardiac repair. *Circ Res* 110, 159-173.
138. He J, Liu D, Zhao L, Zhou D, Rong J, Zhang L and Xia Z (2022). Myocardial ischemia/reperfusion injury: mechanisms of injury and implications for management (Review). *Exp Ther Med* 23, 430.
139. Bell RM, Mocanu MM and Yellon DM (2011). Retrograde heart perfusion: the Langendorff technique of isolated heart perfusion. *J Mol Cell Cardiol* 50, 940-950.
140. Cadete VJ, Arcand SA, Chaharyn BM, Doroszko A, Sawicka J, Mousseau DD and Sawicki G (2013). Matrix metalloproteinase-2 is activated during ischemia/reperfusion in a model of myocardial infarction. *Can J Cardiol* 29, 1495-1503.
141. Lalu MM, Pasini E, Schulze CJ, Ferrari-Vivaldi M, Ferrari-Vivaldi G, Bachetti T and Schulz R (2005). Ischaemia-reperfusion injury activates matrix metalloproteinases in the human heart. *Eur Heart J* 26, 27-35.
142. Skrzypiec-Spring M, Urbaniak J, Sapa-Wojciechowska A, Pietkiewicz J, Orda A, Karolko B, Danielewicz R, Bil-Lula I, Woźniak M, Schulz R and Szeląg A (2021). Matrix metalloproteinase-2 inhibition in acute ischemia-reperfusion heart injury-cardioprotective properties of carvedilol. *Pharmaceuticals (Basel)* 14, 1276.
143. Bishopric NH, Andreka P, Slepak T and Webster KA (2001). Molecular mechanisms of apoptosis in the cardiac myocyte. *Curr Opin Pharmacol* 1, 141-150.

144. Chakrabarti S, Hoque AN and Karmazyn M (1997). A rapid ischemia-induced apoptosis in isolated rat hearts and its attenuation by the sodium-hydrogen exchange inhibitor HOE 642 (cariporide). *J Mol Cell Cardiol* 29, 3169-3174.
145. Bialik S, Geenen DL, Sasson IE, Cheng R, Horner JW, Evans SM, Lord EM, Koch CJ and Kitsis RN (1997). Myocyte apoptosis during acute myocardial infarction in the mouse localizes to hypoxic regions but occurs independently of p53. *J Clin Invest* 100, 1363-1372.
146. Menon B, Singh M, Ross RS, Johnson JN and Singh K (2006). beta-Adrenergic receptor-stimulated apoptosis in adult cardiac myocytes involves MMP-2-mediated disruption of beta1 integrin signaling and mitochondrial pathway. *Am J Physiol Cell Physiol* 290, C254-261.
147. Grimes CA and Jope RS (2001). The multifaceted roles of glycogen synthase kinase 3beta in cellular signaling. *Prog Neurobiol* 65, 391-426.
148. Shen J, O'Brien D and Xu Y (2006). Matrix metalloproteinase-2 contributes to tumor necrosis factor alpha induced apoptosis in cultured rat cardiac myocytes. *Biochem Biophys Res Commun* 347, 1011-1020.
149. Bencsik P, Pálóczi J, Kocsis GF, Pipis J, Beleczi I, Varga ZV, Csonka C, Görbe A, Csont T and Ferdinandy P (2014). Moderate inhibition of myocardial matrix metalloproteinase-2 by ilomastat is cardioprotective. *Pharmacol Res* 80, 36-42.
150. Arcamone F, Cassinelli G, Fantini G, Grein A, Orezzi P, Pol C and Spalla C (1969). Adriamycin, 14-hydroxydaunomycin, a new antitumor antibiotic from *S. peucetius* var. *caesius*. *Biotechnol Bioeng* 11, 1101-1110.
151. Di Marco A, Gaetani M and Scarpinato B (1969). Adriamycin (NSC-123,127): a new antibiotic with antitumor activity. *Cancer Chemother Rep* 53, 33-37.
152. Bloom MW, Hamo CE, Cardinale D, Ky B, Nohria A, Baer L, Skopicki H, Lenihan DJ, Gheorghide M, Lyon AR and Butler J (2016). Cancer therapy-related cardiac dysfunction and heart failure: part 1: definitions, pathophysiology, risk factors, and imaging. *Circ Heart Fail* 9, e002661.
153. Von Hoff DD, Layard MW, Basa P, Davis HL, Jr., Von Hoff AL, Rozenzweig M and Muggia FM (1979). Risk factors for doxorubicin-induced congestive heart failure. *Ann Intern Med* 91, 710-717.
154. Alexander J, Dainiak N, Berger HJ, Goldman L, Johnstone D, Reduto L, Duffy T, Schwartz P, Gottschalk A and Zaret BL (1979). Serial assessment of doxorubicin cardiotoxicity with quantitative radionuclide angiocardiology. *N Engl J Med* 300, 278-283.
155. Buzdar AU, Marcus C, Smith TL and Blumenschein GR (1985). Early and delayed clinical cardiotoxicity of doxorubicin. *Cancer* 55, 2761-2765.

156. Volkova M and Russell R, 3rd (2011). Anthracycline cardiotoxicity: prevalence, pathogenesis and treatment. *Curr Cardiol Rev* 7, 214-220.
157. Swain SM, Whaley FS and Ewer MS (2003). Congestive heart failure in patients treated with doxorubicin: a retrospective analysis of three trials. *Cancer* 97, 2869-2879.
158. Bristow MR, Thompson PD, Martin RP, Mason JW, Billingham ME and Harrison DC (1978). Early anthracycline cardiotoxicity. *Am J Med* 65, 823-832.
159. Hayek ER, Speakman E and Rehmus E (2005). Acute doxorubicin cardiotoxicity. *N Engl J Med* 352, 2456-2457.
160. Chen Y, Huang T, Shi W, Fang J, Deng H and Cui G (2020). Potential targets for intervention against doxorubicin-induced cardiotoxicity based on genetic studies: a systematic review of the literature. *J Mol Cell Cardiol* 138, 88-98.
161. Davies KJ and Doroshov JH (1986). Redox cycling of anthracyclines by cardiac mitochondria. I. Anthracycline radical formation by NADH dehydrogenase. *J Biol Chem* 261, 3060-3067.
162. Doroshov JH and Davies KJ (1986). Redox cycling of anthracyclines by cardiac mitochondria. II. Formation of superoxide anion, hydrogen peroxide, and hydroxyl radical. *J Biol Chem* 261, 3068-3074.
163. Kotamraju S, Chitambar CR, Kalivendi SV, Joseph J and Kalyanaraman B (2002). Transferrin receptor-dependent iron uptake is responsible for doxorubicin-mediated apoptosis in endothelial cells: role of oxidant-induced iron signaling in apoptosis. *J Biol Chem* 277, 17179-17187.
164. Wang L, Ma W, Markovich R, Chen JW and Wang PH (1998). Regulation of cardiomyocyte apoptotic signaling by insulin-like growth factor I. *Circ Res* 83, 516-522.
165. Childs AC, Phaneuf SL, Dirks AJ, Phillips T and Leeuwenburgh C (2002). Doxorubicin treatment in vivo causes cytochrome C release and cardiomyocyte apoptosis, as well as increased mitochondrial efficiency, superoxide dismutase activity, and Bcl-2:Bax ratio. *Cancer Res* 62, 4592-4598.
166. Tokarska-Schlattner M, Dolder M, Gerber I, Speer O, Wallimann T and Schlattner U (2007). Reduced creatine-stimulated respiration in doxorubicin challenged mitochondria: particular sensitivity of the heart. *Biochim Biophys Acta* 1767, 1276-1284.
167. Kim SY, Kim SJ, Kim BJ, Rah SY, Chung SM, Im MJ and Kim UH (2006). Doxorubicin-induced reactive oxygen species generation and intracellular Ca²⁺ increase are reciprocally modulated in rat cardiomyocytes. *Exp Mol Med* 38, 535-545.
168. Pessah IN (1992). Calcium release channel of sarcoplasmic reticulum: an important target for doxorubicin-mediated cardiotoxicity. *Adv Exp Med Biol* 311, 409-410.

169. Shinlapawittayatorn K, Chattipakorn SC and Chattipakorn N (2022). The effects of doxorubicin on cardiac calcium homeostasis and contractile function. *J Cardiol* 80, 125-132.
170. Takemura G and Fujiwara H (2007). Doxorubicin-induced cardiomyopathy from the cardiotoxic mechanisms to management. *Prog Cardiovasc Dis* 49, 330-352.
171. Spallarossa P, Garibaldi S, Altieri P, Fabbi P, Manca V, Nasti S, Rossettin P, Ghigliotti G, Ballestrero A, Patrone F, Barsotti A and Brunelli C (2004). Carvedilol prevents doxorubicin-induced free radical release and apoptosis in cardiomyocytes in vitro. *J Mol Cell Cardiol* 37, 837-846.
172. Beak J, Huang W, Parker JS, Hicks ST, Patterson C, Simpson PC, Ma A, Jin J and Jensen BC (2017). An oral selective alpha-1A adrenergic receptor agonist prevents doxorubicin cardiotoxicity. *JACC Basic Transl Sci* 2, 39-53.
173. O'Brien ME, Wigler N, Inbar M, Rosso R, Grischke E, Santoro A, Catane R, Kieback DG, Tomeczak P, Ackland SP, Orlandi F, Mellars L, Alland L and Tendler C (2004). Reduced cardiotoxicity and comparable efficacy in a phase III trial of pegylated liposomal doxorubicin HCl (CAELYX/Doxil) versus conventional doxorubicin for first-line treatment of metastatic breast cancer. *Ann Oncol* 15, 440-449.
174. Chan BYH, Roczkowsky A, Moser N, Poirier M, Hughes BG, Ilarraza R and Schulz R (2018). Doxorubicin induces de novo expression of N-terminal-truncated matrix metalloproteinase-2 in cardiac myocytes. *Can J Physiol Pharmacol* 96, 1238-1245.
175. Bai P, Mabley JG, Liaudet L, Virág L, Szabó C and Pacher P (2004). Matrix metalloproteinase activation is an early event in doxorubicin-induced cardiotoxicity. *Oncol Rep* 11, 505-508.
176. Polegato BF, Minicucci MF, Azevedo PS, Carvalho RF, Chiuso-Minicucci F, Pereira EJ, Paiva SA, Zornoff LA, Okoshi MP, Matsubara BB and Matsubara LS (2015). Acute doxorubicin-induced cardiotoxicity is associated with matrix metalloproteinase-2 alterations in rats. *Cell Physiol Biochem* 35, 1924-1933.
177. Spallarossa P, Altieri P, Garibaldi S, Ghigliotti G, Barisione C, Manca V, Fabbi P, Ballestrero A, Brunelli C and Barsotti A (2006). Matrix metalloproteinase-2 and -9 are induced differently by doxorubicin in H9c2 cells: the role of MAP kinases and NAD(P)H oxidase. *Cardiovasc Res* 69, 736-745.
178. Ivanová M, Dovinová I, Okruhlicová L, Tribulová N, Simončíková P, Barteková M, Vlkovičová J and Barančík M (2012). Chronic cardiotoxicity of doxorubicin involves activation of myocardial and circulating matrix metalloproteinases in rats. *Acta Pharmacol Sin* 33, 459-469.
179. Kizaki K, Ito R, Okada M, Yoshioka K, Uchide T, Temma K, Mutoh K, Uechi M and Hara Y (2006). Enhanced gene expression of myocardial matrix metalloproteinases 2 and 9 after acute treatment with doxorubicin in mice. *Pharmacol Res* 53, 341-346.

180. Chen X, Guo Z, Wang P and Xu M (2014). Erythropoietin modulates imbalance of matrix metalloproteinase-2 and tissue inhibitor of metalloproteinase-2 in doxorubicin-induced cardiotoxicity. *Heart Lung Circ* 23, 772-777.
181. Vance JE (1990). Phospholipid synthesis in a membrane fraction associated with mitochondria. *J Biol Chem* 265, 7248-7256.
182. Ruby JR, Dyer RF and Skalko RG (1969). Continuities between mitochondria and endoplasmic reticulum in the mammalian ovary. *Z Zellforsch Mikrosk Anat* 97, 30-37.
183. Missiroli S, Patergnani S, Caroccia N, Pedriali G, Perrone M, Previati M, Wieckowski MR and Giorgi C (2018). Mitochondria-associated membranes (MAMs) and inflammation. *Cell Death Dis* 9, 329.
184. Gao P, Yan Z and Zhu Z (2020). Mitochondria-associated endoplasmic reticulum membranes in cardiovascular diseases. *Front Cell Dev Biol* 8, 604240.
185. Basso V, Marchesan E and Ziviani E (2020). A trio has turned into a quartet: DJ-1 interacts with the IP3R-Grp75-VDAC complex to control ER-mitochondria interaction. *Cell Calcium* 87, 102186.
186. Wu S, Lu Q, Wang Q, Ding Y, Ma Z, Mao X, Huang K, Xie Z and Zou MH (2017). Binding of FUN14 domain containing 1 with Inositol 1,4,5-trisphosphate receptor in mitochondria-associated endoplasmic reticulum membranes maintains mitochondrial dynamics and function in hearts in vivo. *Circulation* 136, 2248-2266.
187. Boyman L, Karbowski M and Lederer WJ (2020). Regulation of mitochondrial ATP production: Ca²⁺ signaling and quality control. *Trends Mol Med* 26, 21-39.
188. Filadi R, Leal NS, Schreiner B, Rossi A, Dentoni G, Pinho CM, Wiehager B, Cieri D, Cali T, Pizzo P and Ankarcona M (2018). TOM70 sustains cell bioenergetics by promoting IP3R3-mediated ER to mitochondria Ca²⁺ transfer. *Curr Biol* 28, 369-382.e366.
189. Matuz-Mares D, González-Andrade M, Araiza-Villanueva MG, Vilchis-Landeros MM and Vázquez-Meza H (2022). Mitochondrial calcium: effects of its imbalance in disease. *Antioxidants (Basel)* 11, 801.
190. Petrungraro C and Kornmann B (2019). Lipid exchange at ER-mitochondria contact sites: a puzzle falling into place with quite a few pieces missing. *Curr Opin Cell Biol* 57, 71-76.
191. Murata M, Peränen J, Schreiner R, Wieland F, Kurzchalia TV and Simons K (1995). VIP21/caveolin is a cholesterol-binding protein. *Proc Natl Acad Sci U S A* 92, 10339-10343.
192. Ramírez CM, Zhang X, Bandyopadhyay C, Rotllan N, Sugiyama MG, Aryal B, Liu X, He S, Kraehling JR, Ulrich V, Lin CS, Velazquez H, Lasunción MA, Li G, Suárez Y, Tellides G, Swirski FK, Lee WL, Schwartz MA, Sessa WC and Fernández-Hernando C (2019). Caveolin-1 regulates atherogenesis by attenuating low-density lipoprotein transcytosis and

- vascular inflammation independently of endothelial nitric oxide synthase activation. *Circulation* 140, 225-239.
193. Luan Y, Luan Y, Yuan RX, Feng Q, Chen X and Yang Y (2021). Structure and function of mitochondria-associated endoplasmic reticulum membranes (MAMs) and their role in cardiovascular diseases. *Oxid Med Cell Longev* 2021, 4578809.
 194. Murphy E and Liu JC (2023). Mitochondrial calcium and reactive oxygen species in cardiovascular disease. *Cardiovasc Res* 119, 1105-1116.
 195. de Brito OM and Scorrano L (2008). Mitofusin 2 tethers endoplasmic reticulum to mitochondria. *Nature* 456, 605-610.
 196. Friedman JR, Lackner LL, West M, DiBenedetto JR, Nunnari J and Voeltz GK (2011). ER tubules mark sites of mitochondrial division. *Science* 334, 358-362.
 197. Shlevkov E, Kramer T, Schapansky J, LaVoie MJ and Schwarz TL (2016). Miro phosphorylation sites regulate Parkin recruitment and mitochondrial motility. *Proc Natl Acad Sci U S A* 113, E6097-e6106.
 198. Cao Y, Xu C, Ye J, He Q, Zhang X, Jia S, Qiao X, Zhang C, Liu R, Weng L, Liu Y, Liu L and Zheng M (2019). Miro2 regulates inter-mitochondrial communication in the heart and protects against TAC-induced cardiac dysfunction. *Circ Res* 125, 728-743.
 199. Gelmetti V, De Rosa P, Torosantucci L, Marini ES, Romagnoli A, Di Rienzo M, Arena G, Vignone D, Fimia GM and Valente EM (2017). PINK1 and BECN1 relocalize at mitochondria-associated membranes during mitophagy and promote ER-mitochondria tethering and autophagosome formation. *Autophagy* 13, 654-669.
 200. McLelland GL, Goiran T, Yi W, Dorval G, Chen CX, Lauinger ND, Krahn AI, Valimehr S, Rakovic A, Rouiller I, Durcan TM, Trempe JF and Fon EA (2018). Mfn2 ubiquitination by PINK1/parkin gates the p97-dependent release of ER from mitochondria to drive mitophagy. *Elife* 7, e32866.
 201. Schroder K and Tschopp J (2010). The inflammasomes. *Cell* 140, 821-832.
 202. Gurung P, Lukens JR and Kanneganti TD (2015). Mitochondria: diversity in the regulation of the NLRP3 inflammasome. *Trends Mol Med* 21, 193-201.
 203. Hamilton C and Anand PK (2019). Right place, right time: localisation and assembly of the NLRP3 inflammasome. *F1000Res* 8, F1000.
 204. Anastacio MM, Kanter EM, Makepeace CM, Keith AD, Zhang H, Schuessler RB, Nichols CG and Lawton JS (2013). Relationship between mitochondrial matrix volume and cellular volume in response to stress and the role of ATP-sensitive potassium channel. *Circulation* 128, S130-135.

205. Nguyen BY, Ruiz-Velasco A, Bui T, Collins L, Wang X and Liu W (2019). Mitochondrial function in the heart: the insight into mechanisms and therapeutic potentials. *Br J Pharmacol* 176, 4302-4318.
206. Brown DA, Perry JB, Allen ME, Sabbah HN, Stauffer BL, Shaikh SR, Cleland JG, Colucci WS, Butler J, Voors AA, Anker SD, Pitt B, Pieske B, Filippatos G, Greene SJ and Gheorghiade M (2017). Expert consensus document: mitochondrial function as a therapeutic target in heart failure. *Nat Rev Cardiol* 14, 238-250.
207. Kühlbrandt W (2015). Structure and function of mitochondrial membrane protein complexes. *BMC Biol* 13, 89.
208. Ernster L and Schatz G (1981). Mitochondria: a historical review. *J Cell Biol* 91, 227s-255s.
209. Protasoni M and Zeviani M (2021). Mitochondrial structure and bioenergetics in normal and disease conditions. *Int J Mol Sci* 22, 586.
210. Colombini M (1989). Voltage gating in the mitochondrial channel, VDAC. *J Membr Biol* 111, 103-111.
211. Galluzzi L, Kepp O, Trojel-Hansen C and Kroemer G (2012). Mitochondrial control of cellular life, stress, and death. *Circ Res* 111, 1198-1207.
212. Stock D, Leslie AG and Walker JE (1999). Molecular architecture of the rotary motor in ATP synthase. *Science* 286, 1700-1705.
213. Bartlett K and Eaton S (2004). Mitochondrial beta-oxidation. *Eur J Biochem* 271, 462-469.
214. Rouault TA and Tong WH (2005). Iron-sulphur cluster biogenesis and mitochondrial iron homeostasis. *Nat Rev Mol Cell Biol* 6, 345-351.
215. Wang C and Youle RJ (2009). The role of mitochondria in apoptosis. *Annu Rev Genet* 43, 95-118.
216. Williams GS, Boyman L and Lederer WJ (2015). Mitochondrial calcium and the regulation of metabolism in the heart. *J Mol Cell Cardiol* 78, 35-45.
217. Grover GJ, Atwal KS, Sleph PG, Wang FL, Monshizadegan H, Monticello T and Green DW (2004). Excessive ATP hydrolysis in ischemic myocardium by mitochondrial F1F0-ATPase: effect of selective pharmacological inhibition of mitochondrial ATPase hydrolase activity. *Am J Physiol Heart Circ Physiol* 287, H1747-1755.
218. Halestrap AP, Clarke SJ and Javadov SA (2004). Mitochondrial permeability transition pore opening during myocardial reperfusion- a target for cardioprotection. *Cardiovasc Res* 61, 372-385.

219. Griffiths EJ and Halestrap AP (1995). Mitochondrial non-specific pores remain closed during cardiac ischaemia, but open upon reperfusion. *Biochem J* 307 (Pt 1), 93-98.
220. Ong SB, Samangouei P, Kalkhoran SB and Hausenloy DJ (2015). The mitochondrial permeability transition pore and its role in myocardial ischemia reperfusion injury. *J Mol Cell Cardiol* 78, 23-34.
221. Piper HM, Abdallah Y and Schäfer C (2004). The first minutes of reperfusion: a window of opportunity for cardioprotection. *Cardiovasc Res* 61, 365-371.
222. Szabó I, De Pinto V and Zoratti M (1993). The mitochondrial permeability transition pore may comprise VDAC molecules. II. The electrophysiological properties of VDAC are compatible with those of the mitochondrial megachannel. *FEBS Lett* 330, 206-210.
223. Morciano G, Bonora M, Campo G, Aquila G, Rizzo P, Giorgi C, Wieckowski MR and Pinton P (2017). Mechanistic role of mPTP in ischemia-reperfusion injury. *Adv Exp Med Biol* 982, 169-189.
224. Paradies G, Petrosillo G, Pistolese M, Di Venosa N, Serena D and Ruggiero FM (1999). Lipid peroxidation and alterations to oxidative metabolism in mitochondria isolated from rat heart subjected to ischemia and reperfusion. *Free Radic Biol Med* 27, 42-50.
225. Picca A, Mankowski RT, Burman JL, Donisi L, Kim JS, Marzetti E and Leeuwenburgh C (2018). Mitochondrial quality control mechanisms as molecular targets in cardiac ageing. *Nat Rev Cardiol* 15, 543-554.
226. Suliman HB and Piantadosi CA (2016). Mitochondrial quality control as a therapeutic target. *Pharmacol Rev* 68, 20-48.
227. Nakai A, Yamaguchi O, Takeda T, Higuchi Y, Hikoso S, Taniike M, Omiya S, Mizote I, Matsumura Y, Asahi M, Nishida K, Hori M, Mizushima N and Otsu K (2007). The role of autophagy in cardiomyocytes in the basal state and in response to hemodynamic stress. *Nat Med* 13, 619-624.
228. Fan H, He Z, Huang H, Zhuang H, Liu H, Liu X, Yang S, He P, Yang H and Feng D (2020). Mitochondrial quality control in cardiomyocytes: a critical role in the progression of cardiovascular diseases. *Front Physiol* 11, 252.
229. Marin TL, Gongol B, Zhang F, Martin M, Johnson DA, Xiao H, Wang Y, Subramaniam S, Chien S and Shyy JY (2017). AMPK promotes mitochondrial biogenesis and function by phosphorylating the epigenetic factors DNMT1, RBBP7, and HAT1. *Sci Signal* 10, eaaf7478.
230. Puigserver P, Wu Z, Park CW, Graves R, Wright M and Spiegelman BM (1998). A cold-inducible coactivator of nuclear receptors linked to adaptive thermogenesis. *Cell* 92, 829-839.

231. Dorn GW, 2nd, Vega RB and Kelly DP (2015). Mitochondrial biogenesis and dynamics in the developing and diseased heart. *Genes Dev* 29, 1981-1991.
232. van der Blik AM, Shen Q and Kawajiri S (2013). Mechanisms of mitochondrial fission and fusion. *Cold Spring Harb Perspect Biol* 5, a011072.
233. Maneechote C, Palee S, Chattipakorn SC and Chattipakorn N (2017). Roles of mitochondrial dynamics modulators in cardiac ischaemia/reperfusion injury. *J Cell Mol Med* 21, 2643-2653.
234. Youle RJ and van der Blik AM (2012). Mitochondrial fission, fusion, and stress. *Science* 337, 1062-1065.
235. Cao YL, Meng S, Chen Y, Feng JX, Gu DD, Yu B, Li YJ, Yang JY, Liao S, Chan DC and Gao S (2017). MFN1 structures reveal nucleotide-triggered dimerization critical for mitochondrial fusion. *Nature* 542, 372-376.
236. Filadi R, Pendin D and Pizzo P (2018). Mitofusin 2: from functions to disease. *Cell Death Dis* 9, 330.
237. Song Z, Chen H, Fiket M, Alexander C and Chan DC (2007). OPA1 processing controls mitochondrial fusion and is regulated by mRNA splicing, membrane potential, and Yme1L. *J Cell Biol* 178, 749-755.
238. Zanna C, Ghelli A, Porcelli AM, Karbowski M, Youle RJ, Schimpf S, Wissinger B, Pinti M, Cossarizza A, Vidoni S, Valentino ML, Rugolo M and Carelli V (2008). OPA1 mutations associated with dominant optic atrophy impair oxidative phosphorylation and mitochondrial fusion. *Brain* 131, 352-367.
239. Ni HM, Williams JA and Ding WX (2015). Mitochondrial dynamics and mitochondrial quality control. *Redox Biol* 4, 6-13.
240. Taguchi N, Ishihara N, Jofuku A, Oka T and Mihara K (2007). Mitotic phosphorylation of dynamin-related GTPase Drp1 participates in mitochondrial fission. *J Biol Chem* 282, 11521-11529.
241. Wu S, Zhou F, Zhang Z and Xing D (2011). Mitochondrial oxidative stress causes mitochondrial fragmentation via differential modulation of mitochondrial fission-fusion proteins. *Febs J* 278, 941-954.
242. Ashrafi G and Schwarz TL (2013). The pathways of mitophagy for quality control and clearance of mitochondria. *Cell Death Differ* 20, 31-42.
243. Narendra DP, Jin SM, Tanaka A, Suen DF, Gautier CA, Shen J, Cookson MR and Youle RJ (2010). PINK1 is selectively stabilized on impaired mitochondria to activate Parkin. *PLoS Biol* 8, e1000298.

244. Seirafi M, Kozlov G and Gehring K (2015). Parkin structure and function. *Febs J* 282, 2076-2088.
245. Chan NC, Salazar AM, Pham AH, Sweredoski MJ, Kolawa NJ, Graham RL, Hess S and Chan DC (2011). Broad activation of the ubiquitin-proteasome system by Parkin is critical for mitophagy. *Hum Mol Genet* 20, 1726-1737.
246. Sedlackova L and Korolchuk VI (2019). Mitochondrial quality control as a key determinant of cell survival. *Biochim Biophys Acta Mol Cell Res* 1866, 575-587.
247. Hales KG and Fuller MT (1997). Developmentally regulated mitochondrial fusion mediated by a conserved, novel, predicted GTPase. *Cell* 90, 121-129.
248. Mozdy AD and Shaw JM (2003). A fuzzy mitochondrial fusion apparatus comes into focus. *Nat Rev Mol Cell Biol* 4, 468-478.
249. Chen H, Detmer SA, Ewald AJ, Griffin EE, Fraser SE and Chan DC (2003). Mitofusins Mfn1 and Mfn2 coordinately regulate mitochondrial fusion and are essential for embryonic development. *J Cell Biol* 160, 189-200.
250. Papanicolaou KN, Kikuchi R, Ngoh GA, Coughlan KA, Dominguez I, Stanley WC and Walsh K (2012). Mitofusins 1 and 2 are essential for postnatal metabolic remodeling in heart. *Circ Res* 111, 1012-1026.
251. Mourier A, Motori E, Brandt T, Lagouge M, Atanassov I, Galinier A, Rappl G, Brodesser S, Hultenby K, Dieterich C and Larsson NG (2015). Mitofusin 2 is required to maintain mitochondrial coenzyme Q levels. *J Cell Biol* 208, 429-442.
252. Chen Y and Dorn GW, 2nd (2013). PINK1-phosphorylated mitofusin 2 is a parkin receptor for culling damaged mitochondria. *Science* 340, 471-475.
253. Zhao T, Huang X, Han L, Wang X, Cheng H, Zhao Y, Chen Q, Chen J, Cheng H, Xiao R and Zheng M (2012). Central role of mitofusin 2 in autophagosome-lysosome fusion in cardiomyocytes. *J Biol Chem* 287, 23615-23625.
254. Parra V, Eisner V, Chiong M, Criollo A, Moraga F, Garcia A, Härtel S, Jaimovich E, Zorzano A, Hidalgo C and Lavandero S (2008). Changes in mitochondrial dynamics during ceramide-induced cardiomyocyte early apoptosis. *Cardiovasc Res* 77, 387-397.
255. Chen Y, Csordás G, Jowdy C, Schneider TG, Csordás N, Wang W, Liu Y, Kohlhaas M, Meiser M, Bergem S, Nerbonne JM, Dorn GW, 2nd and Maack C (2012). Mitofusin 2-containing mitochondrial-reticular microdomains direct rapid cardiomyocyte bioenergetic responses via interorganelle Ca²⁺ crosstalk. *Circ Res* 111, 863-875.
256. McLelland GL, Goiran T, Yi W, Dorval G, Chen CX, Lauinger ND, Krahn AI, Valimehr S, Rakovic A, Rouiller I, Durcan TM, Trempe JF and Fon EA (2018). Mfn2 ubiquitination by PINK1/parkin gates the p97-dependent release of ER from mitochondria to drive mitophagy. *Elife* 7.

257. Misko A, Jiang S, Wegorzewska I, Milbrandt J and Baloh RH (2010). Mitofusin 2 is necessary for transport of axonal mitochondria and interacts with the Miro/Milton complex. *J Neurosci* 30, 4232-4240.
258. Lehninger AL and Wadkins CL (1962). Oxidative phosphorylation. *Annu Rev Biochem* 31, 47-78.
259. Nicholls DG and Ferguson SJ (2013). 5- Respiratory chains. Bioenergetics (fourth edition). Nicholls DG and Ferguson SJ. Boston, *Academic Press*, 91-157.
260. Nolfi-Donagan D, Braganza A and Shiva S (2020). Mitochondrial electron transport chain: oxidative phosphorylation, oxidant production, and methods of measurement. *Redox Biol* 37, 101674.
261. Wilson DF (2017). Oxidative phosphorylation: regulation and role in cellular and tissue metabolism. *J Physiol* 595, 7023-7038.
262. Hatefi Y, Haavik AG, Fowler LR and Griffiths DE (1962). Studies on the electron transfer system. XLII. Reconstitution of the electron transfer system. *J Biol Chem* 237, 2661-2669.
263. Manoj KM (2018). Aerobic respiration: criticism of the proton-centric explanation involving rotary adenosine triphosphate synthesis, chemiosmosis principle, proton pumps and electron transport chain. *Biochem Insights* 11, 1178626418818442.
264. Wojtovich AP, Smith CO, Haynes CM, Nehrke KW and Brookes PS (2013). Physiological consequences of complex II inhibition for aging, disease, and the mKATP channel. *Biochim Biophys Acta* 1827, 598-611.
265. Stine ZE, Altman BJ, Hsieh AL, Gouw AM and Dang CV (2014). Deregulation of the cellular energetics of cancer cells. Pathobiology of human disease. McManus LM and Mitchell RN. San Diego, *Academic Press*, 444-455.
266. Efremov RG, Baradaran R and Sazanov LA (2010). The architecture of respiratory complex I. *Nature* 465, 441-445.
267. Iverson TM (2013). Catalytic mechanisms of complex II enzymes: a structural perspective. *Biochim Biophys Acta* 1827, 648-657.
268. Cecchini G (2003). Function and structure of complex II of the respiratory chain. *Annu Rev Biochem* 72, 77-109.
269. Li Y, Park JS, Deng JH and Bai Y (2006). Cytochrome c oxidase subunit IV is essential for assembly and respiratory function of the enzyme complex. *J Bioenerg Biomembr* 38, 283-291.
270. Nobes CD, Brown GC, Olive PN and Brand MD (1990). Non-ohmic proton conductance of the mitochondrial inner membrane in hepatocytes. *J Biol Chem* 265, 12903-12909.

271. Stock D, Gibbons C, Arechaga I, Leslie AG and Walker JE (2000). The rotary mechanism of ATP synthase. *Curr Opin Struct Biol* 10, 672-679.
272. Boyer PD (1997). The ATP synthase- a splendid molecular machine. *Annu Rev Biochem* 66, 717-749.
273. Suzuki T, Ueno H, Mitome N, Suzuki J and Yoshida M (2002). F(0) of ATP synthase is a rotary proton channel. Obligatory coupling of proton translocation with rotation of c-subunit ring. *J Biol Chem* 277, 13281-13285.
274. Klusch N, Murphy BJ, Mills DJ, Yildiz Ö and Kühlbrandt W (2017). Structural basis of proton translocation and force generation in mitochondrial ATP synthase. *Elife* 6, e33274.
275. Boyman L, Chikando AC, Williams GS, Khairallah RJ, Kettlewell S, Ward CW, Smith GL, Kao JP and Lederer WJ (2014). Calcium movement in cardiac mitochondria. *Biophys J* 107, 1289-1301.
276. Wacquier B, Combettes L and Dupont G (2019). Cytoplasmic and mitochondrial calcium signaling: a two-way relationship. *Cold Spring Harb Perspect Biol* 11, a035139.
277. Robert V, Gurlini P, Tosello V, Nagai T, Miyawaki A, Di Lisa F and Pozzan T (2001). Beat-to-beat oscillations of mitochondrial $[Ca^{2+}]$ in cardiac cells. *Embo j* 20, 4998-5007.
278. Mohsin AA, Thompson J, Hu Y, Hollander J, Lesnefsky EJ and Chen Q (2020). Endoplasmic reticulum stress-induced complex I defect: central role of calcium overload. *Arch Biochem Biophys* 683, 108299.
279. Santulli G, Xie W, Reiken SR and Marks AR (2015). Mitochondrial calcium overload is a key determinant in heart failure. *Proc Natl Acad Sci U S A* 112, 11389-11394.
280. Green D and Kroemer G (1998). The central executioners of apoptosis: caspases or mitochondria? *Trends Cell Biol* 8, 267-271.
281. Susin SA, Zamzami N, Castedo M, Hirsch T, Marchetti P, Macho A, Daugas E, Geuskens M and Kroemer G (1996). Bcl-2 inhibits the mitochondrial release of an apoptogenic protease. *J Exp Med* 184, 1331-1341.
282. Susin SA, Lorenzo HK, Zamzami N, Marzo I, Snow BE, Brothers GM, Mangion J, Jacotot E, Costantini P, Loeffler M, Larochette N, Goodlett DR, Aebersold R, Siderovski DP, Penninger JM and Kroemer G (1999). Molecular characterization of mitochondrial apoptosis-inducing factor. *Nature* 397, 441-446.
283. Miramar MD, Costantini P, Ravagnan L, Saraiva LM, Haouzi D, Brothers G, Penninger JM, Peleato ML, Kroemer G and Susin SA (2001). NADH oxidase activity of mitochondrial apoptosis-inducing factor. *J Biol Chem* 276, 16391-16398.
284. Sevrioukova IF (2011). Apoptosis-inducing factor: structure, function, and redox regulation. *Antioxid Redox Signal* 14, 2545-2579.

285. Daugas E, Susin SA, Zamzami N, Ferri KF, Irinopoulou T, Larochette N, Prévost MC, Leber B, Andrews D, Penninger J and Kroemer G (2000). Mitochondrio-nuclear translocation of AIF in apoptosis and necrosis. *Faseb J* 14, 729-739.
286. Otera H, Ohsakaya S, Nagaura Z, Ishihara N and Mihara K (2005). Export of mitochondrial AIF in response to proapoptotic stimuli depends on processing at the intermembrane space. *Embo j* 24, 1375-1386.
287. Norberg E, Gogvadze V, Ott M, Horn M, Uhlén P, Orrenius S and Zhivotovsky B (2008). An increase in intracellular Ca^{2+} is required for the activation of mitochondrial calpain to release AIF during cell death. *Cell Death Differ* 15, 1857-1864.
288. Fonseca AC, Ferreiro E, Oliveira CR, Cardoso SM and Pereira CF (2013). Activation of the endoplasmic reticulum stress response by the amyloid-beta 1-40 peptide in brain endothelial cells. *Biochim Biophys Acta* 1832, 2191-2203.
289. Joza N, Susin SA, Daugas E, Stanford WL, Cho SK, Li CY, Sasaki T, Elia AJ, Cheng HY, Ravagnan L, Ferri KF, Zamzami N, Wakeham A, Hakem R, Yoshida H, Kong YY, Mak TW, Zúñiga-Pflücker JC, Kroemer G and Penninger JM (2001). Essential role of the mitochondrial apoptosis-inducing factor in programmed cell death. *Nature* 410, 549-554.
290. Susin SA, Daugas E, Ravagnan L, Samejima K, Zamzami N, Loeffler M, Costantini P, Ferri KF, Irinopoulou T, Prévost MC, Brothers G, Mak TW, Penninger J, Earnshaw WC and Kroemer G (2000). Two distinct pathways leading to nuclear apoptosis. *J Exp Med* 192, 571-580.
291. Joshi A, Bondada V and Geddes JW (2009). Mitochondrial micro-calpain is not involved in the processing of apoptosis-inducing factor. *Experimental neurology* 218, 221-227.
292. Yuste VJ, Moubarak RS, Delettre C, Bras M, Sancho P, Robert N, d'Alayer J and Susin SA (2005). Cysteine protease inhibition prevents mitochondrial apoptosis-inducing factor (AIF) release. *Cell Death Differ* 12, 1445-1448.
293. Moubarak RS, Yuste VJ, Artus C, Bouharrour A, Greer PA, Menissier-de Murcia J and Susin SA (2007). Sequential activation of poly(ADP-ribose) polymerase 1, calpains, and Bax is essential in apoptosis-inducing factor-mediated programmed necrosis. *Mol Cell Biol* 27, 4844-4862.
294. Gustafsson AB and Gottlieb RA (2008). Heart mitochondria: gates of life and death. *Cardiovasc Res* 77, 334-343.
295. Kuwana T, Mackey MR, Perkins G, Ellisman MH, Latterich M, Schneider R, Green DR and Newmeyer DD (2002). Bid, Bax, and lipids cooperate to form supramolecular openings in the outer mitochondrial membrane. *Cell* 111, 331-342.
296. Jürgensmeier JM, Xie Z, Deveraux Q, Ellerby L, Bredesen D and Reed JC (1998). Bax directly induces release of cytochrome c from isolated mitochondria. *Proc Natl Acad Sci U S A* 95, 4997-5002.

297. Nakamura M, Wang NP, Zhao ZQ, Wilcox JN, Thourani V, Guyton RA and Vinten-Johansen J (2000). Preconditioning decreases Bax expression, PMN accumulation and apoptosis in reperfused rat heart. *Cardiovasc Res* 45, 661-670.
298. Hochhauser E, Kivity S, Offen D, Maulik N, Otani H, Barhum Y, Pannet H, Shneyvays V, Shainberg A, Goldshtaub V, Tobar A and Vidne BA (2003). Bax ablation protects against myocardial ischemia-reperfusion injury in transgenic mice. *Am J Physiol Heart Circ Physiol* 284, H2351-2359.
299. Guo H, Callaway JB and Ting JP (2015). Inflammasomes: mechanism of action, role in disease, and therapeutics. *Nat Med* 21, 677-687.
300. Martinon F, Burns K and Tschopp J (2002). The inflammasome: a molecular platform triggering activation of inflammatory caspases and processing of proIL-beta. *Mol Cell* 10, 417-426.
301. Chaplin DD (2010). Overview of the immune response. *J Allergy Clin Immunol* 125, S3-23.
302. Chen GY and Nuñez G (2010). Sterile inflammation: sensing and reacting to damage. *Nat Rev Immunol* 10, 826-837.
303. Medzhitov R and Janeway C, Jr. (2000). Innate immunity. *N Engl J Med* 343, 338-344.
304. Zhu X, Huang H and Zhao L (2022). PAMPs and DAMPs as the bridge between periodontitis and atherosclerosis: the potential therapeutic targets. *Front Cell Dev Biol* 10, 856118.
305. Cerretti DP, Kozlosky CJ, Mosley B, Nelson N, Van Ness K, Greenstreet TA, March CJ, Kronheim SR, Druck T, Cannizzaro LA, Huebner K and Black RA (1992). Molecular cloning of the interleukin-1 beta converting enzyme. *Science* 256, 97-100.
306. Keller M, Rüegg A, Werner S and Beer HD (2008). Active caspase-1 is a regulator of unconventional protein secretion. *Cell* 132, 818-831.
307. Takeuchi O and Akira S (2010). Pattern recognition receptors and inflammation. *Cell* 140, 805-820.
308. Wang Z, Zhang S, Xiao Y, Zhang W, Wu S, Qin T, Yue Y, Qian W and Li L (2020). NLRP3 inflammasome and inflammatory diseases. *Oxid Med Cell Longev* 2020, 4063562.
309. Bauernfeind FG, Horvath G, Stutz A, Alnemri ES, MacDonald K, Speert D, Fernandes-Alnemri T, Wu J, Monks BG, Fitzgerald KA, Hornung V and Latz E (2009). Cutting edge: NF-kappaB activating pattern recognition and cytokine receptors license NLRP3 inflammasome activation by regulating NLRP3 expression. *J Immunol* 183, 787-791.

310. Rodgers MA, Bowman JW, Fujita H, Orazio N, Shi M, Liang Q, Amatya R, Kelly TJ, Iwai K, Ting J and Jung JU (2014). The linear ubiquitin assembly complex (LUBAC) is essential for NLRP3 inflammasome activation. *J Exp Med* 211, 1333-1347.
311. He WT, Wan H, Hu L, Chen P, Wang X, Huang Z, Yang ZH, Zhong CQ and Han J (2015). Gasdermin D is an executor of pyroptosis and required for interleukin-1 β secretion. *Cell Res* 25, 1285-1298.
312. Zhou R, Yazdi AS, Menu P and Tschopp J (2011). A role for mitochondria in NLRP3 inflammasome activation. *Nature* 469, 221-225.
313. Yu J, Nagasu H, Murakami T, Hoang H, Broderick L, Hoffman HM and Horng T (2014). Inflammasome activation leads to caspase-1-dependent mitochondrial damage and block of mitophagy. *Proc Natl Acad Sci U S A* 111, 15514-15519.
314. Zhang J, Huang L, Shi X, Yang L, Hua F, Ma J, Zhu W, Liu X, Xuan R, Shen Y, Liu J, Lai X and Yu P (2020). Metformin protects against myocardial ischemia-reperfusion injury and cell pyroptosis via AMPK/NLRP3 inflammasome pathway. *Aging (Albany NY)* 12, 24270-24287.
315. Wang X, Li X, Liu S, Brickell AN, Zhang J, Wu Z, Zhou S and Ding Z (2020). PCSK9 regulates pyroptosis via mtDNA damage in chronic myocardial ischemia. *Basic Res Cardiol* 115, 66.
316. Qiu Z, Lei S, Zhao B, Wu Y, Su W, Liu M, Meng Q, Zhou B, Leng Y and Xia ZY (2017). NLRP3 inflammasome activation-mediated pyroptosis aggravates myocardial ischemia/reperfusion injury in diabetic rats. *Oxid Med Cell Longev* 2017, 9743280.
317. Mezzaroma E, Toldo S, Farkas D, Seropian IM, Van Tassell BW, Salloum FN, Kannan HR, Menna AC, Voelkel NF and Abbate A (2011). The inflammasome promotes adverse cardiac remodeling following acute myocardial infarction in the mouse. *Proc Natl Acad Sci U S A* 108, 19725-19730.
318. Sandanger Ø, Ranheim T, Vinge LE, Bliksøen M, Alfsnes K, Finsen AV, Dahl CP, Askevold ET, Florholmen G, Christensen G, Fitzgerald KA, Lien E, Valen G, Espevik T, Aukrust P and Yndestad A (2013). The NLRP3 inflammasome is up-regulated in cardiac fibroblasts and mediates myocardial ischaemia-reperfusion injury. *Cardiovasc Res* 99, 164-174.
319. Mastrocola R, Collino M, Penna C, Nigro D, Chiazza F, Fracasso V, Tullio F, Alloatti G, Pagliaro P and Aragno M (2016). Maladaptive modulations of NLRP3 inflammasome and cardioprotective pathways are involved in diet-induced exacerbation of myocardial ischemia/reperfusion injury in mice. *Oxid Med Cell Longev* 2016, 3480637.
320. Mastrocola R, Penna C, Tullio F, Femminò S, Nigro D, Chiazza F, Serpe L, Collotta D, Alloatti G, Cocco M, Bertinaria M, Pagliaro P, Aragno M and Collino M (2016). Pharmacological inhibition of NLRP3 inflammasome attenuates myocardial

- ischemia/reperfusion injury by activation of RISK and mitochondrial pathways. *Oxid Med Cell Longev* 2016, 5271251.
321. Palade GE and Siekevitz P (1956). Liver microsomes; an integrated morphological and biochemical study. *J Biophys Biochem Cytol* 2, 171-200.
 322. Porter KR and Kallman FL (1952). Significance of cell particulates as seen by electron microscopy. *Ann N Y Acad Sci* 54, 882-891.
 323. Wang S, Binder P, Fang Q, Wang Z, Xiao W, Liu W and Wang X (2018). Endoplasmic reticulum stress in the heart: insights into mechanisms and drug targets. *Br J Pharmacol* 175, 1293-1304.
 324. Schwarz DS and Blower MD (2016). The endoplasmic reticulum: structure, function and response to cellular signaling. *Cell Mol Life Sci* 73, 79-94.
 325. Jan CH, Williams CC and Weissman JS (2014). Principles of ER cotranslational translocation revealed by proximity-specific ribosome profiling. *Science* 346, 1257521.
 326. Walter P and Blobel G (1981). Translocation of proteins across the endoplasmic reticulum. II. Signal recognition protein (SRP) mediates the selective binding to microsomal membranes of in-vitro-assembled polysomes synthesizing secretory protein. *J Cell Biol* 91, 551-556.
 327. Chaudhuri TK and Paul S (2006). Protein-misfolding diseases and chaperone-based therapeutic approaches. *Febs J* 273, 1331-1349.
 328. Clapham DE (2007). Calcium signaling. *Cell* 131, 1047-1058.
 329. Foskett JK, White C, Cheung KH and Mak DO (2007). Inositol trisphosphate receptor Ca^{2+} release channels. *Physiol Rev* 87, 593-658.
 330. Endo M (2009). Calcium-induced calcium release in skeletal muscle. *Physiol Rev* 89, 1153-1176.
 331. Lytton J, Westlin M and Hanley MR (1991). Thapsigargin inhibits the sarcoplasmic or endoplasmic reticulum Ca-ATPase family of calcium pumps. *J Biol Chem* 266, 17067-17071.
 332. Fawcett DW (1961). The sarcoplasmic reticulum of skeletal and cardiac muscle. *Circulation* 24, 336-348.
 333. Stein O and Stein Y (1968). Lipid synthesis, intracellular transport, and storage: electron microscopic radioautographic study of the rat heart perfused with tritiated oleic acid. *J Cell Biol* 36, 63-77.
 334. Bers DM (2002). Cardiac excitation-contraction coupling. *Nature* 415, 198-205.

335. Cohen FE and Kelly JW (2003). Therapeutic approaches to protein-misfolding diseases. *Nature* 426, 905-909.
336. van Spaendonck-Zwarts KY, van Hessem L, Jongbloed JD, de Walle HE, Capetanaki Y, van der Kooij AJ, van Langen IM, van den Berg MP and van Tintelen JP (2011). Desmin-related myopathy. *Clin Genet* 80, 354-366.
337. McLendon PM and Robbins J (2015). Proteotoxicity and cardiac dysfunction. *Circ Res* 116, 1863-1882.
338. Sano R and Reed JC (2013). ER stress-induced cell death mechanisms. *Biochim Biophys Acta* 1833, 3460-3470.
339. Bravo R, Parra V, Gatica D, Rodriguez AE, Torrealba N, Paredes F, Wang ZV, Zorzano A, Hill JA, Jaimovich E, Quest AF and Lavandero S (2013). Endoplasmic reticulum and the unfolded protein response: dynamics and metabolic integration. *Int Rev Cell Mol Biol* 301, 215-290.
340. Read A and Schröder M (2021). The unfolded protein response: an overview. *Biology (Basel)* 10, 384.
341. Sidrauski C and Walter P (1997). The transmembrane kinase Ire1p is a site-specific endonuclease that initiates mRNA splicing in the unfolded protein response. *Cell* 90, 1031-1039.
342. Shen X, Ellis RE, Lee K, Liu CY, Yang K, Solomon A, Yoshida H, Morimoto R, Kurnit DM, Mori K and Kaufman RJ (2001). Complementary signaling pathways regulate the unfolded protein response and are required for *C. elegans* development. *Cell* 107, 893-903.
343. Cao SS and Kaufman RJ (2012). Unfolded protein response. *Curr Biol* 22, R622-626.
344. Bertolotti A, Zhang Y, Hendershot LM, Harding HP and Ron D (2000). Dynamic interaction of BiP and ER stress transducers in the unfolded-protein response. *Nat Cell Biol* 2, 326-332.
345. Calton M, Zeng H, Urano F, Till JH, Hubbard SR, Harding HP, Clark SG and Ron D (2002). IRE1 couples endoplasmic reticulum load to secretory capacity by processing the XBP-1 mRNA. *Nature* 415, 92-96.
346. Scheuner D, Song B, McEwen E, Liu C, Laybutt R, Gillespie P, Saunders T, Bonner-Weir S and Kaufman RJ (2001). Translational control is required for the unfolded protein response and in vivo glucose homeostasis. *Mol Cell* 7, 1165-1176.
347. Ameri K and Harris AL (2008). Activating transcription factor 4. *Int J Biochem Cell Biol* 40, 14-21.

348. Wang Y, Shen J, Arenzana N, Tirasophon W, Kaufman RJ and Prywes R (2000). Activation of ATF6 and an ATF6 DNA binding site by the endoplasmic reticulum stress response. *J Biol Chem* 275, 27013-27020.
349. Rutkowski DT and Hegde RS (2010). Regulation of basal cellular physiology by the homeostatic unfolded protein response. *J Cell Biol* 189, 783-794.
350. Riaz TA, Junjappa RP, Handigund M, Ferdous J, Kim HR and Chae HJ (2020). Role of endoplasmic reticulum stress sensor IRE1 α in cellular physiology, calcium, ROS signaling, and metaflammation. *Cells* 9, 1160.
351. Hennigs JK, Burhenne N, Stähler F, Winnig M, Walter B, Meyerhof W and Schmale H (2008). Sweet taste receptor interacting protein CIB1 is a general inhibitor of InsP3-dependent Ca²⁺ release in vivo. *J Neurochem* 106, 2249-2262.
352. Yoon KW, Cho JH, Lee JK, Kang YH, Chae JS, Kim YM, Kim J, Kim EK, Kim SE, Baik JH, Naik UP, Cho SG and Choi EJ (2009). CIB1 functions as a Ca²⁺-sensitive modulator of stress-induced signaling by targeting ASK1. *Proc Natl Acad Sci U S A* 106, 17389-17394.
353. Son SM, Byun J, Roh SE, Kim SJ and Mook-Jung I (2014). Reduced IRE1 α mediates apoptotic cell death by disrupting calcium homeostasis via the InsP3 receptor. *Cell Death Dis* 5, e1188.
354. Minamino T and Kitakaze M (2010). ER stress in cardiovascular disease. *J Mol Cell Cardiol* 48, 1105-1110.
355. Yao Y, Lu Q, Hu Z, Yu Y, Chen Q and Wang QK (2017). A non-canonical pathway regulates ER stress signaling and blocks ER stress-induced apoptosis and heart failure. *Nat Commun* 8, 133.
356. Rasheva VI and Domingos PM (2009). Cellular responses to endoplasmic reticulum stress and apoptosis. *Apoptosis* 14, 996-1007.
357. Amen OM, Sarker SD, Ghildyal R and Arya A (2019). Endoplasmic reticulum stress activates unfolded protein response signaling and mediates inflammation, obesity, and cardiac dysfunction: therapeutic and molecular approach. *Front Pharmacol* 10, 977.
358. Drazner MH (2011). The progression of hypertensive heart disease. *Circulation* 123, 327-334.
359. Yang KC, Jay PY, McMullen JR and Nerbonne JM (2012). Enhanced cardiac PI3K α signalling mitigates arrhythmogenic electrical remodelling in pathological hypertrophy and heart failure. *Cardiovasc Res* 93, 252-262.
360. Li H, Korennykh AV, Behrman SL and Walter P (2010). Mammalian endoplasmic reticulum stress sensor IRE1 signals by dynamic clustering. *Proc Natl Acad Sci U S A* 107, 16113-16118.

361. Urano F, Wang X, Bertolotti A, Zhang Y, Chung P, Harding HP and Ron D (2000). Coupling of stress in the ER to activation of JNK protein kinases by transmembrane protein kinase IRE1. *Science* 287, 664-666.
362. Nishitoh H, Saitoh M, Mochida Y, Takeda K, Nakano H, Rothe M, Miyazono K and Ichijo H (1998). ASK1 is essential for JNK/SAPK activation by TRAF2. *Mol Cell* 2, 389-395.
363. Davis RJ (2000). Signal transduction by the JNK group of MAP kinases. *Cell* 103, 239-252.
364. Harding HP, Zhang Y, Zeng H, Novoa I, Lu PD, Calton M, Sadri N, Yun C, Popko B, Paules R, Stojdl DF, Bell JC, Hettmann T, Leiden JM and Ron D (2003). An integrated stress response regulates amino acid metabolism and resistance to oxidative stress. *Mol Cell* 11, 619-633.
365. Yang Y, Liu L, Naik I, Braunstein Z, Zhong J and Ren B (2017). Transcription factor C/EBP homologous protein in health and diseases. *Front Immunol* 8, 1612.
366. Wang XZ and Ron D (1996). Stress-induced phosphorylation and activation of the transcription factor CHOP (GADD153) by p38 MAP Kinase. *Science* 272, 1347-1349.
367. Tsukano H, Gotoh T, Endo M, Miyata K, Tazume H, Kadomatsu T, Yano M, Iwawaki T, Kohno K, Araki K, Mizuta H and Oike Y (2010). The endoplasmic reticulum stress-C/EBP homologous protein pathway-mediated apoptosis in macrophages contributes to the instability of atherosclerotic plaques. *Arterioscler Thromb Vasc Biol* 30, 1925-1932.
368. Hu H, Tian M, Ding C and Yu S (2018). The C/EBP homologous protein (CHOP) transcription factor functions in endoplasmic reticulum stress-induced apoptosis and microbial infection. *Front Immunol* 9, 3083.
369. Shimizu K, Takahama S, Endo Y and Sawasaki T (2012). Stress-inducible caspase substrate TRB3 promotes nuclear translocation of procaspase-3. *PLoS One* 7, e42721.
370. Ohoka N, Yoshii S, Hattori T, Onozaki K and Hayashi H (2005). TRB3, a novel ER stress-inducible gene, is induced via ATF4-CHOP pathway and is involved in cell death. *Embo j* 24, 1243-1255.
371. Lugea A, Tischler D, Nguyen J, Gong J, Gukovsky I, French SW, Gorelick FS and Pandolfi SJ (2011). Adaptive unfolded protein response attenuates alcohol-induced pancreatic damage. *Gastroenterology* 140, 987-997.
372. Engin F, Yermalovich A, Nguyen T, Hummasti S, Fu W, Eizirik DL, Mathis D and Hotamisligil GS (2013). Restoration of the unfolded protein response in pancreatic β cells protects mice against type 1 diabetes. *Sci Transl Med* 5, 211ra156.
373. Fu HY, Okada K, Liao Y, Tsukamoto O, Isomura T, Asai M, Sawada T, Okuda K, Asano Y, Sanada S, Asanuma H, Asakura M, Takashima S, Komuro I, Kitakaze M and Minamoto T (2010). Ablation of C/EBP homologous protein attenuates endoplasmic reticulum-

- mediated apoptosis and cardiac dysfunction induced by pressure overload. *Circulation* 122, 361-369.
374. Hamada H, Suzuki M, Yuasa S, Mimura N, Shinozuka N, Takada Y, Suzuki M, Nishino T, Nakaya H, Koseki H and Aoe T (2004). Dilated cardiomyopathy caused by aberrant endoplasmic reticulum quality control in mutant KDEL receptor transgenic mice. *Mol Cell Biol* 24, 8007-8017.
375. Yamaguchi O, Higuchi Y, Hirotsu S, Kashiwase K, Nakayama H, Hikoso S, Takeda T, Watanabe T, Asahi M, Taniike M, Matsumura Y, Tsujimoto I, Hongo K, Kusakari Y, Kurihara S, Nishida K, Ichijo H, Hori M and Otsu K (2003). Targeted deletion of apoptosis signal-regulating kinase 1 attenuates left ventricular remodeling. *Proc Natl Acad Sci U S A* 100, 15883-15888.
376. Li RJ, He KL, Li X, Wang LL, Liu CL and He YY (2015). Salubrinal protects cardiomyocytes against apoptosis in a rat myocardial infarction model via suppressing the dephosphorylation of eukaryotic translation initiation factor 2 α . *Mol Med Rep* 12, 1043-1049.
377. Park CS, Cha H, Kwon EJ, Sreenivasiah PK and Kim DH (2012). The chemical chaperone 4-phenylbutyric acid attenuates pressure-overload cardiac hypertrophy by alleviating endoplasmic reticulum stress. *Biochem Biophys Res Commun* 421, 578-584.
378. Wang S, Wang Z, Fan Q, Guo J, Galli G, Du G, Wang X and Xiao W (2016). Ginkgolide K protects the heart against endoplasmic reticulum stress injury by activating the inositol-requiring enzyme 1 α /X box-binding protein-1 pathway. *Br J Pharmacol* 173, 2402-2418.
379. Glembotski CC (2008). The role of the unfolded protein response in the heart. *J Mol Cell Cardiol* 44, 453-459.
380. Thuerauf DJ, Marcinko M, Gude N, Rubio M, Sussman MA and Glembotski CC (2006). Activation of the unfolded protein response in infarcted mouse heart and hypoxic cultured cardiac myocytes. *Circ Res* 99, 275-282.
381. Cao SS and Kaufman RJ (2014). Endoplasmic reticulum stress and oxidative stress in cell fate decision and human disease. *Antioxid Redox Signal* 21, 396-413.
382. van der Vlies D, Makkinje M, Jansens A, Braakman I, Verkleij AJ, Wirtz KW and Post JA (2003). Oxidation of ER resident proteins upon oxidative stress: effects of altering cellular redox/antioxidant status and implications for protein maturation. *Antioxid Redox Signal* 5, 381-387.
383. Szegezdi E, Duffy A, O'Mahoney ME, Logue SE, Mylotte LA, O'Brien T and Samali A (2006). ER stress contributes to ischemia-induced cardiomyocyte apoptosis. *Biochem Biophys Res Commun* 349, 1406-1411.
384. Miyazaki Y, Kaikita K, Endo M, Horio E, Miura M, Tsujita K, Hokimoto S, Yamamuro M, Iwawaki T, Gotoh T, Ogawa H and Oike Y (2011). C/EBP homologous protein

- deficiency attenuates myocardial reperfusion injury by inhibiting myocardial apoptosis and inflammation. *Arterioscler Thromb Vasc Biol* 31, 1124-1132.
385. Ruan Y, Zeng J, Jin Q, Chu M, Ji K, Wang Z and Li L (2020). Endoplasmic reticulum stress serves an important role in cardiac ischemia/reperfusion injury (Review). *Exp Ther Med* 20, 268.
386. Cao L, Chen Y, Zhang Z, Li Y and Zhao P (2019). Endoplasmic reticulum stress-induced NLRP1 inflammasome activation contributes to myocardial ischemia/reperfusion injury. *Shock* 51, 511-518.
387. Wang ZV, Deng Y, Gao N, Pedrozo Z, Li DL, Morales CR, Criollo A, Luo X, Tan W, Jiang N, Lehrman MA, Rothermel BA, Lee AH, Lavandero S, Mammen PPA, Ferdous A, Gillette TG, Scherer PE and Hill JA (2014). Spliced X-box binding protein 1 couples the unfolded protein response to hexosamine biosynthetic pathway. *Cell* 156, 1179-1192.
388. Martindale JJ, Fernandez R, Thuerauf D, Whittaker R, Gude N, Sussman MA and Glembotski CC (2006). Endoplasmic reticulum stress gene induction and protection from ischemia/reperfusion injury in the hearts of transgenic mice with a tamoxifen-regulated form of ATF6. *Circ Res* 98, 1186-1193.
389. Jian L, Lu Y, Lu S and Lu C (2016). Chemical chaperone 4-phenylbutyric acid reduces cardiac ischemia/reperfusion injury by alleviating endoplasmic reticulum stress and oxidative stress. *Med Sci Monit* 22, 5218-5227.
390. Soeller C and Cannell MB (1999). Examination of the transverse tubular system in living cardiac rat myocytes by 2-photon microscopy and digital image-processing techniques. *Circ Res* 84, 266-275.
391. Eisner DA, Caldwell JL, Kistamás K and Trafford AW (2017). Calcium and excitation-contraction coupling in the heart. *Circ Res* 121, 181-195.
392. Orchard C and Brette F (2008). t-Tubules and sarcoplasmic reticulum function in cardiac ventricular myocytes. *Cardiovasc Res* 77, 237-244.
393. Nakai J, Imagawa T, Hakamat Y, Shigekawa M, Takeshima H and Numa S (1990). Primary structure and functional expression from cDNA of the cardiac ryanodine receptor/calcium release channel. *FEBS Lett* 271, 169-177.
394. Meissner G (2004). Molecular regulation of cardiac ryanodine receptor ion channel. *Cell Calcium* 35, 621-628.
395. Wang SQ, Song LS, Lakatta EG and Cheng H (2001). Ca²⁺ signalling between single L-type Ca²⁺ channels and ryanodine receptors in heart cells. *Nature* 410, 592-596.
396. Solaro RJ and Rarick HM (1998). Troponin and tropomyosin: proteins that switch on and tune in the activity of cardiac myofilaments. *Circ Res* 83, 471-480.

397. Hilgemann DW, Collins A and Matsuoka S (1992). Steady-state and dynamic properties of cardiac sodium-calcium exchange. Secondary modulation by cytoplasmic calcium and ATP. *J Gen Physiol* 100, 933-961.
398. Kawase Y and Hajjar RJ (2008). The cardiac sarcoplasmic/endoplasmic reticulum calcium ATPase: a potent target for cardiovascular diseases. *Nat Clin Pract Cardiovasc Med* 5, 554-565.
399. Guo A, Zhang C, Wei S, Chen B and Song LS (2013). Emerging mechanisms of T-tubule remodelling in heart failure. *Cardiovasc Res* 98, 204-215.
400. Orchard CH, Bryant SM and James AF (2013). Do t-tubules play a role in arrhythmogenesis in cardiac ventricular myocytes? *J Physiol* 591, 4141-4147.
401. Gómez AM, Valdivia HH, Cheng H, Lederer MR, Santana LF, Cannell MB, McCune SA, Altschuld RA and Lederer WJ (1997). Defective excitation-contraction coupling in experimental cardiac hypertrophy and heart failure. *Science* 276, 800-806.
402. Zhang HB, Li RC, Xu M, Xu SM, Lai YS, Wu HD, Xie XJ, Gao W, Ye H, Zhang YY, Meng X and Wang SQ (2013). Ultrastructural uncoupling between T-tubules and sarcoplasmic reticulum in human heart failure. *Cardiovasc Res* 98, 269-276.
403. Wei S, Guo A, Chen B, Kutschke W, Xie YP, Zimmerman K, Weiss RM, Anderson ME, Cheng H and Song LS (2010). T-tubule remodeling during transition from hypertrophy to heart failure. *Circ Res* 107, 520-531.
404. He J, Conklin MW, Foell JD, Wolff MR, Haworth RA, Coronado R and Kamp TJ (2001). Reduction in density of transverse tubules and L-type Ca^{2+} channels in canine tachycardia-induced heart failure. *Cardiovasc Res* 49, 298-307.
405. Song LS, Sobie EA, McCulle S, Lederer WJ, Balke CW and Cheng H (2006). Orphaned ryanodine receptors in the failing heart. *Proc Natl Acad Sci U S A* 103, 4305-4310.
406. Hong T, Yang H, Zhang SS, Cho HC, Kalashnikova M, Sun B, Zhang H, Bhargava A, Grabe M, Olgin J, Gorelik J, Marbán E, Jan LY and Shaw RM (2014). Cardiac BIN1 folds T-tubule membrane, controlling ion flux and limiting arrhythmia. *Nat Med* 20, 624-632.
407. Crossman DJ, Young AA, Ruygrok PN, Nason GP, Baddeley D, Soeller C and Cannell MB (2015). T-tubule disease: relationship between t-tubule organization and regional contractile performance in human dilated cardiomyopathy. *J Mol Cell Cardiol* 84, 170-178.
408. Kolstad TR, van den Brink J, MacQuaide N, Lunde PK, Frisk M, Aronsen JM, Norden ES, Cataliotti A, Sjaastad I, Sejersted OM, Edwards AG, Lines GT and Louch WE (2018). Ryanodine receptor dispersion disrupts Ca^{2+} release in failing cardiac myocytes. *Elife* 7, e39427.

409. Piacentino V, 3rd, Weber CR, Chen X, Weisser-Thomas J, Margulies KB, Bers DM and Houser SR (2003). Cellular basis of abnormal calcium transients of failing human ventricular myocytes. *Circ Res* 92, 651-658.
410. Chopra N, Yang T, Asghari P, Moore ED, Huke S, Akin B, Cattolica RA, Perez CF, Hlaing T, Knollmann-Ritschel BE, Jones LR, Pessah IN, Allen PD, Franzini-Armstrong C and Knollmann BC (2009). Ablation of triadin causes loss of cardiac Ca²⁺ release units, impaired excitation-contraction coupling, and cardiac arrhythmias. *Proc Natl Acad Sci U S A* 106, 7636-7641.
411. Takeshima H, Komazaki S, Nishi M, Iino M and Kangawa K (2000). Junctophilins: a novel family of junctional membrane complex proteins. *Mol Cell* 6, 11-22.
412. Pinali C, Bennett H, Davenport JB, Trafford AW and Kitmitto A (2013). Three-dimensional reconstruction of cardiac sarcoplasmic reticulum reveals a continuous network linking transverse-tubules: this organization is perturbed in heart failure. *Circ Res* 113, 1219-1230.
413. Ziman AP, Gómez-Viquez NL, Bloch RJ and Lederer WJ (2010). Excitation-contraction coupling changes during postnatal cardiac development. *J Mol Cell Cardiol* 48, 379-386.
414. Garbino A and Wehrens XH (2010). Emerging role of junctophilin-2 as a regulator of calcium handling in the heart. *Acta Pharmacol Sin* 31, 1019-1021.
415. Nishi M, Mizushima A, Nakagawara K and Takeshima H (2000). Characterization of human junctophilin subtype genes. *Biochem Biophys Res Commun* 273, 920-927.
416. Beavers DL, Landstrom AP, Chiang DY and Wehrens XH (2014). Emerging roles of junctophilin-2 in the heart and implications for cardiac diseases. *Cardiovasc Res* 103, 198-205.
417. Landstrom AP, Kellen CA, Dixit SS, van Oort RJ, Garbino A, Weisleder N, Ma J, Wehrens XH and Ackerman MJ (2011). Junctophilin-2 expression silencing causes cardiocyte hypertrophy and abnormal intracellular calcium-handling. *Circ Heart Fail* 4, 214-223.
418. Minamisawa S, Oshikawa J, Takeshima H, Hoshijima M, Wang Y, Chien KR, Ishikawa Y and Matsuoka R (2004). Junctophilin type 2 is associated with caveolin-3 and is down-regulated in the hypertrophic and dilated cardiomyopathies. *Biochem Biophys Res Commun* 325, 852-856.
419. van Oort RJ, Garbino A, Wang W, Dixit SS, Landstrom AP, Gaur N, De Almeida AC, Skapura DG, Rudy Y, Burns AR, Ackerman MJ and Wehrens XH (2011). Disrupted junctional membrane complexes and hyperactive ryanodine receptors after acute junctophilin knockdown in mice. *Circulation* 123, 979-988.
420. Wagner E, Lauterbach MA, Kohl T, Westphal V, Williams GS, Steinbrecher JH, Streich JH, Korff B, Tuan HT, Hagen B, Luther S, Hasenfuss G, Parlitz U, Jafri MS, Hell SW, Lederer WJ and Lehnart SE (2012). Stimulated emission depletion live-cell super-

- resolution imaging shows proliferative remodeling of T-tubule membrane structures after myocardial infarction. *Circ Res* 111, 402-414.
421. Brandenburg S, Pawlowitz J, Eikenbusch B, Peper J, Kohl T, Mitronova GY, Sossalla S, Hasenfuss G, Wehrens XH, Kohl P, Rog-Zielinska EA and Lehnart SE (2019). Junctophilin-2 expression rescues atrial dysfunction through polyadic junctional membrane complex biogenesis. *JCI Insight* 4, e127116.
 422. Reynolds JO, Chiang DY, Wang W, Beavers DL, Dixit SS, Skapura DG, Landstrom AP, Song LS, Ackerman MJ and Wehrens XH (2013). Junctophilin-2 is necessary for T-tubule maturation during mouse heart development. *Cardiovasc Res* 100, 44-53.
 423. Landstrom AP, Weisleder N, Batalden KB, Bos JM, Tester DJ, Ommen SR, Wehrens XH, Claycomb WC, Ko JK, Hwang M, Pan Z, Ma J and Ackerman MJ (2007). Mutations in JPH2-encoded junctophilin-2 associated with hypertrophic cardiomyopathy in humans. *J Mol Cell Cardiol* 42, 1026-1035.
 424. Beavers DL, Wang W, Ather S, Voigt N, Garbino A, Dixit SS, Landstrom AP, Li N, Wang Q, Olivotto I, Dobrev D, Ackerman MJ and Wehrens XHT (2013). Mutation E169K in junctophilin-2 causes atrial fibrillation due to impaired RyR2 stabilization. *J Am Coll Cardiol* 62, 2010-2019.
 425. Llach A, Mazevet M, Mateo P, Villejouvert O, Ridoux A, Rucker-Martin C, Ribeiro M, Fischmeister R, Crozatier B, Benitah JP, Morel E and Gómez AM (2019). Progression of excitation-contraction coupling defects in doxorubicin cardiotoxicity. *J Mol Cell Cardiol* 126, 129-139.
 426. Wang YX and Korth M (1995). Effects of doxorubicin on excitation-contraction coupling in guinea pig ventricular myocardium. *Circ Res* 76, 645-653.
 427. Ondrias K, Borgatta L, Kim DH and Ehrlich BE (1990). Biphasic effects of doxorubicin on the calcium release channel from sarcoplasmic reticulum of cardiac muscle. *Circ Res* 67, 1167-1174.
 428. Altomare C, Lodrini AM, Milano G, Biemmi V, Lazzarini E, Bolis S, Pernigoni N, Torre E, Arici M, Ferrandi M, Barile L, Rocchetti M and Vassalli G (2021). Structural and electrophysiological changes in a model of cardiotoxicity induced by anthracycline combined with trastuzumab. *Front Physiol* 12, 658790.
 429. Keung EC, Toll L, Ellis M and Jensen RA (1991). L-type cardiac calcium channels in doxorubicin cardiomyopathy in rats morphological, biochemical, and functional correlations. *J Clin Invest* 87, 2108-2113.
 430. Li X, Xu G, Wei S, Zhang B, Yao H, Chen Y, Liu W, Wang B, Zhao J and Gao Y (2019). Lingguizhugan decoction attenuates doxorubicin-induced heart failure in rats by improving TT-SR microstructural remodeling. *BMC Complement Altern Med* 19, 360.

431. Olson RD, Gambliel HA, Vestal RE, Shadle SE, Charlier HA, Jr. and Cusack BJ (2005). Doxorubicin cardiac dysfunction: effects on calcium regulatory proteins, sarcoplasmic reticulum, and triiodothyronine. *Cardiovasc Toxicol* 5, 269-283.
432. Gambliel HA, Burke BE, Cusack BJ, Walsh GM, Zhang YL, Mushlin PS and Olson RD (2002). Doxorubicin and C-13 deoxydoxorubicin effects on ryanodine receptor gene expression. *Biochem Biophys Res Commun* 291, 433-438.
433. Baines CP, Zhang J, Wang GW, Zheng YT, Xiu JX, Cardwell EM, Bolli R and Ping P (2002). Mitochondrial PKCepsilon and MAPK form signaling modules in the murine heart: enhanced mitochondrial PKCepsilon-MAPK interactions and differential MAPK activation in PKCepsilon-induced cardioprotection. *Circ Res* 90, 390-397.
434. Polster BM, Basañez G, Etxebarria A, Hardwick JM and Nicholls DG (2005). Calpain I induces cleavage and release of apoptosis-inducing factor from isolated mitochondria. *J Biol Chem* 280, 6447-6454.
435. Omura S, Iwai Y, Hirano A, Nakagawa A, Awaya J, Tsuchya H, Takahashi Y and Masuma R (1977). A new alkaloid AM-2282 OF *Streptomyces* origin. Taxonomy, fermentation, isolation and preliminary characterization. *J Antibiot (Tokyo)* 30, 275-282.
436. Chae HJ, Kang JS, Byun JO, Han KS, Kim DU, Oh SM, Kim HM, Chae SW and Kim HR (2000). Molecular mechanism of staurosporine-induced apoptosis in osteoblasts. *Pharmacol Res* 42, 373-381.
437. Verma RP and Hansch C (2007). Matrix metalloproteinases (MMPs): chemical-biological functions and (Q)SARs. *Bioorg Med Chem* 15, 2223-2268.
438. Bassiouni W, Ali MAM and Schulz R (2021). Multifunctional intracellular matrix metalloproteinases: implications in disease. *FEBS J*.
439. Stammers AN, Susser SE, Hamm NC, Hlynsky MW, Kimber DE, Kehler DS and Duhamel TA (2015). The regulation of sarco(endo)plasmic reticulum calcium-ATPases (SERCA). *Can J Physiol Pharmacol* 93, 843-854.
440. Johansson AC, Steen H, Ollinger K and Roberg K (2003). Cathepsin D mediates cytochrome c release and caspase activation in human fibroblast apoptosis induced by staurosporine. *Cell Death Differ* 10, 1253-1259.
441. Olguín-Albuerne M, Domínguez G and Morán J (2014). Effect of staurosporine in the morphology and viability of cerebellar astrocytes: role of reactive oxygen species and NADPH oxidase. *Oxid Med Cell Longev* 2014, 678371.
442. Sasaki T, Kishi M, Saito M, Tanaka T, Higuchi N, Kominami E, Katunuma N and Murachi T (1990). Inhibitory effect of di- and tripeptidyl aldehydes on calpains and cathepsins. *J Enzyme Inhib* 3, 195-201.

443. Ali MA, Stepanko A, Fan X, Holt A and Schulz R (2012). Calpain inhibitors exhibit matrix metalloproteinase-2 inhibitory activity. *Biochem Biophys Res Commun* 423, 1-5.
444. Ali MA, Kandasamy AD, Fan X and Schulz R (2013). Hydrogen peroxide-induced necrotic cell death in cardiomyocytes is independent of matrix metalloproteinase-2. *Toxicol In Vitro* 27, 1686-1692.
445. Li F, Leier A, Liu Q, Wang Y, Xiang D, Akutsu T, Webb GI, Smith AI, Marquez-Lago T, Li J and Song J (2020). Procleave: predicting protease-specific substrate cleavage sites by combining sequence and structural information. *Genomics Proteomics Bioinformatics* 18, 52-64.
446. Musaogullari A, Mandato A and Chai YC (2020). Role of glutathione depletion and reactive oxygen species generation on caspase-3 activation: a study with the kinase inhibitor staurosporine. *Front Physiol* 11, 998.
447. Olguín-Albuerne M, Ramos-Pittol JM, Coyoy A, Martínez-Briseño CP, Domínguez G and Morán J (2016). Peroxynitrite is involved in the apoptotic death of cultured cerebellar granule neurons induced by staurosporine, but not by potassium deprivation. *Neurochem Res* 41, 316-327.
448. Yang Y, Candelario-Jalil E, Thompson JF, Cuadrado E, Estrada EY, Rosell A, Montaner J and Rosenberg GA (2010). Increased intranuclear matrix metalloproteinase activity in neurons interferes with oxidative DNA repair in focal cerebral ischemia. *J Neurochem* 112, 134-149.
449. Cao G, Xing J, Xiao X, Liou AK, Gao Y, Yin XM, Clark RS, Graham SH and Chen J (2007). Critical role of calpain I in mitochondrial release of apoptosis-inducing factor in ischemic neuronal injury. *J Neurosci* 27, 9278-9293.
450. Wang Y, Kim NS, Li X, Greer PA, Koehler RC, Dawson VL and Dawson TM (2009). Calpain activation is not required for AIF translocation in PARP-1-dependent cell death (parthanatos). *J Neurochem* 110, 687-696.
451. Andrabi SA, Dawson TM and Dawson VL (2008). Mitochondrial and nuclear cross talk in cell death: parthanatos. *Ann N Y Acad Sci* 1147, 233-241.
452. Mashimo M, Onishi M, Uno A, Tanimichi A, Nobeyama A, Mori M, Yamada S, Negi S, Bu X, Kato J, Moss J, Sanada N, Kizu R and Fujii T (2020). The 89-kDa PARP1 cleavage fragment serves as a cytoplasmic PAR carrier to induce AIF-mediated apoptosis. *J Biol Chem* 296, 100046.
453. Wang J and Zhou H (2020). Mitochondrial quality control mechanisms as molecular targets in cardiac ischemia-reperfusion injury. *Acta Pharm Sin B* 10, 1866-1879.
454. Disatnik MH, Ferreira JC, Campos JC, Gomes KS, Dourado PM, Qi X and Mochly-Rosen D (2013). Acute inhibition of excessive mitochondrial fission after myocardial infarction prevents long-term cardiac dysfunction. *J Am Heart Assoc* 2, e000461.

455. Yang Y, Zhao L and Ma J (2017). Penethylidene hydrochloride preconditioning provides cardiac protection in a rat model of myocardial ischemia/reperfusion injury via the mechanism of mitochondrial dynamics mechanism. *Eur J Pharmacol* 813, 130-139.
456. Uchikado Y, Ikeda Y and Ohishi M (2022). Current understanding of the pivotal role of mitochondrial dynamics in cardiovascular diseases and senescence. *Front Cardiovasc Med* 9, 905072.
457. Chen Q, Thompson J, Hu Y, Dean J and Lesnefsky EJ (2019). Inhibition of the ubiquitous calpains protects complex I activity and enables improved mitophagy in the heart following ischemia-reperfusion. *Am J Physiol Cell Physiol* 317, C910-921.
458. Chen M, He H, Zhan S, Krajewski S, Reed JC and Gottlieb RA (2001). Bid is cleaved by calpain to an active fragment in vitro and during myocardial ischemia/reperfusion. *J Biol Chem* 276, 30724-30728.
459. Chen Q, Paillard M, Gomez L, Ross T, Hu Y, Xu A and Lesnefsky EJ (2011). Activation of mitochondrial μ -calpain increases AIF cleavage in cardiac mitochondria during ischemia-reperfusion. *Biochem Biophys Res Commun* 415, 533-538.
460. Wang W, Zhang F, Li L, Tang F, Siedlak SL, Fujioka H, Liu Y, Su B, Pi Y and Wang X (2015). MFN2 couples glutamate excitotoxicity and mitochondrial dysfunction in motor neurons. *J Biol Chem* 290, 168-182.
461. Shan S, Liu Z, Li L, Zhang C, Kou R and Song F (2022). Calpain-mediated cleavage of mitochondrial fusion/fission proteins in acetaminophen-induced mice liver injury. *Hum Exp Toxicol* 41, 9603271221108321.
462. Latz E, Xiao TS and Stutz A (2013). Activation and regulation of the inflammasomes. *Nat Rev Immunol* 13, 397-411.
463. Perry CG, Kane DA, Lanza IR and Neuffer PD (2013). Methods for assessing mitochondrial function in diabetes. *Diabetes* 62, 1041-1053.
464. Rossello X, Hall AR, Bell RM and Yellon DM (2016). Characterization of the Langendorff perfused isolated mouse heart model of global ischemia-reperfusion injury: impact of ischemia and reperfusion length on infarct size and LDH release. *J Cardiovasc Pharmacol Ther* 21, 286-295.
465. Kuznetsov AV, Veksler V, Gellerich FN, Saks V, Margreiter R and Kunz WS (2008). Analysis of mitochondrial function in situ in permeabilized muscle fibers, tissues and cells. *Nat Protoc* 3, 965-976.
466. Berman HM, Battistuz T, Bhat TN, Bluhm WF, Bourne PE, Burkhardt K, Feng Z, Gilliland GL, Iype L, Jain S, Fagan P, Marvin J, Padilla D, Ravichandran V, Schneider B, Thanki N, Weissig H, Westbrook JD and Zardecki C (2002). The protein data bank. *Acta Crystallogr D Biol Crystallogr* 58, 899-907.

467. Biasini M, Bienert S, Waterhouse A, Arnold K, Studer G, Schmidt T, Kiefer F, Gallo Cassarino T, Bertoni M, Bordoli L and Schwede T (2014). SWISS-MODEL: modelling protein tertiary and quaternary structure using evolutionary information. *Nucleic Acids Res* 42, W252-258.
468. Jumper J, Evans R, Pritzel A, Green T, Figurnov M, Ronneberger O, Tunyasuvunakool K, Bates R, Žídek A, Potapenko A, Bridgland A, Meyer C, Kohl SAA, Ballard AJ, Cowie A, Romera-Paredes B, Nikolov S, Jain R, Adler J, Back T, Petersen S, Reiman D, Clancy E, Zielinski M, Steinegger M, Pacholska M, Berghammer T, Bodenstein S, Silver D, Vinyals O, Senior AW, Kavukcuoglu K, Kohli P and Hassabis D (2021). Highly accurate protein structure prediction with AlphaFold. *Nature* 596, 583-589.
469. Eckhard U, Huesgen PF, Schilling O, Bellac CL, Butler GS, Cox JH, Dufour A, Goebeler V, Kappelhoff R, Keller UAD, Klein T, Lange PF, Marino G, Morrison CJ, Prudova A, Rodriguez D, Starr AE, Wang Y and Overall CM (2016). Active site specificity profiling of the matrix metalloproteinase family: proteomic identification of 4300 cleavage sites by nine MMPs explored with structural and synthetic peptide cleavage analyses. *Matrix Biol* 49, 37-60.
470. Hom J and Sheu SS (2009). Morphological dynamics of mitochondria- a special emphasis on cardiac muscle cells. *J Mol Cell Cardiol* 46, 811-820.
471. Spinelli JB and Haigis MC (2018). The multifaceted contributions of mitochondria to cellular metabolism. *Nat Cell Biol* 20, 745-754.
472. Murphy E and Steenbergen C (2008). Mechanisms underlying acute protection from cardiac ischemia-reperfusion injury. *Physiol Rev* 88, 581-609.
473. Raturi A and Simmen T (2013). Where the endoplasmic reticulum and the mitochondrion tie the knot: the mitochondria-associated membrane (MAM). *Biochim Biophys Acta* 1833, 213-224.
474. Liu Q, Zhang D, Hu D, Zhou X and Zhou Y (2018). The role of mitochondria in NLRP3 inflammasome activation. *Mol Immunol* 103, 115-124.
475. Kanneganti TD, Ozören N, Body-Malapel M, Amer A, Park JH, Franchi L, Whitfield J, Barchet W, Colonna M, Vandenabeele P, Bertin J, Coyle A, Grant EP, Akira S and Núñez G (2006). Bacterial RNA and small antiviral compounds activate caspase-1 through cryopyrin/Nalp3. *Nature* 440, 233-236.
476. Mariathasan S, Weiss DS, Newton K, McBride J, O'Rourke K, Roose-Girma M, Lee WP, Weinrauch Y, Monack DM and Dixit VM (2006). Cryopyrin activates the inflammasome in response to toxins and ATP. *Nature* 440, 228-232.
477. Liu X, Li M, Chen Z, Yu Y, Shi H, Yu Y, Wang Y, Chen R and Ge J (2022). Mitochondrial calpain-1 activates NLRP3 inflammasome by cleaving ATP5A1 and inducing mitochondrial ROS in CVB3-induced myocarditis. *Basic Res Cardiol* 117, 40.

478. Usui F, Shirasuna K, Kimura H, Tatsumi K, Kawashima A, Karasawa T, Yoshimura K, Aoki H, Tsutsui H, Noda T, Sagara J, Taniguchi S and Takahashi M (2015). Inflammasome activation by mitochondrial oxidative stress in macrophages leads to the development of angiotensin II-induced aortic aneurysm. *Arterioscler Thromb Vasc Biol* 35, 127-136.
479. Zhang X, Hong S, Qi S, Liu W, Zhang X, Shi Z, Chen W, Zhao M and Yin X (2019). NLRP3 inflammasome is involved in calcium-sensing receptor-induced aortic remodeling in SHR. *Mediators Inflamm* 2019, 6847087.
480. Liu W, Zhang X, Zhao M, Zhang X, Chi J, Liu Y, Lin F, Fu Y, Ma D and Yin X (2015). Activation in M1 but not M2 macrophages contributes to cardiac remodeling after myocardial infarction in rats: a critical role of the calcium sensing receptor/NLRP3 inflammasome. *Cell Physiol Biochem* 35, 2483-2500.
481. Olmedo I, Pino G, Riquelme JA, Aranguiz P, Díaz MC, López-Crisosto C, Lavandero S, Donoso P, Pedrozo Z and Sánchez G (2020). Inhibition of the proteasome preserves Mitofusin-2 and mitochondrial integrity, protecting cardiomyocytes during ischemia-reperfusion injury. *Biochim Biophys Acta Mol Basis Dis* 1866, 165659.
482. Dong G, Chen T, Ren X, Zhang Z, Huang W, Liu L, Luo P and Zhou H (2016). Rg1 prevents myocardial hypoxia/reoxygenation injury by regulating mitochondrial dynamics imbalance via modulation of glutamate dehydrogenase and mitofusin 2. *Mitochondrion* 26, 7-18.
483. Thai PN, Seidlmayer LK, Miller C, Ferrero M, Dorn GW, II, Schaefer S, Bers DM and Dedkova EN (2019). Mitochondrial quality control in aging and heart failure: influence of ketone bodies and mitofusin-stabilizing peptides. *Front Physiol* 10, 382.
484. Wu QR, Zheng DL, Liu PM, Yang H, Li LA, Kuang SJ, Lai YY, Rao F, Xue YM, Lin JJ, Liu SX, Chen CB and Deng CY (2021). High glucose induces Drp1-mediated mitochondrial fission via the Orail calcium channel to participate in diabetic cardiomyocyte hypertrophy. *Cell Death Dis* 12, 216.
485. Ong SB, Subrayan S, Lim SY, Yellon DM, Davidson SM and Hausenloy DJ (2010). Inhibiting mitochondrial fission protects the heart against ischemia/reperfusion injury. *Circulation* 121, 2012-2022.
486. Chen Y, Liu Y and Dorn GW, 2nd (2011). Mitochondrial fusion is essential for organelle function and cardiac homeostasis. *Circ Res* 109, 1327-1331.
487. Ainbinder A, Boncompagni S, Protasi F and Dirksen RT (2015). Role of mitofusin-2 in mitochondrial localization and calcium uptake in skeletal muscle. *Cell Calcium* 57, 14-24.
488. Adebayo M, Singh S, Singh AP and Dasgupta S (2021). Mitochondrial fusion and fission: the fine-tune balance for cellular homeostasis. *Faseb J* 35, e21620.
489. Hom J, Yu T, Yoon Y, Porter G and Sheu SS (2010). Regulation of mitochondrial fission by intracellular Ca²⁺ in rat ventricular myocytes. *Biochim Biophys Acta* 1797, 913-921.

490. Toldo S, Mezzaroma E, Mauro AG, Salloum F, Van Tassell BW and Abbate A (2015). The inflammasome in myocardial injury and cardiac remodeling. *Antioxid Redox Signal* 22, 1146-1161.
491. Perri ER, Thomas CJ, Parakh S, Spencer DM and Atkin JD (2015). The unfolded protein response and the role of protein disulfide isomerase in neurodegeneration. *Front Cell Dev Biol* 3, 80.
492. Hetz C (2012). The unfolded protein response: controlling cell fate decisions under ER stress and beyond. *Nat Rev Mol Cell Biol* 13, 89-102.
493. Mori K (2009). Signalling pathways in the unfolded protein response: development from yeast to mammals. *J Biochem* 146, 743-750.
494. Almanza A, Carlesso A, Chintla C, Creedican S, Doultzinos D, Leuzzi B, Luís A, McCarthy N, Montibeller L, More S, Papaioannou A, Püschel F, Sassano ML, Skoko J, Agostinis P, de Belleruche J, Eriksson LA, Fulda S, Gorman AM, Healy S, Kozlov A, Muñoz-Pinedo C, Rehm M, Chevet E and Samali A (2019). Endoplasmic reticulum stress signalling - from basic mechanisms to clinical applications. *Febs J* 286, 241-278.
495. Simmen T, Lynes EM, Gesson K and Thomas G (2010). Oxidative protein folding in the endoplasmic reticulum: tight links to the mitochondria-associated membrane (MAM). *Biochim Biophys Acta* 1798, 1465-1473.
496. Bassiouni W, Valencia R, Mahmud Z, Seubert JM and Schulz R (2023). Matrix metalloproteinase-2 proteolyzes mitofusin-2 and impairs mitochondrial function during myocardial ischemia-reperfusion injury. *Basic Res Cardiol* 118, 29.
497. Sanches M, Duffy NM, Talukdar M, Thevakumaran N, Chiovitti D, Canny MD, Lee K, Kurinov I, Uehling D, Al-awar R, Poda G, Prakesch M, Wilson B, Tam V, Schweitzer C, Toro A, Lucas JL, Vuga D, Lehmann L, Durocher D, Zeng Q, Patterson JB and Sicheri F (2014). Structure and mechanism of action of the hydroxy-aryl-aldehyde class of IRE1 endoribonuclease inhibitors. *Nat Commun* 5, 4202.
498. Cuanalo-Contreras K, Schulz J, Mukherjee A, Park KW, Armijo E and Soto C (2022). Extensive accumulation of misfolded protein aggregates during natural aging and senescence. *Front Aging Neurosci* 14, 1090109.
499. Malhotra JD and Kaufman RJ (2007). Endoplasmic reticulum stress and oxidative stress: a vicious cycle or a double-edged sword? *Antioxid Redox Signal* 9, 2277-2293.
500. Jin JK, Blackwood EA, Azizi K, Thuerauf DJ, Fahem AG, Hofmann C, Kaufman RJ, Doroudgar S and Glembotski CC (2017). ATF6 decreases myocardial ischemia/reperfusion damage and links ER stress and oxidative stress signaling pathways in the heart. *Circ Res* 120, 862-875.
501. Bi X, Zhang G, Wang X, Nguyen C, May HI, Li X, Al-Hashimi AA, Austin RC, Gillette TG, Fu G, Wang ZV and Hill JA (2018). Endoplasmic reticulum chaperone GRP78

- protects heart from ischemia/reperfusion injury through Akt activation. *Circ Res* 122, 1545-1554.
502. Tian F, Zhou X, Wikström J, Karlsson H, Sjöland H, Gan LM, Borén J and Akyürek LM (2009). Protein disulfide isomerase increases in myocardial endothelial cells in mice exposed to chronic hypoxia: a stimulatory role in angiogenesis. *Am J Physiol Heart Circ Physiol* 297, H1078-1086.
503. Shemorry A, Harnoss JM, Guttman O, Marsters SA, Kőmúves LG, Lawrence DA and Ashkenazi A (2019). Caspase-mediated cleavage of IRE1 controls apoptotic cell commitment during endoplasmic reticulum stress. *Elife* 8, e47084.
504. Castro MM, Fuah J, Ali M, Sung M, Schulz J, Kondo MY, Fan X, Holt A and Schulz R (2013). Inhibitory effects of caspase inhibitors on the activity of matrix metalloproteinase-2. *Biochem Pharmacol* 86, 469-475.
505. Lin JH, Li H, Yasumura D, Cohen HR, Zhang C, Panning B, Shokat KM, Lavail MM and Walter P (2007). IRE1 signaling affects cell fate during the unfolded protein response. *Science* 318, 944-949.
506. Steiger D, Yokota T, Li J, Ren S, Minamisawa S and Wang Y (2018). The serine/threonine-protein kinase/endoribonuclease IRE1 α protects the heart against pressure overload-induced heart failure. *J Biol Chem* 293, 9652-9661.
507. Lee JG, Dahi S, Mahimkar R, Tulloch NL, Alfonso-Jaume MA, Lovett DH and Sarkar R (2005). Intronic regulation of matrix metalloproteinase-2 revealed by in vivo transcriptional analysis in ischemia. *Proc Natl Acad Sci U S A* 102, 16345-16350.
508. Liu Y, Zhang H, Yan L, Du W, Zhang M, Chen H, Zhang L, Li G, Li J, Dong Y and Zhu D (2018). MMP-2 and MMP-9 contribute to the angiogenic effect produced by hypoxia/15-HETE in pulmonary endothelial cells. *J Mol Cell Cardiol* 121, 36-50.
509. He G (2010). Electron paramagnetic resonance oximetry and redoximetry. *Methods Mol Biol* 594, 85-105.
510. Rutkowski DT, Arnold SM, Miller CN, Wu J, Li J, Gunnison KM, Mori K, Sadighi Akha AA, Raden D and Kaufman RJ (2006). Adaptation to ER stress is mediated by differential stabilities of pro-survival and pro-apoptotic mRNAs and proteins. *PLoS Biol* 4, e374.
511. Han J, Back SH, Hur J, Lin YH, Gildersleeve R, Shan J, Yuan CL, Krokowski D, Wang S, Hatzoglou M, Kilberg MS, Sartor MA and Kaufman RJ (2013). ER-stress-induced transcriptional regulation increases protein synthesis leading to cell death. *Nat Cell Biol* 15, 481-490.
512. Lahiri SK, Quick AP, Samson-Couterie B, Hulsurkar M, Elzenaar I, van Oort RJ and Wehrens XHT (2020). Nuclear localization of a novel calpain-2 mediated junctophilin-2 C-terminal cleavage peptide promotes cardiomyocyte remodeling. *Basic Research in Cardiology* 115, 49.

513. Mitra N, Sinha S, Ramya TN and Suroolia A (2006). N-linked oligosaccharides as outfitters for glycoprotein folding, form and function. *Trends Biochem Sci* 31, 156-163.
514. Lee HS, Qi Y and Im W (2015). Effects of N-glycosylation on protein conformation and dynamics: protein Data Bank analysis and molecular dynamics simulation study. *Sci Rep* 5, 8926.
515. Lis H and Sharon N (1993). Protein glycosylation. Structural and functional aspects. *Eur J Biochem* 218, 1-27.
516. Ednie AR, Deng W, Yip KP and Bennett ES (2019). Reduced myocyte complex N-glycosylation causes dilated cardiomyopathy. *Faseb J* 33, 1248-1261.
517. Johansen PB (1981). Doxorubicin pharmacokinetics after intravenous and intraperitoneal administration in the nude mouse. *Cancer Chemother Pharmacol* 5, 267-270.
518. Barpe DR, Rosa DD and Froehlich PE (2010). Pharmacokinetic evaluation of doxorubicin plasma levels in normal and overweight patients with breast cancer and simulation of dose adjustment by different indexes of body mass. *Eur J Pharm Sci* 41, 458-463.
519. Castro MM, Rizzi E, Figueiredo-Lopes L, Fernandes K, Bendhack LM, Pitol DL, Gerlach RF and Tanus-Santos JE (2008). Metalloproteinase inhibition ameliorates hypertension and prevents vascular dysfunction and remodeling in renovascular hypertensive rats. *Atherosclerosis* 198, 320-331.
520. Hariya A, Takazawa K, Yamamoto T and Amano A (2004). ONO-4817, a novel matrix metalloproteinase inhibitor, attenuates allograft vasculopathy in a rat cardiac transplant. *J Heart Lung Transplant* 23, 1163-1169.
521. Kumar S, Ratnikov BI, Kazanov MD, Smith JW and Cieplak P (2015). CleavPredict: a platform for reasoning about matrix metalloproteinases proteolytic events. *PLoS One* 10, e0127877.
522. Rodrigues JP, Levitt M and Chopra G (2012). KoBaMIN: a knowledge-based minimization web server for protein structure refinement. *Nucleic Acids Res* 40, W323-328.
523. Lüthy R, Bowie JU and Eisenberg D (1992). Assessment of protein models with three-dimensional profiles. *Nature* 356, 83-85.
524. Bazan C, Torres Barba D, Blomgren P and Paolini P (2011). Image processing techniques for assessing contractility in isolated neonatal cardiac myocytes. *Int J Biomed Imaging* 2011, 729732.
525. Lahiri SK, Quick AP, Samson-Couterie B, Hulsurkar M, Elzenaar I, van Oort RJ and Wehrens XHT (2020). Nuclear localization of a novel calpain-2 mediated junctophilin-2 C-terminal cleavage peptide promotes cardiomyocyte remodeling. *Basic Res Cardiol* 115, 49.

526. Guo A, Hall D, Zhang C, Peng T, Miller JD, Kutschke W, Grueter CE, Johnson FL, Lin RZ and Song LS (2015). Molecular determinants of calpain-dependent cleavage of junctophilin-2 protein in cardiomyocytes. *J Biol Chem* 290, 17946-17955.
527. Kandasamy AD, Chow AK, Ali MA and Schulz R (2010). Matrix metalloproteinase-2 and myocardial oxidative stress injury: beyond the matrix. *Cardiovasc Res* 85, 413-423.
528. Guo A, Wang Y, Chen B, Wang Y, Yuan J, Zhang L, Hall D, Wu J, Shi Y, Zhu Q, Chen C, Thiel WH, Zhan X, Weiss RM, Zhan F, Musselman CA, Pufall M, Zhu W, Au KF, Hong J, Anderson ME, Grueter CE and Song LS (2018). E-C coupling structural protein junctophilin-2 encodes a stress-adaptive transcription regulator. *Science* 362, eaan3303.
529. Chen B, Guo A, Zhang C, Chen R, Zhu Y, Hong J, Kutschke W, Zimmerman K, Weiss RM, Zingman L, Anderson ME, Wehrens XH and Song LS (2013). Critical roles of junctophilin-2 in T-tubule and excitation-contraction coupling maturation during postnatal development. *Cardiovasc Res* 100, 54-62.
530. Wu HD, Xu M, Li RC, Guo L, Lai YS, Xu SM, Li SF, Lü QL, Li LL, Zhang HB, Zhang YY, Zhang CM and Wang SQ (2012). Ultrastructural remodelling of Ca²⁺ signalling apparatus in failing heart cells. *Cardiovasc Res* 95, 430-438.
531. Wallace KB, Sardão VA and Oliveira PJ (2020). Mitochondrial determinants of doxorubicin-induced cardiomyopathy. *Circ Res* 126, 926-941.
532. Montaine D, Marechal X, Preau S, Baccouch R, Modine T, Fayad G, Lancel S and Nevriere R (2011). Doxorubicin induces mitochondrial permeability transition and contractile dysfunction in the human myocardium. *Mitochondrion* 11, 22-26.
533. Prisco SZ, Hartweck LM, Kazmirczak F, Mendelson JB, Deng SL, Lahiri SK, Wehrens XHT and Prins KW (2023). Junctophilin-2 regulates mitochondrial metabolism. *bioRxiv*.
534. Sheibani M, Azizi Y, Shayan M, Nezamoleslami S, Eslami F, Farjoo MH and Dehpour AR (2022). Doxorubicin-induced cardiotoxicity: an overview on pre-clinical therapeutic approaches. *Cardiovasc Toxicol* 22, 292-310.
535. Bøtker HE, Cabrera-Fuentes HA, Ruiz-Meana M, Heusch G and Ovize M (2020). Translational issues for mitoprotective agents as adjunct to reperfusion therapy in patients with ST-segment elevation myocardial infarction. *J Cell Mol Med* 24, 2717-2729.
536. Ramachandra CJA, Hernandez-Resendiz S, Crespo-Avilan GE, Lin YH and Hausenloy DJ (2020). Mitochondria in acute myocardial infarction and cardioprotection. *EBioMedicine* 57, 102884.
537. Davidson SM, Ferdinandy P, Andreadou I, Bøtker HE, Heusch G, Ibáñez B, Ovize M, Schulz R, Yellon DM, Hausenloy DJ and Garcia-Dorado D (2019). Multitarget strategies to reduce myocardial ischemia/reperfusion injury: JACC review topic of the week. *J Am Coll Cardiol* 73, 89-99.

538. Zhang C, He S, Li Y, Li F, Liu Z, Liu J and Gong J (2017). Bisoprolol protects myocardium cells against ischemia/reperfusion injury by attenuating unfolded protein response in rats. *Sci Rep* 7, 11859.
539. Clemente-Moragón A, Gómez M, Villena-Gutiérrez R, Lalama DV, García-Prieto J, Martínez F, Sánchez-Cabo F, Fuster V, Oliver E and Ibáñez B (2020). Metoprolol exerts a non-class effect against ischaemia-reperfusion injury by abrogating exacerbated inflammation. *Eur Heart J* 41, 4425-4440.
540. Kim GT, Chun YS, Park JW and Kim MS (2003). Role of apoptosis-inducing factor in myocardial cell death by ischemia-reperfusion. *Biochem Biophys Res Commun* 309, 619-624.
541. Boettcher M and McManus MT (2015). Choosing the right tool for the job: RNAi, TALEN, or CRISPR. *Mol Cell* 58, 575-585.
542. Sutherland FJ and Hearse DJ (2000). The isolated blood and perfusion fluid perfused heart. *Pharmacol Res* 41, 613-627.
543. Liao R, Podesser BK and Lim CC (2012). The continuing evolution of the Langendorff and ejecting murine heart: new advances in cardiac phenotyping. *Am J Physiol Heart Circ Physiol* 303, H156-167.
544. Skrzypiec-Spring M, Grotthus B, Szelag A and Schulz R (2007). Isolated heart perfusion according to Langendorff- still viable in the new millennium. *J Pharmacol Toxicol Methods* 55, 113-126.
545. Du XJ (2004). Gender modulates cardiac phenotype development in genetically modified mice. *Cardiovasc Res* 63, 510-519.
546. Ostadal B and Ostadal P (2014). Sex-based differences in cardiac ischaemic injury and protection: therapeutic implications. *Br J Pharmacol* 171, 541-554.
547. Johnson MS, Moore RL and Brown DA (2006). Sex differences in myocardial infarct size are abolished by sarcolemmal KATP channel blockade in rat. *Am J Physiol Heart Circ Physiol* 290, H2644-2647.
548. Booth EA and Lucchesi BR (2008). Estrogen-mediated protection in myocardial ischemia-reperfusion injury. *Cardiovasc Toxicol* 8, 101-113.
549. Fels JA and Manfredi G (2019). Sex differences in ischemia/reperfusion injury: the role of mitochondrial permeability transition. *Neurochem Res* 44, 2336-2345.
550. Givvimani S, Pushpakumar S, Veeranki S and Tyagi SC (2014). Dysregulation of Mfn2 and Drp-1 proteins in heart failure. *Can J Physiol Pharmacol* 92, 583-591.
551. Park SM, Kang TI and So JS (2021). Roles of XBP1s in transcriptional regulation of target genes. *Biomedicines* 9, 791.

552. Beriault DR and Werstuck GH (2013). Detection and quantification of endoplasmic reticulum stress in living cells using the fluorescent compound, thioflavin T. *Biochim Biophys Acta* 1833, 2293-2301.
553. Osowski CM and Urano F (2011). Measuring ER stress and the unfolded protein response using mammalian tissue culture system. *Methods Enzymol* 490, 71-92.
554. Willis MS, Parry TL, Brown DI, Mota RI, Huang W, Beak JY, Sola M, Zhou C, Hicks ST, Caughey MC, D'Agostino RB, Jr., Jordan J, Hundley WG and Jensen BC (2019). Doxorubicin exposure causes subacute cardiac atrophy dependent on the striated muscle-specific ubiquitin ligase MuRF1. *Circ Heart Fail* 12, e005234.
555. Chatterjee K, Zhang J, Honbo N and Karliner JS (2010). Doxorubicin cardiomyopathy. *Cardiology* 115, 155-162.
556. Eppenberger HM, Hertig C and Eppenberger-Eberhardt M (1994). Adult rat cardiomyocytes in culture: a model system to study the plasticity of the differentiated cardiac phenotype at the molecular and cellular levels. *Trends Cardiovasc Med* 4, 187-193.
557. Ehler E, Moore-Morris T and Lange S (2013). Isolation and culture of neonatal mouse cardiomyocytes. *J Vis Exp* 2013, 50154.
558. Moulin M, Piquereau J, Mateo P, Fortin D, Rucker-Martin C, Gressette M, Lefebvre F, Gresikova M, Solgadi A, Veksler V, Garnier A and Ventura-Clapier R (2015). Sexual dimorphism of doxorubicin-mediated cardiotoxicity: potential role of energy metabolism remodeling. *Circ Heart Fail* 8, 98-108.
559. Lounas A, Lebrun A, Laflamme I, Vernoux N, Savage J, Tremblay M, Germain M and Richard FJ (2022). A 3D analysis revealed complex mitochondria morphologies in porcine cumulus cells. *Sci Rep* 12, 15403.
560. Liu J, Li L, Yang Y, Hong B, Chen X, Xie Q and Han H (2020). Automatic reconstruction of mitochondria and endoplasmic reticulum in electron microscopy volumes by deep learning. *Front Neurosci* 14, 599.
561. Takeshima H, Hoshijima M and Song LS (2015). Ca²⁺ microdomains organized by junctophilins. *Cell Calcium* 58, 349-356.
562. Sharp WW, Fang YH, Han M, Zhang HJ, Hong Z, Banathy A, Morrow E, Ryan JJ and Archer SL (2014). Dynamin-related protein 1 (Drp1)-mediated diastolic dysfunction in myocardial ischemia-reperfusion injury: therapeutic benefits of Drp1 inhibition to reduce mitochondrial fission. *Faseb J* 28, 316-326.
563. Gao T, Shi R, Liu Z, De D, Li R, Chen Y, Pei J and Ding M (2023). Ischemia/reperfusion-induced MiD51 upregulation recruits Drp1 to mitochondria and contributes to myocardial injury. *Biochem Biophys Res Commun* 665, 78-87.

Appendix

A.1. Introduction

Mitochondrial quality control mechanisms are the main regulatory processes that protect the mitochondria against cellular dysfunction [225]. They include: mitobiogenesis, mitochondrial dynamics (fusion and fission) and mitophagy, as discussed earlier [226]. They preserve mitochondrial function and ensure that there are enough healthy mitochondria to meet the energy and homeostatic demands of the cell. Therefore, impaired mitochondrial quality control can be associated with cellular dysfunction such that which occurs in cardiac disease [227].

Among these regulatory mechanisms are mitochondrial dynamics which involve fusion and fission. Fusion is the merging of two distinct, partially damaged mitochondria to allow the recycling of undamaged mitochondrial proteins, and is regulated by Mfn-1 and -2 (for outer mitochondrial membrane fusion) and OPA-1 (for inner mitochondrial membrane fusion) [233, 234]. On the other hand, fission is the division of mitochondria into two separate organelles to eliminate the damaged segments, and is regulated by Drp-1 [234]. Finally, mitophagy is the removal of the damaged mitochondria by autophagosome-lysosomal degradation, and is mediated by the interaction of PINK1 with parkin [242].

Myocardial IR injury is associated with mitochondrial dysfunction, as discussed earlier [224]. Failure of mitochondrial quality control to protect the mitochondria will result in accumulation of damaged mitochondria which predisposes cellular dysfunction due to the induction of mPTP opening, increased RONS production and impaired ATP synthesis [218, 246]. Therefore, keeping an optimal balance amongst the mitochondrial quality control proteins is critical to protect the mitochondria and, subsequently, prevent cardiac contractile dysfunction during IR injury.

Here I investigated how specific mitochondrial quality control regulatory proteins are affected during myocardial IR injury and whether the changes in Mfn-2 and Drp-1 in mitochondria are dependent on the duration of ischemia and/or reperfusion. I also investigated whether MMP-2, activated during IR injury, contributes to the associated changes in these proteins.

A.2. Methods

A.2.1. Isolated heart perfusion

Hearts from male C57BL/6J mice were isolated and subjected to *in vitro* IR injury in Langendorff perfusion mode as described in **Chapter 2 (section 2.2)**.

To evaluate the changes in mitochondrial protein levels in IR hearts during a shorter period of ischemia or at early reperfusion, following 40 min of baseline aerobic perfusion, the hearts were subjected to different durations of ischemia and/or reperfusion as follows: 30 min ischemia and 40 min reperfusion (I30-R40), 20 min ischemia and 40 min reperfusion (I20-R40), or 30 min ischemia and 5 min reperfusion (I30-R5), and compared to hearts perfused aerobically for the same durations (110, 100 or 75 min, respectively) as controls.

A.2.2. Preparation of ventricular extracts

Frozen heart ventricles were ground, homogenized and subjected to subcellular fractionation as described in **Chapter 2 (section 2.3)**, to obtain cytosolic or mitochondria-enriched fractions.

A.2.3. Immunoblotting

To measure the level of a protein of interest in cytosolic or mitochondria-enriched fractions obtained from heart ventricles, 30-35 μg total protein was separated on 4-15% SDS-polyacrylamide gels as described in **Chapter 2 (section 2.6)**.

The following primary antibodies were used: anti-Mfn-2 (1:1000, Cat#9482s, Cell Signaling), Drp-1 (1:500, Cat#8570s, Cell Signaling), PINK1 (1:500, Cat#ab23707, Abcam), parkin (1:1000, Cat#2132s, Cell Signaling), α -tubulin (1:2000, Cat#ab7750, Abcam) as a cytosolic fraction loading control, and VDAC (1:1000, Cat#ab14734, Abcam) as a mitochondria-enriched fraction loading control.

A.2.4. Statistics

Data are expressed as the mean \pm SEM of n independent experiments (where n represents an individual mouse heart sample). For multiple comparisons, one-way ANOVA followed by Dunnett's post-hoc test was used. For the comparison of two groups, unpaired student t-test was used (GraphPad Prism version 8, La Jolla, CA, USA). Statistical significance was considered at $p < 0.05$.

A.3. Results

A.3.1. Hearts subjected to shorter ischemia showed improved recovery of cardiac contractile function

Subjecting mouse heart to a shorter ischemic duration of 20 min (compared to 30 min used in most other studies in this thesis) resulted in less reduction in post-ischemic recovery of contractile function (%LVDP baseline 59.26 ± 8.99 , $n=3$) compared to 30 min ischemia (%LVDP

baseline 26.05 ± 4.61 , $n=3$) and similar results were obtained when measuring the rates of contraction and relaxation (**Figure A.1**).

A.3.2. IR-mediated reduction in mitochondrial Mfn-2 level occurs during early reperfusion and with shorter ischemia

To investigate whether Mfn-2 level in mitochondria-enriched fraction is affected by the duration of ischemia or the time of reperfusion. I also measured the level of Mfn-2 in the mitochondria-enriched fractions obtained from hearts perfused for different time points (I20-R40, I30-R40 and I30-R5). In all three IR groups, the level of Mfn-2 in the mitochondria-enriched fraction was significantly reduced in IR hearts compared to the corresponding aerobic controls perfused for the same duration regardless of the time of ischemia or reperfusion ($p < 0.05$) (**Figures A.2 A-C**).

A.3.3. Changes in mitochondrial Drp-1 showed a different pattern than Mfn-2

The pattern of changes in mitochondrial fission protein, Drp-1, was very different than for Mfn-2. While the level of Drp-1 in mitochondria-enriched fractions was significantly reduced in IR hearts subjected to 30 min ischemia and 40 min reperfusion (I30-R40) compared to aerobic controls, its level was significantly upregulated in IR hearts subjected to shorter ischemic duration of 20 min (I20-R40) as well as at 5 min reperfusion after 30 min ischemia (I30-R5) compared to aerobic controls (**Figures A.2 D-F**).

A.3.4. MMP-2 inhibition preserves mitochondrial and cytosolic Drp-1 levels during IR injury

In hearts subjected to 30 min ischemia and 40 min reperfusion, the levels of Drp-1 in both mitochondria-enriched and cytosolic fractions were significantly reduced compared to aerobic controls. These reductions in mitochondrial or cytosolic Drp-1 levels were significantly attenuated by the MMP-2 preferring inhibitors, ARP-100 or ONO-4817 (**Figures A.3 A and B**).

A.3.5. IR induces a reduction in mitochondrial parkin, but not PINK1

In hearts subjected to 30 min ischemia and 40 min reperfusion, there were no significant changes in the level of the mitophagy protein PINK1 in mitochondria-enriched fractions amongst the different groups (**Figure A.4 A**). On the other hand, the level of parkin was significantly reduced in mitochondria-enriched fractions obtained from IR hearts compared to aerobic controls, while the MMP-2 preferring inhibitors, ARP-100 or ONO-4817, attenuated this reduction ($p < 0.05$) (**Figure A.4 B**).

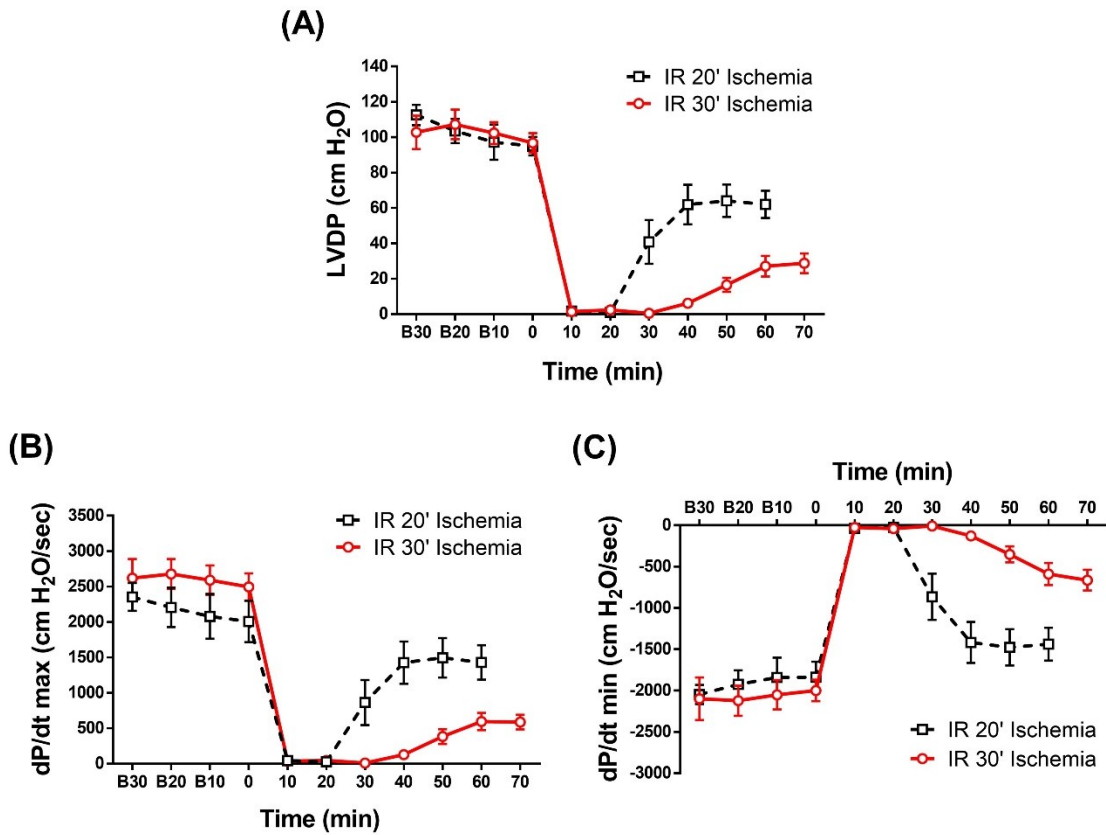


Figure A.1. Cardiac contractile function in hearts subjected to IR injury with different durations of ischemia. Changes in (A) left ventricular developed pressure (LVDP), (B) dP/dt_{max} , or (C) dP/dt_{min} , during IR injury in hearts subjected to 20 or 30 min ischemia followed by 40 min reperfusion ($n=3$ hearts per group).

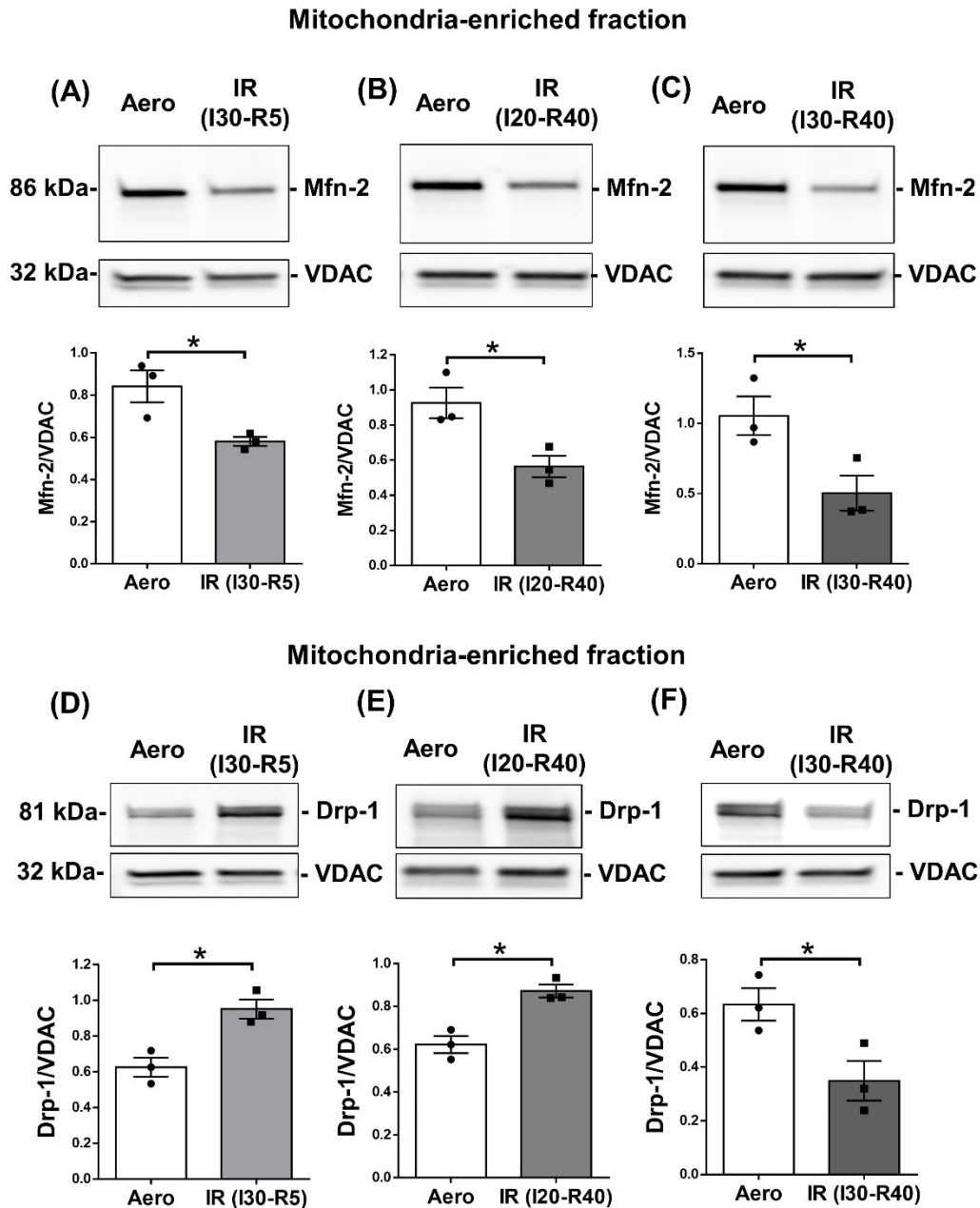


Figure A.2. Changes in mitochondrial Mfn-2 and Drp-1 levels in hearts subjected to different durations of ischemia and/or reperfusion. (A-C) Representative immunoblots (upper panels) and quantitative measurements (lower panels) of Mfn-2 level in mitochondria-enriched fraction from IR hearts perfused for (A) 30 min ischemia/5 min reperfusion (I30-R5), (B) 20 min ischemia/40 min reperfusion (I20-R40) or (C) 30 min ischemia/40 min reperfusion (I30-R40) compared to aerobic control (Aero). (D-F) Representative immunoblots (upper panels) and quantitative measurements (lower panels) of Drp-1 level in mitochondria-enriched fraction from IR hearts perfused for (D) I30-R5, (E) I20-R40 or (F) I30-R40 compared to aerobic control (Aero) (n=3 hearts per group). *p<0.05 vs. the corresponding aerobic group by unpaired student t-test.

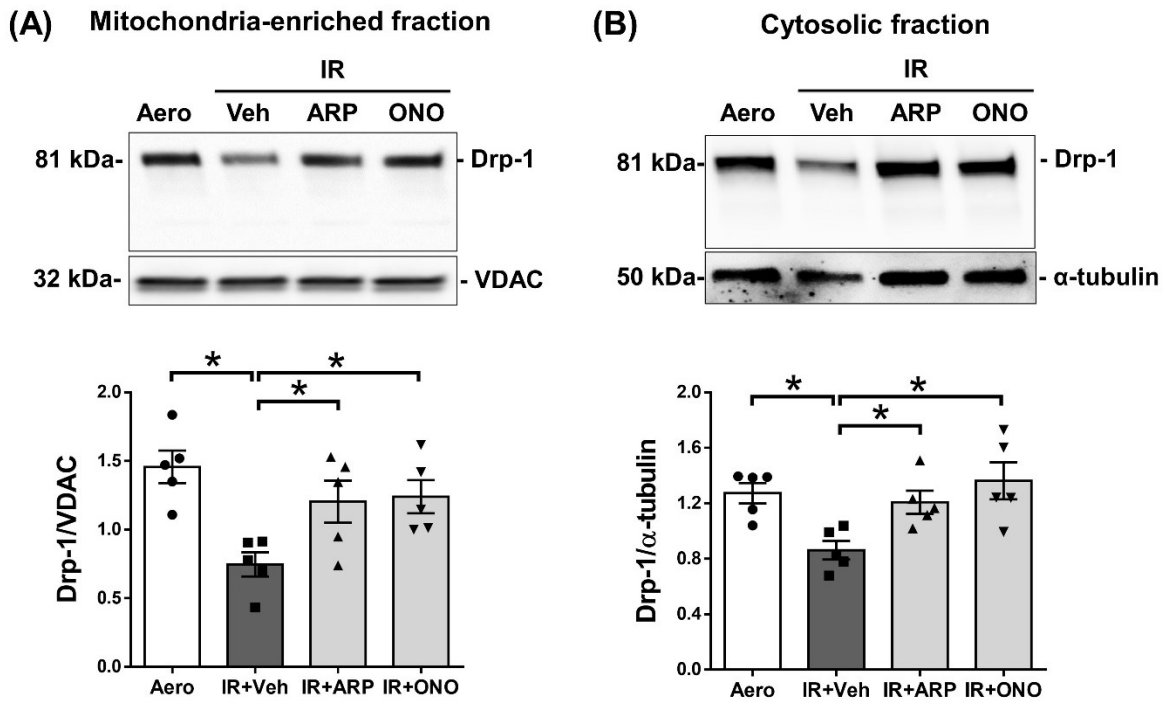


Figure A.3. MMP-2 preferring inhibitors attenuate IR injury-induced reduction in Drp-1 level. Representative immunoblots (upper panels) and quantitative measurements (lower panels) of Drp-1 level in (A) mitochondria-enriched fraction or (B) cytosolic fraction from I30-R40 hearts in absence or presence of ARP-100 (ARP, 10 μ M), ONO-4817 (ONO, 50 μ M) or DMSO vehicle (Veh) compared to aerobic control (Aero) (n=5 hearts per group). *p<0.05 by one-way ANOVA followed by Dunnett's post-hoc test.

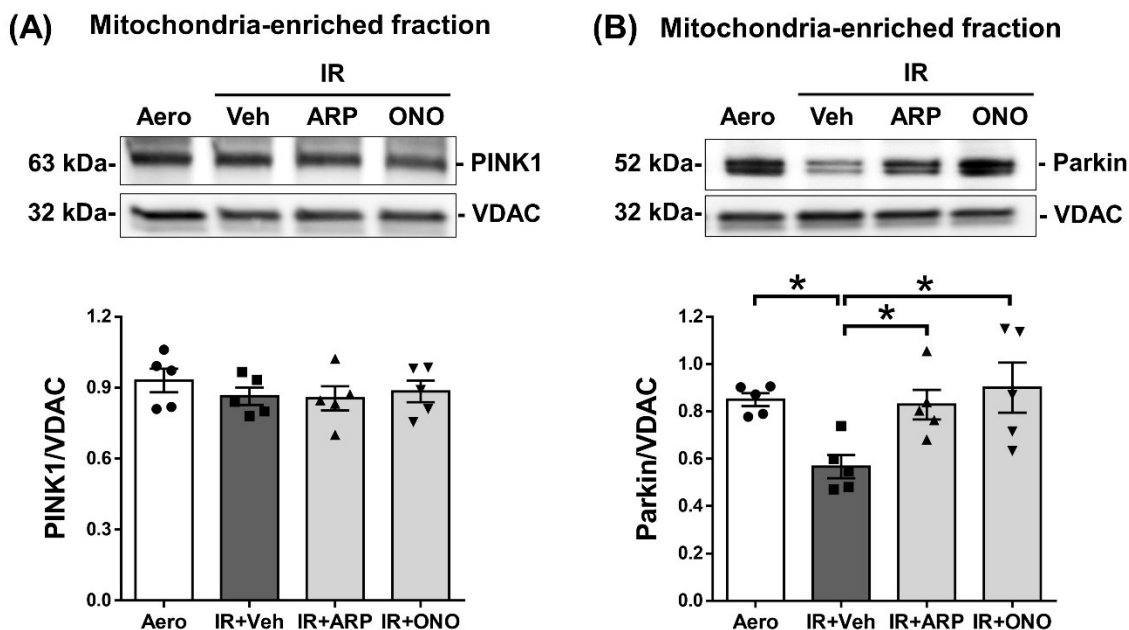


Figure A.4. MMP-2 preferring inhibitors attenuate IR injury-induced reduction in mitochondrial parkin. Representative immunoblots (upper panels) and quantitative measurements (lower panels) of (A) PINK1 or (B) parkin level in mitochondria-enriched fraction from I30-R40 hearts in absence or presence of ARP-100 (ARP, 10 μ M), ONO-4817 (ONO, 50 μ M) or DMSO vehicle (Veh) compared to aerobic control (Aero) (n=5 hearts per group). *p<0.05 by one-way ANOVA followed by Dunnett's post-hoc test.

A.4. Discussion

As I discovered in **Chapter 4**, MMP-2 activated during IR injury proteolyzes the mitochondrial fusion protein, Mfn-2. Here I show that both hearts subjected to 20 or 30 min ischemia followed by 40 min reperfusion had lower levels of mitochondrial Mfn-2 compared to aerobic controls, although the post-ischemic recovery of cardiac function is higher in hearts subjected to 20 min ischemia compared to those subjected to 30 min. I showed that, using our model of the isolated, perfused mouse heart, MMP-2 is activated in hearts subjected to 30 min ischemia (see **Chapter 4**), and it is also reported to be activated in rat hearts subjected to 20 min ischemia which induces stunning injury [8]. Mfn-2 loss also appears to start at early reperfusion (5 min) after 30 min ischemia. This is consistent with the pattern of intracellular MMP-2 activation during IR. Peroxynitrite, which activates MMP-2, peaks in heart tissue during IR injury in the first 30 seconds of reperfusion [45], which in turn induces MMP-2 activation within 2-5 minutes of reperfusion [8].

In contrast to Mfn-2, the changes in mitochondrial Drp-1 levels during IR showed a very different pattern. Drp-1 is a cytosolic protein and is recruited to the outer mitochondrial membrane to induce fission in response to stimuli that trigger mitochondrial damage [238, 239]. Our data shows that Drp-1 is upregulated in mitochondria from hearts subjected to short duration of ischemia (20 min) as well as at 5 min reperfusion following 30 min ischemia, which could occur as a cardioprotective effect to protect against mitochondrial damage. This is consistent with previous studies reporting increased Drp-1 recruitment to mitochondria and its activation during myocardial IR injury [562, 563]. However, with longer IR duration (30 min ischemia and 40 min reperfusion), both mitochondrial and cytosolic Drp-1 are downregulated in IR hearts, which could be a consequence of persistent mitochondrial damage. MMP-2 seems to play a role in Drp-1

dysregulation during IR injury as MMP-2 inhibition protected against its loss. Whether this is a direct or indirect effect of the proteolytic activity of MMP-2 requires further investigation.

Another mitochondrial quality control process that could be affected by MMP-2 activation is mitophagy. Although the level of PINK1 in mitochondria was not affected by IR injury, the level of mitochondrial parkin was reduced in IR hearts. This could be attributed to the loss in Mfn-2, as Mfn-2 is required for parkin translocation from the cytosol to mitochondria which in turn induces mitophagy to get rid of damaged mitochondria [256]. Cardiac-specific knockout of Mfn-2 in the mouse heart reduced parkin recruitment to mitochondria, resulting in defective mitophagy [252]. This reduction in parkin was attenuated by MMP-2 inhibition which could be due to preserving mitochondrial Mfn-2. Further studies are required to understand the role of MMP-2 in mitophagy.

In conclusion, MMP-2 activated during IR injury contributes to the loss in the mitochondrial quality control proteins, Mfn-2, Drp-1 and parkin which eventually leads to mitochondrial and cardiac dysfunction. The changes in mitochondrial Mfn-2, but not Drp-1, during IR occur rapidly upon reperfusion and with shorter duration of ischemia which is consistent with the reported pattern of MMP-2 activation during IR. Inhibition of MMP-2 activity can protect against cardiac contractile dysfunction by preserving mitochondrial quality control proteins.